CATALYTIC ROUTES FOR HYDROXYALKYLATION OF PHENOLS FOLLOWED BY OXIDATION FOR THE SYNTHESIS OF FLAVOURING AND FRAGRANCE AGENT

A THESIS SUBMITTED TO

UNIVERSITY OF PUNE

FOR THE DEGREE OF

DOCTOR OF PHILOSOPHY

(IN CHEMISTRY)

BY

Mr. Ajit C. Garade

Research Guide

Dr. Chandrashekhar V. Rode

CHEMICAL ENGINEERING AND PROCESS DEVELOPMENT DIVISION

NATIONAL CHEMICAL LABORATORY

PUNE- 411 008, INDIA

January-2011

Certificate of the Guide

Certified that the work incorporated in the thesis entitled **"Catalytic routes for hydroxyalkylation of phenols followed by oxidation for the synthesis of flavouring and fragrance agent"** submitted by **Mr. Ajit C. Garade** was carried out by the candidate under my supervision/guidance. Such material as has been obtained from other sources has been duly acknowledged in the thesis.

January, 2011

Dr. Chandrashekhar V. Rode
(Supervisor/Research Guide)

Declaration by the Candidate

I declare that the thesis entitled **"Catalytic routes for hydroxyalkylation of phenols followed by oxidation for the synthesis of flavouring and fragrance agent"** submitted by me for the degree of Doctor of Philosophy is the record of work carried out by me during the period from 11-07-2007 to 31-12-2010 under the guidance of **Dr. C. V. Rode** and has not formed the basis for the award of any degree, diploma, associateship, fellowship, titles in this or any other University or other institution of Higher learning.

I further declare that the material obtained from other sources has been duly acknowledged in the thesis.

January, 2011 Ajit C. Garade

Dedicated to my beloved Father and Mother…

Acknowledgement

I wish to express my sincere gratitude to my research guide, ***Dr. C. V. Rode****, Scientist, 'F' Chemical Engineering and Process Development Division, National Chemical Laboratory (NCL), Pune, for his constant support, invaluable guidance, numerous discussions, constructive suggestions and encouragement during the course of this work. He has been a constant source of inspiration to me during my stay at NCL. His enthusiastic attitude, innovative ideas, and scientific knowledge have inspired me profoundly. I will be remaining ever grateful to him for his teaching, guidance, and wonderful personality. It has been an intellectually stimulating and rewarding experience to work with him.*

I would like to thank head of the Chemical Engineering and Process Development Division, Dr. B. D. Kulkarni, for providing me all the divisional facilities required for my research work.

I would like to thank Dr. S. Sivaram (former Director) and Dr. S. Pal, Director, NCL, Pune, for allowing me to carry out research and providing all infrastructural facilities at NCL. I am grateful to University Grant Commission (UGC), New Delhi for awarding me the research fellowship.

I would like to thank Dr. M. Shirai, AIST, Sendai, Japan and Dr. R. C. Chikate of Abasaheb Garware College, Pune for very useful scientific discussions during the period of my research.

I take this opportunity to express my deepest sense of gratitude towards Dr. K. R. Patil, Dr. C. S. Gopinath, Dr. A. S. Kumbhar, Dr. P. N. Joshi, Dr. P. P. Wadgaonkar, Dr. Vaidya, Mr. P. B. Jadkar for their timely help, constant support, and valuable guidance.

I owe my special thanks to all scientific and non scientific staff of NCL. I would like to thank Mr. R. K. Jha, Ms. Violet, Mr. A. B. Gaikwad, Mr. Raheja, Mr. Patane, Mr. Kamble, Mr. Dure, Mr. Wanjale, Mr. Shinde, Mr. Nalavade, for their help and cooperation in completing my research work successfully.

I also wish to thank my seniors and my friends, Dr. Indresh, Dr. Vikas, Dr. Amit, Dr. Nitin, Dr. Anand, Dr. Shashi, Dr. Nandu, Dr. Kapil, Dr. Mahesh D., Jayprakash, Prashant, Vivek, Amit, Makarand, Savita, Sandeep, Piplad, Amol, Ajay G., Pravin,

Mahadev, Sachin, Narayan, Nitin, Ajay Jha, Sumit, Yogesh, Ms.Rasika, Ms. Mandakini, Ms. Prema, and all other research scholars and friends in NCL who are not named in person, for their valuable suggestions and helping hand.

Words are not enough to express my love and gratitude to my family members. It gives me great pleasure to thanks my parents, my sisters for always providing unconditional support and helping me over the years. Thanks to my dear wife for being patient and supportive all the time particularly during the tough writing stage of the thesis.

Ajit Chandrakant Garade

List of Contents:

List of Tables

List of Schemes

List of Figures

Chapter III

Chapter IV

Abbreviations

BET	Brunauer-Emmett-Teller
BJH	Barrett-Joyner-Halenda
B/L ratio	Brønsted to Lewis acid sites ratio
BNT	Bentonite
BPA	Bisphenol A
DAM	2, 2'-methylenebis (4-methylphenol)
DEPT	Distortionless enhanced polarization transfer
DTA	Differential thermal analysis
E_a	Energy of activation
EDX	Energy dispersive X-ray
FT-IR	Fourier- transform infrared spectroscopy
FWHM	Full width at half maximum
GC	Gas chromatography
$H_3PW_{12}O_{40}$ / DTP	Dodecatungstophosphoric acid
HBA	Hydroxybenzyl alcohol
HPA	Heteropolyacids
HPLC	High performance liquid chromatography
HT	High temperature
LT	Low temperature
Mont K10	Montmorillonite K10
NMR	Nuclear magnetic resonance
^{31}P-MAS NMR	^{31}P- Magic angle spinning NMR
PHB	*p*-Hydroxybenzaldehyde
PHBA	*p*-Hydroxybenzoic acid
PHBAlc	*p*-Hydroxybenzyl alcohol
p-VAlc	*p*-Vanillyl alcohol
S_{BET}	BET surface area
SEM	Scanning electron microscopy
SiO_2	Fumed silica

TG	Thermogravimetry
TPD	Temperature programmed desorption
TPR	Temperature programmed reduction
TS-1	Titanium silicate
XPS	X-ray photoelectron spectroscopy
XRD	X-ray diffraction

ABSTRACT OF THESIS

Catalytic routes for hydroxyalkylation of phenols followed by oxidation for the synthesis of flavouring and fragrance agent

The environmental friendly processes using solid catalysts for the fine chemicals have been the subject of research due to increased stringent effluent regulations in recent times and demand for high purity products particularly in fragrance/flavour, food, polymer additives and pharmaceutical applications. The processes involving condensation, hydroxyalkylation and oxidation of variety of substrates leading to important hydroxylated/oxygenated products can be developed by employing suitable solid catalysts. One such example is the hydroxyalkylation of phenols with aldehyde or ketone, which is a reaction of interest for the production of drugs, polymers and food additives [1, 2]. A well known industrially important category of compounds synthesized by hydroxyalkylation of phenols is, bisphenols which are widely used in plastic and rubber industries and as precursors for the synthesis of many benzophenone derivatives in perfumes and pharmaceutical industries. Similarly, hydroxymethylation of 2-methoxyphenol (guaiacol) to yield 3-methoxy-4-hydroxybenzyl alcohol (*p*-vanillyl alcohol) represents one of the steps in the synthesis of 3-methoxy-4-hydroxybenzaldehyde (*p*-vanillin), a well known flavouring agent in food and confectionary. Hydroxyalkylation is conventionally carried out using Lewis type acids like $AlCl_3$, Brønsted acids (e.g. HCl, H_2SO_4 etc) as well as bases which pose several major drawbacks as given below.

1) Difficulties in the separation and recovery of a pure product.
2) Handling of the toxic reagents is cumbersome.
3) Problems due to corrosive nature of reagents.
4) Formation of inorganic wastes due to use of reagents in the stoichiometric quantities.

In order to overcome these problems, a novel catalytic route is proposed using various solid catalysts such as heteropolyacids, zeolites, ion exchange resins, clays etc. for hydroxyalkylation of phenols. Among various solid acid catalysts, zeolites were found to exhibit better activity for hydroxyalkylation of phenols, but a major problem associated with these catalysts is deactivation of the catalyst due to deposition of bulky and higher molecular weight condensation products formed during the progress of the reaction [3]. Hence, it is of great practical importance to develop active and reusable solid acid catalysts having higher activity and selectivity for hydroxyalkylation of phenols. It is well known that the acidic characteristics of solid acids can be suitably modified by dispersing them on proper supports, by incorporating/exchanging metal ions, changing the ratio of Si/Al etc [4]. Such modifications in the solid acids also lead to change in reaction pathways. In the present thesis work, I have developed variety of solid catalysts involving dodecatungstophosphoric acid (DTP) impregnated on various supports like silica, montmorillonite and bentonite for hydroxyalkylation of phenols as well as γ-Fe_2O_3 and Co-saponite catalysts for side chain oxidation of hydroxyalkylated products into corresponding high value aldehyde products which extensively used in flavour/fragrance, food and polymer additives.

OBJECTIVES OF THE PRESENT INVESTIGATION

- Preparation of surface modified solid acid materials such as clays, silica etc. with tuned acidity and strength by impregnating dodecatungstophosphoric acid on them.
- Detail characterization of prepared catalysts using various techniques such as BET, NH_3-TPD, FTIR, pyridine IR, XRD, EDX, SEM, and by ^{31}P-CP MASNMR.
- Activity testing of above catalysts for hydroxyalkylation of phenol, *p*-cresol and guaiacol.
- Preparation of γ-Fe_2O_3 and Co-saponite catalysts by various methods and their detailed characterization.

- Activity testing of prepared catalysts for oxidation of hydroxyalkylated intermediates.
- Optimization of reaction conditions for the best catalysts.
- Interpretation of activity results based on the characterization data.

OUTLINE OF THE THESIS

The thesis is divided into seven chapters with appropriate references given at the end of each chapter.

Chapter 1 provides the concept of catalysis and green chemistry, general introduction to the hydroxyalkylation reactions, types of solid acid catalysts used for hydroxyalkylation of phenols, summary of literature on hydroxyalkylation of phenols and oxidation of side chain of phenol derivatives. At the end of this chapter, scope and objectives of the thesis are given.

Chapter 2 includes detailed experimental procedures used for preparation of various solid catalysts, their characterization and activity testing for hydroxyalkylation and oxidation reactions.

Chapter 3 explains hydroxyalkylation of phenol to give bisphenol F using dodecatungstophosphoric acid (DTP) impregnated on supports like silica and montmorillonite K10, their detail characterization and co-relation between observed catalyst activity results and characterization data.

Heteropolyacids like DTP are widely used as solid acid catalysts owing to their inherent Brønsted acidity. However for the hydroxyalkylation of phenol to give bisphenol F, the catalysts with proper acidity and strength are required in order to achieve high selectivity to bisphenol F. Acidity of DTP could be tuned suitably by dispersing it on proper supports like silica and montmorillonite K10. Surface hydroxyl groups of silica and montmorillonite supports interacted with DTP and forms $(SiOH_2)^+$ $(H_2PW_{12}O_{40})^-$ species depending upon DTP loading. This interaction of DTP with silica or montmorillonite supports leads to the localization of DTP protons thereby increasing their proximity to the Keggin anion because of the decrease in proton mobility [5]. Such surface modification

of supports due to impregnation of DTP enhanced their acidity and strength and thereby their activity for hydroxyalkylation of phenol to give bisphenol F.

In our study, various % of DTP supported on silica and montmorillonite were prepared by wet impregnation method. From NH_3-TPD measurement, the nature of acid sites of both parent SiO_2 and mont K10 was found to be significantly altered beyond 10% DTP loading. Both the supports beyond 10% DTP loading exhibited two types of acid sites both in low and high temperature regions whose strength was found to depend upon their textural properties and the extent of interactions with bulk DTP. Pyridine-IR studies showed that the ratio of Brønsted to Lewis acid sites (B/L) increased with increase in DTP loading. ^{31}P CPMAS NMR of 20% DTP/SiO_2 showed broadening of signal at -15.49, indicating interaction of DTP with surface silanol groups of silica, leading to higher acidity of silica after DTP dispersion on it.

Among various catalysts screened for the hydroxyalkylation of phenol to bisphenol F, 20% DTP impregnated on silica and montmorillonite K10 showed excellent activity with > 90% selectivity to bisphenol F. An increase in total acidity and acid sites in a high temperature region as well as surface modification of supports was found to be responsible for their high catalyst activity and selectivity as evidenced by NH_3-TPD, pyridine IR and ^{31}P CPMAS NMR. Effect of various reaction parameters on activity and bisphenol F selectivity was also studied [6, 7].

Chapter 4 demonstrates the hydroxyalkylation of *p*-cresol to give 2, 2'-methylenebis (4-methylphenol) [DAM] using DTP impregnated on bentonite (BNT) and commercial montmorillonite in a batch as well as continuous operation.

DTP supported on bentonite (20% DTP/BNT) was prepared by wet impregnation method and characterized by various techniques like BET, NH_3-TPD, Py-IR, XRD, and by ^{31}P CPMAS NMR. This catalyst gave 95% product yield with 94% selectivity to 2, 2'-methylenebis (4-methylphenol), DAM for the hydroxyalkylation of *p*-cresol with formaldehyde at 353 K and for a mole ratio of 5. Ammonia-TPD results showed that an increase in total concentration of acid sites from 4.9 of parent BNT to 11.6 $\mu molS^{-1}$ NH_3 of 20% DTP/BNT due to a strong interaction of protons of bulk DTP with surface

hydroxyl groups of BNT as evidenced by ^{31}P-CP MASNMR studies, was responsible for its high activity and selectivity.

Catalyst activity of commercial montmorillonite was also compared with that of TS-1 and bulk DTP having different acid strength for the hydroxyalkylation of *p*-cresol with formaldehyde. Among the three catalysts, montmorillonite showed highest activity (32% conversion with > 90% selectivity to DAM) for hydroxyalkylation of *p*-cresol. Ammonia TPD studies of various catalysts showed that an appropriate combination of both strong and weak acid sites of montmorillonite was mainly responsible rather than only the stronger acidity of bulk DTP for its highest catalyst activity for selective hydroxyalkylation of *p*-cresol to DAM [8].

Activities of various montmorillonite K catalysts were also evaluated for the continuous hydroxyalkylation of *p*-cresol to DAM in a fixed bed reactor. Among various catalysts screened, montmorillonite KSF/O showed excellent performance (26% conversion of *p*-cresol with > 90% selectivity to DAM). The effect of various reaction parameters such as mole ratio, temperature and catalyst concentration on the conversion of *p*-cresol and DAM selectivity was also studied in both batch and fixed bed reactors. Very low conversion of *p*-cresol (< 4%) was observed in the batch reactor as compared to the fixed bed reactor under the same reaction conditions [9].

In Chapter 5, hydroxyalkylation of guaiacol followed by oxidation of hydroxyalkylated intermediate to give *p*-vanillin, is discussed. Although H-mordenite has been reported as a solid acid catalyst for hydroxyalkylation of guaiacol to vanillol, the mole ratio of guaiacol to formaldehyde used was as high as 1:15. In our work we could achieve the highest selectivity of 46% to vanillol over 10% DTP/SiO_2, for the mole ratio of guaiacol to formaldehyde as low as 1:3. Ammonia TPD studies showed that the concentration of acid sites of SiO_2 in low temperature region (373-473 K) was significantly altered after impregnation of 10% DTP on SiO_2. The highest catalyst activity and selectivity of 10% DTP/SiO_2 as compared to other catalysts was mainly due to its acidic sites present in a low temperature region and stabilization of the intermediate carbocation by heteropolyanions of DTP. The effect of various reaction parameters like mole ratio,

catalyst concentration, temperature and the reaction time on guaiacol conversion and product selectivity was also investigated.

Oxidation of *p*-vanillyl alcohol (hydroxyalkylated intermediate) which is a second step in the synthesis of *p*-vanillin was carried out using Co-saponite catalysts with different Co loading (5-30%). These catalysts were prepared by precipitation method [10, 11] and characterized by XRD, TPR, TG, FT-IR, Raman and N_2-adsorption etc. Among the various catalysts, 13% Co-saponite showed highest activity (99% selectivity to *p*-vanillin with 55% conversion of *p*-vanillyl alcohol) for oxidation of *p*-vanillyl alcohol to *p*-vanillin. The distribution ratios of Co_3O_4/CoO phases increased from 0.84 to 1.67 with increase in Co loading from 5 to 13%, leading to its highest activity and selectivity [12].

In Chapter 6, studies on oxidation of *p*-hydroxybenzyl alcohol to *p*-hydroxybenzaldehyde (PHB) using γ-Fe_2O_3 (maghemite) catalysts has been presented.

I prepared highly pure single phase γ-Fe_2O_3 by a simple protocol involving co-precipitation using NH_4OH. XRD pattern showed major reflections at 2θ of 30.3^o (220), 35.8^o (311), 44.5^o (400) and 63^o (440) characteristic of γ-Fe_2O_3. The characteristic doublet of Fe $2p_{3/2}$ and $2p_{1/2}$ were observed as photoelectron peaks at 710.6 and 724.12 eV respectively, which confirmed Fe_2O_3 species. Two different morphologies due to precipitation carried out at two different temperatures (278 and 368 K) were observed in SEM analysis. Both LT and HT samples of γ-Fe_2O_3 particles showed about three times higher activities (80-84% conversion with 90-94% selectivity to oxidation products) than that shown by the bulk Fe_2O_3 for the air oxidation of *p*-hydroxybenzylalcohol under mild conditions [13].

Chapter 7 summarizes the work presented in all the chapters and general conclusions arrived from the discussed results.

References

1. A. de Angelis, P. Ingallina, C. Perego, *Ind. Eng. Chem. Res.* 43 (2004) 1169.
2. C. V. Rode, A. C. Garade, R. C. Chikate, *Catal. Surv. Asia* 13 (2009) 205.
3. A. Corma, H. Garcia, J. Miralles, *Micropor. Mesopor. Mater.* 43 (2001) 161.
4. A. C. Garade, P. S. Niphadkar, P. N. Joshi, C. V. Rode, *Chem. Lett.* 39 (2010) 126.
5. P. Madhusudhan Rao, A. Wolfson, S. Kababya, S. Vega, M. V. Landau, *J. Catal.* 232 (2005) 210.
6. A. C. Garade, V. S. Kshirsagar, C. V. Rode, *Appl. Catal. A: Gen.* 354 (2009) 176.
7. A. C. Garade, V. S. Kshirsagar, R. B. Mane, A. A. Ghalwadkar, U. D. Joshi, C. V. Rode, *Appl. Clay Sci.* 48 (2010) 164.
8. A. C. Garade, V. R. Mate, C. V. Rode, *Appl. Clay Sci.* 43 (2009) 113.
9. A. C. Garade, A. M. Hengne, T. N. Deshpande, S. V. Shaligram, M. Shirai, C. V. Rode, *J. Chem. Eng. Jpn.* 42 (2009) 782.
10. V. S. Kshirsagar, A. C. Garade, K. R. Patil, M. Shirai, C. V. Rode, *Top. Catal.* 52 (2009) 784.
11. V. S. Kshirsagar, A. C. Garade, K. R. Patil, R. K. Jha, C. V. Rode, *Ind. Eng. Chem. Res.* 48 (2009) 9423.
12. A. C. Garade, N. S. Biradar, S. M. Joshi, V. S. Kshirsagar, R. K. Jha, C. V. Rode, *Appl. Clay Sci.* (2010) doi:10.1016/j.clay.2010.10.026.
13. A. C. Garade, M. Bharadwaj, S. V. Bhagwat, A. A. Athawale, C. V. Rode, *Catal. Commun.* 10 (2009) 485.

Chapter I

Introduction and literature survey

1.1. CATALYSIS

With increasing concern of the environmental problems, the importance and economical significance of catalysis in various industries such as chemical, petrochemical, biochemical as well as polymer is exponentially increased during last couple of decades. More than 80% of the present industrial processes established since 1980, use catalysts. The term "catalysis" was first defined by Berzelius in 1835 [1]. *Catalysis is a phenomenon in which chemical reactions are accelerated by small quantities of foreign substances, called catalysts.* A suitable catalyst can enhance the rate of a thermodynamically feasible reaction but cannot change the position of the thermodynamic equilibrium. The catalytic reaction is a cyclic process and according to a simplified model, the reactant or reactants form a complex with the catalyst, thereby opening an alternate pathway for their transformation into the product or products. After completion of the reaction, the catalyst is released and the next catalytic cycle can proceed [2].

The rate of chemical reaction at a given temperature is generally decided by the energy of activation. *The energy of activation is the minimum amount of energy the reactants must acquire before they could react.*

For a reaction A $\longrightarrow$ B, it is necessary that the molecules of A must be activated to transition state X^* before they get converted into product B. A state of equilibrium exists between A, B and X^* which is represented as,

$$A \rightleftharpoons X^* \rightleftharpoons B$$

The energy profile diagram for the above reaction with and without catalyst is presented in Figure 1.1.

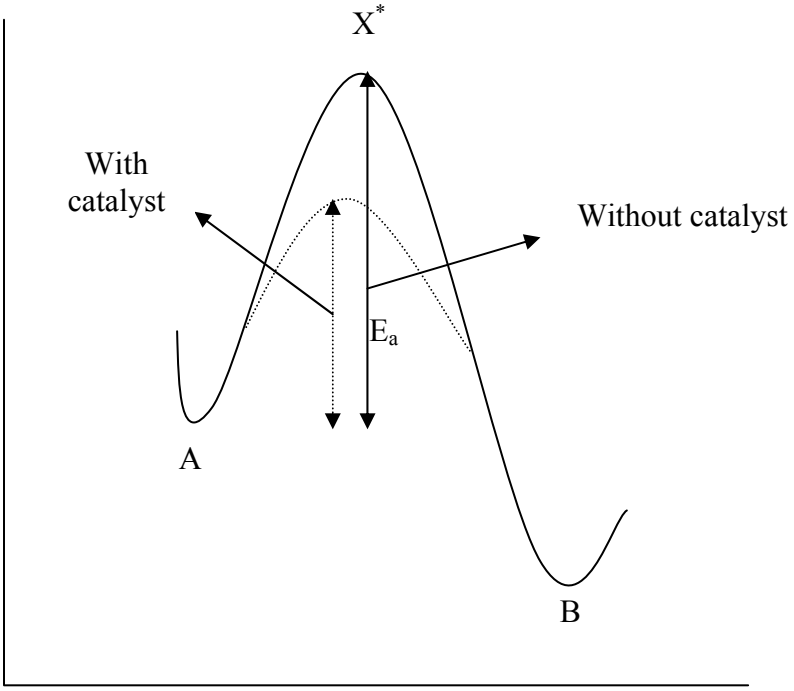

Figure 1.1. Energy profile diagram [3]

The absorption of energy E_a (energy of activation) by molecules of A converts them to an activated complex X^*. When X^* gets converted into product B, more heat will be evolved since energy of B is lower than that of A. The energy of activation is a lower for a reaction carried out in the presence of a catalyst as compared to an un-catalyzed reaction. Therefore, the rate of a catalytic reaction is very high as compared to that in absence of a catalyst [3].

Catalysts are broadly classified as homogeneous and heterogeneous, depending on their physical form in which they are present in the respective catalytic process (Figure 1.2). If the catalyst and reactants form a common physical phase, then the reaction is called *homogeneously catalyzed reaction*. Acids, bases such as HCl, NaOMe etc. and transition metal complexes/compounds such as carbonyls complexes of Co, Fe, and Rh are typical examples of homogeneous *catalysts*.

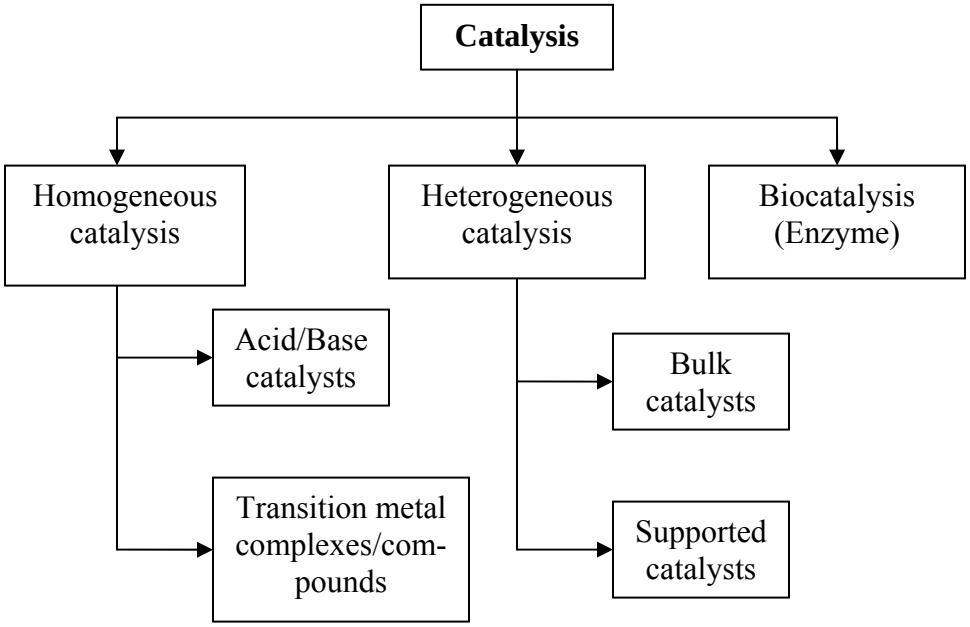

Figure 1.2. Classification of catalysis

Example of *homogeneously catalyzed* reaction is the esterfication of methanol with acetic acid using conc. HCl (Figure 1.3a) to give methyl acetate.

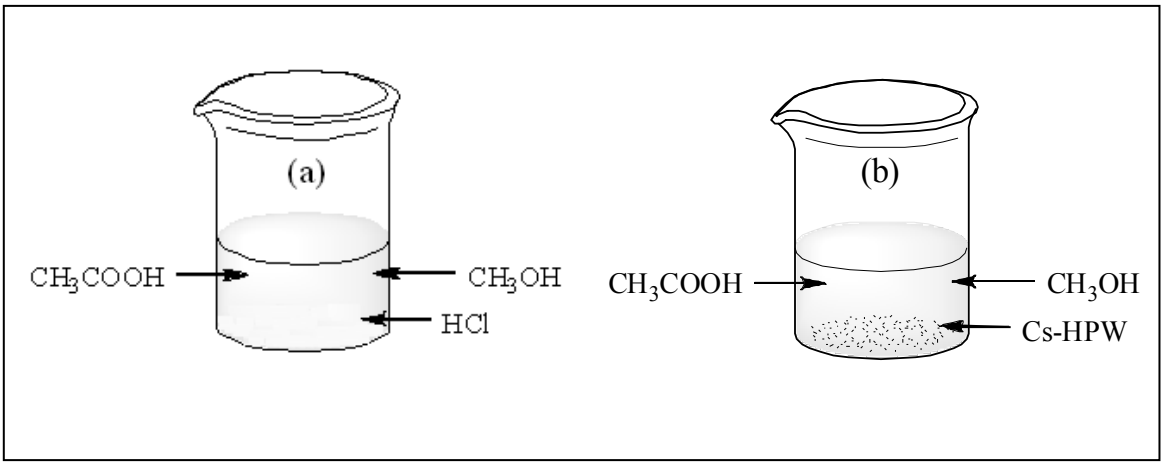

Figure 1.3. Esterfication of methanol with acetic acid over (a) HCl, homogeneous catalysis and (b) Cs-HPW, heterogeneous catalysis

In *heterogeneous catalysis,* the catalyst and reactants form separate physical phases. Typical *heterogeneous catalysts* are bulk solid catalysts such as metal oxides and supported catalysts such as heteropolyacids supported on alumina, carbon and silica etc. Example of *heterogeneously catalyzed* reaction is ammonia synthesis by reacting N_2 and H_2 over promoted iron catalysts in the gas phase [4] and esterfication of methanol with acetic acid using Cs substituted heteropolyacids (Cs-HPW) solid catalyst (Figure 1.3b). Heterogeneous catalysts have several advantages over homogeneous catalysts [5] such as

1. Easy separation and recycle by simple filtration
2. Fixed-bed and continuous flow operations for enhanced productivity
3. Commercial utility on a large scale due to the economic benefits over batch operations and/or reduced expense of catalyst recovery and recycle
4. High conversion and selectivity to the desired product

Bio-catalysis involves the processes in which enzymes or microorganisms catalyze various processes. Famous example of bio-catlysis is ethanol fermentation by *Saccharomyces cerevisiae* [6]. Although such catalysts are homogenous, these can be immobilized on various carriers such as porous glass, SiO_2, and organic polymers, in order to facilitate their separation on a commercial scale. Other examples of biochemical reactions are, isomerization of glucose to fructose using enzymes such as glucoamylase immobilized on SiO_2, and the conversion of acrylonitrile to acrylamide by cells of corynebacteria entrapped in a polyacrylamide gel.

From 1940, numerous catalytic reactions were commercialized on industrial scales [7-16]. Some of the important catalytic processes are presented in Table 1.1.

Table 1.1. Industrially important catalytic processes [7-16]

Year of commerci-alization	Process	Catalyst	Products	Company
1940-1960	Dehydrogenation	Cr_2O_3 – Fe_2O_3	Butadiene from *n*-butane;	Phillips Petroleum Company, Delaware [7]
	Oxidation of aromatics	V_2O_5/TiO_2	Phthalic anhydride from naphthalene and *o*-xylene;	BASF Aktiengesellschaft, Germany [8]
	Polymerization (Ziegler –Natta)	$TiCl_4$ – $Al(C_2H_5)_3$	Polyethylene from ethylene;	Solvay & Cie, Belgium [9]
1961-1980	Steam reforming	Ni –α-Al_2O_3	Co, (CO_2), and H_2 from methane;	Texaco Inc., USA [10]
	Ammoxidation	Bi phosphomolybdate	Acrylonitrile from propene	Eastman Kodak Company, USA [11]

1981-2000	Alkylation (Mobil –Badger)	Modified zeolite (ZSM-5)	Ethylbenzene from ethylene;	Mobil Oil Corporation, USA [12]
	Oxidation (Monsanto)	Vanadyl phosphate	Maleic anhydride from *n*-butane	E. I. Du Pont de Numours and Company, Wilmington [13]
	Oxidation with H_2O_2 (Enichem)	Ti- silicalite	Hydroquinone and catechol from phenol;	Council of Scientific industrial Research, India [14]
2001-2010	Epoxidation, dehydration followed by hydrogenation	Metal hydroxide	Hexamethylene diamine from butadiene	Degussa AG, USA [15]
	Hydroformyla-tion, oxidation followed by hydrogenation	Rh-complexes	6-Amino-caproic acid from 3-pentenenitrile	E. I. du Pont de Nemours and Company Wilmington [16]

1.2. GREEN CHEMISTRY

In recent years, the term "environmental catalysis" and "green chemistry" are frequently used. *Green Chemistry is the science that deals with "carrying out chemical activities-including chemical design, manufacture, use, and disposal-such that hazardous substance will not be used and generated"* [17]. Twelve principles of green chemistry are given below.

Twelve principle of green chemistry [18]

1. It is better to prevent waste than to treat or clean up waste after it is formed.
2. Synthetic methods should be designed to maximize the incorporation of all materials used in the process into the final product.
3. Wherever practicable, synthetic methodologies should be designed to use and generate substances that possess little or no toxicity to human health and the environment.
4. Chemical products should be designed to preserve efficacy of function while reducing toxicity.
5. The use of auxiliary substances (e.g. solvents, separation agents, etc.) should not be made unnecessary wherever possible and, innocuous when used.
6. Energy requirements should be recognized for their environmental and economic impacts and should be minimized. Synthetic methods should be conducted at ambient temperature and pressure.
7. A raw material or feedstock should be renewable rather than depleting wherever technically and economically practicable.
8. Reduce derivatives - Unnecessary derivatization (blocking group, protection/ deprotection, temporary modification) should be avoided whenever possible.
9. Catalytic reagents (as selective as possible) are superior to stoichiometric reagents.
10. Chemical products should be designed so that at the end of their function they do not persist in the environment and break down into innocuous degradation products.
11. Analytical methodologies need to be further developed to allow for real-time, in-process monitoring and control prior to the formation of hazardous substances.
12. Substances and the form of a substance used in a chemical process should be chosen to minimize potential for chemical accidents, including releases, explosions, and fires.

There are several examples of green processes among which the topic of my thesis, hydroxyalkylation of phenols to give bisphenols and/or hydroxybenzyl alcohol (HBAlc) and side chain oxidation of phenol derivatives into corresponding aldehydes over solid catalysts is an important process being developed and commercialized [19]. Catalytic routes often satisfy most of the criteria listed above; hence, my work on developing new catalysts for hydroxyalkylation of phenol to bisphenols is directly relevant to the concept of "green chemistry". This has been elaborated in details in section 1.3 below.

1.3. HYDROXYALKYLATION

1.3.1. Hydroxyalkylation of aromatics

Hydroxyalkylation is an electrophilic substitution reaction in which one or more hydrogen atom(s) of an aromatic ring are replaced by hydroxyalkyl group(s). The general mechanistic pathway for the hydroxyalkylation of aromatic in presence of acidic catalysts /reagents is presented in Scheme 1.1.

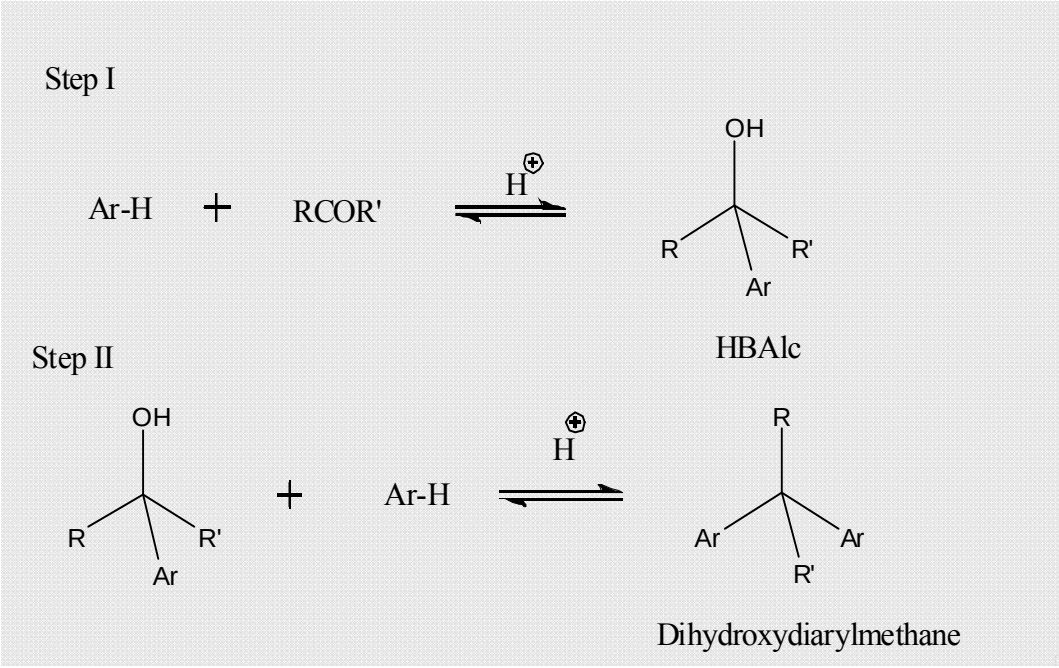

Scheme 1.1. Formation of HBAlc and dihydroxydiarylmethane by hydroxyalkylation of aromatics

In the hydroxyalkylation reaction, aldehyde or ketone reacts with an aromatic compound to form HBAlc. The reaction usually does not stop at this stage and alcohol which formed initially reacts further with another molecule of aromatic compound to give dihydroxydiarylmethane. The reactivity of aldehyde (or ketone) strongly depends upon the nature of substituents attached to the carbonyl carbon. Aliphatic aldehydes e.g. formaldehyde (R and R'=H) are very reactive as compared to aromatic aldehydes. Electron withdrawing groups (e.g. NO_2) present on aromatic ring generally facilitate the hydroxyalkylation reaction [20].

The products obtained by the hydroxyalkylation or hydroxyalkylation/oxidation processes are of great commercial importance and widely used as flavouring and fragrance agents in pharmaceutical and food industries. Among various flavouring and fragrance agents, *p*-vanillin, *p*-hydroxybenzaldehyde (PHB) and benzophenone derivatives are well known and commonly used in consumer products. Due to the high production cost (Table 1.2) from natural resources, these compounds are generally prepared by chemical processes e.g. the cost of vanillin extracted from vanilla pods has increased up to $1200 per kilo in 2001, in contrast to the price of synthetic vanillin, stable at < $15 per kilo [21, 22].

Table 1.2. Production cost of *p*-vanillin from natural resource (vanilla bean) and synthetic route [21-23]

Year	*p*-vanillin from vanilla bean		*p*-vanillin from synthetic route		Industry
	Metric Tons	U. S. $/kg	Metric Tons	U. S. $/kg	
1924	360	19.8	-	18	Salvo Chemical Corporation, USA; Marathon Paper Mill Company, USA
1934	360	7.7	-	6	
1971	-	11-18.5	-	11	
1980	-	88-101	-	11-12	Ontario Pulp and Paper, Canada
1991	498	33.3	4500-5500	11-14	
1992	437	27.6	4500-5500	11-14	
2001	1800	1200	~10000	15	

The cheapest and simplest conventional route to synthesize such flavouring and fragrance agents is the hydroxyalkylation of phenols followed by the oxidation of side chain of phenol derivatives formed as an intermediate hydroxyalkylated product using reagents like quaternary ammonium compound, sulfuric acid, chromic acid etc. [24] which pose several environmental as well as reagents handling problems [25]. Due to immense commercial importance of these compounds, developing cheaper and eco-friendly routes for the hydroxyalkylation and oxidation processes are of great practical importance. Several chemical processes were reported for the production of flavouring and fragrance agents, among which first one was reported by Rhodia for vanillin using solid catalysts (Scheme 1.2) [26]. This process is evidently superior to the processes based on the use of conventional reagents in stoichiometric amounts for the production of vanillin, from both economic and environmental viewpoints.

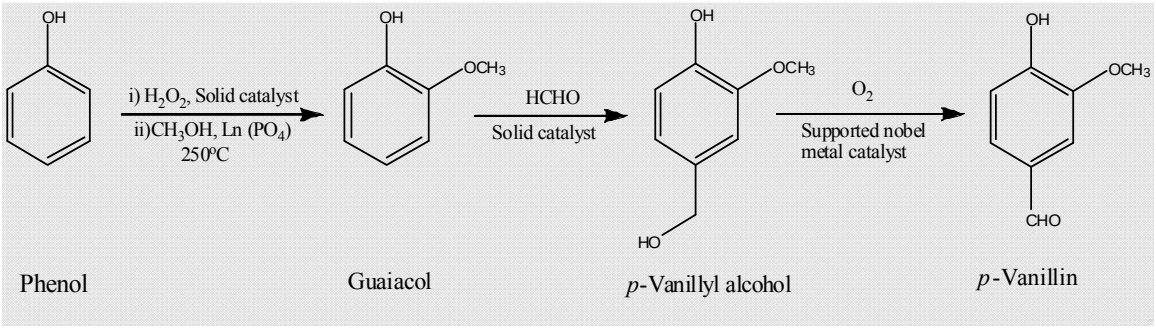

Scheme 1.2. Catalytic Rhodia process for vanillin [26]

Another important class of chemical compounds synthesized by the hydroxyalkylation of phenols with formaldehyde is bisphenols, also known as dihydroxydiarylmethane. Besides their use in the synthesis of benzophenone derivatives aforementioned, bisphenols are also widely used as antioxidant and chemical intermediates for the preparation of epoxide resins and polycarbonate in polymer industries [27-30]. Bisphenols are mainly produced in Japan, and its production (bisphenol F) is estimated to be about 3000 metric tons per year [31]. The most important bisphenols other than bisphenol F are bisphenol A and bisphenol Z which are produced by condensation of phenol with acetone and cyclohexanone respectively. World capacity of bisphenol A is 2.67 million metric tons (2001) and the four main global producers are, General Electric (25% of world installed capacity), Bayer (16% of world installed capacity), Shell (12% of world installed capacity) and Dow Chemical Corp. (10% of world installed capacity) [27]. The worldwide production of bisphenol Z is about 1360 metric tons per year [32] which is widely used for production of polycarbonate film [33].

1.3.2. Hydroxyalkylation process mediated by conventional reagents

As mentioned in section 1.3.1., hydroxyalkylation processes are conventionally carried out using strong mineral acids (HCl, H_2SO_4, H_3PO_4) as well as bases. Some of the industrially important products derived from the hydroxyalkylation of phenol using conventional reagents are summarized in Table 1.3.

Table 1.3. Industrially important products derived from hydroxyalkylation of phenol

Aromatic	Aldehyde/ Ketone	Product (s)	Reagents	Industry
Phenol Guaiacol	Formaldehyde	Hydroxybenzyl alcohol Vanillyl alcohol	Quarternary ammonium salt NaOH	The Dow Chemical Company, USA [34]; Mitsubishi Petrochemical Company Ltd., Japan [35]
Phenol	Formaldehyde	Bisphenol F	HCl, H_2SO_4 or Oxalic acid	Dainippon Ink & Chemicals, Japan [36]
Phenol	Acetone	Bisphenol A	HCl	Mitsui Toatsu Chemicals, Inc., Japan [37]
Phenol	Cyclohexa-none	Bisphenol Z	HCl or H_2SO_4	Maruzen Oil Co., Ltd., Japan [38]

Although, these reagents give acceptable yields of the desired product, the conventional processes based on the stoichiometric use of reagents have some of the following major drawbacks:

i) Difficulties in the separation and recovery of pure product from the reaction medium

ii) Handling of reagents due to their corrosive nature and toxicity

iii) Formation of inorganic wastes due to use of reagents in the stoichiometric quantities

Another disadvantage of mineral acids/reagents based processes is its higher production cost as compared to the solid acid catalyzed processes. In a fixed-bed reactor (for the ion exchange-resin process) and a continuous stirred tank reactor (for HCl-catalyzed process), acetone and phenol react with each other to produce bisphenol A along with other side products. Because of corrosion problems, relevant parts of the HCl-catalyzed process plant have to be made of monel alloys (i.e., heat exchangers) or must be glass lined (i.e., reactors). On the other hand, the whole plant for the process based on ion-exchange resins is made of 304 or 316 L stainless steel, which is less expensive. This difference has an important influence on the total cost of the plant. In fact, for example, a bisphenol A plant using ion exchange-resin catalyst to produce 200 million pounds per year requires a total project investment of about $101,000,000, compared to about $244,000,000 for a plant using HCl catalyst [39].

Presently, several conventional processes based on stoichiometric use of reagents are being replaced by solid acid catalysts in order to overcome the above drawbacks and in particular to improve the process economics [40-42].

1.3.3. Solid acid catalysts for hydroxyalkylation of phenols

Solid acid catalysts are the materials in the solid state which exhibits the Brønsted and /or Lewis acidity and have the following advantages over conventional acid reagents:

1) Required in catalytic amount unlike mineral acids which are used in stoichiometric equivalent or in excess
2) Easy separation and recovery
3) Reusability and lower toxicity
4) Higher selectivity to the desired product
5) No formation of inorganic waste

The catalyst activity of solid acids for the hydroxyalkylation of phenols mainly depends upon their properties e.g. acidity and strength, particle size, morpholgy etc. which in turn depend upon their structure. The solid acid catalysts reported for the hydroxyalkylation of phenols are: heteropolyacids [43], clays [44], and zeolites [45]. The structure and properties of these catalysts are described in detail below.

1.3.3.1. Heteropolyacids

Heteropolyacids (HPA) are hydrogen form of heteropolyanions formed by condensation of more than two types of oxoanion. Heteropolyanions are composed of oxides of addenda atoms (V, Nb, Mo, W, etc.) and heteroatoms (P, Si, etc.) [46]. The structures of heteropolyacids are classified into several groups based on the similarity of the composition e.g. Keggin-type, $XM_{12}O_{40}^{n-}$ [47]; Silverton-type, $XM_{12}O_{42}^{n-}$ [48]; Dawson-type, $X_2M_{18}O_{62}^{n-}$ [49]; Strandberg-type, $X_2M_5O_{23}^{n-}$; Anderson-type, $XM_6O_{24}^{n-}$ and Lindqvist-type, $XM_6O_{24}^{n-}$, where X is a heteroatom and M is an addenda atom [50]. Among various structures aforementioned, Keggin-type heteropolyacids are widely used as solid catalysts for various organic transformations due to their higher activity and thermal stability [51, 52]. The catalyst activity and properties of heteropolyacids depend upon their structure. HPA in solid state shows hierarchical structures which are classified into primary, secondary and tertiary.

1.3.3.1.1. Structure of heteropolyacids

a) Primary structure

The primary structure of heteropolyanion consists of clusters of the metal oxide. The first characterized and the best known of these is the Keggin heteropolyanion typically represented by the formula $XM_{12}O_{40}^{n-}$, where X is the central atom (Si^{4+}, P^{5+}, etc.) and M is a metal ion (Mo^{6+} or W^{6+}). The Keggin anion is composed of a central tetrahedron XO_4 surrounded by 12 edges and corners sharing metal-oxygen octahedra, MO_6 (Figure 1.4). The octahedra are arranged in four M_3O_{13} groups. Each group is formed by three octahedra sharing edges and having a common oxygen atom which is also shared with the central tetrahedron XO_4 [53]. A typical primary structure of an heteropolyacid $H_3PW_{12}O_{40}$ is given in Figure 1.4.

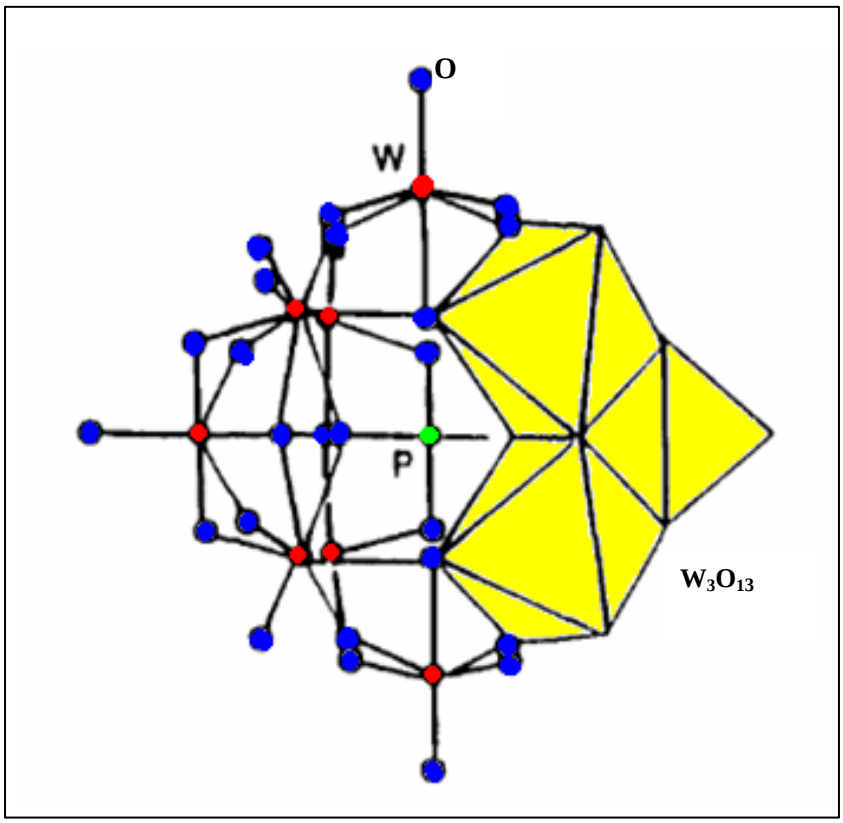

Figure 1.4. Primary structure of heteropolyacid (HPA) in the solid state [51]

b) Secondary structure

The secondary structure is the three-dimensional (usually regular) arrangement consisting of polyanions, counter cations and water molecules (Figure 1.5). The secondary structure is flexible to different extents depending on the counter cation and the structure of the polyanion, and is the basis of bulk-type catalysis of solid HPA catalysts discussed later in section 1.3.3.1.2.

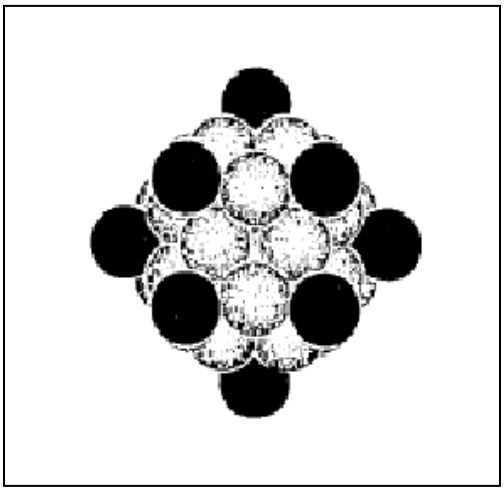

Figure 1.5. Secondary structure of HPA [53]

c) Tertiary structure

The tertiary structure of HPA (Figure 1.6) represents the manner in which the secondary structure assembles into solid particles and relates to properties such as particle size, surface area, and pore structure, and plays an important role in heterogeneous catalysis [53].

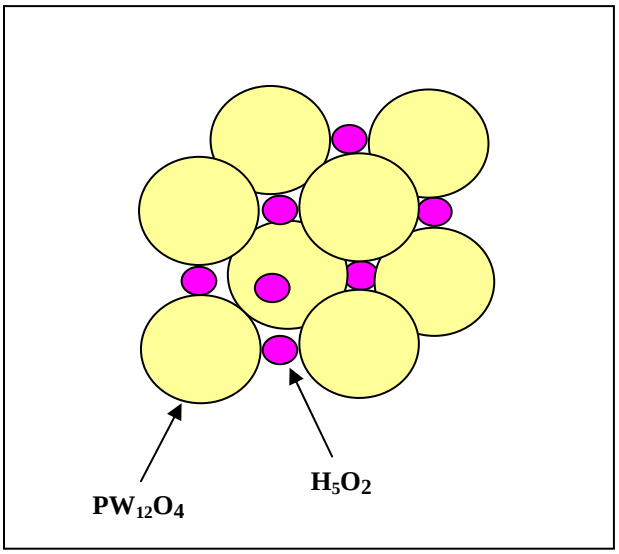

Figure 1.6. Tertiary structure of HPA [53]

1.3.3.1.2. Types of catalysis using solid heteropolyacids

Generally, three different modes of catalysis are observed using solid HPAs (Figure 1.7). Surface-type catalysis (a) takes place on the solid surface involving two-dimensional reaction field: on outer surface and pore wall. In types (b) and (c) as shown in Figure 1.7, the reaction fields are three-dimensional in contrast to the surface-type catalysis [54]. Three dimensional reaction field involves outer surface, pore wall and pseudo bulk liquid at high temperature. When the diffusion of reactant molecules in the solid (diffusion in the lattice rather than pores) is faster than the reaction, the solid bulk forms a pseudo-liquid phase in which catalytic reaction can proceed (Figure 1.7 b). In this instance, reactant molecules in the gas or liquid phase penetrate in between the polyanions (primary structure), sometimes expanding the distance between the polyanions, and react inside the bulk solid. The products come out to the surface and are released to the gas or liquid phase. In the pseudoliquid phase, such catalysts appear as solids but behave like liquids (solvent). As the active sites in the solid bulk *e.g.* protons, take part in catalysis, very high catalytic activities are often observed in the bulk phase.

The second bulk-type catalysis [bulk-type (II), Figure 1.7 c] is found in oxidation processes at high temperature when the diffusion of redox carriers (protons and electrons in this case) is rapid in the solid bulk, and the whole bulk participates in the reduction–oxidation cycle. Solid HPAs containing cations of low ionic radii to charge ratio (H^+, Na^+, Cu^{2+}, *etc.*) readily absorb small polar molecules and tend to exhibit pseudoliquid behaviour and are soluble in water. Cs and NH_4 salts (scarcely soluble in water, due to low solvation energy) usually show only surface-type catalysis.

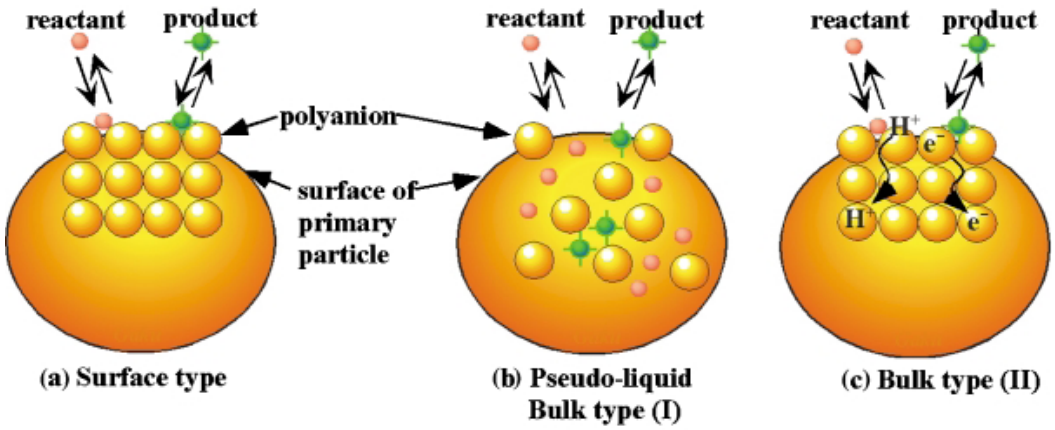

Figure 1.7. Three types of catalysis for solid heteropoly compounds: (a) surface type; (b) pseudoliquid: bulk type (I), (c) bulk type (II) [54]

1.3.3.1.3. Characteristics of heteropolyacids

1. HPAs have very high solubility in polar solvents such as water, lower alcohol, ketones, ethers, esters etc. and insoluble in non-polar solvents like hydrocarbons [55].
2. Solid HPAs possess purely Brønsted acidity and are stronger than other solid acids such as SiO_2-Al_2O_3, H_3PO_4/SiO_2, HX and HY zeolites. The acid strength of crystalline HPAs decreases in the order: PW > SiW ≥ PMo > SiMo which is identical to that in solutions [56].
3. HPAs have a fairly high thermal stability. The Keggin-type PW, SiW, PMo and SiMo decompose at 738, 718, 648 and 623 K respectively [57].

1.3.3.1.4. Supported HPAs

Supported HPA catalysts are important for applications in various organic transformations because bulk HPAs have a low specific surface (1-5 m^2 /g). The acidity and catalytic activity of supported HPAs depends on the type of the carrier, the HPA loading and conditions of pretreatment etc. Acidic or neutral substances such as SiO_2, active carbon, acidic ion-exchange resin etc., are suitable as supports [58, 59] while basic solids like MgO tend to decompose HPA [60].

HPA on Silica

The acidity and strength of HPA can be tuned properly by impregnating it on a suitable support like silica. Silica contains surface silanol groups which interact with protons of bulk DTP. This interaction leads to the localization of DTP protons thereby increasing their proximity to the Keggin anion because of the decrease in proton mobility [61, 62]. The interaction between HPA and silica could be studied by ^{1}H and ^{31}P magic-angle spinning (MAS) NMR studies [63, 64]. During impregnation of HPA (< 10%) on silica in aqueous solution, two HPA species were observed viz. HPA with intact Keggin unit and Keggin anion formed due to protonation with silanol group, ($SiOH_2^+$) ($H_2PW_{12}O_{40}^-$) denoted by A and B respectively [64]. The presence of A and B was shown by Kozhevnikov et al. at -15 ppm and at -11 to -14 ppm respectively in ^{31}P-MAS NMR [65]. The relative amount of species A and B depends on HPA loading nevertheless, A is always dominating irrespective of HPA loading. At higher HPA loadings of 30-50%, only A is practically present on the silica surface; while at lower loadings, both species exist. The amount of B increases with decrease in HPA loading. In contrast, catalysts prepared by impregnation of HPA in *methanol* contain exclusively Keggin type A over the whole range of HPA loading [65].

HPA on Mesoporous Molecular Sieve

Developing shape selective catalysts has been attempted by incorporating HPA into the pores of zeolite matrix. The large molecular size of HPA (12 Å) is a major constraint for its incorporation into the small pore size of normal zeolites. Hence mesoporous pure-silica molecular sieve MCM- 41 is a good alternative to zeolites due to its large pore size (32Å) [66]. Keggin structure is retained on the MCM-41 surface for HPA loading higher than 20 wt%; however at lower loadings a partial decomposition of HPA to P_2W_{21} species was observed [65]. An excellent dispersion of HPA is achieved on the MCM-41 due to its higher surface area of 1250 m^2/g. Formation of crystal phase is not seen even at HPA loadings as high as 50 wt% on MCM-41, which enables to develop catalysts with a wide range of HPA loadings necessary for excellent activity and shape selectivity in industrial applications e.g. liquid-phase phenol alkylation [67].

HPA on Carbon

HPAs supported on H_3PO_4 activated carbon exhibit an excellent stability against leaching, and therefore are widely used as solid acid catalysts for fixed bed operation [68]. As evidenced by IR and ^{31}P MAS NMR, HPA supported on H_3PO_4 activated carbon was found to retain its Keggin structure at loading > 5 wt%, however at lower loadings, a line broadening was observed due to the strong interaction of HPA with carbon [69]. HPAs form finely dispersed species on the carbon surface and no HPA crystal phase is developed even at the HPA loading as high as 45 wt% [69].

1.3.3.2. Clays

Clay minerals are layer silicates of the phyllosilicate family having two-dimensional structure, in which the basic building blocks are the Si (O, OH) tetrahedra and the M (O, $OH)_6$ octahedra (where M = Al^{3+}, Mg^{2+}, Fe^{3+} or Fe^{2+}) [44]. The alternate sheets of tetrahedra and octahedra give rise to the layers (thick 0.7 nm ca.) of the 1:1 minerals (kaolinites or serpentinites for M = Al^{3+} or Mg^{2+}, respectively), while in the layers of the 2:1 type clays (thick 1.0 nm ca.) a sheet of octahedra is sandwiched between two sheets of Si-tetrahedra (Figure 1.8) [70, 71]. Clay minerals can be dioctahedral or trioctahedral, based on the number of octahedral sites per unit cell occupied, which in turn depends essentially on the cation present (for example, Al^{3+} or Mg^{2+}) in the octahedral sheets. Clays are divided into two broad groups: (a) cationic and (b) anionic. The negatively charged alumino-silicate layers, in cationic clays have cations in the interlayer space to balance the charge, while the anionic clays have anions and water molecules located interstitially to balance the positively charged metal hydroxide layers [72]. Due to the presence of external -OH groups and the isomorphous substitution of Si^{4+} by Al^{3+} ions, clays exhibit Brønsted as well as Lewis acidity with versatile applications for several organic transformations [73-79] e.g. montmorillonite K10 (2:1 type clays belonging to smectite group) having Brønsted as well as Lewis acid sites [80, 81] are widely used as the catalysts or supports. In montmorillonite, isomorphous substitution of Al^{3+} by Mg^{2+} takes place in octahedral sheet.

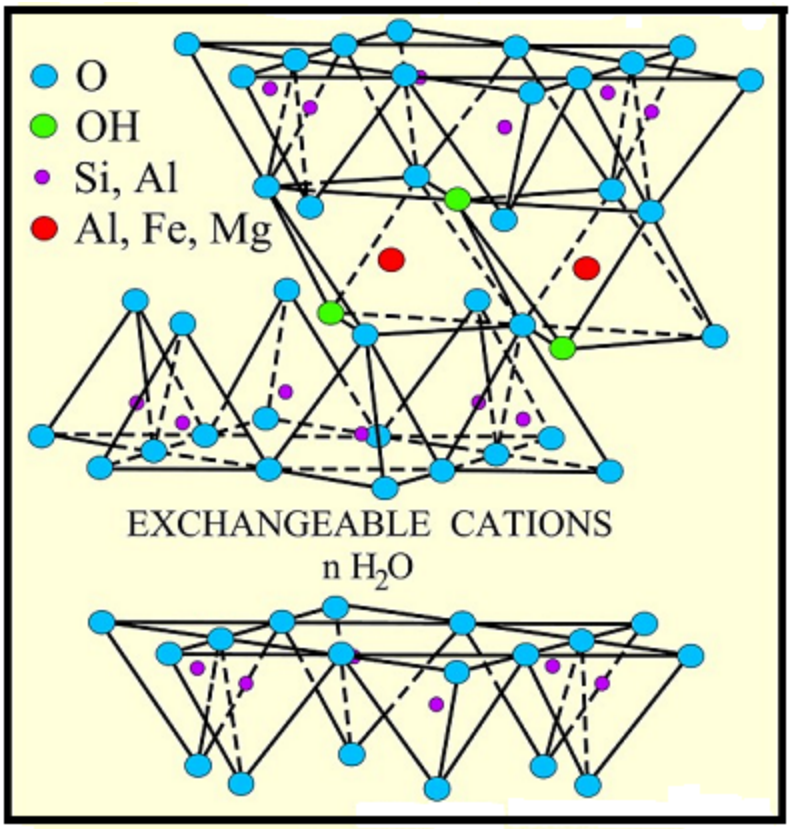

Figure 1.8. Structure of montmorillonite clay [81]

1.3.3.3. Zeolites

Zeolites are microporous aluminosilicates in which the tetrahedral primary building blocks (TO_4, T is Si, Al) are linked through oxygen, producing a three-dimensional network containing channels and cavities of molecular dimensions (Figure 1.9) [82, 83]. The general formula of zeolites in the as-synthesized form is: $xM_2/nO.xA1_2O_3.ySiO_2.wH_2O$ where M is a cation which can belong to the group IA or IIA or can be an organic cation, while *n* is the cation valence, and w represents moles of water contained in the zeolite voids.

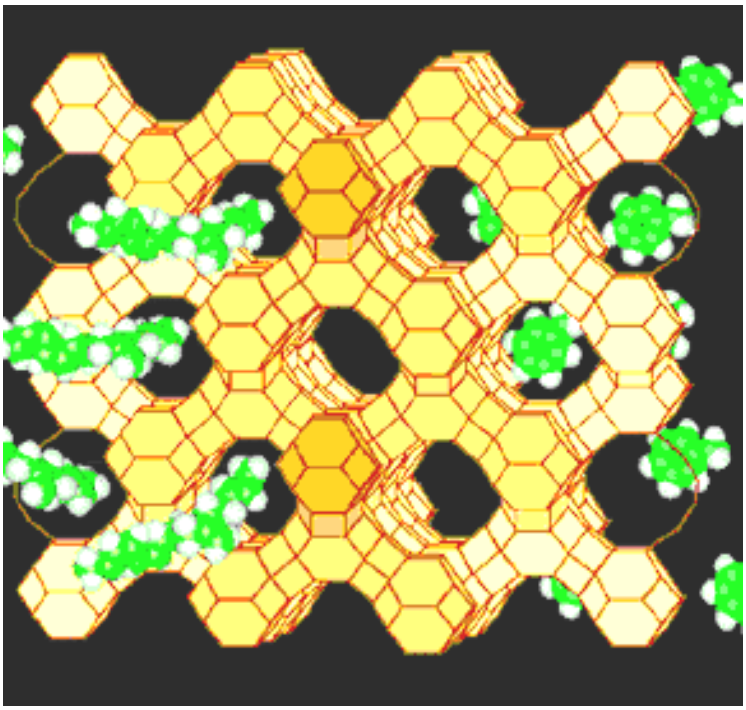

Figure 1.9. Structure of zeolites [83]

Zeolites are generally prepared by hydrothermal method [84, 85]. Small-pore zeolites contain 6- or 8-membered rings (diameter *d*: 2.8<*d* <4 ˚A), medium-pore zeolites contain 10-membered rings (5<*d* <6 ˚A) and the openings of large-pore zeolites are constructed of 12- membered rings (*d* >7 ˚A). Examples of small pore zeolites are sodalite and zeolite A, of medium-pore zeolites ZSM-type zeolites, while large-pore zeolites include faujasites and zeolites X and Y. The H forms of zeolites develop strong Brønsted acidity and play a major role in many large-scale industrial processes [86, 87]. Characteristic properties of these structurally well-defined solids are selective sorption of small molecules (molecular sieves), ion exchange, and large surface areas [82].

Zeolite structure containing only SiO_2 tetrahedra would be electrically neutral and no acidity would be developed on its surface. Brønsted acid sites are developed when Si^{4+} is isomorphically substituted by a trivalent metal cation, for instance $A1^{3+}$, and a negative charge is created in the lattice, which is compensated by a proton. The proton is attached

to the oxygen atom connected to neighbor silicon and aluminum atoms, resulting in the so-called bridged hydroxyl group which is the site responsible for the Brønsted acidity of zeolites [88]. Therefore zeolites also were thought as appropriate catalysts for the hydroxyalkylation of phenols. Although zeolites showed good activity for hydroxyalkylation of phenols, a major problem associated with these catalysts is their small pore size which restricts diffusion of reactants and products through their voids. Secondly, in case of smaller dimension reactants, bulky and high molecular weight condensation products are possible which block the pores during the progress of a reaction, hence poisoning the catalyst [89].

1.3.3.4. Ion-exchange resin

Ion exchange resins, having sulfonated crosslinked polystyrene functionality are widely used in industry for many decades. The term "ion exchange resin" refers to an organic polymeric resin that exchanges ions with a liquid that contains ions with the same charge. Ion-exchange resins are typically synthesized from the hydrocarbon monomers (usually styrene and divinylbenzene) by copolymerization and catalytically active functional groups e.g. $–SO_3OH$ are added in a later step by sulfonation of the copolymer with concentrated sulfuric acid. Sulfonic acid groups in presence of excess water are fully dissociated and the catalyst can be regarded as an aqueous solution of a strong acid in presence of an inert solid polymer. On the other hand, when only small amount of water is present, the $–SO_3OH$ groups remain undissociated and act themselves as catalytic sites. Infrared spectroscopy has been used to characterize the interaction of$–SO_3OH$ groups with each other. In a dry resin, with enough flexibility of the polymer network and a sufficiently high concentration of $–SO_3OH$ groups, these groups are bonded strongly with each other through hydrogen bonding (Figure 1.10).

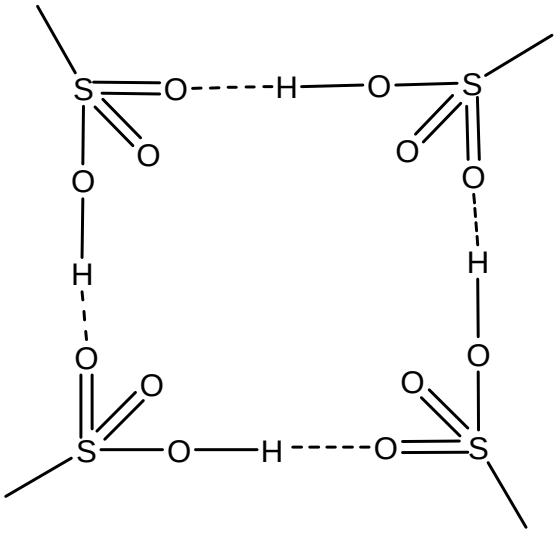

Figure 1.10. Hydrogen bonded network of sulfonic acid groups in ion-exchange resin [90]

When water is added to the dry resin, it is entrapped into the network by breaking the bonds between the acid groups and forming hydrogen bonds within the network as shown in Figure 1.11 [90].

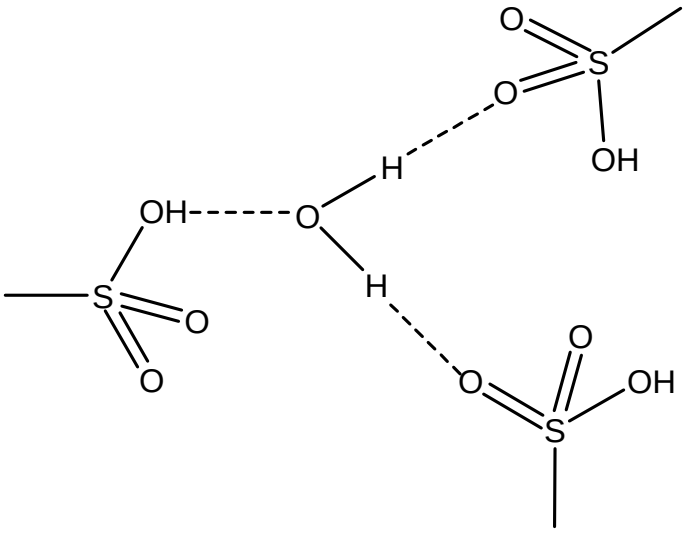

Figure 1.11. Hydrogen bonded network of sulfonic acid groups in ion-exchange resin in presence of water [90]

Although ion-exchange resins are widely used for various organic transformations such as hydroxyalkylation of phenols, their application and reusability is confined to the reactions carried out at < 393 K [90].

1.4. LITERATURE SURVEY ON HYDROXYALKYLATION OF PHENOLS

Several solid acid catalysts as well as reagents have been reported in the literature (Table 1.4) for the hydroxyalkylation of phenols [91-120]. Various mineral acids like HCl, H_2SO_4, H_3PO_4 were used for the hydroxyalkylation of phenol to give bisphenol [91-94], however these reagents based processes have several major drawbacks like difficulties in the separation, corrosion, toxicity and formation of inorganic wastes mentioned in section 1.4.2. In order to overcome these drawbacks, various solid acid catalysts were reported for the hydroxyalkylation of phenols. Among various ion exchange resins screened for the hydroxyalkylation of phenol, sulfonic acid-type cation exchange resin (Diaion SK104) along with 3-pyridinemethanethiol showed higher activity (93% conversion of acetone with 95% selectivity to bisphenol A) [97]. Several other ion exchange resin catalysts were also reported for hydroxyalkylation of phenols. Inaba et al. reported Lewatit SC-102 ion exchange resin which showed 96% conversion of acetone with 85% selectivity to bisphenol A [96] while sulfonated styrene ion exchange resin was reported by Faler and Loucks which showed 66% conversion of acetone with 99% selectivity to bisphenol A [98]. Polysiloxane catalyst having $–SO_3H$ group showed 88% conversion of acetone with 96% selectivity to bisphenol A for the hydroxyalkylation of phenol with acetone [99]. Although these ion exchange resin catalysts showed better activity, they suffer from major disadvantages like thermal instability and reusability.

Various zeolite catalysts were also used for hydroxyalkylation of various phenols. Alvaro et al. reported USY-zeolite which gave 47% yield of diphenylmethane [100] while protonic zeolites like MOR, MFI and BEA were reported by Barthel et al. which showed 46% total product yield with 57% selectivity to diarylmethane [101]. ZSM-5 catalyst showed 40% total product yield with 90% selectivity to bisphenol F [102] for the hydroxyalkylation of phenol to give bisphenol F. β-type zeolite for hydroxyalkylation of phenol gave selectivity to bisphenol F as high as 99% with 95% conversion of

formaldehyde in hydroxyalkylation of phenol [106]. Perego and De Angelis reported Toyosoda HSH-320 HUA zeolite with modified acidity by varying Si/Al ratio which showed 90% conversion of acetone and 60% selectivity to bisphenol A [107]. For bisphenol A formation, the same group of Perego et al. reported amorphous aluminosilcate which gave 72% conversion of acetone with 62% selectivity to bisphenol A [109]. Various other zeolites like Al:MCM-41 and H-β have been reported by Jana et al. for bisphenol F with 91% selectivity and 34 and 68% product yield respectively [104, 108]. Cavani et al. studied another industrially important hydroxyalkylation reaction of guaiacol to vanillyl alcohol (VAlc), by varying Si/Al ratio in H-mordenite catalysts [111,112]. They found that the highest selectivity of 60-70% to VAlc could be achieved for an optimum Si/Al ratio of 23. Corma et al. reported layered zeolite ITQ-2 catalyst comprising balance combination of acidity and strength as the highly active and selective catalyst (100% conversion of paraformaldehyde with 91% selectivity to diarylmethane) for the hydroxyalkylation of bis-1, 1'-(2-methoxy-naphthyl) methane with paraformaldehyde to give diarylmethane [110].

Among heteropolyacid catalysts, Udayakumar et al. reported 30% HPA/MCM-41 catalyst for hydroxyalkylation of phenol which gave 34% yield of dihydroxy-diarylmethane [114]. Yadav and Kirthivasan have reported DTP-K10 catalysts for hydroxyalkylation of phenol to give bisphenol A with 23% conversion of phenol and 60% selectivity to bisphenol A [115].

Since, heteropolyacids are not much explored for the hydroxyalkylation of phenol due to their low surface area (5-8 m^2/g) and high solubility in polar solvent, the present work is undertaken to improve activity and reusability of heteropolyacids by impregnating them on appropriate supports. Secondly, for selective hydroxyalkylation of phenol, the catalysts with desired acidity and strength are highly essential. In this thesis, several solid acid catalysts with tuned acidity and strength were prepared by dispersing DTP on various supports and tested for hydroxyalkylation of phenol and its derivatives under mild conditions [116-120]. The catalytic performance of various commercial montmorilonite catalysts with varying acidity and strength were also evaluated for the hydroxyalkylation of phenol.

Table 1.4. Summary of the literature for the hydroxyalkylation of phenols [91-120]

Sr. No.	Catalyst/ Reagent	Reactant (s)	Product	Reaction conditions	Yield/ Conversion (%)	Product selectivity (%)	Refs.
1	HCl	Phenol, Acetone, 15% MeSNa solution	Bisphenol A	323 K	11 (DY)	-	91
2	Conc. HCl	Phenol, Acetone	Bisphenol A	318 K; 2 h	9 (TPY)	98	92
3	H_2SO_4, HCl	Phenol, Acetone	Bisphenol A	333 K; 10 min	87 (AC)	92	93
4	Phosphoric acid	Phenol, Formald-ehyde	Bisphenol F	323-353 K; P to F mole ratio, 6-50	91 (DY)	91	94
5	Tetramethyl ammonium hydroxide	Phenol, Paraform-aldehyde	PHBAlc	323 K; P to F mole ratio, 2; 115 h	30 (PFC)	82	95
7	Acidic ion exchange resin (Lewatit SC-102)	Phenol, Acetone	Bisphenol A	358 K; 8 h	96 (AC)	85	96

8	Sulfonic acid-type cation exchange resin (Diaion SK104) along with 3-Pyridinemeth-anethiol	Phenol, Acetone	Bisphenol A	358 K; 1h	93 (AC)	95	97
9	Sulfonated styrene ion exchange resin	Phenol, Acetone	Bisphenol A	348 K; 1 h	66 (AC)	99	98
10	Polysiloxane catalyst having $–SO_3H$ group	Phenol, Acetone	Bisphenol A	348 K; 24 h	88 (AC)	96	99
11	USY zeolite (Si/Al= 17.5)	Benzene/ Anisole/ N,N-Dimethyl aniline, Benzalde-hyde	Diphenyl methane	383-423 K; 8 h	47 (DY)	-	100
12	Protonic Zeolites (Y-FAU, MOR, MFI & BEA)	Anisole, Chloral	Diaryl methane	323 K; 8 h	46 (TPY)	57	101
13	ZSM-5	Phenol (85), 40% Formald-ehyde (40)	Bisphenol F	393 K; 4 h	40 (TPY)	90	102

14	ZSM-12, ERB-1, Zeolite Y, H-β-Zeolite	Phenol (100), Acetone (20)	Bisphenol A	453 K; P to A mole ratio, 5; 12 h,	76-99 (AC)	20-76	103
15	H-β-zeolite (Si/Al=75)	Phenol, Formald-ehyde	Bisphenol F	363 K; P to F mole ratio, 30; 15 min	68 (TPY)	91	104
16	H-mordenite (Si/Al=10)	Anisole (28), Paraform-aldehyde (7)	Diaryl methane	6 h	57 (PFC) [at 333 K in Supercri tical CO_2] 20 [at 383 K in toluene]	98 97	105
17	β-type zeolite	Phenol, Formald-ehyde	Bisphenol F	393 K; 4 h	95 (FC)	99	106
18	Zeolite (Toyosoda HSH-320 HUA)	Phenol (100), Acetone (20)	Bisphenol A	453 K; P to A mole ratio, 5; 12 h	90 (AC)	60	107
19	Al:MCM-41 (Si/Al=70)	Phenol, Formald-ehyde	Bisphenol F	363 K; P to F mole ratio, 30; 15 min	34 (TPY)	91	108

20	Amorphous aluminosili-cate	Phenol, Acetone	Bisphenol A	423 K; P to A mole ratio, 5; 6 h	72 (AC)	62	109
21	ITQ-2	Bis-1,1'-(2-methoxy-naphthyl) methane (5), Paraform-aldehyde (1)	Diaryl methane	323 K; 24 h	100 (PFC)	91	110
22	H-mordenite (Si/Al=23)	Guaiacol, Formald-ehyde	VAlc	353 K; 2 h	41 (GC)	70	111
24	H-mordenite (Si/Al=23)	Guaiacol, Formald-ehyde	VAlc	338 K; 2 h	41 (GC)	70	112
25	Ion exchange montmorillo-nite	Phenol, Acetone	Bisphenol A	373 K; 2 h	32 (DY)	-	113
26	HPA/Si-MCM-41	Phenol, Benzald-ehyde	DAM	393 K; PH/ ALD mole ratio, 3; 3 h	34 (DY)	-	114
27	DTP-K10	Phenol, Acetone	Bisphenol A	408 K; P to A mole ratio, 5; 4 h	23 (AC)	60	115

28	Mont KSF/O	*p*-cresol, Formald-ehyde	2,2'-methylenebis-(4-methylphenol)	343 K; PC to F mole ratio,5; flow rate, 3 mL/h	26 (PCC)	91	116
29	20% DTP/SiO_2	Phenol, Formald-ehyde	Bisphenol F	353 K; P to F mole ratio, 5; 1 h	34 (TPY)	90	117
30	20% DTP/Mont K10	Phenol, Formald-ehyde	Bisphenol F	353 K; P to F mole ratio, 5; 1 h	28 (PC)	90	118
31	20% DTP/Bento-nite	*p*-Cresol, Formald-ehyde	2,2'-Methylenebis-(4-methylp-henol)	353 K; PC to F mole ratio,5; 1 h	95 (TPY)	94	119
32	Sn/Si-MCM-41	*p*-Cresol, Formald-ehyde	2,2'-Methylenebis-(4-methylp-henol)	363 K; PC to F mole ratio,5; 2 h	70 (TPY)	88	120

Note: AC = Acetone Conversion; FC = Formaldehyde conversion; DY = Diarylmethane Yield; TPY = Total Product Yield; GC = Guaiacol Yield; PFC = Paraformaldehyde Conversion; PCC = *p*-Cresol Conversion; PC = Phenol Conversion.

1.5. LITERATURE SUMMARY ON OXIDATION OF PHENOL DERIVATIVES

Oxidation is a process which involves loss of electron or addition of oxygen or removal of hydrogen. Oxidation of side chain of phenol derivatives (hydroxyalkylated intermediate) e.g. 4-hydroxy-3-methoxy benzyl alcohol, 4-hydroxy benzyl alcohol into corresponding aldehyde is an industrially important reaction used in food, perfumes and cosmetics industries. Conventionally, oxidation reactions are carried out using strong oxidants like pyridinium chlorochromate, pyridinium dichromate, aqueous sulfuric acid-acetone-chromic acid, potassium permangnate, potassium dichromate, lead tetra acetate, sodium chlorite and osmium tetraoxide [121, 122] which pose serious effluent problems. Due to the detrimental effects of these conventional toxic and corrosive reagents on the environment and stringent environmental laws and regulations set up all over the world, the use of eco-friendly catalysts for oxidation has increased exponentially in the fine and bulk chemical industries during the last couple of decades [123-126]. Since atmospheric air is the most abundant and cheapest primary oxygen donor without having any waste disposal problem, several catalytic oxidation reactions of substituted hydroxybenzyl alcohol (hydroxyalkylated intermediate) are reported using air/oxygen as an oxidant during last couple of decades which are summarized in Table 1.5.

Table 1.5. Literature summary on oxidation of phenol derivatives [127-138]

Sr. No.	Catalyst	Reactant	Product	Reaction conditions	Yield/ Conv (%)	Product select-ivity (%)	Refs.
1	Au/Fe_2O_3	OHBAlc	OHB	323 K; O_2 pressure, 1 atm.; 2 h	90	92	127

2	Co-salen	Veratryl alcohol	Veratryl aldehyde	353 K; *pH* =12.5	TOF = 28 h^{-1}	-	128
3	2% Au-PVP	PHBAlc	PHB	300 K; air, 1 atm.; 8 h	91 (Y)	-	129
4	4.1%Pd/H-Beta	Piperonyl alcohol	Piperonyl-aldehyde	353 K; air, 1 atm.; 1 h	28	100	130
5	2%Pt/C	PHBAlc	PHB	373 K; O_2 pressure, 20 bar; 16 h	> 99	>99	131
6	Ru/TiO_2	*p*-VAlc	*p*-Vanillin	353 K; O_2 pressure, 80 bar; 2h	46 (Y)	55	132
7	Au/CeO_2	*p*-VAlc	*p*-Vanillin	323 K; O_2 pressure, 1 atm.; 2 h	96	98	133
8	Polyanili-ne supported vanadium catalyst	PHBAlc	PHB	373 K; O_2 pressure, 1 atm.; 9 h	96 (Y)	-	134
9	9% Pt/SKT-4 (Carbon)	*p*-VAlc	*p*-Vanillin	353 K; air, atm.; 1 h	94	95	135

10	Cu-Mn oxide/C	PHBAlc	PHB	353 K; O_2 pressure, 0.4 MPa; 3.5 h	83	99	136
11	Mo-V-O	PHBAlc	PHB	353 K; O_2 pressure, 1 atm.; 24 h	83	99	137
12	Cu-Al hydrotalc-ite/*rac*-BINOL	PHBAlc	PHB	278 K; air, 1 atm.; 12 h	75 (Y)		138

Note: Y = (%) Yield

Milone et al. reported gold supported on different oxides like Fe_2O_3, ZnO, CaO and Al_2O_3 for liquid phase oxidation of *o*-hydroxybenzyl alcohol (OHBAlc) [127]. Very high catalyst activity (90% conversion with > 90% selectivity to salicylic aldehyde) was obtained with these catalysts under milder reaction conditions. The presence of gold strongly enhanced the catalytic activity of iron oxide, which was practically inactive under the same reaction conditions. It was shown that the liquid phase oxidation of OHBAlc followed a first order reaction rate law with respect to the organic substrate and zero order with respect to the oxygen partial pressure. Various cobalt salen as well as substituted cobalt salen complexes were studied as catalysts by Kervinen et al. for dioxygen activation in the oxidation of veratryl alcohol in basic aqueous conditions [128]. Among various complexes, unsubstituted Co-salen complex showed best performance giving TOF up to 28 at 353 K and *pH* 12.5. Tsunoyama et al. reported size-specific catalytic activity of polymer-stabilized gold nanoclusters for PHBAlc oxidation in water [129]. Smaller size (1.3 nm) gold nanoclusters exhibit higher catalytic activity (rate [k] = 27 x 10^{-2} h^{-1}) than larger (9.5 nm) homologues (rate [k] = 95 x 10^{-6} h^{-1}) and palladium nanoclusters of comparable size (1.5 and 2.2 nm) which showed a reaction rate

of 1.8 x 10^{-2} and 6.2 x 10^{-2} h^{-1} respectively. The catalyst activity of various Pd/H-Beta catalysts with different Si/Al ratio prepared by an impregnation method was evaluated in selective oxidation of piperonyl alcohol to piperonylaldehyde at 353 K [130]. Among various catalysts screened, 4.1% Pd-H-Beta showed highest activity giving 100% selectivity to piperonylaldehyde with 28% conversion of piperonyl alcohol at 353 K after 1 h. Air oxidation of PHBAlc using Pt/C catalysts gave > 99% selectivity to PHB with > 99% conversion of PHBAlc under mild air pressure (20 bar) at 373 K [131]. The solvent was found to play the most important role in deciding the product selectivity. Kockritz et al. reported Ru/TiO_2 catalyst for oxidation of VAlc which gave 55% selectivity to vanillin with 46% yield at 353 K [132]. The dispersion of catalytically active centers influenced the catalyst activity significantly. A collaborative effect of gold and CeO_2 support for oxidation of various alcohols such as VAlc was studied by Abad et al. [133]. Au/CeO_2 showed very high (96%) conversion of VAlc with 98% selectivity to vanillin at 323 K under mild (1 atm.) oxygen pressure after 2 h. M. Reddy et al. reported polyaniline supported vanadium catalyst for air oxidation of PHBAlc under molecular oxygen which showed 96% yield of PHB at 373 K [134]. Several Pt and Pd catalysts deposited on various carbon supports were reported by Tarasov, among which 9% Pt/SKT-4 catalysts showed best activity giving 94% conversion of *p*-VAlc with 95% selectivity to *p*-vanillin [135]. Yang et al. reported Cu-Mn oxide/C as a highly stable and recyclable catalyst for oxidation of PHBAlc [136]. The activity of catalyst for oxidation PHBAlc was significantly increased in presence of 2, 2, 6, 6-tetramethylpiperidyl-1-oxyl (TEMPO). 10 wt% Cu-Mn oxide/C along with 5 mol % TEMPO showed excellent catalyst activity (99% selectivity to PHB with 83% conversion of PHBAlc) for oxidation of PHBAlc. Crystalline Mo-V-O catalyst was studied by Wang and Ueda for selective oxidation of alcohols with molecular oxygen [137]. Very high (99%) selectivity to PHB with 83% conversion of PHBAlc was achieved at 353 K. Kantam et al. reported Cu-Al-Hydrotalcite/rac-BINOL catalyst for oxidation of PHBAlc which gave 75% yield of PHB [138].

Owing to inherent property of cobalt to form a redox couple necessary for oxidation reaction, several heterogeneous cobalt catalysts were reported for oxidation reaction. As a

part of our research activities on designing and developing solid catalysts, various heterogeneous cobalt catalysts were reported recently for oxidation of side chain of phenol derivatives [139-144]. In the present thesis work, Co-saponite and γ-Fe_2O_3 catalysts are reported for liquid phase oxidation of *p*-VAlc and PHBAlc respectively under mild conditions [145, 146].

1.6. SCOPE AND OBJECTIVES OF PRESENT INVESTIGATION

Hydroxyalkylation of phenols gives two types of products viz. dihydroxydiarylmethane compounds and substituted hydroxybenzyl alcohols depending on reaction conditions and mole ratio of phenolic compound to the carbonyl compound. Further oxidation of substituted hydroxybenzyl alcohol derivatives (hydroxyalkylated intermediate) gives corresponding aldehydes and acids of commercial importance. Mainly zeolites, resins and homogeneous cobalt catalysts were mainly used for hydroxyalkylation and oxidation reactions respectively. However major problems associated with these catalysts are (i) deactivation of the catalysts due to pore blockage (ii) thermal instability (iii) use of very high phenol to formaldehyde ratio and (iv) formation of inactive, OH-bridged Co complexes under aqueous basic conditions causing catalyst deactivation. Hence, there is still scope to develop active, selective, and reusable solid catalysts for the hydroxyalkylation and oxidation reactions by modifying the surface (acidity, strength etc.) as well as redox properties respectively. The major objective of this thesis is to design and develop highly active and selective solid catalysts for hydroxyalkylation of phenols and oxidation of side chain of phenol derivatives (hydroxyalkylated intermediate). Specific objectives of present study are given below:

- Preparation of surface modified solid acid materials such as clays, silica etc. with enhanced acidity and strength by impregnating dodecatungstophosphoric acid on them.
- Detail characterization of prepared catalysts using various techniques such as BET, NH_3-TPD, FTIR, pyridine IR, XRD, EDX, SEM, and by ^{31}P-CP MASNMR.

- Activity testing of above catalysts for hydroxyalkylation of phenol, *p*-cresol and guaiacol.
- Preparation of γ-Fe_2O_3 and Co-saponite catalysts by various methods and their detailed characterization.
- Activity testing of prepared catalysts for liquid phase air oxidation of hydroxyalkylated intermediates.
- Optimization of reaction conditions for the best catalysts.
- Interpretation of activity results based on the characterization data.

1.7. REFERENCES

1. J. J. Berzelius, *Ann. Chim. Phys.* 61 (1836) 146.
2. K. J. Laidler, J. H. Meiser, *Physical Chemistry*, Benjamin/Cummings, 1982.
3. S. A. Topham in: J. R. Anderson, M. Boudart (eds.): *Catalysis: Science and Technology*, Vol.7, Springer, Berlin, 1987, p. 1.
4. B. Herzog, D. Herein, R. Schlogl, *Appl. Catal. A: Gen.* 141 (1996) 71.
5. G. Ertl, H. Knozinger, J. Weitkamp (eds.), *Handbook of Heterogeneous Catalysis*, Wiley-VCH, Weinheim, 1997.
6. Z. Yu, H. Zhang, *Bioresour. Technol.* 90 (2003) 95.
7. E. W. Pitzer, B. Okla, *US Pat. 2866791* (1958).
8. K. Blechschmitt, P. Reuter, F. Wirth, P. Hornberger, *US Pat. 4077984* (1978).
9. F. Bloyaert , W. Brussels, E. Leblon, M. Jean, *US Pat. 3214417* (1965).
10. T. G. Dorawala, R. R. Renhard, *US Pat. 4046869* (1977).
11. H. S. Young, E. L. McDaniel, *US Pat. 3386923* (1968).
12. F. G. Dwyer, *US Pat. 4107224* (1978).
13. T. A. Bither, *US Pat. 4699485* (1985).
14. P. Ratnasamy, S. Sivasanker, *US Pat. 5493061* (1996).
15. C. Brasse, T. Haas, R. Weber, J. Neuroth, *US Pat. 0212298* (2003).
16. E. E. Bunel, T. A. Koch, R. Ozer, S. K. Sengupta, *US Pat. 6372939* (2002).
17. P. T. Anastas, T. C. Williamson, *Green Chemistry*, Oxford University Press, New York, 1998.
18. P. T. Anastas, J. C. Warner, *Green Chemistry: Theory and Practice*, Oxford University Press, New York, 1998.
19. C. Moreau, S. Razigade. Trousseller, A. Finiels, F. Fazula, L.Gilbert, *US Pat. 5811587* (1998).
20. Jerry March, *Advanced Organic Chemistry*, 4th eds. John Wiley and Sons (1992).
21. D. G. Diddams, J. K. Krum in: *Kirk–Othmer Encyclopedia of Chemical Technology*, 2nd ed., Vol. 21, Interscience: New York, 1970, p. 183.
22. W. Haynes, *This Chemical Age*, 2nd ed., Knopf: New York, 1942, p. 37.
23. M. B. Hocking, *J. Chem. Edu.* 74 (1997) 1055.

24. H. Iwane, T. Sugawara, N. Suzuki, K. Kaneko, *US Pat. 5220079* (1993).
25. M. Okihama, J. Kunitake, *Japanese Pat. 08198790* (1996).
26. R. A. Sheldon, H. van Bekkum, *Fine Chemicals through Heterogeneous Catalysis*, Wiley-VCH, Weinheim, 2001, p. 13.
27. A. de Angelis, P. Ingallina, C. Perego, *Ind. Eng. Chem. Res.* 43 (2004) 1169.
28. M. Okihama, J. Kunitake, *Japanese Pat. 08268943* (1996).
29. M. Okihama, J. Kunitake, *Japanese Pat. 09067287* (1996).
30. M. Huglin, G. Knight, W. Wright, *Die Makromolekulare Chemie* 152 (1972) 67.
31. E. O. Camara, T. Kaelin, G. Toki, Bisphenol A, *Chemical economics handbooks,* SRI International, Menlo Park, CA (2001).
32. B. Suresh, M. Yoneyama, Cyclohexanol-cyclohexanone, *Chemical economics handbook,* SRI International, Menlo Park, CA (2002).
33. W. Hesse, *Ullmann's encyclopedia of industrial chemistry*, Vol A19, Wiley-VCH, Weinheim, Germany, p. 313.
34. W. C. Muench, T. S. Hormel, P. M. Kirchhoff, L. A. Robbins, *US Pat. 4205188* (1980).
35. H. Iwane, T. Sugawara, N. Suzuki, K. Kaneko, *US Pat. 5220079* (1993).
36. M. Okihama, J. Kunitake, *Japanese Pat. 08198790* (1996).
37. K. Takashi, I. Shigeru, M. Yoshio *Japanese Pat. 01211544* (1989).
38. Maruzen Oil Co., Ltd., Japan, *Japanese Pat. 57035532* (1982).
39. Bisphenol A, *Chem Systems Report 01/02-6*; Process Evaluation/Research Planning Program, Chem Systems: San Francisco, CA, (2002).
40. A. Chakrabarti, M. M. Sharma, *React. Polym.* 20 (1993) 1.
41. A. Corma, *Chem. Rev.* 97 (1997) 2373.
42. J. H. Westbrook, R. L. Fleischer, *Intermetallic Compounds*, John Wiley and Sons: New York (2000).
43. T. Okuhara, N. Mizuno, M. Misono, *Adv. Catal.* 41 (1996) 113.
44. A. Vaccari, *Catal. Today* 41 (1998) 53.
45. A. Corma, *Chem. Rev.* 95 (1995) 559.
46. M. Misono, *Catal. Rev. Sci. Eng.* 29 (1987) 269.

47. M. T. Pope, *Heteropoly and Isopoly Oxometalates*, Springer-Verlag, Berlin, 1983.
48. L. Pettersson, I. Anderson, L.O. Ohman, *Inorg. Chem.* 25 (1986) 4726.
49. H. D'Amour, *Acta Crystallogr. B* 32 (1976) 729.
50. J. S. Anderson, *Nature,* 140 (1937) 850.
51. G. D. Yadav, H. G. Manyar, *Micro. Meso. Mater.* 63 (2003) 85.
52. V. K. Diez, B. J. Marcos, C. R. Apesteguia, J. I. Di Cosimo, *Appl. Catal. A: Gen.* 358 (2009) 95.
53. N. Mizuno, M. Misono, *Chem. Rev*. 98 (1998) 199.
54. M. Misono, *Chem. Commun.* (2001) 1141.
55. I. V. Kozhevnikov, *Chem. Rev.* 98 (1998) 171.
56. M. Misono, N. Mizuno, K. Katamura, A. Kasai, Y. Konishi, K. Sakata, T. Okuhara, Y. Yoneda, *Bull. Chem. Soc. Jpn.* 55 (1982) 400.
57. V. F. Chuvaev, K. I. Popov, V. I. Spitsyn, *Dokl. Akad. Nauk. SSSR* 255 (1980) 892.
58. Y. Izumi, R. Hasebe, K. Urbe, *J. Catal.* 84 (1983) 402.
59. M. A. Schwegler, H. van Bekkum, N. A. de Munck, *Appl. Catal.* 74 (1991) 191.
60. M. Misono, *Catal. Rev. Sci. Eng.* 30 (1988) 339.
61. P. Madhusudhan Rao, A. Wolfson, S. Kababya, S. Vega, M. V. Landau, *J. Catal*. 232 (2005) 210.
62. V. M. Mastikhin, S. M. Kulikov, A. V. Nosov, I. V. Kozhevnikov, I. L. Mudrakovsky, M. N. Timofeeva, *J. Mol. Catal.* 60 (1990) 65.
63. K. Mohana Rao, R. Gobetto, A. Iannibello, A. Zecchina, *J. Catal*. 119 (1989) 512.
64. F. Lefebvre, *J. Chem. Soc., Chem. Commun.* (1992) 756.
65. I. V. Kozhevnikov, K. R. Kloetstra, A. Sinnema, H. W. Zandbergen, H. van Bekkum, *J. Mol. Catal. A: Chem.* 114 (1996) 287.
66. C. T. Kresge, D. O. Marler, G. S. Rav, B. H. Rose, *US Pat. 5366945* (1994).
67. I. V. Kozhevnikov, A. Sinnema, R. J. J. Jansen, K. Pamin, H. van Bekkum, Catal. Lett. 30 (1995) 241.
68. Y. Izumi, K. Urbe, *Chem. Lett.* (1981) 663.

69. I. V. Kozhevnikov, A. Sinnema, R. J. J. Jansen, H. van Bekkum, *Catal. Lett.* 27 (1994) 187.
70. R. A. Schoonheydt, in: H. van Bekkum, E. M. Flanigen, J. C. Jansen (Eds.), *Introduction to Zeolite. Science and Practice*, Elsevier, Amsterdam, 1991, p. 201.
71. G. W. Bridley, G. Brown (Eds.), *Crystal Structure of Clay Minerals and their X-ray Identification*, Monograph 5 of the Mineralogical Society, Longman, London, 1980.
72. W. T. Reichle, *Solid State Ionics* 22 (1986) 135.
73. A. Cornelis, P. Laszlo, Janssen, *Chimica Acta* 8 (1990) 3.
74. P. Laszlo, *Acc. Chem. Res.* 19 (1986) 121.
75. A. Elsen, P. Grobet, M. Keung, H. Leeman, R. Schoonheydt, H. Toufar (Eds.), *Proceedings of Euroclay'95*, Leuven (B), 1995.
76. A. Cornelis, P. Laszlo, *Synthesis* (1985) 909.
77. A. Cornelis, A. Gerstmans, P. Laszlo, A. Mathy, I. Zieba, *Catal. Lett.* 6 (1990) 103.
78. G. D. Yadav, N. Kirthivasan, *J. Chem. Soc., Chem. Commun*. (1995) 203.
79. B. Singh, J. Patial, P. Sharma, S. G. Agarwal, G. N. Qazi, S. Maity, *J. Mol. Catal. A: Chem.* 266 (2007) 215.
80. S. Stackhouse, P. V. Coveney, E. Sandre, *J. Am. Chem. Soc.* 123 (2001) 11764.
81. T. J. Pinnavaia, *Science*, 220 (1983) 365.
82. R. M. Barrer: *Hydrothermal Chemistry of Zeolites*, Academic Press, London, 1982.
83. R. M. Barrer, Trans. Far. Soc. 40 (1944) 559.
84. C. S. Cundy, P. A. Cox, Chem. Rev. 103 (2003) 663.
85. G. J. A. A. Soler-Illia, C. Sanchez, B. Lebeau, J. Patarin, *Chem. Rev.* 102 (2002) 4093.
86. P. B. Venuto, P. S. Landis, *Adv. Catal.* 18 (1968) 259.
87. P. B. Venuto, *Microporous Mater.* 2 (1994) 297.
88. A. Corma, *Chem. Rev.* 95 (1995) 559.
89. A. Sanjuan, G. Aguirre, M. Alvaro, H. Garcia, *Appl. Catal. B* 15 (1998) 247.

90. G. Ertl, H. Knozinger, J. Weitkamp (eds.), *Handbook of Heterogeneous Catalysis*, Wiley-VCH, Weinheim, 2008, p.278.
91. F. Matsunaga, T. Nishimura, E. Miyake, K. Baba, *Japanese Pat. 61012640* (1986).
92. Mitsui Toatsu Chemicals, Inc., Japan, *Japanese Pat. 60038335* (1985).
93. Mitsubishi Chemical Industries Co., Ltd., Japan, *Japnese Pat. 57112588* (1982).
94. M. Okihama, Y. Kunitake, *Japanese Pat. 9067287* (1997).
95. H. Iwane, T. Sugawara, N. Suzuki, K. Kaneko, *US Pat.5220079* (1993).
96. S. Inaba, T. Yamamori, Y. Morimoto, *Japanese Pat. 61078741* (1986).
97. T. Maki, T. Masuyama, T. Yokoyama, Y. Fujiyama, *Eur. Pat. 45959* (1982).
98. G. R. Faler, G. R. Loucks, *US Pat. 4424283* (1984).
99. H. Nakamura, M. Inomata, K. Takahashi, S. Yoshinaga, *Japenese Pat. 2000281607* (2000).
100. M. Alvaro, H. Garcia, A. Sanjuan, M. Espla, *Appl. Catal., A: Gen.* 175 (1998) 105.
101. N. Barthel, A. Finiels, C. Moreau, R. Jacquot, M. Spagnol, *Top. Catal.* 13 (2000) 269.
102. M. G. Clerici, G. Bellussi, *US pat. 4895988* (1990).
103. C. Perego, A. De Angelis, *World Pat. 02/096847* (2002).
104. S. K. Jana, T. Okamoto, T. Kugita, S. Namba, *Appl. Catal. A: Gen.*288 (2005) 80.
105. M. Alvaro, D. Das, M. Cano, H. Garcia, *J. Catal.* 219 (2003) 464.
106. T. Shimizu, K. Tsumura, *Japanese Pat. 11269113* (1999).
107. C. Perego, A. De Angelis, *US pat. 6872859* (2005).
108. S. K. Jana, T. Kugita, S. Namba, *Appl. Catal. A: Gen.* 266 (2004) 245.
109. C. Perego, A. De Angelis, A. Carati, C. Flego, R. Millini, C. Rizzo, G. Bellussi, *Appl. Catal. A: Gen.* 307 (2006) 128.
110. A. Corma, H. Garcia, J. Miralles, *Micropor. Mesopor. Mater.* 43 (2001) 161.
111. M. Bolognini, F. Cavani, L. Dal Pozzo, L. Maselli, F. Zaccarelli, B. Bonelli, M. Armandi, E. Garrone, *Appl. Catal. A: Gen.* 272 (2004) 115.

112. F. Cavani, M. Corrado, R. Mezzogori, *J. Mol. Catal. A: Chem.* 182-183 (2002) 447.
113. Fukada, H. Okubo, T. Terashima, K. Inoue, *Japanese Pat. 10017509* (1998).
114. S. Udayakumar, S. Ajaikumar, A. Pandurangan, *Appl. Catal. A: Gen.* 302 (2006) 86.
115. G. D. Yadav, N. Kirthivasan, *Appl. Catal. A: Gen.* 154 (1997) 29.
116. A. C. Garade, A. M. Hengne, T. N. Deshpande, S. V. Shaligram, M. Shirai, C. V. Rode, *J. Chem. Eng. Jpn.* 42 (2009) 782.
117. A. C. Garade, V. S. Kshirsagar, C. V. Rode, *Appl. Catal. A: Gen.* 354 (2009) 176.
118. A. C. Garade, V. S. Kshirsagar, R. B. Mane, A. A. Ghalwadkar, C. V. Rode, *Appl. Clay Sci.* 48 (2010) 164.
119. A. C. Garade, V. S. Kshirsagar, A. Jha, C. V. Rode, *Catal. Commun*. 11 (2010) 942.
120. A. C. Garade, P. S. Niphadkar, P. N. Joshi, C. V. Rode, *Chem. Lett*. 39 (2010) 126.
121. F. A. Luzzio, *Org. React*. 53 (1998) 1.
122. R. A. Sheldon, H. van Bekkum, *Fine Chemicals through Heterogeneous Catalysis*, Wiley-VCH, Weinheim, 2001, p. 1.
123. I. W. C. E. Arends, R. A. Sheldon, *Appl. Catal. A: Gen.* 212 (2001) 175.
124. D. E. De Vos, M. Dams, B. F. Sels, P. A. Jacobs, *Chem. Rev*. 102 (2002) 3615.
125. D.C. Bailey, S.H Langer, *Chem. Rev*. 81 (1981) 109.
126. B.C. Gates, *Stud. Surf. Sci. Catal*. 29 (1986) 4153.
127. C. Milone, R. Ingoglia, G. Neri, A. Pistone, S. Galvagno, Appl. Catal. A: Gen. 211 (2001) 251.
128. K. Kervinen, P. Lahtinen, T. Repo, M. Svahn, M. Leskelä, Catal. Today 75 (2002) 183.
129. H. Tsunoyama, H. Sakurai, Y. Negishi, T. Tsukuda, *J. Am. Chem. Soc.* 127 (2005) 9374.

130. O. P. Tkachenko, L. M. Kustov, A. L. Tarasov, K. V. Klementiev, N. Kumar, D. Y. Murzin, *Appl. Catal. A: Gen.* 359 (2009) 144.

131. P. Korovchenko, C. Donze, P. Gallezot, M. Besson, *Catal. Today,* 121 (2007) 13.

132. A. Kockritz, M. Sebek, A. Dittmar, J. Radnik, A. Bruckner, U. Bentrup, M. M. Pohl, H. Hugl, W. Magerlein, *J. Mol. Catal. A: Chem.* 246 (2006) 85.

133. A. Abad, P. Concepcion, A. Corma, H. Garcia, *Angew. Chem. Int. Ed.* 44 (2005) 4066.

134. S. R. Reddy, S. Das, T. Punniyamurthy, *Tetrahedron Lett.* 45 (2004) 3561.

135. A. L. Tarasov, L.M. Kustov, A.A. Bogolyubov, A.S. Kiselyov, V.V. Semenov, *Appl. Catal. A: Gen.* 366 (2009) 227.

136. G.Yang, W. Zhu, P. Zhang, H. Xue, W. Wang, J. Tian, M. Song, *Adv. Synth. Catal.* 350 (2008) 542.

137. F. Wang, W. Ueda, *Catal. Today,* 144 (2009) 358.

138. M. Lakshmi Kantam, R. Arundhathi, P. R. Likhar, D. Damodara, Adv. Synth. Catal. 351 (2009) 2633.

139. C. V. Rode, V. S. Kshirsagar, J. M. Nadgeri, K. R. Patil, *Ind. Eng. Chem. Res*. 46 (2007) 8413.

140. V. S. Kshirsagar, J. M. Nadgeri, P. R. Tayade, C. V. Rode, *Appl. Catal. A: Gen*. 339 (2008) 28.

141. V. S. Kshirsagar, S. Vijayanand, H. S. Potdar, P. A. Joy, K. R. Patil, C. V. Rode, *Chem. Lett*. 37 (2008) 310.

142. V. S. Kshirsagar, K. R. Patil, M. Shirai, C. V. Rode, *Top. Catal*. 52 (2009) 784.

143. V. S. Kshirsagar, A. C. Garade, K. R. Patil, R. K. Jha, C. V. Rode, *Ind. Eng. Chem. Res* 48 (2009) 9423.

144. V. S. Kshirsagar, A. C. Garade, K. R. Patil, A. Yamaguchi, M. Shirai, C. V. Rode, *Appl. Catal. A: Gen.* 370 (2009) 16.

145. A. C. Garade, M. Bhardwaj, S. V. Bhagwat, A. A. Athawale, C. V. Rode, *Catal. Commun*. 10 (2009) 485.

146. A. C. Garade, N. S. Biradar, S. M. Joshi, V. S. Kshirsagar, R. K. Jha, C. V. Rode, *Appl*. *Clay Sci.* (2010) doi: 10.1016/j.clay.2010.10.026.

Chapter II

Experimental and physico-chemical characterization

The activity of the prepared catalysts generally depends upon their textural properties such as surface area, acidity, morphology etc. which in turn depends upon their method of preparation [1, 2]. Hence, selection of proper method of preparation of catalysts and their detailed characterization are very crucial in order to understand the structure-activity correlation. Present chapter describes details of procedures followed for the preparation of various catalysts, catalyst characterization and activity testing of the prepared catalysts for hydroxyalkylation and oxidation reactions.

2.1. MATERIALS

Silica (SiO_2), montmorillonite K10, *p*-hydroxybenzyl alcohol, PHBAlc (99%), *p*-vanillyl alcohol, *p*-VAlc (99%), guaiacol (99%) were purchased from Sigma-Aldrich, Bangalore, India. Montmorillonite KSF/O, montmorillonite KP-10, aluminium pillared clay, Amberlyst-15 were purchased from Fluka, Germany. Phenol (98%), *p*-cresol (98%), formalin solution (37% formaldehyde, 10-13% methanol, 50-55% water), toluene (98%), ferric chloride (98%), $(NH_4)_2SO_4.FeSO_4.H_2O$ (98%), and dodecatungstophosphoric acid, DTP (98%) were purchased from Loba chemie, Mumbai, India. Sodium silicate (99%), aluminum nitrate (99%), sodium hydroxide (98%), cobalt acetate (99%) and urea (99%) were purchased from Sd fine, India. Bentonite was procured from Ashapura, India.

2.2. CATALYST PREPARATION

2.2.1. DTP impregnated catalysts

In a typical procedure, DTP impregnated on silica (20% DTP/SiO_2) catalyst was prepared as follows. Four g of SiO_2 was added slowly to the solution of 1 g of DTP in 40 mL methanol with constant stirring over a period of 20 min. The slurry was stirred for 6 h at room temperature and the solvent was evaporated under vacuum. The catalyst formed was dried in an oven at 383 K for 2 h. 10% and 40% DTP/SiO_2 catalysts were also prepared in a similar way. [3]. A schematic of the preparation method is shown in Figure 2.1.

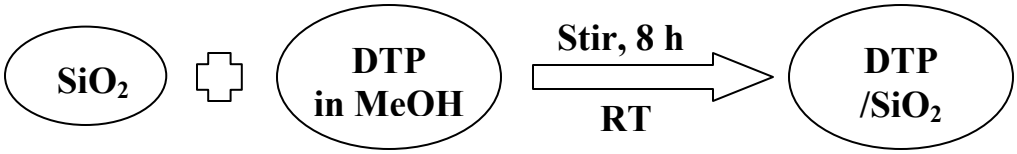

Figure 2.1. Preparation of DTP/SiO_2 catalyst

DTP impregnated on various other clay materials such as montmorillonite K10, bentonite etc. were also prepared in a similar way, as follows.

4 g of mont K10 was added to the solution of 1 g of DTP in 100 mL methanol with constant stirring over a period of 20 min. The dispersion was stirred for 24 h at room temperature and the solvent was evaporated under vacuum. The catalyst was dried at 383 K for 2 h and then calcined at 573 K for 6 h. 5, 10, 40 and 60% DTP/Mont K10 catalysts were also prepared by the similar method [4].

Bentonite (BNT) impregnated with 20% DTP (20% DTP/BNT) catalyst was also prepared by a wet impregnation method. Four g of BNT was added slowly to the solution of 1 g of DTP in 50 mL methanol with constant stirring over a period of 20 minutes. The slurry was stirred for 8 h at room temperature and the solvent was evaporated under vacuum. The catalyst formed was dried in an oven at 393 K for 2 h and then calcined at 573 K for 5 h [5].

2.2.2. Preparation of Co-saponite catalysts

In a typical procedure, a slurry of sodium silicate (17.97 g), aluminium nitrate (3.13 g) and sodium hydroxide (0.391 g) was made in deionized water and was stirred for half an hour at 363 K. After obtaining the homogeneous mixture, cobalt acetate (3.0 g) and urea (15 g) were added. This whole mixture was stirred for 12 h at 363 K. After cooling, Co-saponite cake was filtered, washed with distilled water and then dried in a static air furnace at 383 K. Following this procedure, Co-saponite catalysts were prepared with Co content varying in the range of 5–30% [6, 7]. A flow chart of the preparation method is shown in Figure 2.2.

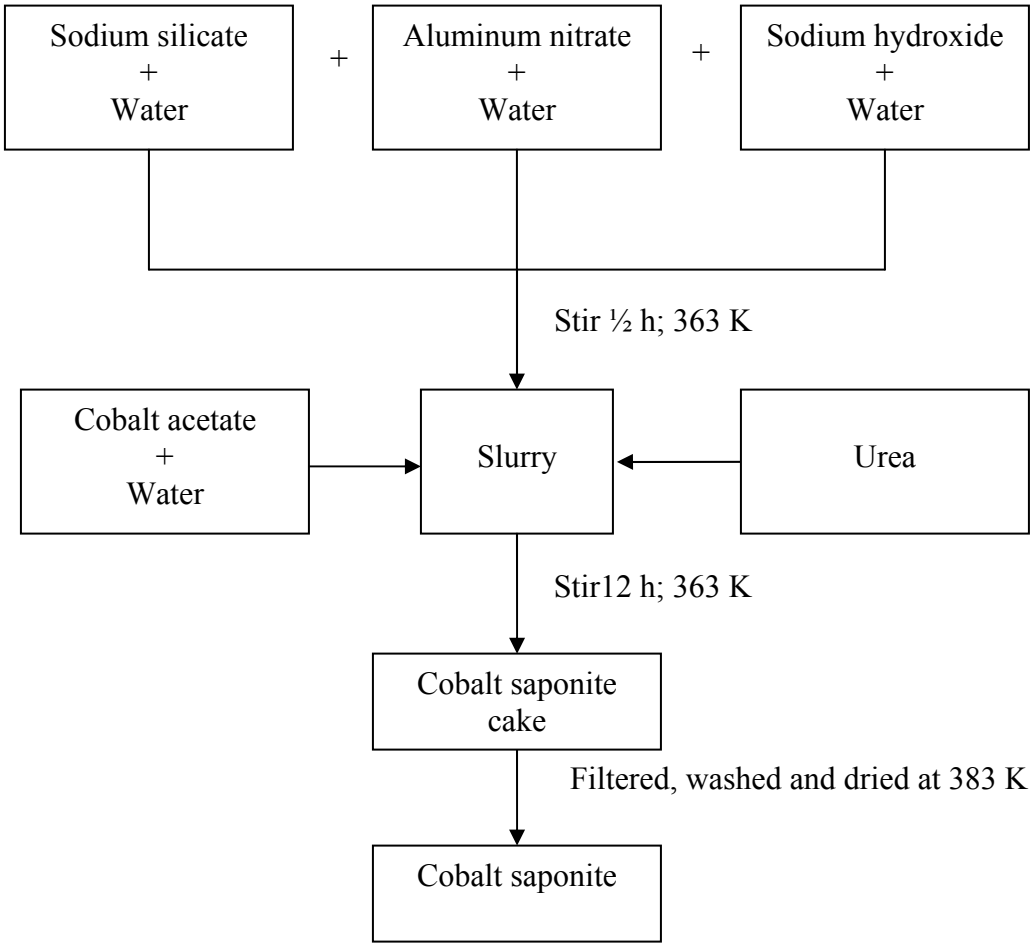

Figure 2.2. Preparation of Co-saponite catalyst

2.2.3. Preparation of γ-Fe_2O_3 catalysts

The iron oxide particles were synthesized by adopting a simple chemical protocol. Aqueous solutions in the mole ratio of 1:2, of $FeCl_3$, $(NH_4)_2SO_4.FeSO_4.H_2O$ were mixed together in a beaker. To the above solution, 0.8 mL of 1 M HCl was added. This mixture was then added drop wise to a flask containing 250 mL of NH_4OH solution with constant stirring under nitrogen atmosphere. The precipitation was carried out at two different temperatures viz. 278 and 368 K. After complete addition of the precursor solution, the

whole mixture was stirred further for a period of 3 h. The product was seen to appear as a black precipitate. The precipitate was washed with double distilled water till the pH of mother liquor decreased to about 8–8.5. The washed and clean products were then dried in an oven at 353 K for 6 h [8]. A flow chart of the preparation scheme is shown in Figure 2.3.

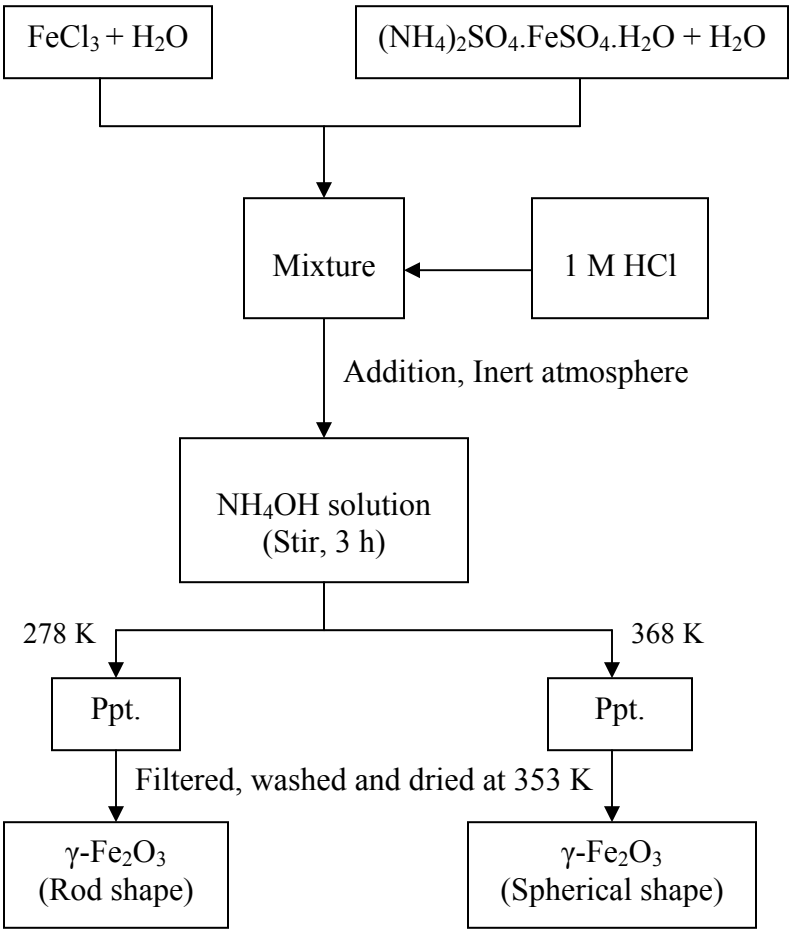

Figure 2.3. Preparation of γ-Fe_2O_3 catalyst

2.3. PHYSICO-CHEMICAL CHARACTERIZATION

2.3.1. X-ray diffraction

The X-ray diffraction furnishes a rapid, accurate method for identifying crystalline phases, particle size etc. of the catalyst [9, 10]. This method involves the interaction between the incident monochromatized X-rays (like Cu K_α or Mo K_α source) with the atoms of a periodic lattice of the solid material. X-rays scattered by atoms in an ordered lattice interfere constructively in directions given by Bragg's law:

$$n\lambda = 2\ d\ \sin\theta \qquad \text{.....(2.1)}$$

where, n = 1, 2, 3 (integer called order of the reflection)

λ is the wavelength of the X-rays, Å

d is the distance between two lattice planes, Å,

θ is the angle (deg.) between the incoming X-rays and the normal to the reflecting lattice plane [11].

The interplanar distances or d-spacings are calculated from the values of the peaks observed from the above Bragg's equation. The width of diffraction peaks carries information on the dimensions of the reflecting planes.

For crystals with size below 100 nm, line broadening occurs due to incomplete destructive interference in scattering directions where the X-rays are out of phase. The crystallite size can be calculated from the Debye- Scherrer equation, as given below:

$$D_{hkl} = 0.9\lambda / \beta\cos\theta \qquad \text{.....(2.2)}$$

where D_{hkl} is volume averaged particle diameter, Å

λ is X-ray wavelength, Å

β is full width at half maximum (FWHM), radian.

and θ is diffraction angle, deg.

For example, the particle size of prepared 40% DTP/SiO_2 catalyst was calculated from XRD data (Chapter 3, Figure 3.1d) as follows:

Data: λ = 1.54178 Å; β (FWHM) = 0.011868237 rad; $\theta = 12.69^{o}$ (β and θ were measured from XRD graph)

Particle size (D) = (0.9 x 1.54178) / (0.011868237 x Cos12.69) = <u>117.82 Å</u>

X-ray powder diffraction patterns of all the catalysts reported in this thesis were recorded on a Rigaku, D-Max III VC model, using nickel-filtered Cu Kα radiation (λ =1.5418 Å).

2.3.2. Surface area measurement

The common method for measuring surface area of the catalyst is based on the theory developed by Brunauer, Emmett and Teller in 1938 considering the concept of multilayer adsorption [12].

The isotherm points are transformed into the linear version of BET equation:

$$P/V\ (P_o-P) = 1/V_mC + [(C-1)/V_mC]\ (P/P_o) \quad \ldots\ldots\ (2.3)$$

where P is the adsorption equilibrium pressure (Pa),

P_o is the saturation vapor pressure of the adsorbate at the experimental temperature (Pa),

V is the volume of gas adsorbed at pressure P (cm^3),

V_m is the volume of adsorbate required for monolayer coverage (cm^3),

and C is constant related to the heat of adsorption and liquefaction [12].

A plot of $P/V\ (P_o-P)$ vs. (P/P_o) yields a straight line usually in the range $0.05 \leq P/P_o \leq 0.35$. The monolayer volume V_m is given by 1/(S+I), where S is the slope, which is equal to $(C-1)/V_mC$ and I is the intercept, which is equal to $1/V_mC$.

The surface area of the catalyst (S_{BET}) is related to V_m by the equation:

$$S_{BET} = (V_m/22414)\ N_a\ \sigma \quad \ldots\ldots\ (2.4)$$

where N_a is the Avogadro number and σ is mean cross sectional area covered by one adsorbate molecule. The σ value generally used for N_2 is 0.162 nm^2.

The specific BET surface area of the catalyst was measured by N_2 physisorption at liquid nitrogen temperature (77 K) using a Quantachrome CHEMBET 3000 instrument. All the samples were dried at 573 K for 2 h before N_2 physisorption.

N_2 adsorption-desorption isotherms of the catalysts were obtained at liquid N_2 temperature (77 K) using Quantachrome Nova-1200 adsorption unit. About 200 mg of sample was degassed at 473 K for about 4 h till the residual pressure was < 10^{-3} Torr. The isotherms were analyzed in a conventional manner and the pore size distribution was calculated using the Barrett-Joyner-Halenda (BJH) method [13].

2.3.3. Temperature programmed desorption of ammonia (NH_3-TPD)

Ammonia-TPD technique is generally used to determine the acidity and acid strength of the solid catalysts and involves monitoring surface or bulk interaction between the solid catalyst and its gaseous environment via continuous analysis of the gas phase composition as the temperature is raised linearly with time [14]. Instrument used for ammonia-TPD study consists of a sample holder charged with the catalyst in a furnace that can be temperature programmed and a thermal conductivity detector (TCD) to measure the NH_3 gas in the gas mixture before and after interaction.

Ammonia temperature programmed desorption (TPD) measurements of all the catalysts were done on a CHEMBET 3000 by: (i) pre-treating the sample at 473 K in a flow of nitrogen, (ii) adsorption of ammonia at room temperature, and (iii) desorption of adsorbed ammonia with a heating rate 10 K min^{-1} starting from the adsorption temperature to 900 K. The (%) distribution of acidic sites was calculated by measuring the area of desorption peaks in a low and high temperature regions using Origin 6.1 software.

2.3.4. Pyridine FT-IR technique

Pyridine FT-IR is the most widely used technique for determining the nature of acidic sites i.e. Brønsted and/or Lewis present on the catalyst surface [15]. The catalyst having Brønsted acidity shows a peak at 1540 cm^{-1}, while peak at 1450 cm^{-1} can be assigned to Lewis acidity [16]. In this thesis, the Brønsted and Lewis acid sites were determined by

ex-situ FTIR spectroscopy with chemisorbed pyridine. For this purpose, catalyst samples were dried at 383 K for 1 h and then saturated with pyridine vapors in a desiccator containing pyridine for 8 h. Physically adsorbed pyridine was removed by heating the samples at 393 K for 2 h in a continuous flow of nitrogen. FTIR spectra of the samples were recorded on a Shimadzu (Model-820 PC) spectrophotometer under DRIFT (diffuse reflectance infrared Fourier transform) mode.

2.3.5. Scanning electron microscopy (SEM) and energy dispersive X-ray (EDX) techniques

Scanning electron microscopy (SEM) is an important tool for determining the catalyst morphology and particle size in the range of 100 nm to 50 μm. A scanning electron microscope can generate an electron beam scanning back and forth over a solid sample. The interaction between the beam and the sample produces different types of signals providing detailed information about the surface structure and morphology of the sample. When an electron from the beam encounters a nucleus in the sample, the resultant Coulombic attraction leads to a deflection in the electron's path, known as Rutherford elastic scattering. A fraction of these electrons will be completely backscattered, re-emerging from the incident surface of the sample. Since the scattering angle depends on the atomic number of the nucleus, the primary electrons arriving at a given detector position can be used to produce images containing topological and compositional information [17]. The high-energy incident electrons can also interact with the loosely bound conduction band electrons in the sample. However, the amount of energy given to these secondary electrons as a result of the interactions is small, and so they have a very limited range in the sample. Hence, only those secondary electrons that are produced within a very short distance from the surface are able to escape from the sample. As a result, high resolution topographical images can be obtained in this detection mode [18].

The chemical composition and morphology of the sample were determined by energy dispersive X-ray (EDX) attached to SEM (JEOL JSM 500).

2.3.6. X-ray photoelectron spectroscopy (XPS)

The X-ray photoelectron spectroscopy [19-21] is based on the photoelectric effect that involves the interaction of sample surface with X-ray and the measurement of the concomitant photo-emitted electrons energy. The photo-emitted electrons have discrete kinetic energies that are characteristic of the emitting atoms and their bonding states. The kinetic energy, E_k, of these photoelectrons is determined from the energy of the incident X-ray radiation ($h\nu$) and the electron binding energy (E_b) is given as

$$E_k = h\nu - E_b \quad \ldots\ldots (2.5)$$

The experimentally measured energies of the photoelectrons are given as

$$E_k = h\nu - E_b - E_w \quad \ldots.. (2.6)$$

where E_w is the work function of the spectrometer.

The XPS technique is highly surface sensitive due to the short-range mean free path of the photoelectrons that are excited from the solid. The binding energy of the peaks is characteristic of each element. The peak area can be used (with appropriate sensitivity factors) to determine the surface compositions of the material. The shape and the binding energy of the peak vary due to different chemical state of the emitting ion and its surroundings. Hence, XPS can provide chemical bonding information as well. XPS can provide surface elemental analysis essentially for all the elements in the entire periodic table except H and He. The electrons arise from a depth of not greater than about 5 nm are analyzed, hence the technique is surface sensitive.

XPS analysis of all the samples in this thesis was performed on a VG Scientific ESCA-3000 spectrometer using a nonmonochromatized Mg K_α radiation (1253.6 eV). To correct for possible deviations caused by electric charge of the samples, the C1s line at 284.6 eV was taken as an internal standard.

2.3.7. ^{31}P magic angle spinning nuclear magnetic resonance spectroscopy

Nuclear Magnetic Resonance (NMR) spectroscopy gives information on the interaction of a nucleus having a nuclear spin quantum number (I) greater than zero with an external

magnetic field. In a solid-state NMR, the line shape is determined by dipolar and quadrupolar interactions. The lines are usually broader because the rigid structure of the solid phase prevents the averaging of the dipolar interaction by motions. Since, the first order quadrupolar and dipolar interactions are proportional to $(3\cos^2\theta - 1)$, where θ is the angle between an internuclear vector and the magnetic field, these interactions can be removed to a first order approximation by spinning the sample around the so-called magic angle β with respect to the external magnetic field for which $3\cos^2\beta - 1 = 0$, i.e. $\beta = 54.74^{o}$. Hence, this NMR technique is known as Magic Angle Spinning (MAS) [22].

Phosphorus contains only one isotope, ^{31}P, with a nuclear spin of $I = 1/2$. This and the high magnetic moment (which results in a high sensitivity) makes it an interesting nucleus for NMR spectroscopy. Solid state NMR gives insight into the structure of solids and enables us to probe the local environment of a nucleus.

^{31}P-CPMAS NMR spectra were measured at room temperature on a Bruker TOPSPIN AVANCE-300 spectrometer equipped with a Bruker MAS-4 BLCP probe using phosphoric acid as a reference compound for the calibration in NMR. The probe head, rotor (4 mm diameter) and sample tubes were made totally moisture free and 0.1 g sample of catalysts were weighed separately and ^{31}P-CPMAS NMR was recorded using 300 MH_Z Bruker TOPSPIN AVANCE-300 spectrometer. Data acquisition and processing was done by using TOPSPIN software provided by Bruker.

2.3.8. Temperature programmed reduction (TPR)

Temperature programmed reduction (TPR) is used to investigate the reduction behavior of bulk and supported reducible species by increasing the temperature linearly [23]. The basic set up for TPR consists of a sample holder and a thermal conductivity detector to measure the hydrogen content in the gas mixture before and after the reaction. In a typical procedure, the sample is heated with a linear temperature ramp, while a reducing gas (H_2/N_2) mixture flowing over it. The reduction rate is continuously measured by monitoring the change in composition (decrease in H_2 concentration) of the gas mixture after passing through the reactor.

In the present work, TPR experiments were performed on a Quantachrome CHEMBET 3000 instrument using 5% H_2 in N_2 in a temperature range starting from 300 to 1073 K.

2.3.9. Thermal analysis (TG and DTA)

Thermal analysis includes a group of methods by which the physical and chemical properties of a sample are determined as a function of temperature (or time), while the sample is subjected to a controlled temperature program [24]. In thermogravimetry, the change in weight of the sample is monitored as a function of temperature (or time), while differential thermal analysis (DTA) measures the difference in temperature between a sample and a thermally inert reference as the temperature is raised. A plot of this differential provides information on exothermic and endothermic reactions taking place in the sample, which includes phase transitions, dehydration, decomposition, redox, or solid state reactions.

Thermogravimetric analysis (TGA/DTA) were performed on Perkin-Elmer TGA-7 analyzer at a 10 ^{o}C/min scan rate in nitrogen atmosphere.

2.3.10. Mössbauer spectroscopy

Mössbauer spectroscopy is a spectroscopic technique based on the recoil-free, resonant absorption and emission of gamma rays in solids. It provides information on oxidation states, phases, lattice symmetry and lattice vibration [25, 26]. Like NMR spectroscopy, Mössbauer spectroscopy probes tiny changes in the energy levels of an atomic nucleus in response to its environment. Typically, three types of nuclear interaction may be observed: an isomer shift, also known as a chemical shift; quadrupole splitting; and magnetic or hyperfine splitting, also known as the Zeeman effect. The isomer shift (IS) is a consequence of the Coulomb interaction between positively charged nucleus and negatively charged s-electrons. The electric quadrupole splitting is caused by the interaction of electric quadrupole moment with an electric field gradient. Magnetic hyperfine splitting or so-called Zeeman effect arises from the interaction between the nuclear magnetic dipole moment and magnetic field at the nucleus. This interaction splits both nuclear levels and removes all degeneracy. From the eight possible transitions only

six are allowed and the spectrum contains six equidistant peaks, called sextet or sextuplet. The separation between peaks in the spectrum is proportional to magnetic field at the nucleus. Due to the high energy and extremely narrow line widths of gamma rays, Mössbauer spectroscopy is one of the most sensitive techniques in terms of energy (and hence frequency) resolution, capable of detecting change in just a few parts per 10^{11}.

Mössbauer measurements were performed in transmission geometry between 300 and 30 K using constant acceleration spectroscopy with a ^{57}Co (Rh) source. Computer fitting of the spectra was performed to obtain the hyperfine interaction parameters and field distributions; the isomer shift (IS) values were referred to metallic iron foil.

2.4. CATALYST ACTIVITY MEASUREMENT

2.4.1. Hydroxyalkylation of phenol and *p*-cresol to give bisphenols in a batch reactor

The hydroxyalkylation of phenol and *p*-cresol with formaldehyde was carried out in a magnetically stirred glass reactor (capacity 50 mL) fitted with a reflux condenser and an arrangement for temperature control. In a typical experiment, calculated quantity of phenol/ *p*-cresol, formaldehyde, toluene and catalyst were added to the reactor, which was then heated to a desired temperature (353 K) for under stirring.

2.4.2. Continuous hydroxyalkylation of *p*-cresol to give 2, 2'-methylenebis (4-methylphenol)[DAM] over montmorillonite KSF/O catalyst

The continuous hydroxyalkylation of *p*-cresol was carried out in a fixed bed reactor having the catalyst bed length of 5.5 cm and internal diameter of 1.5 cm under similar reaction conditions to that of the batch reactor (Figure 2.4). In the continuous hydroxyalkylation process, *p*-cresol (42.6 mmol), was dissolved in toluene (12 mL), and the whole homogeneous reaction mixture of *p*-cresol, formaldehyde (8.52 mmol) and toluene was fed to the reactor at a constant flow rate of 3.1 mL/h. The temperature of the reactor was kept constant at 343 K and the reaction mixture was discharged from the reactor at a constant flow rate of 3 mL/h. The feed rate (3.1 mL/h) was kept slightly higher than the discharge rate (3 mL/h) in order to avoid drying of the catalyst bed. A flowchart of the continuous hydroxyalkylation process is shown in Figure 2.4.

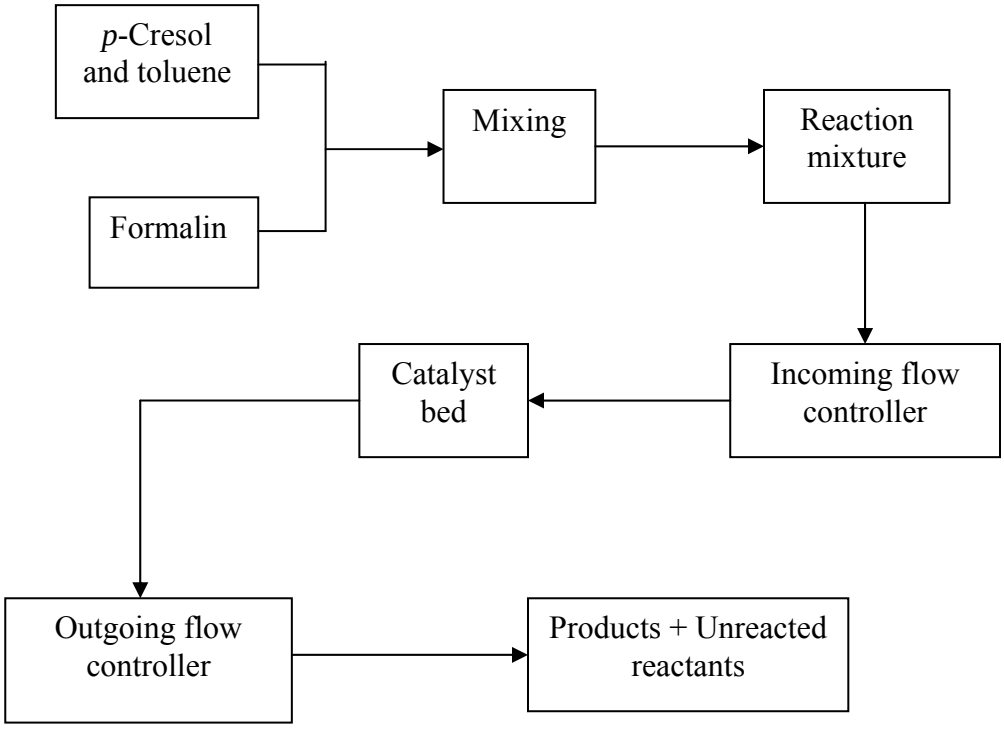

Figure 2.4. Continuous hydroxyalkylation of *p*-cresol in the fixed bed reactor

2.4.3. Hydroxyalkylation of guaiacol to *p*-vanillyl alcohol using DTP impregnated fumed silica catalysts

The hydroxyalkylation of guaiacol with formaldehyde was carried out in a magnetically stirred glass reactor (capacity 50 mL) fitted with a reflux condenser and an arrangement for temperature control. In a typical experiment, guaiacol (8 mmol), formaldehyde (24 mmol) and catalyst (0.11 g/mL) were added to the reactor which was then heated to 353 K for 30 min. The guaiacol conversion and product selectivity were determined by liquid sample analysis using a Hewlett-Packard model high pressure liquid 1050 chromatograph equipped with an ultraviolet detector (λ_{max} = 278) on a 25 cm RP-18 column.

2.4.4. Air oxidation of *p*-hydroxybenzyl and *p*-vanillyl alcohol

The oxidation of *p*-vanillyl alcohol (*p*-VAlc) using Co-saponite catalyst was carried out in a magnetically stirred three necked round bottom flask (capacity 250 mL) fitted with reflux condenser and an arrangement for temperature controller. In a typical oxidation

experiment, the calculated quantities of *p*-VAlc (6.5 mmol), NaOH (26 mmol) and iso-propanol (50 mL) were added to a round bottom flask at 338 K. After homogenizing the reaction mixture, the catalyst (10% mol with respect to *p*-VAlc) was added into the reaction mixture and air was bubbled through the reaction mixture at 60 mL/min under stirring for 3 h.

Similarly, in a typical oxidation experiment of *p*-hydroxybenzyl alcohol (PHBAlc) in water using iron oxide catalyst, the calculated quantities of PHBAlc (8 mmol), NaOH (32 mmol), water (50 mL) and catalyst (0.008 g/mL) were added to a round bottom flask at 370-373 K. Air was bubbled through the reaction mixture at 40 mL/min under stirring for 24 h. The set-up used for oxidation of PHBAlc and *p*-VAlc is shown in Figure 2.5.

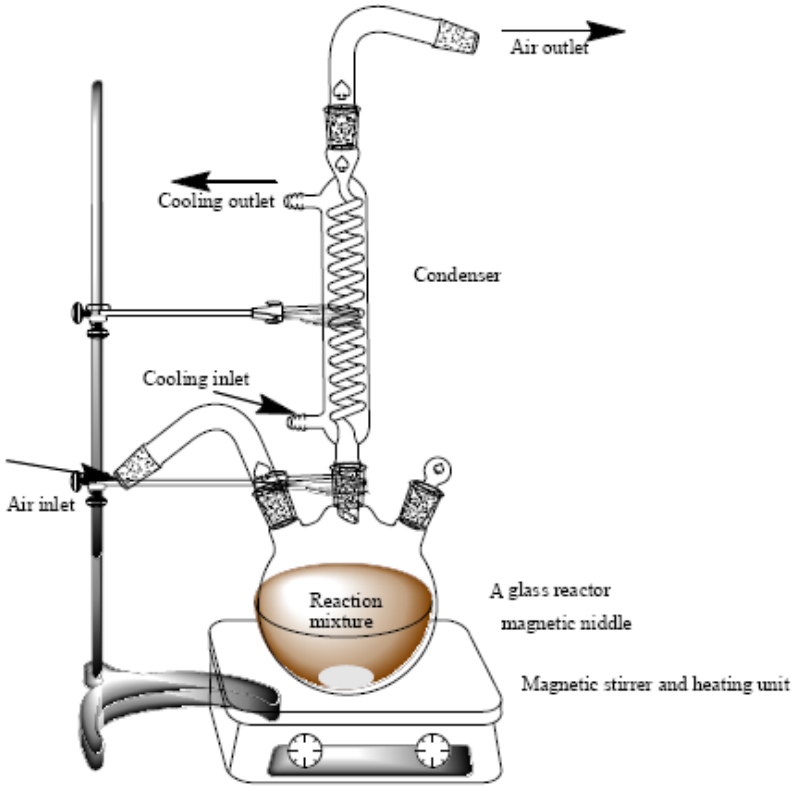

Figure 2.5. Atmospheric experimental set-up for oxidation of *p*-hydroxybenzyl and *p*-vanillyl alcohol

2.5. ANALYTICAL METHOD

The phenol/*p*-cresol conversion and product yield (sum of DAM and trimer based on formaldehyde) and selectivity were determined with an HP6890 series GC System (Hewlett Packard) coupled with FID detector and capillary column (HP-1 capillary column, 30 m length x 0.32 mm i.d.). The injector and detector temperatures were kept at 523 K. The oven temperature was programmed as follows: 353 K (3 min), then 383 K (2 min, with ramp rate of 10 K min^{-1}) and finally 573 K with ramp rate of 10 K min^{-1}.

Helium gas was used as a carrier gas with the flowrate of 20 mL min^{-1}. Authentic samples were used for calibration and quantifying the data.

Analysis of *p*-VAlc and PHBAlc and their oxidation products was done using Hewlett-Packard model 1050 liquid chromatograph equipped with an ultraviolet detector. HPLC analysis was performed on a 25 cm RP-18 column supplied by Hewlett-Packard. The products and reactants were detected using a UV detector at λ_{max}, 254 nm using 35% acetonitrile-water as mobile phase at a column temperature of 308 K and the flow rate of 0.8 mL/min. Samples of 20 μL were injected into the column using an auto sampler.

A typical chromatogram of the reaction crude of oxidation of *p*-VAlc in Figure 2.6 shows the *p*-vanillin as the only oxidation product.

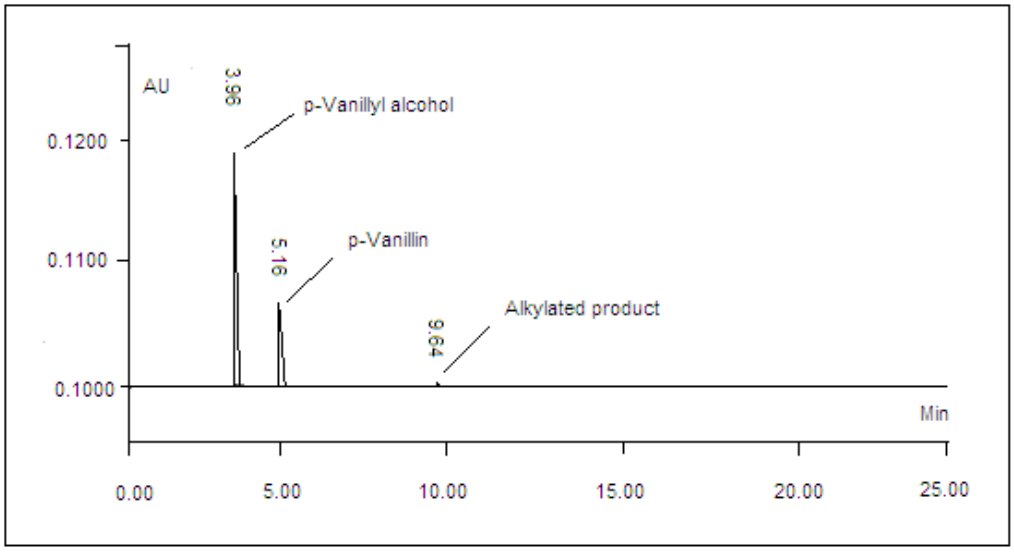

Figure 2.6. Chromatogram of the reaction crude of oxidation of *p*-vanillyl alcohol

2.6. REFERENCES

1. F. Marme, G. Coudurier, J.C. Vedrine, *Microporous Mesoporous Mater.* 22 (1998) 151.
2. S.K. Jana, T. Kugita, S. Namba, *Catal. Lett.* 90 (2003) 143.
3. A. C. Garade, V. S. Kshirsagar, C. V. Rode, *Appl. Catal. A: Gen.* 354 (2009) 176.
4. A. C. Garade, V. S. Kshirsagar, R. B. Mane, A. A. Ghalwadkar, C. V. Rode, *Appl. Clay Sci.* 48 (2010) 164.
5. A. C. Garade, V. S. Kshirsagar, A. Jha, C. V. Rode, *Catal. Commun*. 11 (2010) 942.
6. V. S. Kshirsagar, A. C. Garade, K. R. Patil, M. Shirai, C. V. Rode, *Top. Catal.* 52 (2009) 784.
7. V. S. Kshirsagar, A. C. Garade, K. R. Patil, R. K. Jha, C. V. Rode, *Ind. Eng. Chem. Res*. 48 (2009) 9423.
8. A. C. Garade, M. Bhardwaj, S. S. Bhagwat, A. A. Athawale, C. V. Rode, *Catal. Commun.* 10 (2009) 485.
9. J. W. Niemantsverdriet, *Spectroscopic Methods in Heterogeneous Catalysis*, VCH, Weinheim, 1993, p.82.
10. S. Biz, M. Occelli, *Catal. Rev-Sci. Eng*. 40 (1998) 329.
11. W. H. Bragg, W. L. Bragg, *The Crystalline State*, Vol. 1, McMillan, New York, 1949.
12. S. Brunauer, P. H. Emmett, E. Teller, *J. Am. Chem. Soc.* 60 (1938) 309.
13. E. P. Barrett, L. G. Joyner, P. P. Halenda, *J. Am. Chem. Soc*. 73 (1951) 373.
14. Y. Kamiya, Y. Ooka, C. Obara, R. Ohnishi, T. Fujita, Y. Kurata, K. Tsuji, T. Nakajyo, T. Okuhara, *J. Mol. Catal. A: Chem.* 262 (2007) 77.
15. E. Modrogan, M. H. Valkenberg, W. F. Hoelderich, *J. Catal*. 261 (2009) 177.
16. S. Udayakumar, S. Ajaikumar, A. Pandurangan, *Appl. Catal. A: Gen.* 302 (2006) 86.
17. G. Lawes, *Scanning Electron Microscopy and X-Ray Microanalysis*, John Wiley and Sons Ltd., Chichester, 1987.

18. D. E. Newbury, D. C. Joy, P. Echlin, C. E. Fiori, J. I. Goldstein, *Advanced Scanning Electron Microscopy and X-Ray Microanalysis*, Plenum Press, New York, 1986.
19. A. Carlson, *X-ray Photoelectron Spectroscopy*, Dowden, Hutchinson & Ross: Stroudsburg, PA, 1978.
20. D. Briggs, M. P. seah (Eds.) *Practical Surface Analysis, Vol. 1: Auger and X-ray Photoelectron Spectroscopy*, 2nd ed., Wiley, New York, 1990.
21. S. Huffner, *Photoelectron Spectroscopy*, Springer-Verlag: Berlin, 1995.
22. R. A. Wind in A. I. Popov, K. Hallenga (Eds.), *Modern NMR Techniques and Their Application in Chemistry*, Marcel Dekker, Inc., New York, 1991. p. 156.
23. H. Knözinger in G. Ertl, H. Knözinger, J. Weitkamp (eds.): *Handbook of Heterogeneous Catalysis, Vol. 2*, Wiley-VCH, Weinheim, 1997, p. 676.
24. P. D. Garn: *Thermoanalytical Methods of Investigation*, Academic Press, New York, 1965.
25. A. M. vander Kraan, J. W. Niemantsverdriet in G. J. Lang, J. G. Stevens (eds.): *Industrial Applications of the Mössbauer Effects*, Plenum Press, New York, 1985, p. 609.
26. J. W. Niemantsverdriet, T. Butz in G. Ertl, H. Knözinger, J. Weitkamp (eds.): *Handbook of Heterogeneous Catalysis, Vol. 2*, Wiley-VCH, Weinheim, 1997, p. 512.

Chapter III

Hydroxyalkylation of phenol to bisphenol F

3.1. INTRODUCTION

Hydroxyalkylation of phenol is an industrially important reaction, whose end product e.g. bisphenols F are widely used as a chemical intermediate for the preparation of epoxide resins and polycarbonates in the molding, casting, sealing, coating, encapsulating, adhesive, laminating, reinforced plastics and other chemical industries [1, 2].

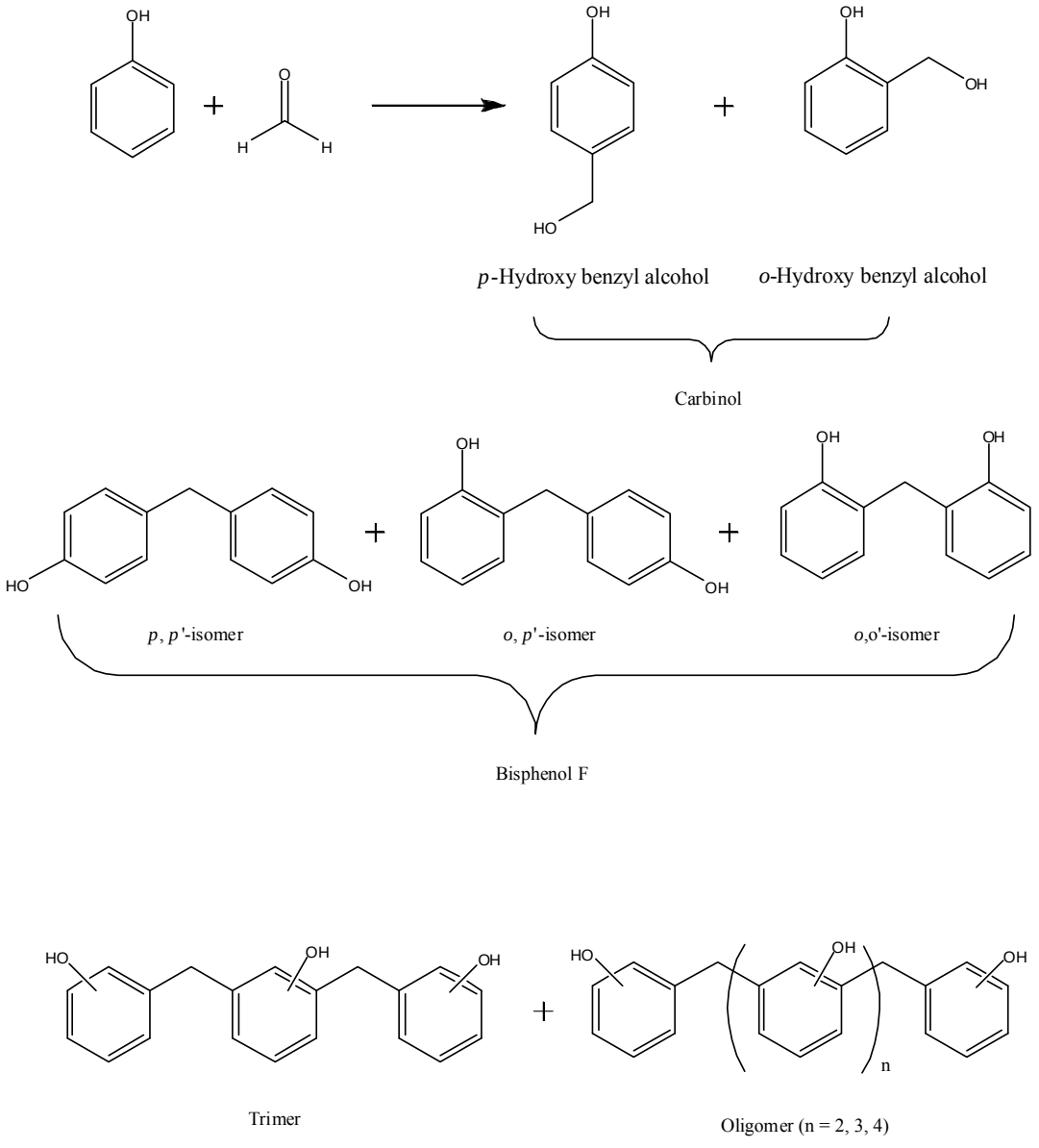

Scheme 3.1. Hydroxyalkylation of phenol with formaldehyde to give Bisphenol F

Bisphenol F is a commercial name for the mixture of bis (2-hydroxyphenyl) methane, bis (4-hydroxyphenyl) methane and 2-hydroxyphenyl-4-hydroxyphenylmethane [$CH_2(C_6H_4OH)_2$] and synthesized by condensing phenol with formaldehyde in presence of acidic catalysts/reagents (Scheme 3.1).

Hydroxyalkylation of phenols is conventionally carried out using toxic and corrosive reagents like phosphoric acid, sulfuric acid etc. which pose several serious environmental and operational problems discussed in chapter 1 (section 1.3.2). Due to increasing demand of bisphenols in various chemical industries and stringent environmental laws and regulations all over the world, several catalytic processes using solid acid catalysts were reported for their synthesis [3-7]. Among various solid acid catalysts, zeolites are mainly used for the hydroxyalkylation of phenols [8-10]. However major problems associated with zeolites are their small pore size which restrict diffusion of reactants and products through their channels/voids and secondly, deactivation of the catalysts due to formation of bulky and high molecular weight condensation products formed during the reaction [11, 12]. Hence developing eco-friendly and reusable solid acid catalysts which give higher activity and bisphenol F selectivity for the hydroxyalkylation of phenol is highly desirable.

Heteropolyacids by virtue of their strong Brønsted acidity [13, 14] is a good alternative to zeolite based hydroxyalkylation processes. Another advantage of heteropolyacids over other solid acid catalysts is the stabilization of intermediate carbocation by heteropoly anion [15, 16]. However for the hydroxyalkylation of phenol to give bisphenol F, the catalysts with proper acidity and strength are required in order to achieve high selectivity to bisphenol F. Acidity of heteropolyacids e.g. dodecatungstophosphoric acid (DTP) could be tuned suitably by dispersing it on proper supports like silica (SiO_2) and montmorillonite K10 (Mont K10) [17-20]. Surface hydroxyl groups of SiO_2 and Mont K10 supports interact with DTP and forms $(SiOH_2)^+$ $(H_2PW_{12}O_{40})^-$ species depending upon DTP loading. This interaction between DTP and SiO_2/Mont K10 supports leads to the localization of DTP protons thereby increasing their proximity to the Keggin anion because of the decrease in proton mobility [21]. Such surface modification of supports due to impregnation of DTP enhanced their acidity and strength and thereby their activity

for hydroxyalkylation of phenol to give bisphenol F. While in case of other supports like MgO and Al_2O_3, they tend to decompose heteropolyacids thereby decrease their activity [14, 22, 23], hence the choice of an appropriate support for DTP dispersion is very crucial in developing new solid acid catalysts.

In this chapter, results on the hydroxyalkylation of phenol to give bisphenol F using various DTP impregnated solid acid catalysts at very low (5:1) phenols to formaldehyde mole ratio are reported [24, 25]. The problems associated with conventional reagents such as toxicity, corrosion and formation of huge amount of inorganic wastes were also minimized by adopting catalyst based routes which is also in accordance with the principles of green chemistry.

3.2. EXPERIMENTAL

DTP impregnated on SiO_2 and Mont K10 catalysts were prepared by wet impregnation method and the detailed experimental procedure of their preparation has been described in chapter 2 (section 2.2.1). The catalysts were characterized by various techniques according to the procedure described in section 2.3. The activity of prepared catalysts was evaluated for the hydroxyalkylation of phenol to give bisphenol F and a typical experimental procedure is described in section 2.4.1.

3.3. RESULTS AND DISCUSSION

3.3.1. DTP impregnated on SiO_2

Hydroxyalkylation of phenol to give bisphenol F was studied using various solid acid catalysts, particularly DTP impregnated on SiO_2 catalysts [24]. The aim of designing DTP/SiO_2 catalysts was to study the effect of DTP loading on acidity and strength of SiO_2 support and their subsequent effect on activity and selectivity in hydroxyalkylation of phenol. A detailed study on characterization of these solid acid catalysts and their activity evaluation for the hydroxyalkylation of phenol is discussed in the following sections.

3.3.1.1. Catalyst characterization

3.3.1.1.1. X-ray diffraction

X-ray diffraction patterns of SiO_2, various percentages of DTP impregnated on SiO_2 (DTP/SiO_2) and bulk DTP are presented in Figure 3.1(a-e).

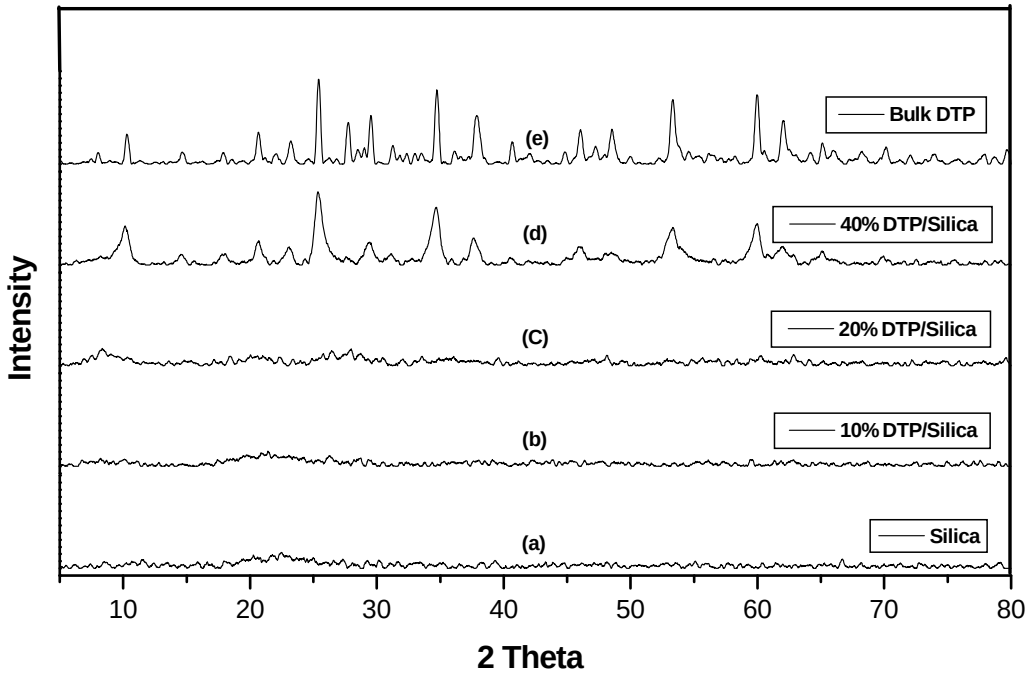

Figure 3.1. XRD patterns of various percentages of DTP supported on SiO_2

DTP/SiO_2 catalysts ≤ 20% DTP loadings showed XRD patterns corresponding to the amorphous materials. No separate crystal phase exists in the 10 and 20% DTP/SiO_2 catalysts (b-c) due to the larger surface area of SiO_2 than parent DTP. This also confirms the high dispersion of DTP on SiO_2 support [19]. The X-ray diffraction pattern of 40% DTP/SiO_2 catalyst shows crystal phases which are characteristic of solid state $H_3PW_{12}O_{40}$. It was clear from the XRD pattern that, for DTP loading < 20% on silica, DTP was dispersed as small crystallites which could not be determined due to amorphous nature of its XRD pattern. As DTP loading increased beyond 20%, these crystallites grew larger (~ 12 nm by Scherrer equation) on SiO_2 [18, 19].

3.3.1.1.2. BET surface area measurement

Table 3.1 presents BET surface areas and NH_3-TPD results of bare SiO_2, various loadings of DTP on SiO_2, DTP and montmorillonite KSF/O samples. Among various solid acid catalysts, the BET surface area of bulk DTP was 8 m^2/g while that of SiO_2 was 256 m^2/g which decreased to 187, 152 and 134 m^2/g for 10, 20 and 40% DTP loadings respectively. This confirmed that DTP (non-porous material) was well dispersed on silica support after impregnation.

3.3.1.1.3. Ammonia-TPD analysis

Figure 3.2 (a-f) shows the NH_3-TPD profiles of bare SiO_2 and montmorillonite KSF/O, DTP and 10, 20, 40% DTP/SiO_2 catalysts. The values of ammonia adsorbed and % distribution of acidic sites based on NH_3 desorption are presented in Table 3.1.

For bulk DTP, the desorption peak of the strongly chemisorbed ammonia appeared at 925 K [19]. Compared to the various DTP/SiO_2 catalysts, an amount of ammonia adsorbed was also maximum (Table 3.1) for bulk DTP catalyst. Thus, the concentration of acidic sites of bulk DTP was the highest with Brønsted characteristics [18, 19]. As compared to the bulk DTP, the parent SiO_2 showed a very low concentration of acidic sites. The concentration of acidic sites of parent SiO_2 enhanced considerably from 1.1 to 6.5 micromoles per unit surface area NH_3 (hereafter $\mu molS^{-1}$ NH_3) by increasing DTP loading from 0 to 40%. Both SiO_2 and 10% DTP/SiO_2 showed only one peak in low temperature region (373-473 K) having acidic site concentrations of 1.1 and 2.1 $\mu molS^{-1}$ NH_3 respectively. Interestingly, the nature of acidic sites was significantly altered beyond 10% DTP loading. 20% DTP/SiO_2 showed two types of acidic sites in low and high temperature regions having acidic site concentrations of 69 and 31% respectively. The concentration of acidic sites in high temperature region doubled (60%) as DTP loading increased from 20 to 40%. Acidic sites of DTP were shifted from 925 to 895 K after impregnation of 20 and 40% DTP on SiO_2.

Table 3.1. Textural properties of the catalysts

Catalysts	$S_{BET}(m^2/g)$	NH_3 adsorbed ($\mu molS^{-1}$)	TPD of NH_3 (%) distribution of acidic sites	
			Region I (LT-Peak)	Region II (HT-Peak)
SiO_2	256	1.1	100	-
10% DTP/SiO_2	187	2.1	100	-
20% DTP/SiO_2	152	3.6	69	31
40% DTP/SiO_2	134	6.5	40	60
DTP	8	163.8	35	65
Montmorillonite KSF/O	128	15.5	25	75

Montmorillonite KSF/O also showed two types of acidic sites having maxima at 425 and 675 K with highest total acidic sites concentration as 15.5 $\mu molS^{-1}$ NH_3. In case of montmorillonite KSF/O, concentration of moderate acidic sites at 675 K was 3 times (75%) higher than that of weak acidic sites (25%) at 425 K.

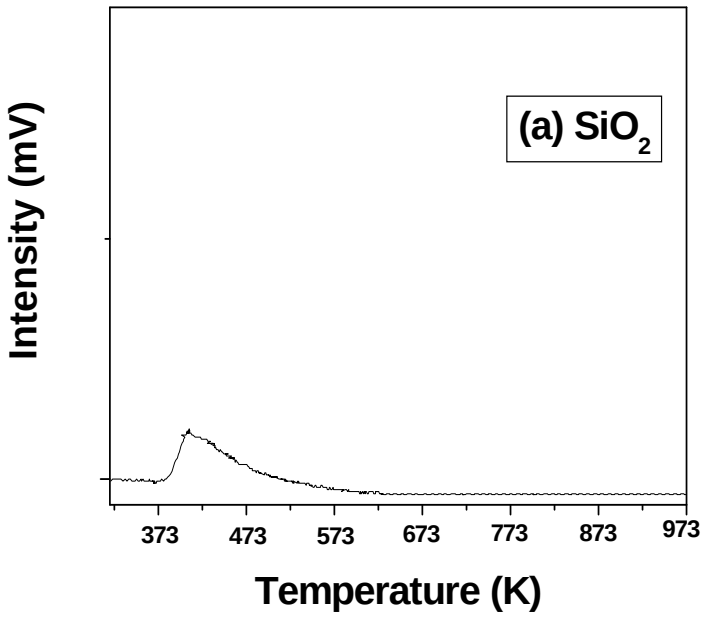

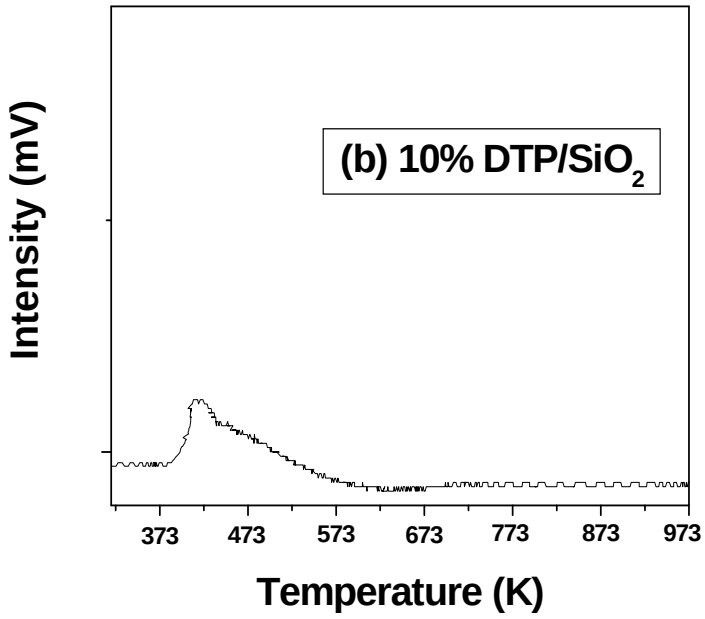
(b) 10% DTP/SiO2
Intensity (mV)
373
473
573
673
773
873
973
Temperature (K)

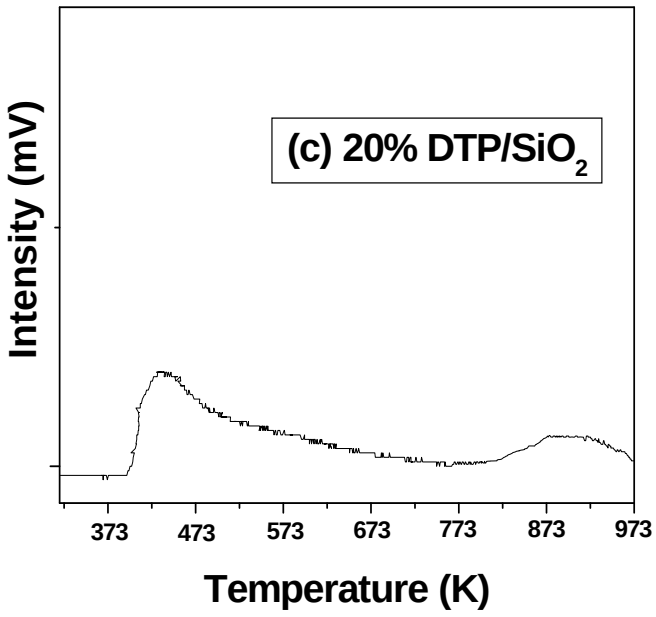
(c) 20% DTP/SiO2
Intensity (mV)
373
473
573
673
773
873
973
Temperature (K)

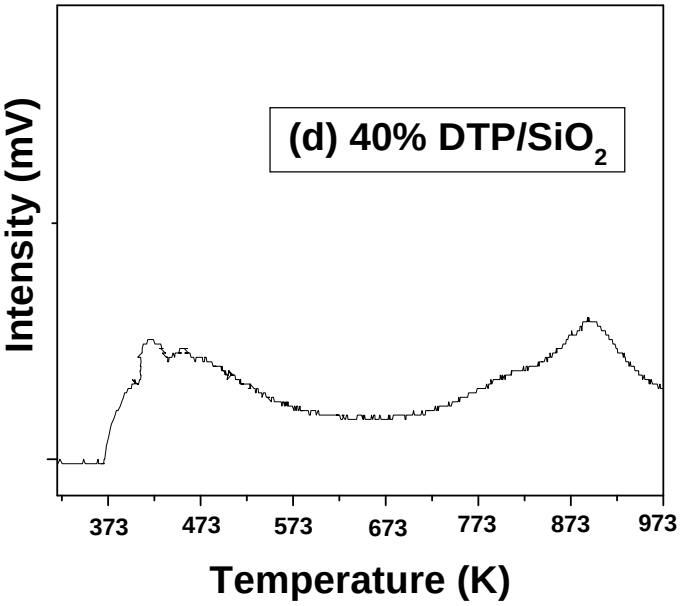
(d) 40% DTP/SiO2
Intensity (mV)
373
473
573
673
773
873
973
Temperature (K)

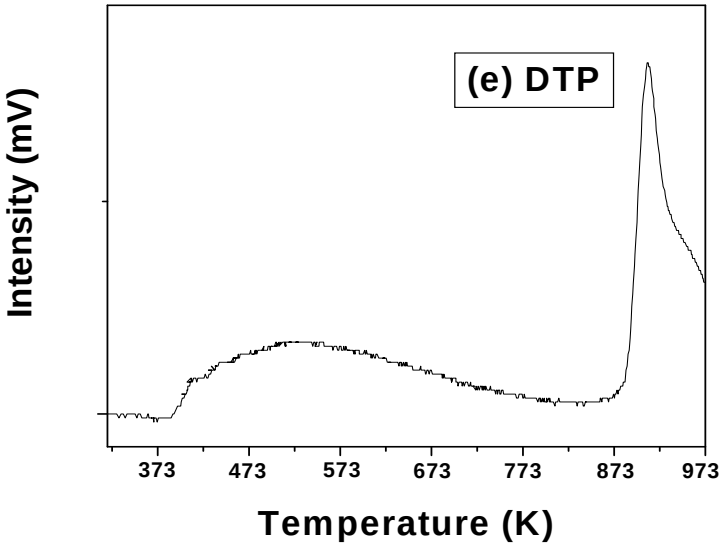
(e) DTP
Intensity (mV)
373
473
573
673
773
873
973
Temperature (K)

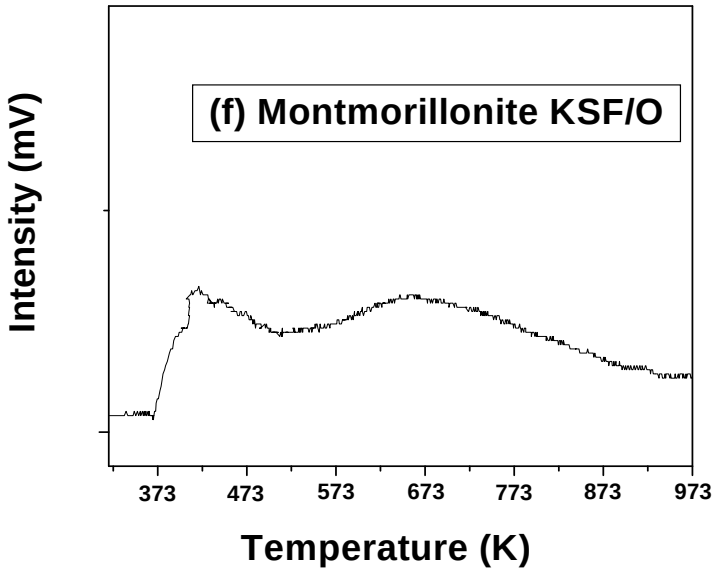

Figure 3.2. NH_3-TPD profile over SiO_2, DTP/SiO_2, DTP and montmorillonite KSF/O

3.3.1.1.4. ^{31}P-CPMAS NMR

^{31}P CPMAS NMR of DTP and 20% DTP on SiO_2 are presented in Figure 3.3. Bulk DTP showed the intense peak at -15.49 ppm that corresponds to the tetrahedral coordination of PO_4 in Keggin unit (Figure 3.3a). As compared to a very sharp peak of DTP at -15.49 ppm, 20% DTP/SiO_2 sample showed a slightly broader peak (Figure 3.3b). This broadening of peak could be due to the interaction of DTP with surface silanol group of SiO_2 [18, 21, 23] as shown in Scheme 3.2.

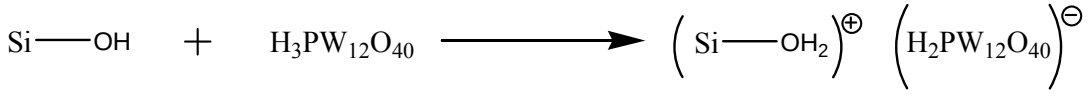

Scheme 3.2. Interaction of dodecatungstophosphoric acid with surface silanol group of silica

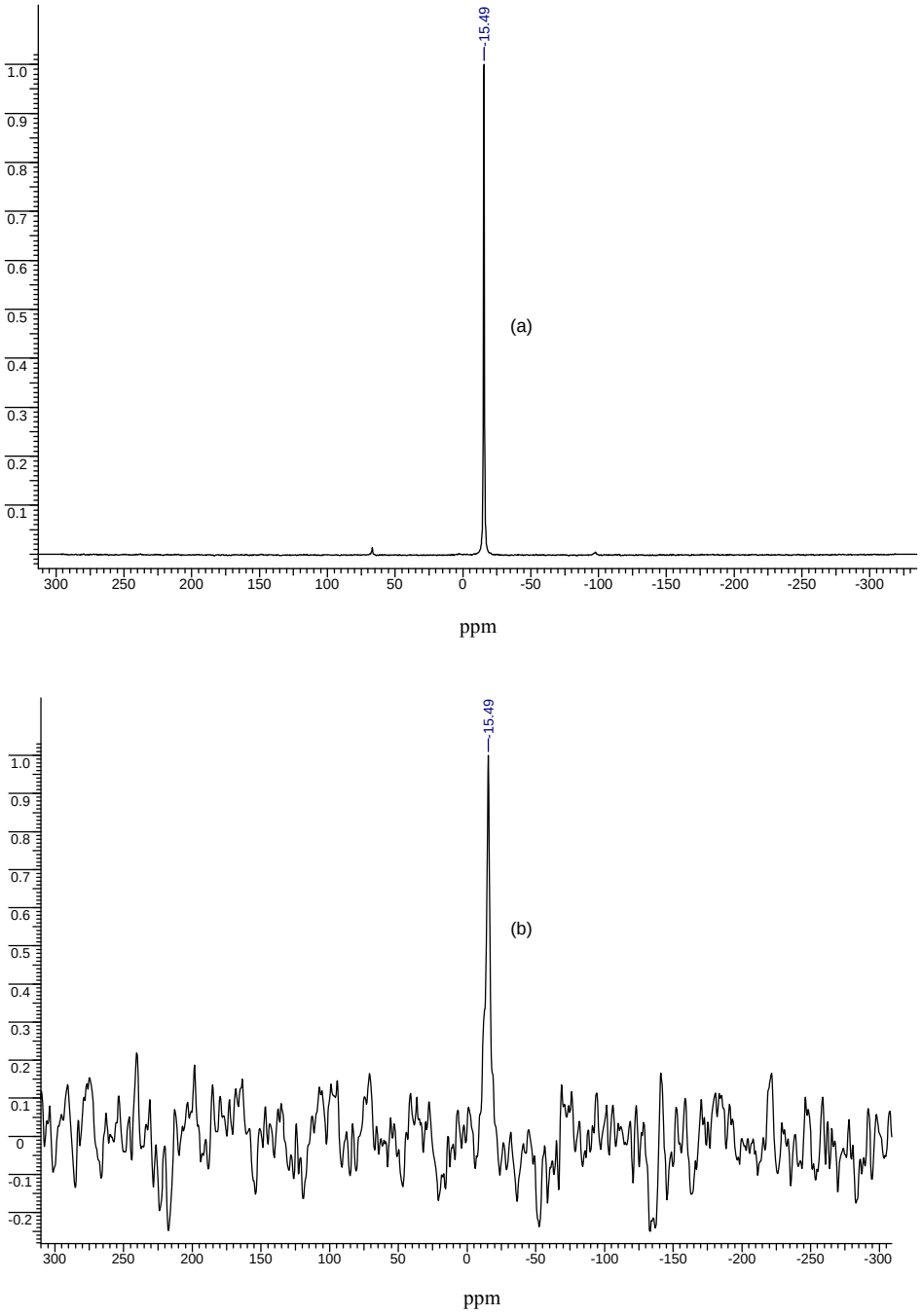

Figure 3.3. ^{31} P CPMAS NMR spectra of (a) Bulk DTP (b) 20% DTP/SiO_2

This interaction between DTP and SiO_2 supports leads to the localization of DTP protons thereby increasing their proximity to the Keggin anion because of the decrease in proton mobility (Figure 3.4). Such surface modification of supports due to impregnation of DTP enhanced their acidity and strength and thereby their activity for hydroxyalkylation of phenol to give bisphenol F.

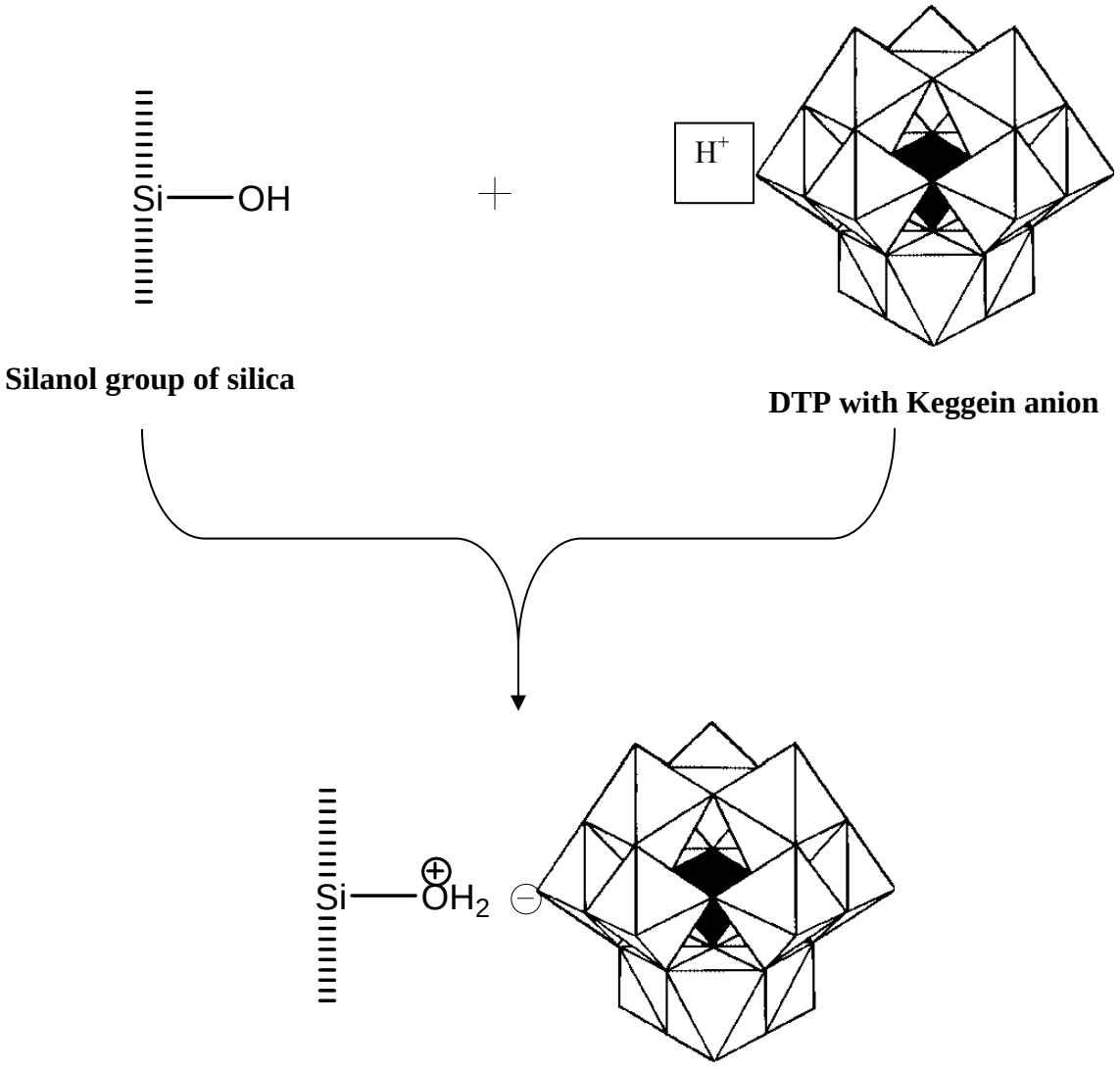

Figure 3.4. Interaction of dodecatungstophosphoric acid having Keggein anion with silanol group of silica

3.3.1.1.5. Scanning electron microscopy (SEM)

Figure 3.5 shows SEM images of (a) SiO_2 and (b) 20% DTP/SiO_2. SEM shows an agglomerated image of the parent SiO_2 with clear boundaries (Figure 3.5a), whereas, 20% DTP/SiO_2 showed wormhole-like precipitate images which could be due to impregnation of DTP on SiO_2 support (Figure 3.5b). Both the samples have irregular shapes and sizes.

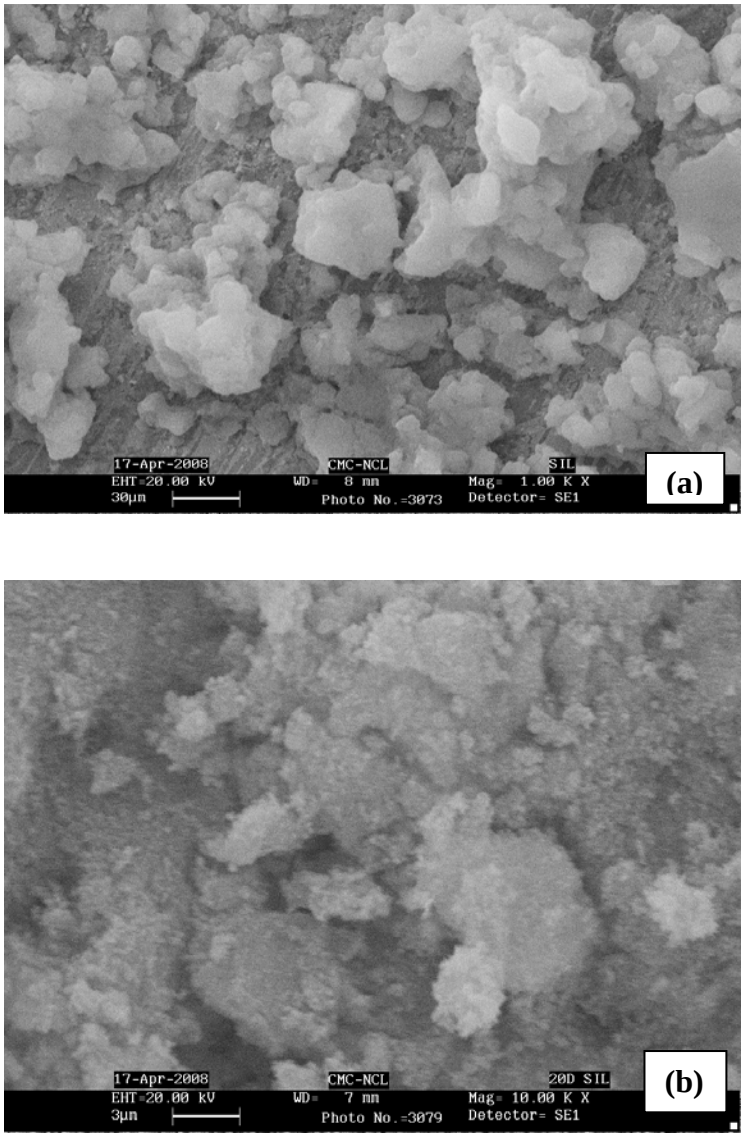

Figure 3.5. SEM image of (a) fumed silica (SiO_2) (b) 20% DTP/SiO_2

3.3.1.2. Catalyst activity measurement

Performances of various catalysts were evaluated in terms of (%) product yields and (%) product selectivity, which are defined as follows:

$$(\%)\ Product\ Yield = \frac{\Sigma\ Actual\ moles\ of\ \ product\ \ formed}{Expected\ moles\ of\ \ product\ \ formed\ based\ on\ \ formaldehyde\ consumed}\ X\ 100 \qquad (3.1)$$

$$(\%)\ Selectivity = \frac{moles\ of\ \ a\ \ product\ \ formed}{\Sigma\ moles\ of\ \ all\ the\ \ product}\ X\ 100 \qquad (3.2)$$

3.3.1.2.1. Catalyst screening

Catalyst activity of various solid acid catalysts for the hydroxyalkylation of phenol is presented in Figure 3.6. Among various catalysts screened, SiO_2 showed the least activity (< 5% product yield) in spite of its highest specific surface area of 256 m^2/g, while bulk DTP showed the highest activity (54% product yield) with the lowest surface area of 8 m^2/g. However, selectivity to bisphenol F was > 80% for SiO_2 and was only 60% (~ 40% trimer) for bulk DTP catalyst (Scheme 3.1). The lowest activity of SiO_2 could be due to its lowest acid strength as well as presence of acid sites in the low temperature (425 K) region. The yield of products increased from 3 to 37% as DTP loading on SiO_2 increased from 0 to 40%. As compared to DTP/SiO_2 catalysts, bulk DTP showed higher product yield (54%) due to its highest acidity (163.8 $\mu molS^{-1}$ NH_3) and strength. With increase in DTP loading on SiO_2 from 10 to 40%, the product yield also started increasing from 15 to 37% mainly because of the increase in total acidity as well as presence of strong acidic sites in the high temperature region (925 K) (Table 3.1).

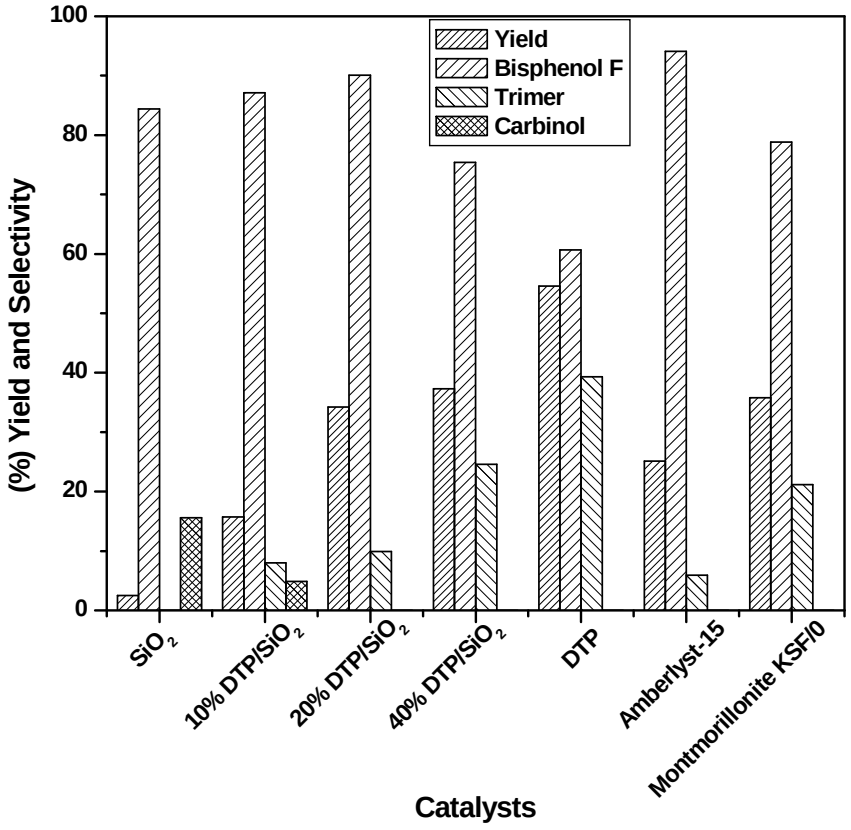

Figure 3.6. Catalyst screening for hydroxyalkylation of phenol
Reaction conditions: phenol, 30.85 mmol; formaldehyde, 6.15 mmol; catalyst concentration, 0.036 g/cm^3; temperature, 353 K; time, 1 h; mole ratio of phenol to formaldehyde, 5; solvent, toluene.

As can be seen from Figure 3.6, formation of the intermediate carbinol (16 and 5%) was observed for SiO_2 and 10% DTP/SiO_2 catalysts, respectively; while its amount decreased steeply to zero as DTP loading increased beyond 10%. The product yield increased from 16 to 34% as DTP loading increased from 10 to 20% while there was a marginal increase in selectivity (87 to 90%) to Bisphenol F. In case of 40% DTP/SiO_2 catalyst, although a slight increase in product yield was observed, there was a dramatic decrease in selectivity (from 90 to 75%) to Bisphenol F. The product selectivities were found to be dependent mainly on distribution of weak and strong acid sites [18]. As can be seen from Figure

3.2b and Table 3.1 that 10% DTP/SiO_2 showed higher acidity (2.1 $\mu molS^{-1}$ NH_3) than SiO_2 (1.1 $\mu molS^{-1}$ NH_3) nevertheless, the nature of acid sites of the former was similar to that of SiO_2 appearing at low temperature of 425 K. Hence, in both the cases the intermediate carbinol was formed while trimer along with the bisphenol F was also observed for 10% DTP/SiO_2 due to its acidity being higher than that of SiO_2 alone. 20% DTP/SiO_2 showed enhanced acidity (3.55 $\mu molS^{-1}$ NH_3) having percentage distribution as 69 and 31% in low and high temperature regions respectively (Figure 3.2c and Table 3.1). Due to enhanced acidity of 20% DTP/SiO_2, the product yield increased to 34% while, the selectivity to bisphenol F increased to 90% (Figure 3.6). Interestingly, the intermediate carbinol was found to be completely converted to bisphenol F and further increase in trimer selectivity (~10%) was also observed. Further increase in DTP loading to 40% caused an enhancement in the acidity (6.5 $\mu molS^{-1}$ NH_3, Table 3.1) with a dramatic change in the distribution of acid sites (Figure 3.2d and Table 3.1). The enhanced acidity of 40% DTP/SiO_2 caused a marginal increase in the product yield (37%); however, the change in the acid sites distribution (Table 3.1) led to a substantial decrease in bisphenol F selectivity (from 90 to 75%, Figure 3.6) and subsequent increase in the selectivity (> 20%) to a trimer. Bisphenol F formed initially, further reacts with phenol to form a trimer and its higher homologues in the presence of 40% DTP/ SiO_2 catalyst which has stronger acidity causing decrease in bisphenol F selectivity.

Other solid acid catalysts such as montmorillonite KSF/O and amberlyst-15 showed 35 and 25% product yield with 79 and 94% bisphenol F selectivity respectively. Montmorillonite KSF/O also showed two types of acid sites (Figure 3.2f and Table 3.1) having higher concentration (75%) of strong acid sites, causing formation of more trimer similar to that observed for 40% DTP/ SiO_2 (Figure 3.6). In the case of amberlyst-15 (resin) catalyst, the total acidity reported was 4.7 mmol/g (88 $\mu molS^{-1}$) [26, 27]; however, its NH_3-TPD profile could not measured to determine the distribution of the weak and strong acid sites, due to its instability at temperature > 373 K. Nevertheless, it showed the highest selectivity (94%) to bisphenol F (Figure 3.6). The observed activity and selectivity pattern and NH_3-TPD characterization of various catalysts studied in this work strongly indicate that not only the total acidity but also an appropriate combination of

both strong and weak acid sites of DTP/SiO_2 are critical for achieving the highest selectivity to Bisphenol F in hydroxyalkylation of phenol.

The catalytic activity of DTP/SiO_2 was also compared with those of conventional homogeneous acid catalysts (hydrochloric and sulfuric acids). Both hydrochloric and sulfuric acids showed high yield of products (40 and 52% respectively); however, a very low selectivity to bisphenol F (27 and 32% respectively) was obtained with these conventional homogenous catalysts. The low bisphenol F selectivity with these mineral acids was due to the predominant formation of trimers and their higher homologues under homogeneous conditions.

It can be seen from Figure 3.6 that amberlyst-15 showed catalytic activity lower (25%) than that for 20% DTP/SiO_2 (34%). It was also found that its catalyst activity significantly decreased by 25-30% for the second reuse, indicating its instability under the reaction conditions. Since, 20% DTP/SiO_2 catalyst was found to be more suitable due to the higher catalyst activity and reusability; further study on hydroxyalkylation of phenol was thus carried out using 20% DTP/SiO_2.

The % distribution of various isomers was also observed in hydroxyalkylation of phenol; among 3 possible isomers, the kinetically controlled 4, 4'-isomer was predominantly formed in a range of 45-48%, while 2, 2'- and 2, 4'-isomers were formed in a range of 10-13% and 39-41% respectively. The % of isomers formed was almost constant for all the catalysts under study except for SiO_2. With SiO_2 the kinetically controlled 4, 4-isomer formed was the highest (67%).

3.3.1.2.2. Effect of mole ratio of phenol to formaldehyde

The effect of mole ratio of phenol to formaldehyde on product yield and bisphenol F selectivity was studied in the range of 1 to 5 for 20% DTP/SiO_2 catalyst by varying the concentration of formaldehyde at a constant phenol concentration; and the results are presented in Figure 3.7.

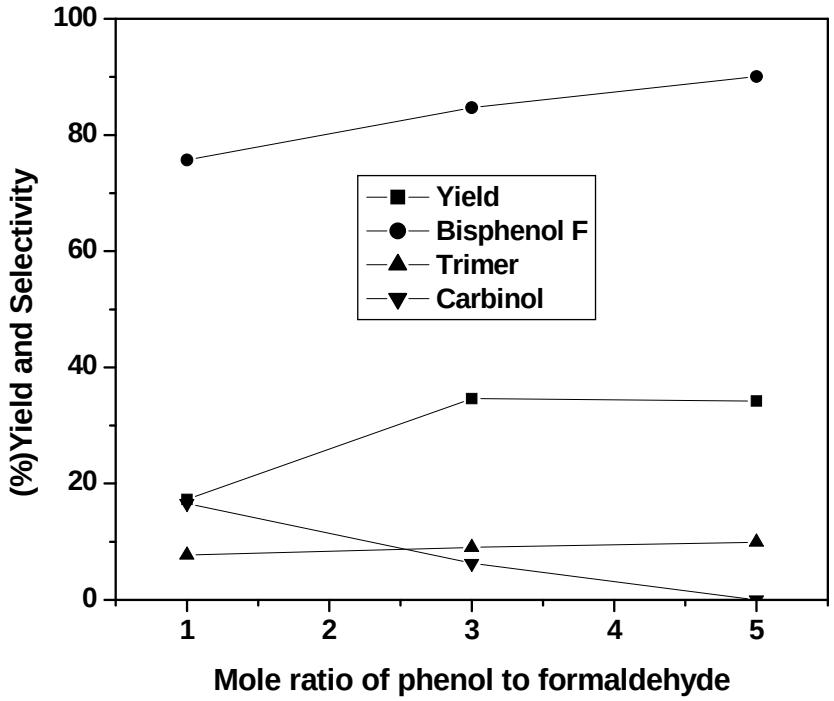

Figure 3.7. Effect of mole ratio of phenol to formaldehyde on product yield and selectivity

Reaction conditions: phenol, 30.85 mmol; catalyst concentration, 0.036 g/cm^3; temperature, 353 K; time, 1 h; catalyst, 20% DTP/SiO_2; solvent, toluene.

The yield of products increased from 17 to 34% as the mole ratio of phenol to formaldehyde increased from 1 to 3. With further increase in mole ratio from 3 to 5, the yield remained almost constant (34%). The lower product yield (17%) was mainly because of the blockage of active sites of the catalyst by more polar water molecules present in excess amount for a mole ratio of 1 as compared to 3 and 5 mole ratios. The selectivity of bisphenol F increased from 75 to 90% and that of trimer from 7 to 10% with increase in mole ratio from 1 to 5. The selectivity to the intermediate, carbinol decreased steeply from 16 to 0% with increase in mole ratio from 1 to 5. The formation of carbinol (16%) at mole ratio 1 was due to the availability of formaldehyde in excessive amount, which minimized the formation of bisphenol F. The 4, 4'-isomer decreased

slightly from 49 to 45% and 2, 2' and 2, 4'-isomer increased from 12 to 13% and from 39 to 42% respectively, with increase in mole ratio from 1 to 5.

3.3.1.2.3. Effect of catalyst concentration

The effect of catalyst concentration in the range of 0.007 to 0.036 g/cm^3 on product yield, selectivity and isomer distribution was also studied; and the results are presented in Figure 3.8.

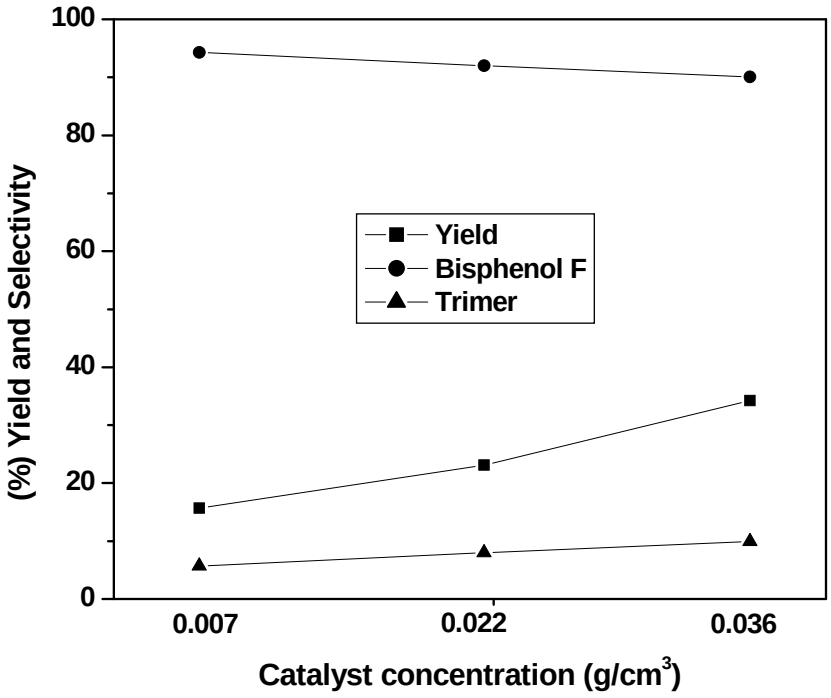

Figure 3.8. Effect of catalyst concentration on product yield and selectivity
Reaction conditions: phenol, 30.85 mmol; formaldehyde, 6.15 mmol; temperature, 353 K; time, 1 h; mole ratio of phenol to formaldehyde, 5; catalyst, 20% DTP/SiO_2; solvent, toluene.

The product yield increased by two fold (from 15 to 34%) as the catalyst concentration increased from 0.007 to 0.036 g/cm^3. This is obvious since with increase in catalyst concentration; the acidic sites also increased, which facilitate the conversion of phenol to

products. However, the selectivity to bisphenol F decreased marginally (94 to 90%) and that of trimer increased from 6 to 10% as the catalyst concentration increased from 0.007 to 0.036 g/cm^3. The slight decrease in bisphenol F selectivity was due to its conversion into a trimer because of an increase in acidic sites at higher catalyst concentration. No significant change was observed in bisphenol F isomers distribution after 1 h with change in catalyst concentration.

3.3.1.2.4. Effect of temperature

Figure 3.9 presents the effect of temperature on product yield, selectivity and isomer distribution. The study was performed in a temperature range of 333 to 353 K at 5 mole ratio of phenol to formaldehyde for 1 h. It was observed that the product yield increased from 22 to 34% with no significant change observed in bisphenol F selectivity as temperature increased from 333 to 353 K. However, 4, 4'-isomer decreased from 49 to 45% while 2, 2' and 2, 4' isomers increased from 11 to 13% and 40 to 42% respectively, with increase in temperature from 333 to 353 K.

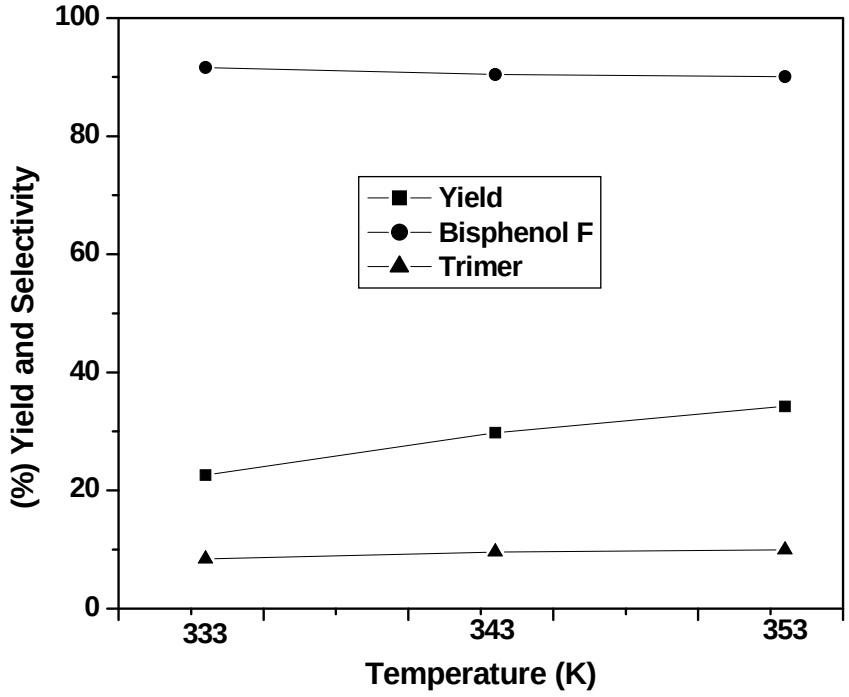

Figure 3.9. Effect of temperature on product yield and selectivity

Reaction conditions: phenol, 30.85 mmol; formaldehyde, 6.15 mmol; catalyst concentration, 0.036 g/cm^3; time, 1 h; mole ratio of phenol to formaldehyde, 5; catalyst, 20% DTP/SiO_2; solvent, toluene.

3.3.1.2.5. Effect of time

The effect of reaction time on the product yield and bisphenol F selectivity was also studied for phenol to formaldehyde mole ratio of 5 at 353 K. It was found that the product yield increased from 0 to 28% with increase in reaction time from 0 to 30 minutes; thereafter it increased slightly from 28 to 34% as reaction time increased from 30 to 60 minutes (Figure 3.10). The selectivity to bisphenol F decreased slightly from 94 to 90% when reaction time increased from 15 to 60 minutes. This slight decrease in selectivity of bisphenol F was mainly because the bisphenol F initially formed reacts further with formaldehyde and phenol to give trimers and their higher homologues.

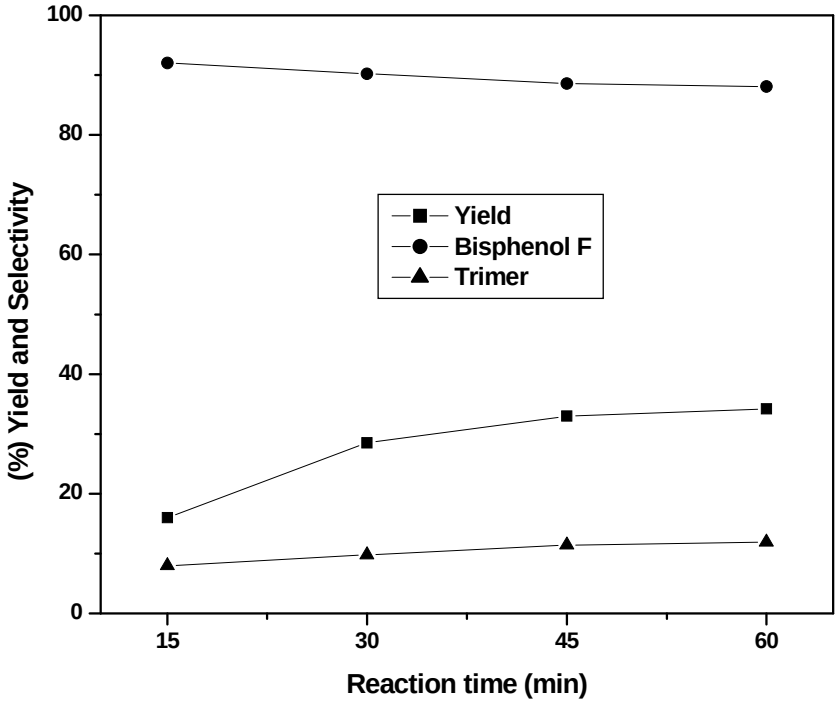

Figure 3.10. Time vs. product yield and selectivity plot

Reaction conditions: phenol, 30.85 mmol; formaldehyde, 6.15 mmol; catalyst concentration, 0.036 g/cm^3; temperature, 353 K; mole ratio of phenol to formaldehyde, 5; catalyst, 20% DTP/SiO_2; solvent, toluene.

3.3.1.2.6. Catalyst recycle

In order to establish the reusability of the catalyst for hydroxyalkylation of phenol, after the first hydroxyalkylation run, the catalyst was filtered and washed with dichloromethane for several times, dried at room temperature and then in an oven at 353 K for 2 h and reused it for subsequent runs. This procedure was followed for two subsequent hydroxyalkylation experiments and the results are shown in Figure 3.11. The catalyst was found to retain its activity even after the second recycle. The product yield slightly decreased from 34 to 29% after the second recycle; this could be because of handling losses of the catalyst. The selectivity to bisphenol F remained almost constant (90%) for all the recycle experiments.

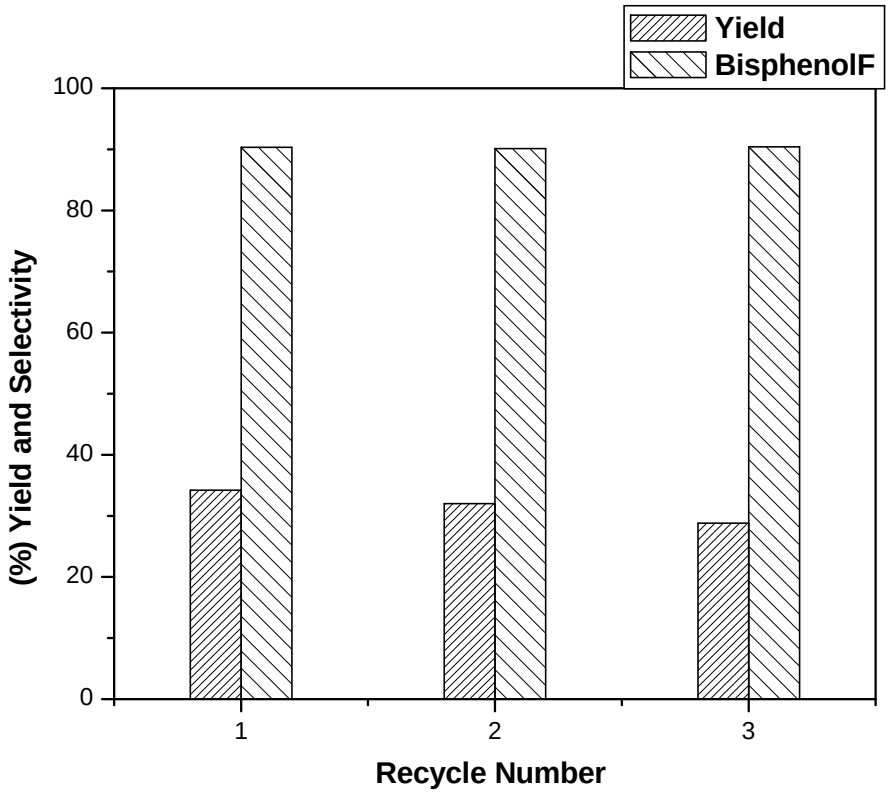

Figure 3.11. Catalyst recycle

Reaction conditions: phenol, 30.85 mmol; formaldehyde, 6.15 mmol; catalyst concentration, 0.036 g/cm^3; temperature, 353 K; time, 1 h; mole ratio of phenol to formaldehyde, 5; catalyst, 20% DTP/SiO_2; solvent, toluene.

3.3.2. DTP impregnated on Montmorillonite K10

DTP impregnated on Mont K10 catalysts were prepared by wet impregnation method [25], characterized by various techniques and their activities were evaluated for the hydroxyalkylation of phenol. The purpose of this study was to examine the effect of alteration in acidity and strength of Mont K10 as well as Brønsted to Lewis acid sites (B/L) ratio on catalyst activity and product selectivity for the hydroxyalkylation of phenol to bisphenol F. A detailed study on characterization of DTP/Mont K10 catalysts and their activity evaluation for the hydroxyalkylation of phenol is discussed in the following sections.

3.3.2.1. Catalyst characterization

3.3.2.1.1. X-ray diffraction

X-ray diffraction patterns of Mont K10, 10 and 20% DTP/Mont K10 are presented in Figure 3.12.

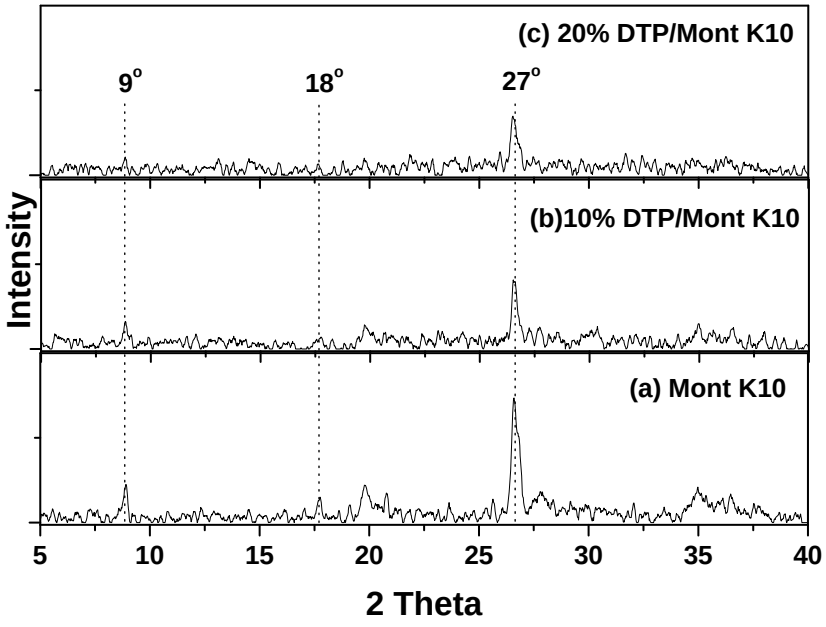

Figure 3.12. X-ray diffraction patterns of (a) Mont K10 (b) 10% DTP/Mont K10 (c) 20% DTP/Mont K10

Mont K10 showed (Figure 3.12a) sharp (0 0 1) and (0 0 3) reflections at $2\theta = 9^o$ and 18^o. The sharp reflection at $2\theta = 27^o$ was assigned to α-quartz phase [28]. 5% DTP/Mont K10 showed XRD pattern similar to that of Mont K10. However, the intensity of reflection decreased significantly, particularly the reflection at $2\theta = 18^o$ almost disappeared after impregnation of 10 and 20% DTP on Mont K10 due to the excellent dispersion of DTP on Mont K10 (Figure 3.12b and c).

3.3.2.1.2. BET surface area measurement

The specific BET surface areas of various solid acid catalysts are presented in Table 3.2.

Table 3.2. Textural properties of various solid acid catalysts

Catalysts	BET surface area (m^2/g)	NH_3 adsorbed (μmol S^{-1})	(%) distribution of acid sites	
			Weak (373-573 K)	Strong (673-973 K)
Mont K10	230	8.1	51	49
5% DTP/Mont K10	201	11	48	52
10% DTP/Mont K10	173	15.2	45	55
20% DTP/Mont K10	130	22.4	39	61
40% DTP/Mont K10	94	41.1	39	61
60% DTP/Mont K10	58	65.3	38	62
DTP	8	163.8	32	68

Among various solid acids, Mont K10 showed the highest (230 m^2/g) specific BET surface area while DTP showed lowest (8 m^2/g) BET surface area. The specific BET surface areas of various catalysts showed the following order: Mont K10 > 5% DTP/Mont K10 > 10% DTP/Mont K10 > 20% DTP/Mont K10 > 40% DTP/Mont K10

> 60% DTP/Mont K10 > DTP. The decrease in surface area with increase in DTP loadings was due to the better dispersion of DTP on Mont K10 which made some pores of Mont K10 inaccessible to N_2.

3.3.2.1.3. Ammonia-TPD

The acid sites and their strength of various catalysts prepared in this work was assessed by NH_3-TPD measurement. NH_3-TPD profiles of Mont K10, bulk DTP and 5- 60% DTP on Mont K10 catalysts are shown in Figure 3.13 and the values of ammonia adsorbed and (%) distribution of acid sites based on ammonia desorption are presented in Table 3.2. The total concentration of acid sites per unit surface area of various catalysts decreased in the following order: DTP > 60% DTP/Mont K10 > 40% DTP/Mont K10 > 20% DTP/Mont K10 > 10% DTP/Mont K10 > 5% DTP/Mont K10 > Mont K10. Among various solid acid catalysts, bulk DTP showed the highest (163.8 $\mu molS^{-1}$ NH_3) concentration of acid sites with sharp desorption peak of ammonia appearing at 925 K [29]. The desorption temperature which reflects the acid strength was also highest for bulk DTP. As compared to bulk DTP, Mont K10 showed low concentration of acid sites (8.1 $\mu molS^{-1}$ NH_3). The concentration of acid sites and (%) distribution of acid sites in high temperature region of Mont K10 increased from 8.1 to 65.3 $\mu molS^{-1}NH_3$ and from 49 to 62% respectively with increase in DTP loading from 0 to 60%. The linear increase in concentration of acid sites with increase in DTP loading shows homogeneous dispersion of DTP particles on Mont K10. Interestingly, sharp desorption peak of bulk DTP at 925 K disappeared and new acid sites were observed for DTP loading up to 20% in a range of 525-725 K while, 40 and 60% DTP-Mont K10 catalysts showed more intense desorption peaks in higher temperature region having maxima at 775 and 885 K respectively. The concentration of acid sites of bulk DTP which reflect total acidity decreased after its dispersion on Mont K10 (Table 3.2). The position of desorption peak of bulk DTP also shifted from 925 K to lower temperatures in the range of 885 – 675 K, for various DTP loadings from 60 to 20% on Mont K10 (Figure 3.13). These results (Table 3.2 and Figure 3.13) indicate that the total acidity and acid strength of bulk DTP decreased and modified significantly after its impregnation at various percentages on

Mont K10. This was also confirmed by studying the change in Brønsted and Lewis acid sites of various catalysts.

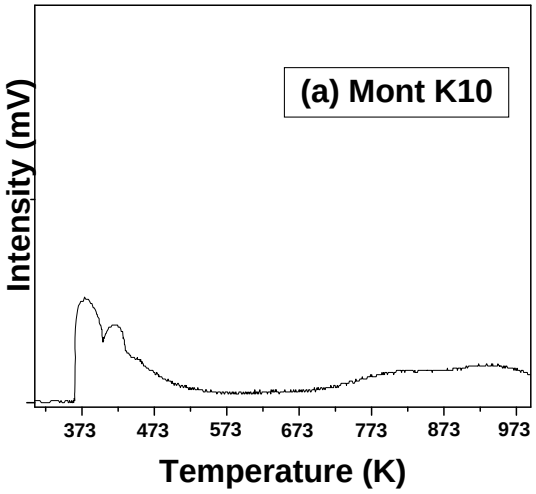

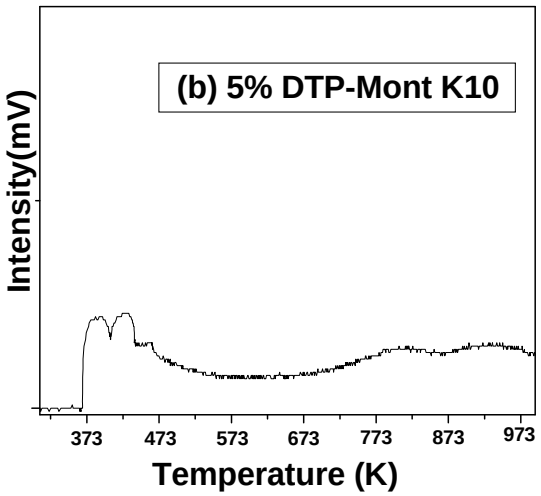

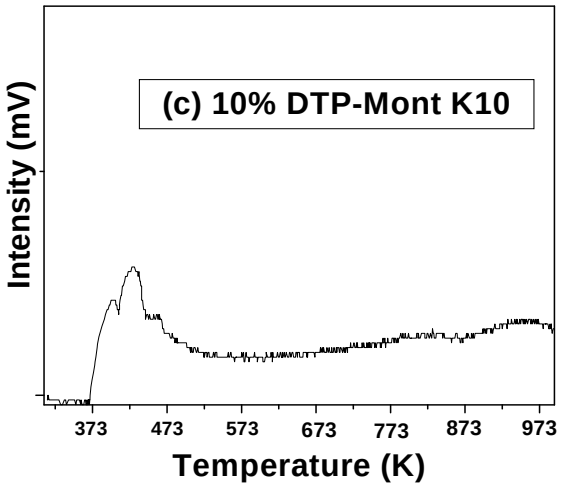

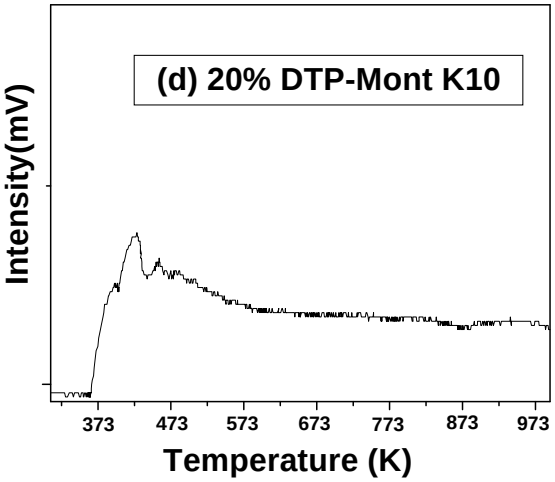

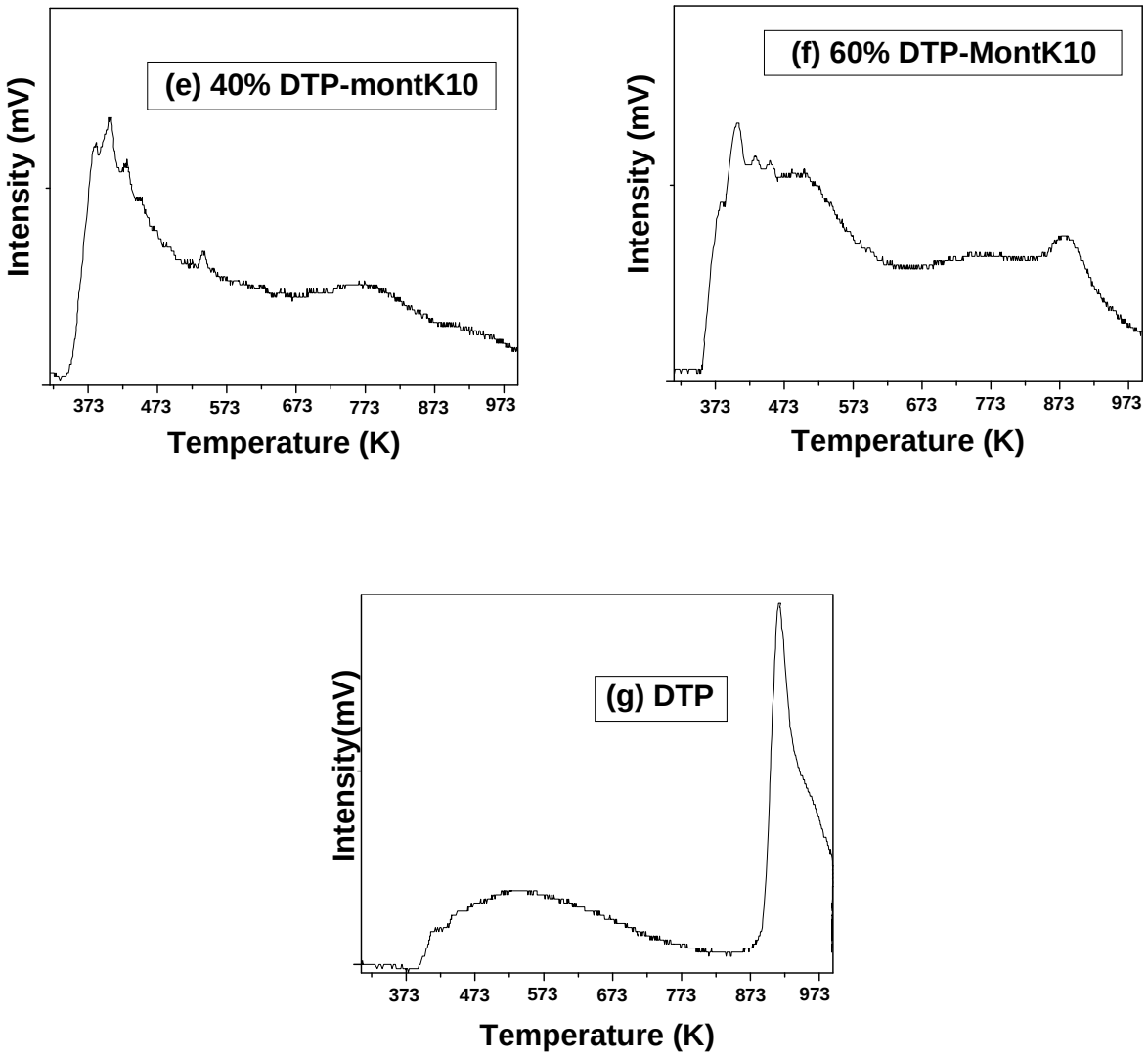

Figure 3.13. Ammonia TPD profiles for various solid acid catalysts

3.3.2.1.4. Pyridine FT-IR analysis

In order to distinguish between Brønsted and Lewis acidity, pyridine FT-IR analysis was carried out. Figure 3.14 presents FT-IR pyridine adsorption spectra of various percentage loadings of DTP on Mont K10. The catalysts showed bands corresponding to Brønsted and Lewis acidity at 1540 and 1442 cm^{-1} respectively. Another band appeared at 1490 cm^{-1} could be assigned to both Brønsted and Lewis acidity.

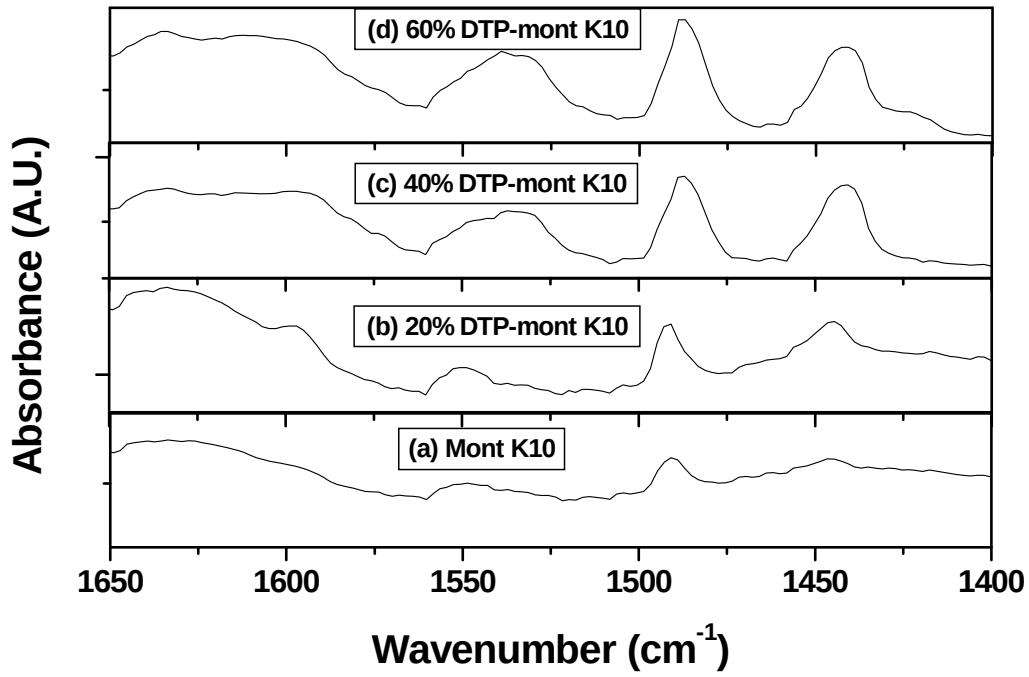

Figure 3.14. FT-IR pyridine adsorption spectra of various percentage of DTP on Mont K10

Figure 3.15 presents the plot of Brønsted to Lewis acid sites (B/L) ratio vs. DTP loading for various DTP/MontK10 catalysts. B/L ratio increased linearly from 0.47 to 1.45 with increase in DTP loading on Mont K10 from 0 to 60%. The increase in B/L ratio or change in quality of acid sites (Figures 3.14 and 3.15) was mainly due to the dispersion of DTP having Brønsted acidity, on Mont K10.

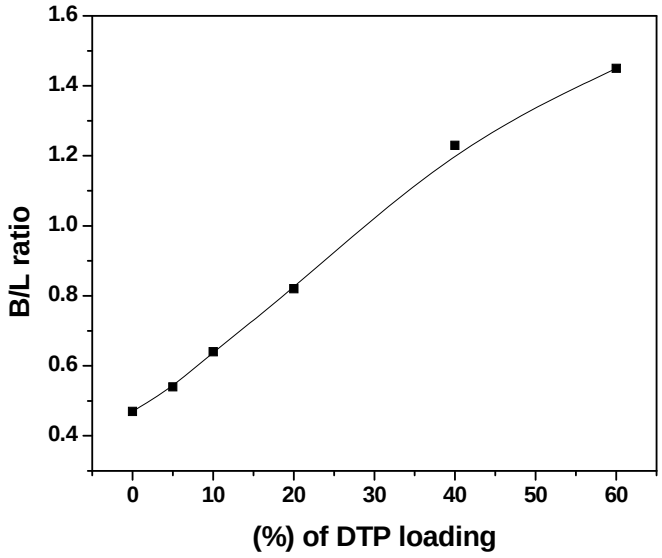

Figure 3.15. B/L ratio vs. DTP loading

Table 3.3 presents percentage composition for various loadings of DTP on Mont K10. The elemental compositions of various DTP/Mont catalysts were in excellent agreement with the theoretical content of elements. These confirmed the successful impregnation of DTP on Mont K10.

Table 3.3. The composition of DTP supported on Mont K10 samples with different DTP loading

Catalysts	Si (Wt%)	O (Wt%)	Mg (Wt%)	Al (Wt%)	P (Wt%)	W (Wt%)
Mont K10	51.8	39.7	1.1	7.4	-	-
5% DTP/Mont K10	51.2	34.9	1.1	7.3	0.7	4.8
10% DTP/Mont K10	47.5	33.8	1.0	7.0	1.1	9.6
20% DTP/Mont K10	41.5	30.5	1.2	5.8	1.6	19.4

3.3.2.2. Activity measurement

3.3.2.2.1. Catalyst screening

Effect of change in total acidity and acid strength of Mont K10 due to the impregnation of various percentages of DTP, on the conversion of phenol and bisphenol F selectivity was studied for phenol to formaldehyde mole ratio of 5 at 353 K (Figure 3.16). The optimum molar ratio of phenol to formaldehyde was kept 5 according to my earlier work [24]. Among various solid acid catalysts, bulk DTP showed the highest conversion of phenol (32%) with a selectivity of 78% to bisphenol F under given reaction conditions. In contrast to bulk DTP, Mont K10 showed 93% selectivity to bisphenol F, however very low conversion of phenol (10%) was observed. The higher conversion of phenol (32%) with bulk DTP was mainly due to its high concentration of acid sites (163.8 μmol S^{-1} NH_3) while lower selectivity (78%) to bisphenol F was mainly due to its high acid strength which facilitates the formation of trimers from initially formed bisphenol F. The low (10%) conversion of phenol with Mont K10 was due to its low (8.1 μmol S^{-1} NH_3) concentration of acid sites. Interestingly, the low acid strength of Mont K10 compared to bulk DTP enhanced bisphenol F selectivity significantly by minimizing the formation of trimers. The conversion of phenol increased from 10 to 28% and selectivity to bisphenol F decreased marginally from 93 to 90% with increase in DTP loading from 0 to 20%. The concentration of acid sites increased from 8.1 to 22.4 μmol S^{-1} NH_3 with increase in DTP loading from 0 to 20% (Figure 3.13 and Table 3.2). This increase in concentration of acid sites facilitates the conversion of phenol into products. The selectivity to bisphenol F decreased marginally from 93 to 90% with increase in DTP loading from 0 to 20%. In the case of further increase in DTP loading up to 60%, although the conversion of phenol slightly increased from 28 to 31% (Figure 3.16), the selectivity to bisphenol F decreased from 90 to 80%. The decrease in selectivity to bisphenol F over 40 and 60% DTP-Mont K10 catalysts was due to their higher acidity (0.041 and 0.065 mmol$S^{-1}NH_3$ respectively) and a higher concentration of acid sites (61-62%) in a high temperature region which facilitated the formation of a trimer.

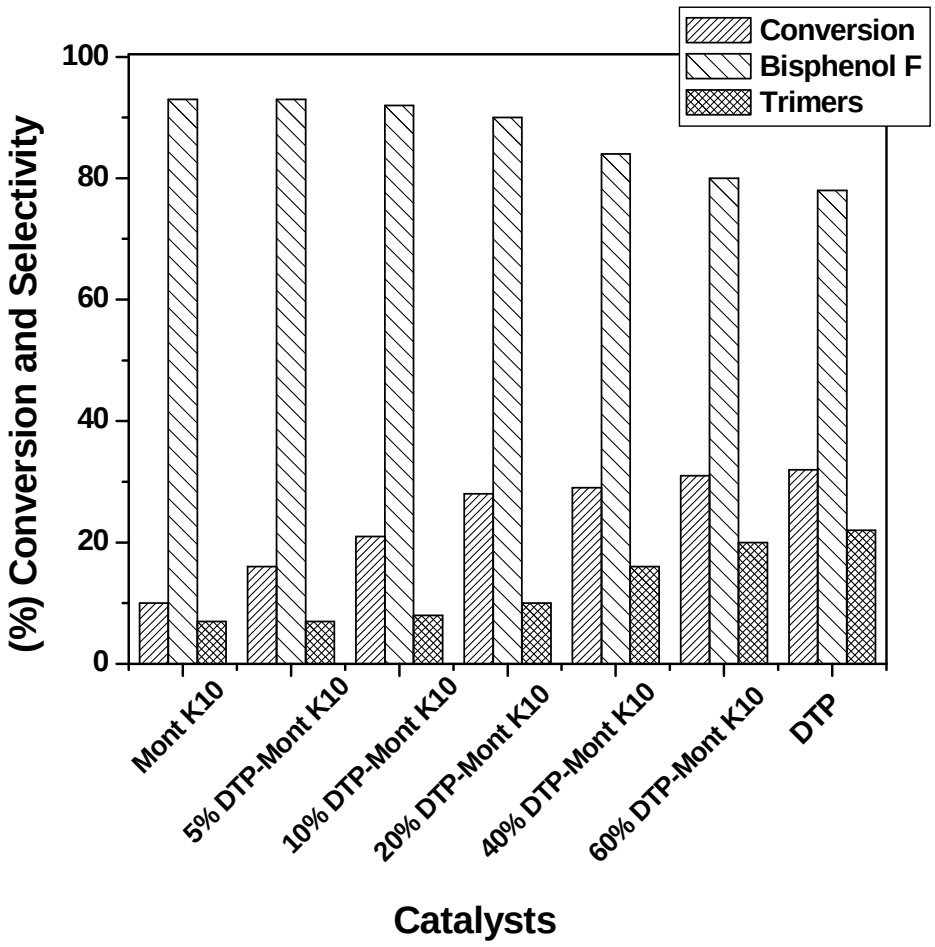

Figure 3.16. Effect of DTP loading on the conversion of phenol and product selectivity Reaction conditions: phenol, 12.5 mmol; formaldehyde, 2.5 mmol; mole ratio of phenol to formaldehyde, 5; catalyst concentration, 0.04 g/cm^3; temperature, 353 K; reaction time, 40 min; solvent, toluene (6 cm^3).

The influence of Brønsted and Lewis acidity on activity and product selectivity was also studied separately and the results are presented in Table 3.4.

Table 3.4. Influence of Brønsted / Lewis acidity on activity and product selectivity

Catalysts	B/L ratio	Conversion (%)	Selectivity (%)	
			Bisphenol F	Trimer
Mont K10	0.47	10	93	7
5% DTP/Mont K10	0.54	16	93	7
10% DTP/Mont K10	0.64	21	92	8
20% DTP/Mont K10	0.82	28	90	10
40% DTP/Mont K10	1.23	29	84	16
60% DTP/Mont K10	1.45	31	80	20

Reaction conditions: phenol, 12.5 mmol; formaldehyde, 2.5 mmol; mole ratio of phenol to formaldehyde, 5; catalyst concentration, 0.04 g/cm^3; temperature, 353 K; reaction time, 40 min; solvent, toluene (6 cm^3).

As discussed earlier, concentration of Brønsted acid sites increased as seen by increase in B/L ratio from 0.47 to 1.45 (Table 3.4) with increase in DTP loading from 0 to 60% on Mont K10. The conversion of phenol also increased from 10 to 28% with increase in B/L ratio from 0.47 to 0.82, thereafter it marginally increased from 28 to 31% with further increase in B/L ratio from 0.82 to 1.45. However, the selectivity to bisphenol F was greatly affected by the B/L ratio. Table 3.4 shows that the selectivity to bisphenol F decreased from 93 to 80% with increase in B/L ratio from 0.47 to 1.45. The lowest selectivity (80%) to bisphenol F over 60% DTP-Mont K10 catalyst was mainly due to the enhanced total acidity and Brønsted acid sites with higher DTP loading, which favor the formation of a trimer by the reaction of bisphenol F with formaldehyde followed by phenol. Thus, Brønsted acid sites played an important role in the hydroxyalkylation of phenol by facilitating first, the formation of methyol carbocation from formaldehyde. The

methyol carbocation then immediately reacted with phenol to give carbinol followed by its further reaction with another molecule of phenol to give bisphenol F [30].

3.3.2.2.2. Effect of reaction time

The effect of reaction time on the phenol conversion and bisphenol F selectivity was also studied for phenol to formaldehyde molar ratio of 5 (Figure 3.17).

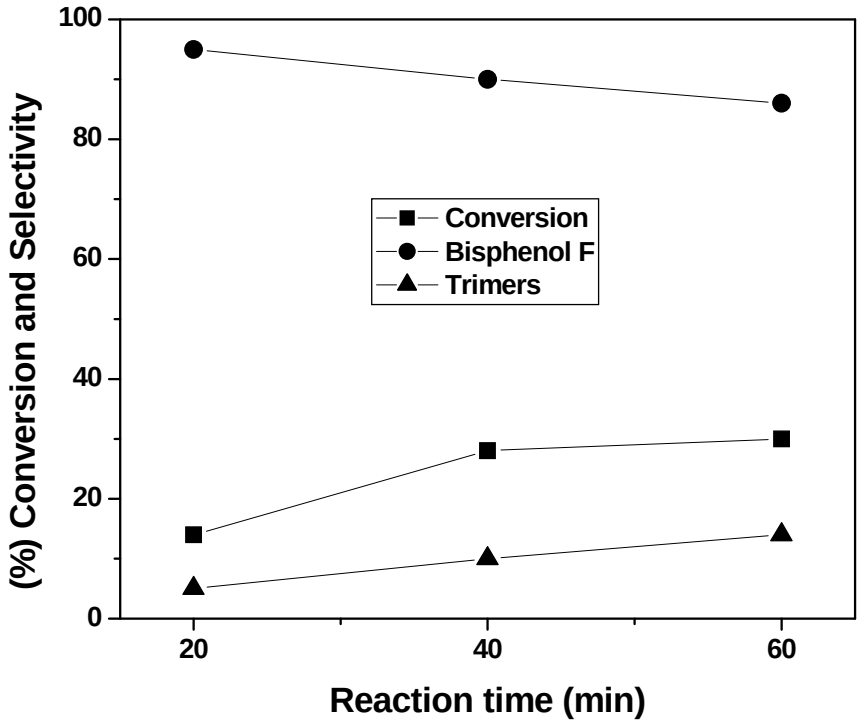

Figure 3.17. Effect of reaction time on the conversion of phenol and product selectivity Reaction conditions: phenol, 12.5 mmol; formaldehyde, 2.5 mmol; mole ratio of phenol to formaldehyde, 5; catalyst concentration (20% DTP/Mont K10), 0.04 g/cm^3; temperature, 353 K; reaction time, 60 min; solvent, toluene (6 cm^3).

Phenol conversion increased from 13 to 30% while the selectivity to bisphenol decreased from 95 to 86% and that of trimers increased from 5 to 14% with increase in reaction time from 20 to 60 min. This decrease in bisphenol F selectivity was mainly due to the

reaction of initially formed bisphenol F with formaldehyde and then with phenol to give trimer.

3.3.2.2.3. Catalyst recycle

Catalyst recycle experiments were carried out using 20% DTP/Mont K10 catalyst according to the procedure discussed in section 3.3.1.2.6 (Figure 3.18). The catalyst was found to retain its activity even after the third recycle experiment without affecting the conversion of phenol (28%). The selectivity to bisphenol F (90%) also remained constant for all the three recycle experiments.

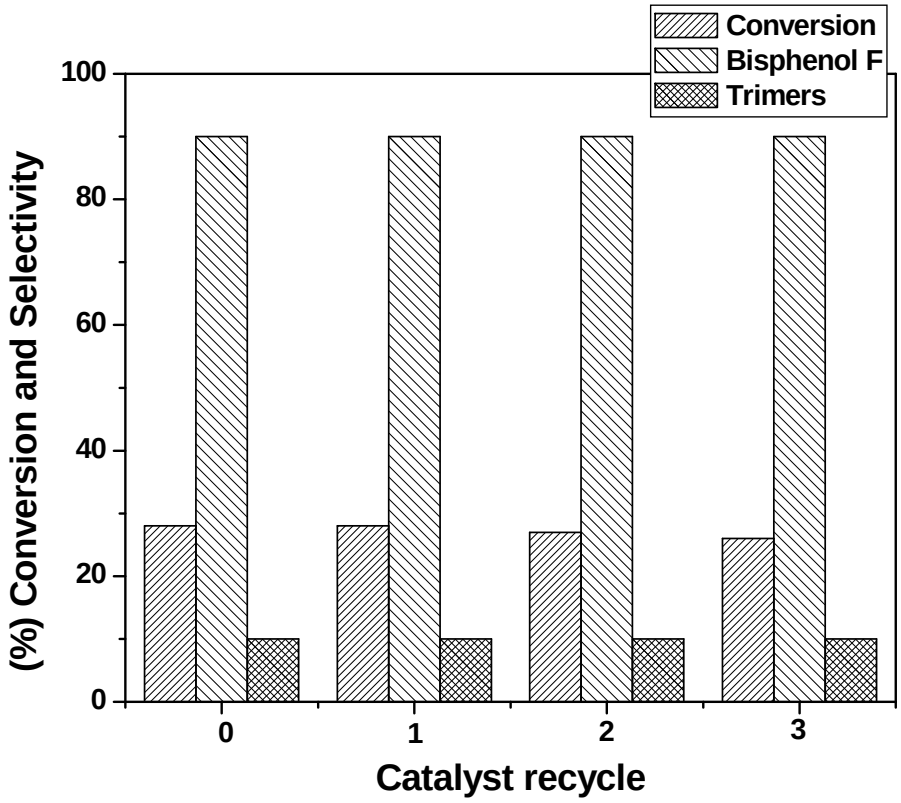

Figure 3.18. Catalyst recycle

Reaction conditions: phenol, 12.5 mmol; formaldehyde, 2.5 mmol; mole ratio of phenol to formaldehyde, 5; catalyst concentration (20% DTP/Mont K10), 0.04 g/cm^3; temperature, 353 K; reaction time, 40 min; solvent, toluene (6 cm^3).

3.3.3. Plausible mechanistic pathway

A plausible mechanistic pathway for the hydroxyalkylation of phenol with formaldehyde to give Bisphenol F (4, 4'-isomer) is shown in Scheme 3.3. In a commercial aqueous solution of formaldehyde (37%), the monomeric form of formaldehyde (around 40% with respect to total formaldehyde) is mostly present in the form of methylene glycol while the remaining 60% of formaldehyde is in oligomeric form (polyoxymethylene glycols and polyoxymethylene hemiacetals) [31]. In the first step, methylene glycol is activated by a proton from the catalyst to form methyol cation (I) with release of a water molecule. The electrophilic attack of methyol cation on phenol takes place in the second step to form a resonance-stabilized carbocation (II). This is followed by a proton transfer from carbocation (II) to the catalyst and a carbinol (*p*-hydroxy benzyl alcohol) (III) is formed with regeneration of the catalyst. The hydroxymethyl group of the carbinol abstracts a proton from the catalyst to form hydroxy benzyl carbocation (IV). Finally, the electrophilic attack of hydroxy benzyl carbocation on the second molecule of phenol followed by a proton transfer to catalyst gives bisphenol F (4, 4'-isomer) (V) with regeneration of the catalyst.

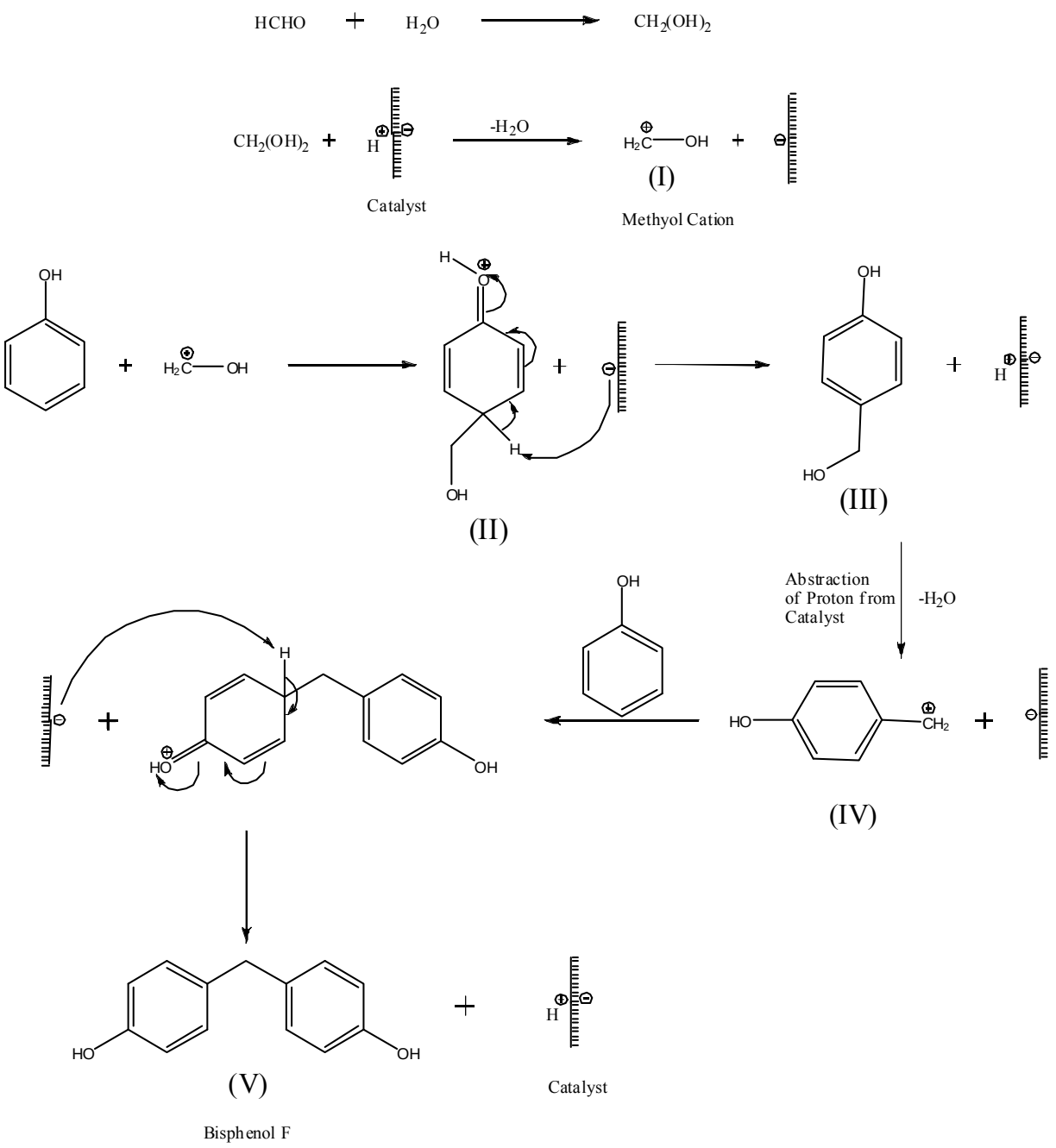

Scheme 3.3. Plausible mechanistic pathway for formation bisphenol F (4, 4'-isomer) via solid acid catalyzed hydroxyalkylation of phenol

3.4. CONCLUSIONS

- Catalysts with different loadings of DTP on SiO_2 and Mont K10 supports were prepared by wet impregnation method.
- Among the various DTP/SiO_2 catalysts with varying DTP loadings (0-40%) screened for the hydroxyalkylation of phenol, 20% DTP/SiO_2 was found to be an effective catalyst giving the highest selectivity of 90% to bisphenol F. The optimum performance (product yield, 34%) with the highest selectivity of 90% to bisphenol F could be due to highly dispersed 20% DTP on SiO_2 giving moderate acidity with an appropriate combination of both strong and weak acid sites, as evidenced by NH_3-TPD studies. Formation of a carbinol intermediate was observed for 10% DTP/SiO_2 catalyst, while a byproduct (trimer) formation was found to be substantial for bulk DTP, 40% DTP/SiO_2 and montmorillonite KSF/O catalysts due to their higher acidity.
- Among various DTP impregnated Mont K10 catalysts screened, 20% DTP/Mont K10 showed the highest activity (90% selectivity to bisphenol F with 28% conversion of phenol) for the hydroxyalkylation of phenol. NH_3-TPD and pyridine IR results showed that the concentration of acid sites and acid strength of Mont K10 were significantly altered after impregnation with DTP. The ratio of Brønsted to Lewis acid sites (B/L) increased from 0.47 to 1.45 with increase in DTP loading from 0 to 60%. This variation in acid sites led to marked differences in their catalyst activity for the hydroxyalkylation of phenol to bisphenol F.
- A plausible reaction pathway has been suggested through methylene glycol activated by a proton from the catalyst to form methyol cation that attacks on phenol to give an intermediate carbinol (*p*-hydroxy benzyl alcohol). Finally, the electrophilic attack of hydroxy benzyl carbocation on the second molecule of phenol followed by a proton transfer to catalyst gives bisphenol F (4, 4'-isomer) (V) with regeneration of the catalyst.

3.5. REFERENCES

1. M. Okihama, J. Kunitake, *Japanese Pat.* 08198790 (1996)
2. A. de Angelis, P. Inagallina, C. Perego, *Ind. Eng. Chem. Res.* 43 (2004) 1169.
3. K. Nowinska, W. Kaleta, *Appl. Catal. A: Gen.* 203 (2000) 91.
4. D. Das, J. Lee, S. Cheng, *Chem. Commun.* (2001) 2178.
5. J. F. Knifton, *US Pat.* 5169992 (1992).
6. C. Perego, A. de Angelis, A. Carati, C. Flego, R. Millini, C. Rizzo, G. Bellussi, *Appl. Catal. A: Gen.* 307 (2006) 128.
7. S. K. Jana, T. Kugita, S. Namba, *Appl. Catal. A: Gen.* 266 (2004) 245.
8. M. Alvaro, D. Das, M. Cano, H. Garcia, *J. Catal.* 219 (2003) 464.
9. N. Barthel, A. Finiels, C. Moreau, R. Jacquot, M. Spagnol, *Top. Catal.* 13 (2000) 269.
10. S. K. Jana, T. Okamoto, T. Kugita, S. Namba, *Appl. Catal. A: Gen.* 288 (2005) 80.
11. M. Alvaro, H. Garcia, A. Sanjuan, M. Espla, *Appl. Catal. A: Gen.* 175 (1998) 105.
12. A. Corma, H. Garcia, J. Miralles, *Micropor. Mesopor. Mater.* 43 (2001) 161.
13. Y. Kamiya, T. Okuhara, M. Misono, A. Miyaji, K. Tsuji, T. Nakajo, *Catal. Surv. Asia* 12 (2008) 101.
14. I. V. Kozhevnikov, *Chem. Rev*. 98 (1998) 171.
15. Y. Izumi, K. Matsuo, K. Urbe, *J. Mol. Catal.* 18 (1983) 299.
16. M. Misono, *Catal. Rev. Sci. Eng.* 29 (1987) 269.
17. N. Mizuno, M. Misono, *Chem. Rev.* 98 (1998) 199.
18. I. V. Kozhevnikov, K. R. Kloetstra, A. Sinnema, H. W. Zandbergen, H. Van Bekkum, *J. Mol. Catal. A: Chem.* 114 (1996) 287.
19. Y. Izumi, R. Hasebe, K. Urbe, *J. Catal.* 84 (1983) 402.
20. W. Kuang, A. Rives, M. Fournier, R. Hubaut, *Appl. Catal. A: Gen.* 250 (2003) 221.
21. P. Madhusudhan Rao, A. Wolfson, S. Kababya, S. Vega, M. V. Landau, *J. Catal*. 232 (2005) 210.
22. N. Mizuno, *Catal. Rev. Sci. Eng.* 30 (1998) 339.

23. V.M. Mastikhin, S.M. Kulikov, A.V. Nosov, I.V. Kozhevnikov, I.L. Mudrakovsky, M.N. Timofeeva, *J. Mol. Catal.* 60 (1990) 65.
24. A. C. Garade, V. S. Kshirsagar, C. V. Rode, *Appl. Catal. A: Gen.* 354 (2009) 176.
25. A. C. Garade, V. S. Kshirsagar, R. B. Mane, A. A.Ghalwadkar, U. D. Joshi, C. V. Rode, *Appl. Clay Sci.* 48 (2010) 164.
26. T. A. Peters, N. E. Benes, A. Holmen, J. T. F. Keurentjes, *Appl. Catal. A: Gen.* 297 (2006) 182.
27. K. Klepacova, D. Mravec, A. Kaszonyi, M. Bajus, *Appl. Catal. A: Gen.* 328 (2007) 1.
28. G. D. Yadav, N. Kirthivasan, *Appl. Catal. A: Gen.* 154 (1997) 29.
29. Y. Kamiya, Y. Ooka, C. Obara, R. Ohnishi, T. Fujita, Y. Kurata, K. Tsuji, T. Nakajyo, T. Okuhara, *J. Mol. Catal. A: Chem.* 262 (2007) 77.
30. Z. Hou, T. Okuhara, *J. Mol. Catal. A: Chem.* 206 (2003) 121.
31. F. Cavani, M. Corrado, R. Mezzogori, *J. Mol. Catal. A: Chem.* 182-183 (2002) 447.

Chapter IV

Hydroxyalkylation of *p*-cresol to 2, 2'-methylenebis (4-methylphenol)

4.1. INTRODUCTION

Due to their distinctive physico-chemical properties such as ion exchange, swelling, high surface area, acidity and strength etc., clay minerals play a major role in various industrial processes [1]. Clays are layered aluminum silicates in which edge of platelets bear silanol or aluminol groups. Secondly, isomorphic substitutions by lower valence metal ion [Si (IV) by Al (III) or Fe (III) in tetrahedra, Al (III) by Mg (II) and Mg (II) by Li (I) in octahedra] create permanent negative charge which is balanced by cation present in the interlayer space [2]. Clays like montmorillonite and bentonite due to their inherent Brønsted as well as Lewis acidity, are widely used as catalysts for many acid catalyzed reactions [3-5], among which the hydroxyalkylation of *p*-cresol with formaldehye (Scheme 4.1) is an important one. The product of this reaction viz. 2, 2'-methylenebis (4-methylphenol) [DAM] is used as an antioxidant in plastic and rubber industries [6].

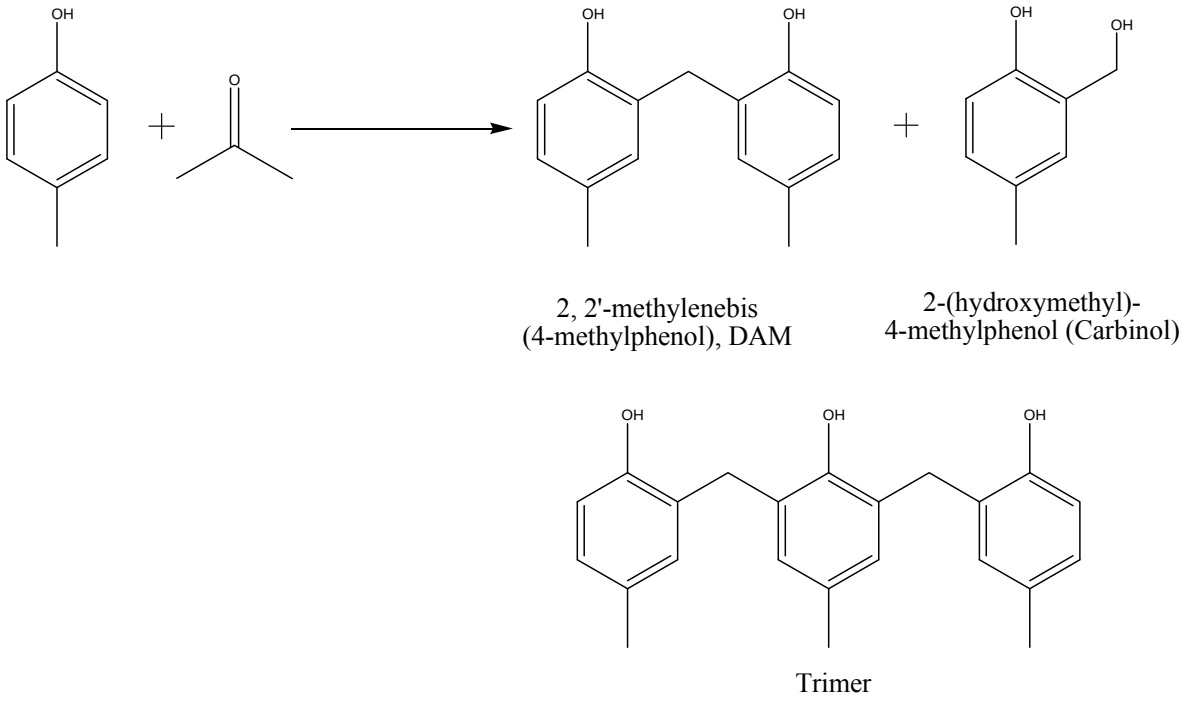

Scheme 4.1. Hydroxyalkylation of *p*-cresol with formaldehyde to give 2, 2'-methylenebis (4-methylphenol), DAM

Conventionally, DAM like bisphenols are synthesized using toxic and corrosive reagents such as phosphoric acid, sulfuric acid etc. Hence designing and developing the solid acid catalysts as well as a process for the hydroxyalkylation of *p*-cresol to give DAM are highly desirable.

Since, hydroxyalkylation of *p*-cresol involves consecutive reactions, designing and developing new catalysts as well as processes which give higher activity and selectivity to DAM is a challenging task in the field of catalysis e.g. with catalyst having weak acidity and strength, predominant formation of carbinol was observed while catalyst having high acidity and strength shows substantial formation of trimer (Scheme 4.1). In this chapter, the hydroxyalkylation of *p*-cresol to give DAM using dodecatungstophosphoric acid (DTP) impregnated on bentonite (BNT) with tuned acidity and commercial montmorillonite is reported [7-9].

4.2. EXPERIMENTAL

DTP impregnated on BNT catalysts (DTP/BNT) were prepared by wet impregnation method and detailed experimental procedure of their preparation has been described in section 2.2.1. The catalysts were characterized by various techniques and the detailed characterization procedure is described in section 2.3. The activities of prepared DTP/BNT and commercial montmorillonite catalysts were evaluated for the hydroxyalkylation of *p*-cresol and its experimental procedure is described in sections 2.4.1 and 2.4.2.

4.3. RESULTS AND DISCUSSION

Hydroxyalkylation of *p*-cresol to DAM was studied using various solid acids. The solid acid catalysts were chosen with varying extent of Brønsted and Lewis acid sites on their surface. The nature and strength of acid sites was also modified by impregnating a heteropolyacid such as DTP on bentonite clay. A detailed study on characterization of these solid acids and their activity evaluation for hydroxyalkylation of *p*-cresol is discussed in the following sections.

4.3.1. DTP impregnated BNT catalyst

Nevertheless, both DTP and BNT alone show the surface acidity, but these if separately used for the hydroxyalkylation of *p*-cresol, show some disadvantages such as (i) DTP, as it is, is soluble in the reaction medium (ii) DAM selectivities are very low (iii) DTP has very low surface area of 8 m^2/g. In order to overcome these drawbacks, it was thought to disperse DTP on BNT, so that truly heterogeneous solid acid catalyst with an appropriate combination of Brønsted and Lewis acidity could be designed. This approach was found to be quite advantageous as evident from the following result and discussions on their structure-activity correlation.

4.3.1.1. Catalyst characterization

4.3.1.1.1. X-ray diffraction

XRD patterns of BNT and 20% DTP/BNT are presented in Figure 4.1.

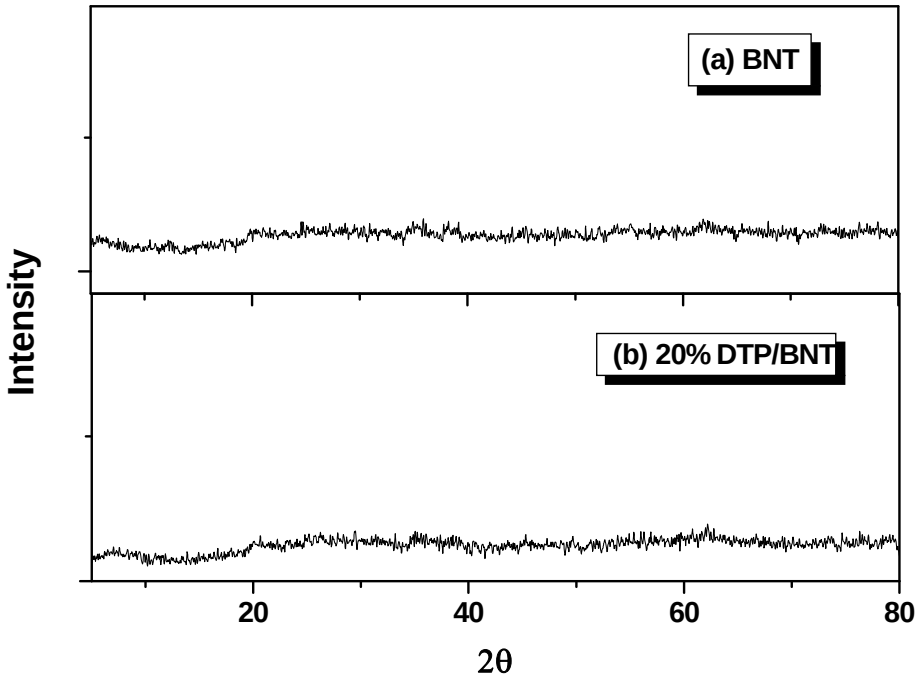

Figure 4.1. XRD patterns of (a) BNT and (b) 20% DTP/BNT

Both parent BNT and 20% DTP/BNT samples showed XRD pattern which is a characteristic of amorphous material. 20% DTP/BNT sample did not show any crystalline phase of bulk DTP, indicating an excellent dispersion of DTP on BNT after impregnation.

4.3.1.1.2. BET surface area measurement

Table 4.1 presents BET surface areas and NH_3-TPD results of various solid acid catalysts. As can be seen from Table 4.1, BET surface area of bulk DTP obtained was 8 m^2/g while that of BNT was 242 m^2/g which decreased to 151 m^2/g after impregnation of 20% DTP. This confirmed that DTP (non-porous material) was well dispersed on BNT support after impregnation. The BET surface areas of various catalysts decreased in the following order: H-β-zeolite > BNT > 20% DTP/ BNT > montmorillonite KSF/O > DTP.

Table 4.1. Textural properties of solid acid catalysts

Catalysts	S_{BET} (m^2/g)	NH_3 adsorbed ($\mu molS^{-1}$)	TPD of NH_3 (%) distribution of acid sites	
			Region I (LT-Peaks)	Region II (HT-Peaks)
BNT	242	4.9	38	62
20% DTP/BNT	151	11.6	40	60
DTP	8	163.8	35	65
Montmorillonite KSF/O	131	15.5	25	75
H-β-Zeolite	650	11.8	63	37

4.3.1.1.3. Ammonia-TPD and pyridine -IR analysis

Figure 4.2 (a–e) shows the NH_3-TPD profiles of various solid acid catalysts, while FT-IR pyridine adsorption spectra of those are presented in Figure 4.3. Among various catalysts, bulk DTP showed the highest concentration of acid sites [163.8 micromoles NH_3 per unit surface area ($\mu molS^{-1}NH_3$), Table 4.1] having a very sharp desorption peak of strongly chemisorbed ammonia at 925 K [10]. Since bulk DTP exhibits purely Brønsted acidity [11], the peaks appeared at 525 and 925 K (Figure 4.2c) having moderate and high acid strength could be assigned to Brønsted acid sites. This was further confirmed by FT-IR pyridine adsorption spectrum of bulk DTP (Figure 4.3c) which showed a peak at 1545 cm^{-1} corresponding to purely Brønsted acidity. Another peak at 1490 cm^{-1} also occurred in the case of bulk DTP, which could be assigned to both Brønsted as well as Lewis acidity. Since, bulk DTP shows only purely Brønsted acidic sites (no peak at 1445 cm^{-1} corresponding to Lewis acidity appeared in the case of bulk DTP), the peak appeared at 1490 cm^{-1} could be assigned to Brønsted acidity.

NH_3-TPD of parent BNT also showed two signals appearing as low (410 K) and high (810 K) temperature regions (Figure 4.2a), which could be assigned to Brønsted and Lewis acid sites respectively [12] and total concentration of acid sites was estimated as 4.9 $\mu molS^{-1}NH_3$. The presence of Brønsted and Lewis acid sites in parent BNT was also confirmed by its FT-IR pyridine adsorption spectrum (Figure 4.3a) which showed peaks at 1445, 1490 and 1545 cm^{-1} and could be assigned to purely Lewis, mixed Brønsted as well as Lewis and purely Brønsted acid sites respectively. Interestingly, the total concentration of acid sites of parent BNT increased significantly from 4.9 to 11.6 $\mu molS^{-1}NH_3$ after impregnation of 20% DTP loading (Figure 4.2, b and Table 4.1), mainly due to the enhancement of Brønsted acid sites that was also evident from a very intense peak (Figure 4.3, b) appearing at 1545 cm^{-1} as compared to a weak peak at 1445 cm^{-1} corresponding to Lewis acidity. This alteration in acidity could be due to the surface modification of BNT by interaction of bulk DTP with its surface hydroxyl groups similar to that of silica [13, 14] which was further confirmed by ^{31}P-CPMAS NMR analysis as discussed later.

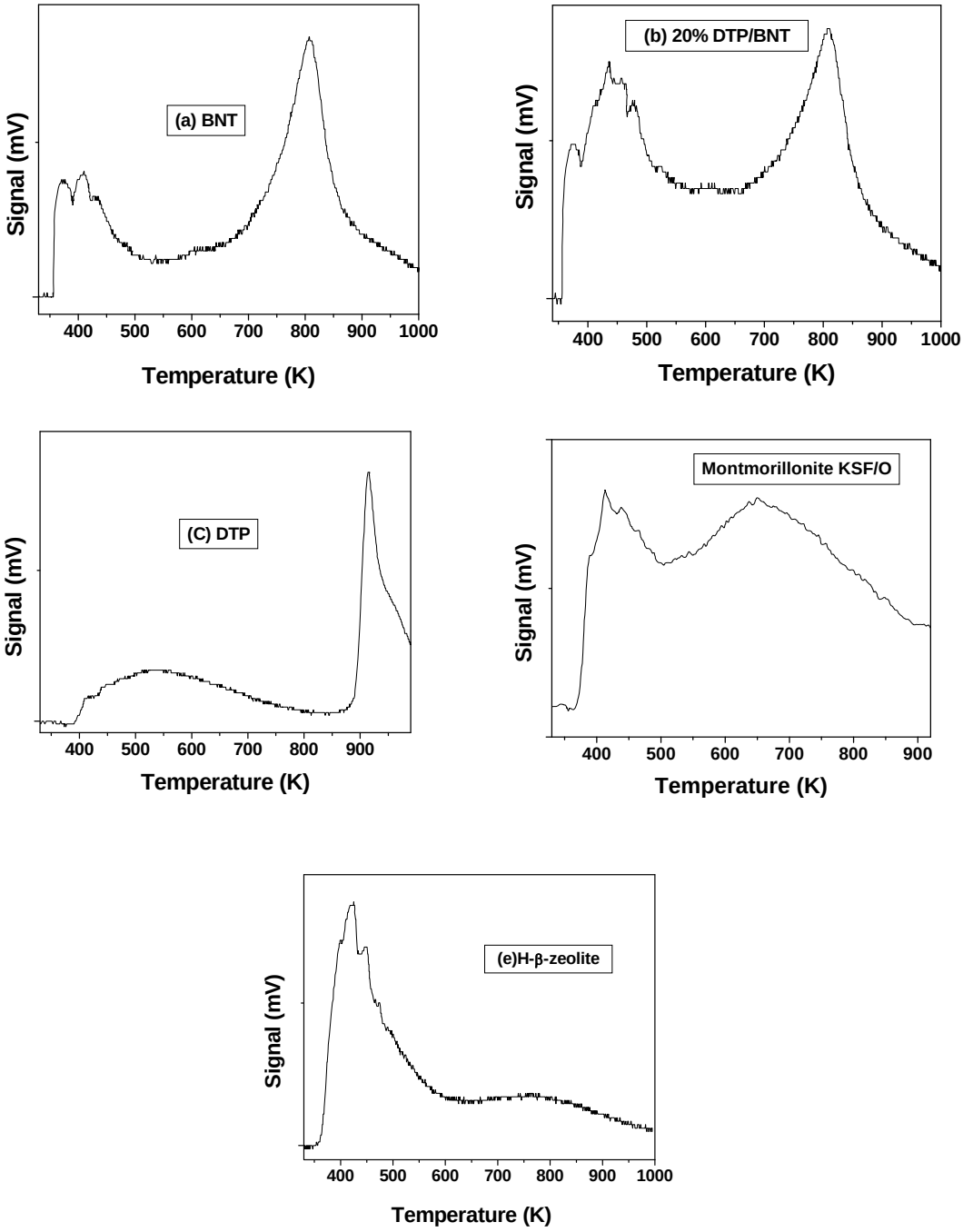

Figure 4.2. Ammonia-TPD profiles for various solid acid catalysts

Montmorillonite KSF/O also showed two types of acid sites having maxima at 425 K and 675 K with highest total acid sites concentration as 15.5 $\mu molS^{-1}NH_3$ (Figure 4.2 d and Table 4.1). In case of montmorillonite KSF/O, concentration of acid sites at high temperature, 675 K was 3 times (75%) higher than that of weak acid sites (25%) at 425 K. As can be seen from Figure 4.3d, montmorillonite KSF/O showed a pyridine desorption peak at 1545 cm^{-1} corresponding to purely Brønsted acid sites. Another peak occurred at 1490 cm^{-1} in FT-IR pyridine adsorption spectrum of montmorillonite KSF/O could be assigned to Brønsted acidity similar to bulk DTP. This also indicates that two adsorption peaks at 425 K and 675 K observed in ammonia-TPD plot of montmorillonite KSF/O were due to the Brønsted acid sites having different acid strengths.

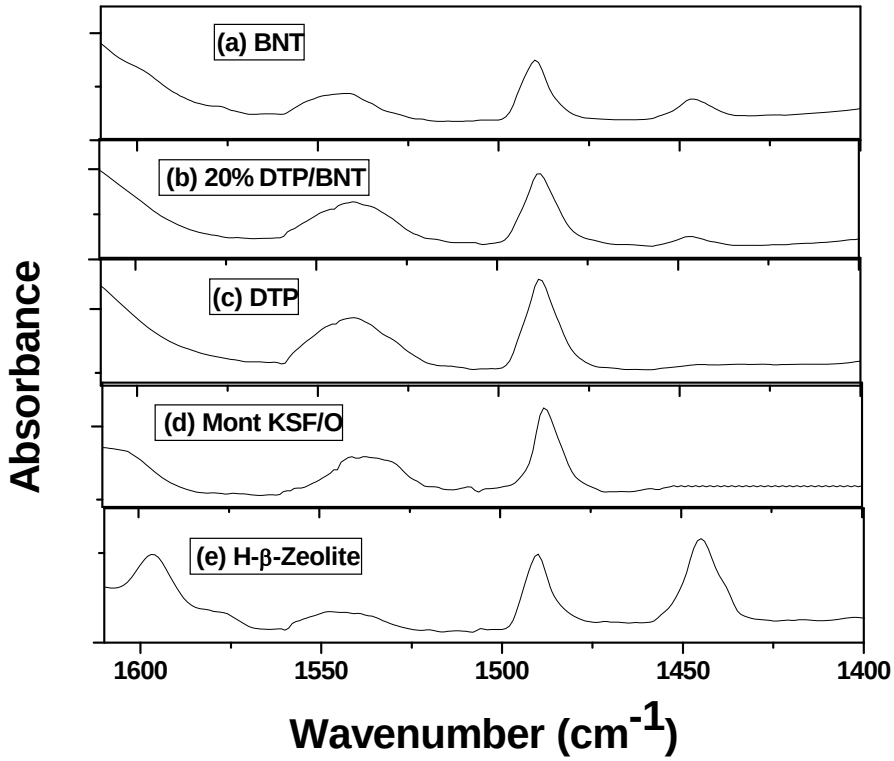

Figure 4.3. FT-IR pyridine adsorption spectra of various solid acid catalysts

H-β-zeolite showed higher concentration of acid sites (63%) in a low temperature region (425 K) having total concentration of acid sites of 11.8 μmolS^{-1} NH_3 (Figure 4.2e and Table 4.1). These acidic sites in a low temperature region could be due to Lewis acidity [15] which was further confirmed by pyridine-IR analysis of H-β-zeolite which showed a very intense peak at 1445 cm^{-1} (Figure 4.3e).

4.3.1.1.4. ^{31}P-CPMAS NMR

Figure 4.4 (a, b) shows ^{31}P-CPMAS NMR of DTP and 20% DTP/BNT. DTP showed a sharp signal at −15.61 ppm that corresponds to tetrahedral co-ordination of PO_4 in the Keggin unit (Chapter 1, Figure 1.3) [16, 17]. Interestingly, 20% DTP/BNT showed a broad signal which shifted towards downfield from −15.61 to −13.7 ppm after impregnation of 20% DTP on it. This broadening of signal could be due to the strong interaction of protons of bulk DTP with surface hydroxyl groups of BNT similar to that observed in case of silica and alumina [18-20]. This interaction leads to the localization of DTP protons thereby increasing their proximity to the Keggin anion because of the decrease in proton mobility as discussed in chapter 3 (section 3.3.1.1.4.) [18]. Such surface as well as acidity modification of BNT due to DTP impregnation enhanced its catalyst activity as discussed below.

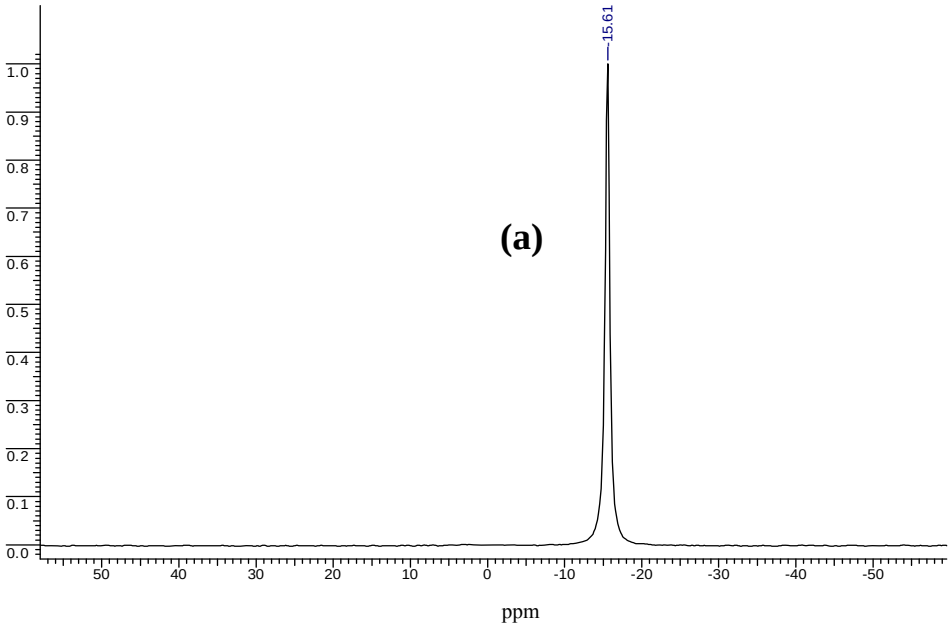

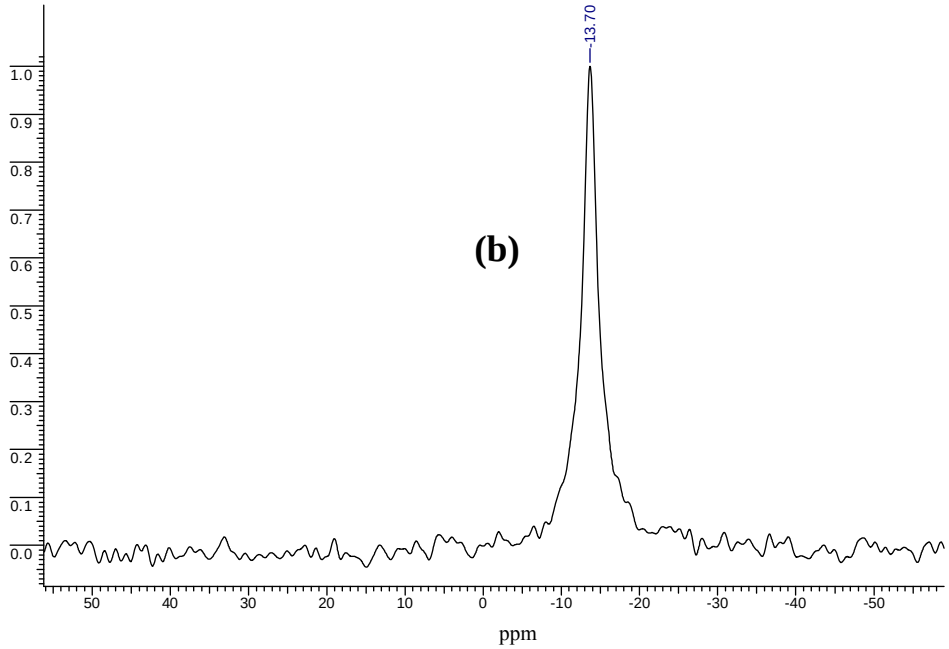

Figure 4.4. ^{31}P- CP MAS NMR spectra of (a) Bulk DTP (b) 20% DTP/BNT

4.3.1.2. Catalyst activity measurement

4.3.1.2.1. Product separation and identification

Hydroxyalkylation of *p*-cresol to the desired DAM product is always accompanied with the formation of carbinol and a trimer due to further reaction of DAM with formaldehyde and phenol as shown in Scheme 4.1. The formation of carbinol was always < 1% while, trimer formation was 5-6% and DAM formed was > 95%. Since the standard samples of DAM and trimer were not available, both these products were separated from the reaction mixture and were thoroughly characterized by ^{1}H-NMR, ^{13}CMR analysis and measuring their physical constants (melting point) as discussed below.

The catalyst was first separated from hot reaction mixture by filtration and the filtrate was then cooled in an ice bath. Toluene was added drop wise into the filtrate till slightly white turbidity appeared (Avoid the excess addition of toluene). The filtrate was then kept overnight at room temperature for crystallization of the trimer which settled as white crystals at the bottom of the flask. The reaction mixture containing DAM, *p*-cresol and

toluene were separated from the trimer by decantation. Toluene was distilled off from the reaction mixture by vacuum distillation on a rotavap and the unreacted *p*-cresol and DAM were separated from each other by column chromatography using 100-200 mesh silica gel column and ethyl acetate/n-hexane as a mobile phase.

The melting points of products viz. DAM and timer are presented in Table 4.2. The melting points of DAM and trimer were matched well with those reported in the literature, thus confirming their structure and purity.

Table 4.2. Physical constant (melting point) of DAM and trimer

Name	**Melting point, K (observed)**	**Melting point, K (reported)**
DAM	398	399
Trimer	487	488

The ^{1}H-NMR spectrum of DAM in $CDCl_3$ is presented in Figure 4.5 and the values of chemical shift of various substituents are given in Table 4.3. The signals at 2.3 and 3.9 ppm confirmed the presence of C**H$_3$**- attached to aromatic ring and C**H$_2$** group flanked between two aromatic rings, respectively. The aromatic protons (Ar-**H**) showed signals at 6.7-7.1 ppm. Two phenolic protons (Ar-O-**H**) also showed a signal in downfield region at ~ 7 ppm.

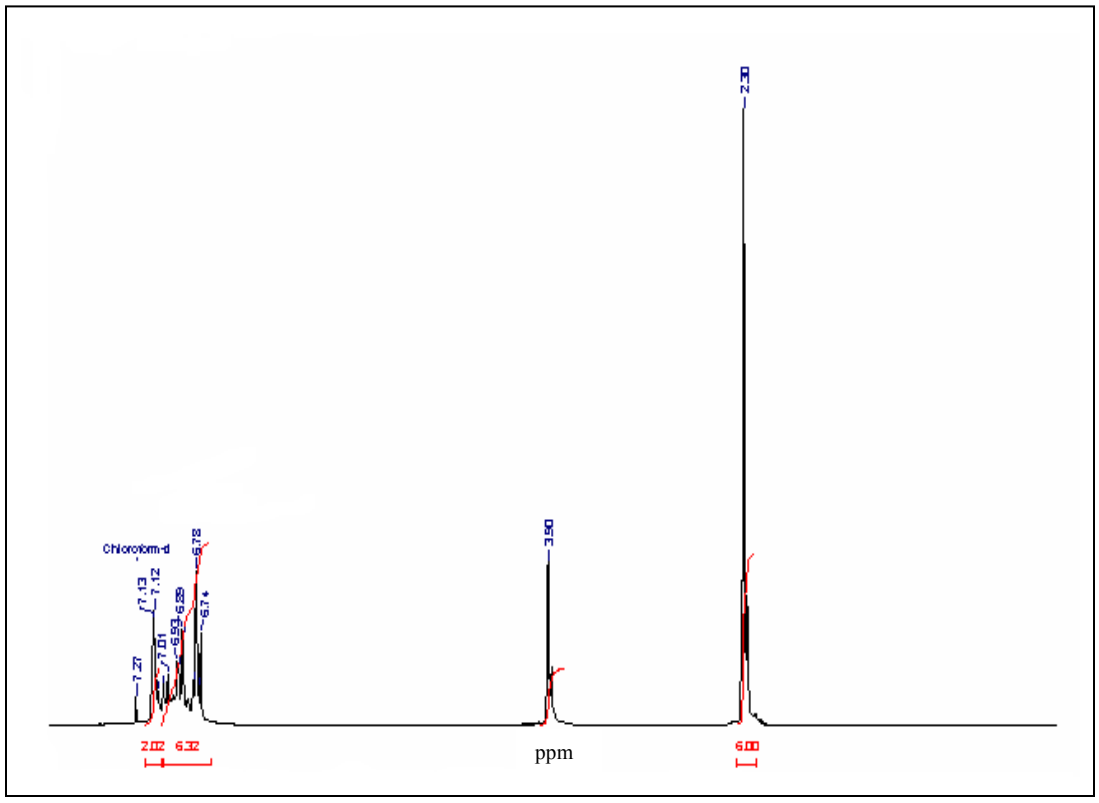

Figure 4.5. ^{1}H-NMR of 2, 2'-methylenebis (4-methylphenol) DAM

Table 4.3. Values of chemical shift for various substituents in ^{1}H-NMR of DAM

Sr. No.	Substituent(s)	No. of protons	Chemical shift (ppm)
1	C**H**$_3$-	6	2.3
2	Ar-C**H**$_2$-Ar	2	3.9
3	Ar-**H**	6	6.7-7.1
4	Ar-O-**H**	2	~ 7

The ^{13}C-NMR spectrum of DAM (in DMSO + $CDCl_3$ solvents) and the values of chemical shift for various substituents are presented in Figure 4.6.

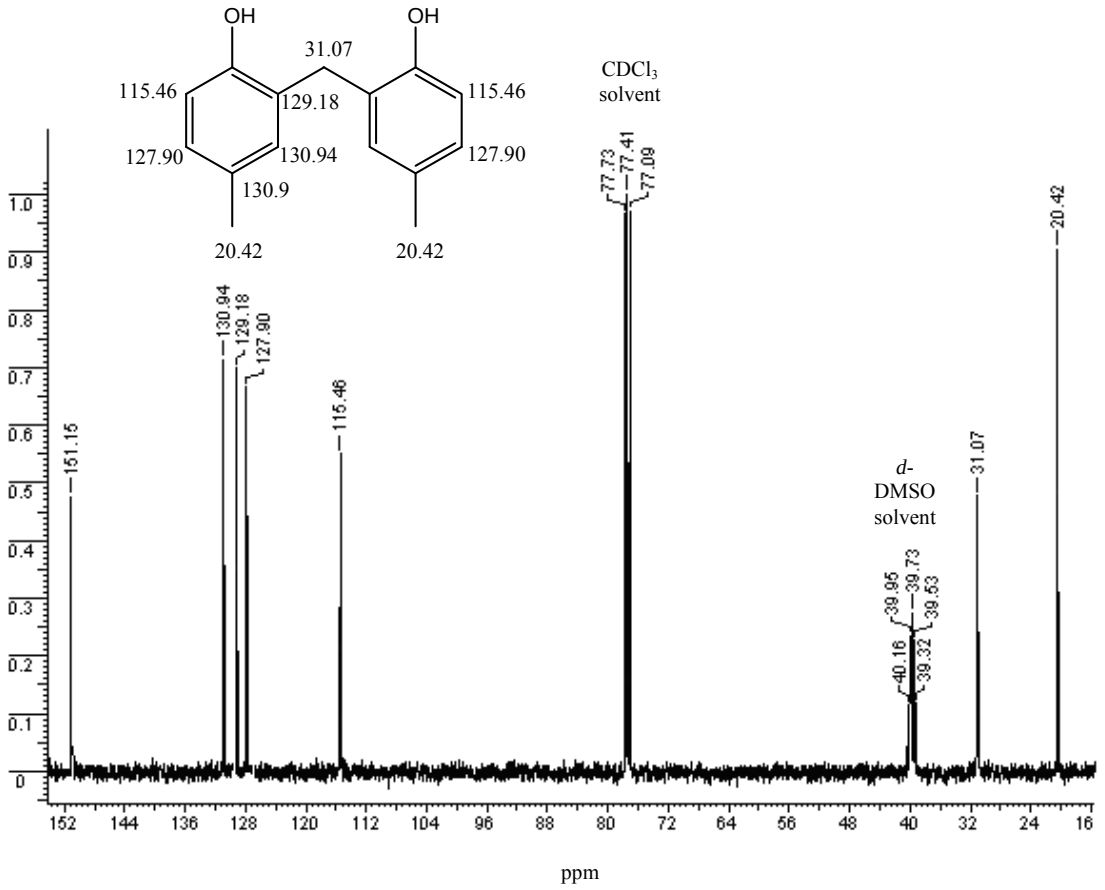

Figure 4.6. ^{13}C-NMR of 2, 2'-methylenebis (4-methylphenol), DAM

Since, DAM and trimers shows almost similar signal for ^{1}H NMR, the structure of DAM was further confirmed by ^{13}C-DEPT (distortionless enhanced polarization transfer) experiment. ^{13}C-DEPT spectrum (Figure 4.7) of DAM shows four positive peaks at 20.42, 115.46, 127.90 and 130.94 ppm. The peak at 20.42 ppm could be assigned to "**C**H_3"carbon attached to the aromatic ring. The other three positive peaks at 115.46, 127.90 and 130.94 ppm correspond to aromatic "**C**H" carbon containing only one hydrogen atom. The occurrence of only one negative peak at 31.07 ppm characteristic of "**C**H_2" carbon indicates the presence of one methylene group attached to the aromatic ring and thus confirmed the structure of DAM.

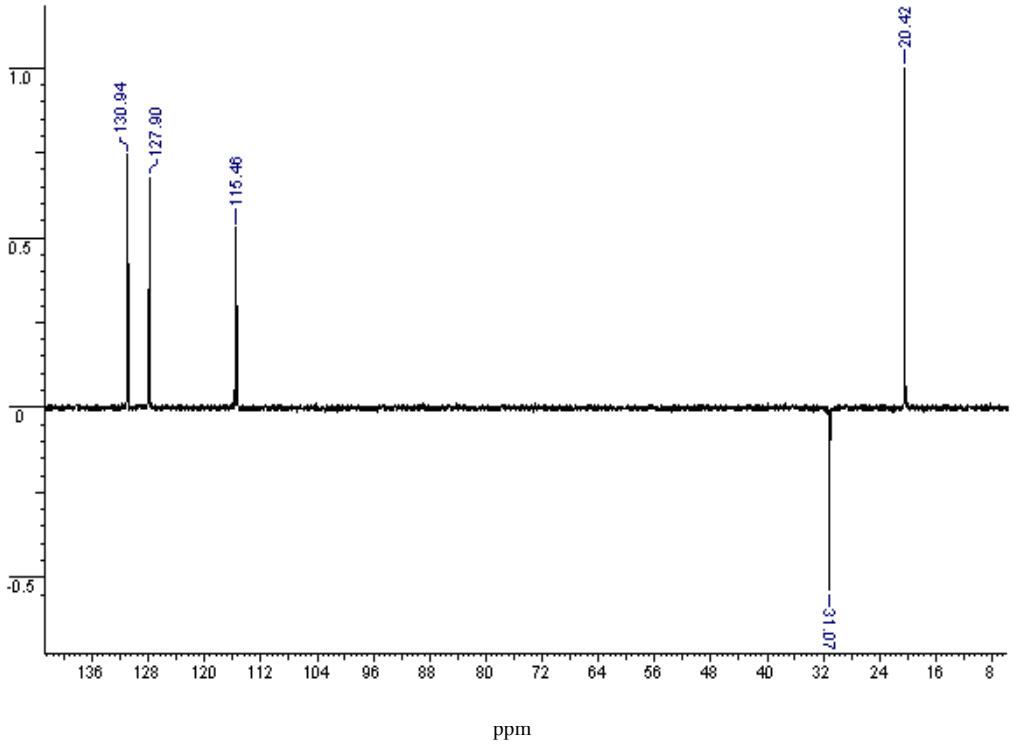

Figure 4.7. ^{13}C-DEPT spectrum of 2, 2'-methylenebis (4-methylphenol), DAM

4.3.1.2.2. Catalyst screening

The catalyst activity results of various solid acid catalysts are presented in Figure 4.8. Performances of various catalysts were evaluated in terms of % product yields and % product selectivity, which are defined as follows:

$$(\%)\ Product\ Yield = \frac{\Sigma\ Actual\ moles\ of\ \ product\ \ formed}{Expected\ moles\ of\ \ product\ \ formed\ based\ on\ \ formaldehyde\ consumed}\ X\ 100 \qquad (4.1)$$

$$(\%)\ Selectivity = \frac{moles\ of\ \ a\ \ product\ \ formed}{\Sigma\ moles\ of\ \ all\ the\ \ products\ \ formed}\ X\ 100 \qquad (4.2)$$

In all the activity measurement experiments, the molar ratio of *p*-cresol to formaldehyde was kept at 5 which was found to be optimum, according to my earlier work (chapter 3, section 3.3.1.2.2).

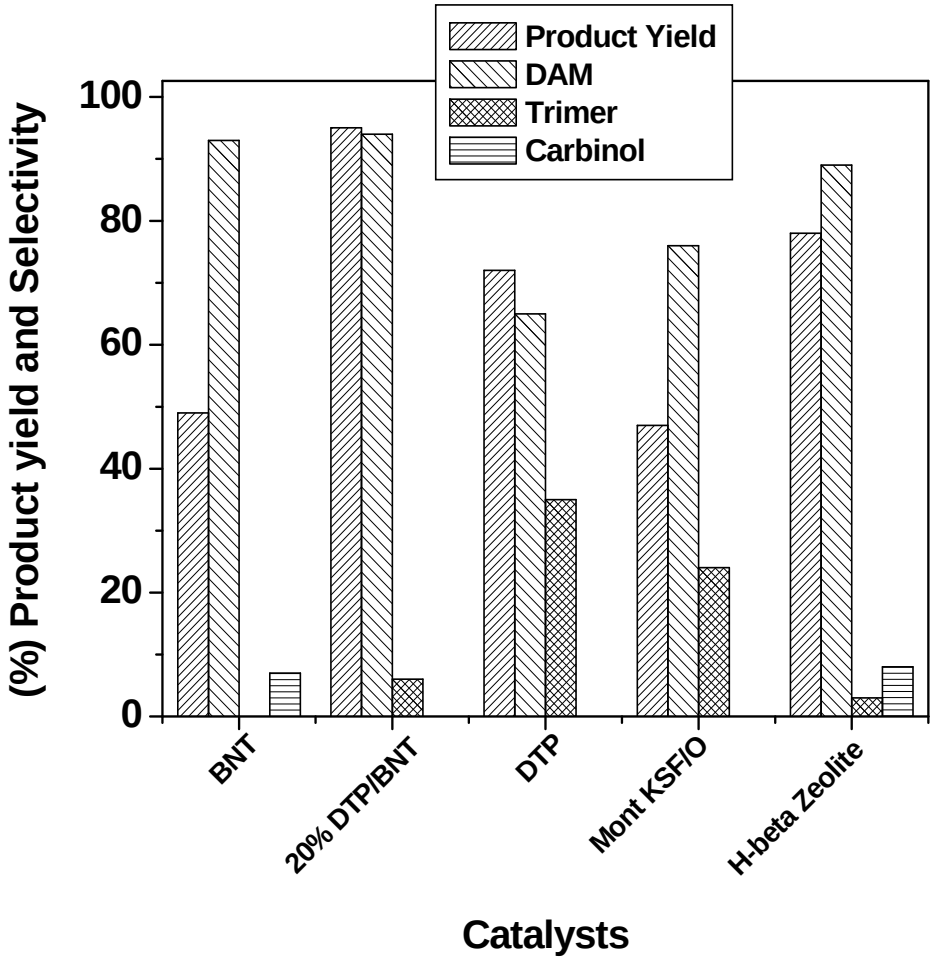

Figure 4.8. Catalyst screening for hydroxyalkylation of *p*-cresol

Reaction conditions: *p*-cresol, 42.5 mmol; formaldehyde, 8.5 mmol; mole ratio of *p*-cresol to formaldehyde, 5; catalyst concentration, 0.03 g/cm^3; temperature, 353 K; time, 1 h; solvent, toluene (12 cm^3).

Among the various catalysts studied for the hydroxyalkylation of *p*-cresol, parent BNT showed 49% product yield with 96 and 4% selectivity to DAM and carbinol respectively, while bulk DTP showed 72% product yield with 65% selectivity to DAM. The lower DAM selectivity with bulk DTP was due to its high acidity (163.8 μmolS^{-1} NH_3) as well as due to presence of only Brønsted acid sites having high strength (65%) in a high

temperature region which facilitates the formation of a trimer by reaction of initially formed DAM with formaldehyde followed by *p*-cresol. Some undetected tarry products were also observed with bulk DTP which resulted into lowering the mass balance from 80 to 85%.

Interestingly, surface modified 20% DTP/BNT catalyst showed the highest product yield of 95% with 94% selectivity to DAM. The highest product yield with 20% DTP/BNT catalyst was due to the increase in total concentration of acid sites especially that of Brønsted acid sites, from 4.9 to 11.6 $\mu molS^{-1}$ NH_3 and the stabilization of intermediate carbocation formed during the reaction by heteropolyanion of DTP (Scheme 4.2) as discussed in chapter 3 (section 3.3.1.2.7.) [21].

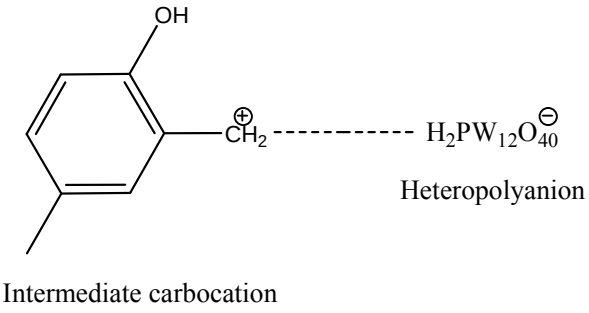

Scheme 4.2. Stabilization of intermediate carbocation by heteropolyanion of DTP

Montmorillonite KSF/O showed 47% product yield, with a lower selectivity (76%) to DAM due to the predominant formation of a trimer (24%) facilitated by its high acidity (15.5 $\mu molS^{-1}$ NH_3) and the presence of Brønsted acid sites (75%) in a high temperature region. Although, H-β-zeolite showed the total acid sites concentration (11.8 $\mu molS^{-1}$ NH_3) similar to 20% DTP/BNT, however lower product yield (78%) with 89% selectivity to DAM was observed with a substantial formation of carbinol (8%) due to the presence of more Lewis acid sites (63%) in a low temperature region.

4.3.1.2.3. Catalyst recycle

Catalyst recycle experiments were carried out using 20% DTP/BNT catalyst according to the procedure discussed in section 3.3.1.2.6. The catalyst was found to retain its activity even after the third recycle experiment showing 95% product yield (Figure 4.9). The selectivity to DAM (94%) remained constant for all the three recycle experiments.

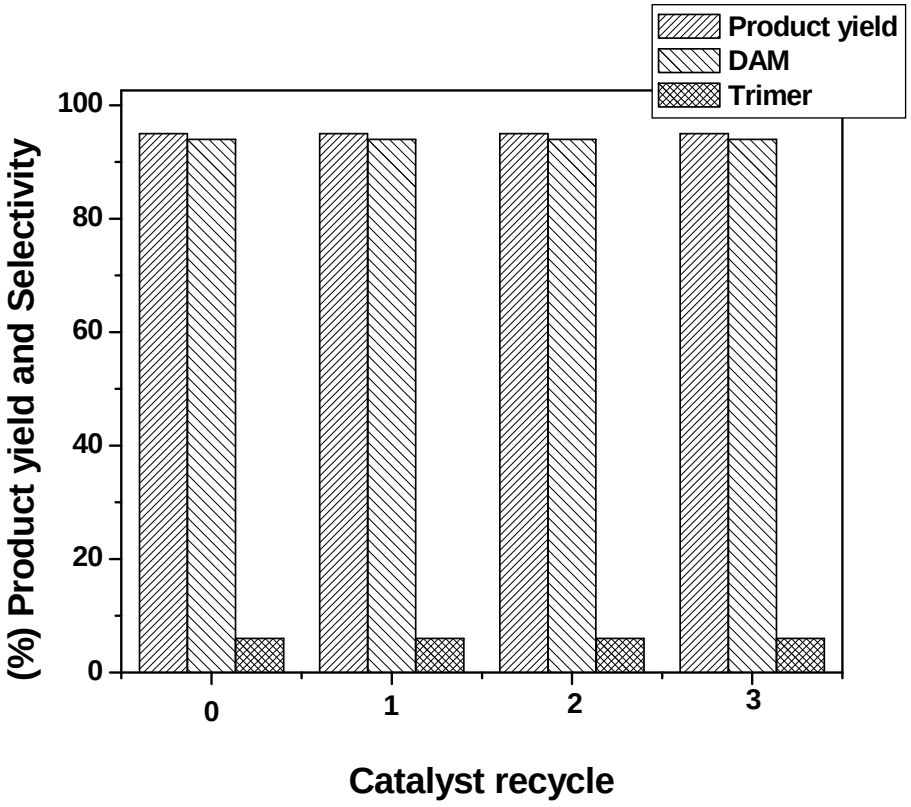

Figure 4.9. Catalyst recycle

Reaction conditions: *p*-cresol, 42.5 mmol; formaldehyde, 8.5 mmol; mole ratio of *p*-cresol to formaldehyde, 5; catalyst concentration, 0.03 g/cm^3; temperature, 353 K; time, 1 h; solvent, toluene (12 cm^3).

4.3.2. Commercial montmorillonite catalyst

The commercial montmorillonite as procured was used for the hydroxyalkylation reaction of *p*-cresol. In this work, montmorillonite was compared with higher surface area material like TS-1 and lower surface area material like bulk DTP, with varying nature and strengths of acid sites on the surface. It was found that neither surface area nor acidity alone are responsible in achieving the highest selectivity to DAM, but the distribution of acid sites are decisive in achieving the highest selectivity to DAM.

4.3.2.1. Catalyst characterization

Table 4.4 presents the specific BET surface areas and NH_3-TPD results of montmorillonite clay, TS-1 and DTP. TS-1 showed the highest surface area of 410 m^2/g while that of DTP was as low as 8 m^2/g. The surface areas of various catalysts were in the following order: TS-1 > montmorillonite clay > DTP.

Table 4.4. Textural properties of the catalysts

Catalysts	S_{BET} (m^2/g)	NH_3 adsorbed ($\mu molS^{-1}$)	TPD of NH_3 (%) distribution of acid sites	
			Region I (LT-Peaks)	Region II (HT-Peaks)
Montmorillonite	60	40	64	36
TS-1	410	2.9	100	-
DTP	8	163.8	35	65

NH_3-TPD profiles of montmorillonite clay, TS-1 and DTP are shown in Figure 4.10 and the values of ammonia adsorbed are presented in Table 4.4. DTP showed two desorption peaks, one for the strongly chemisorbed ammonia at 925 K (curve b, in Figure 4.10) and another at 525 K having the highest total acid site concentration of 163.8 $\mu molS^{-1}$ NH_3. Montmorillonite sample also exhibited two desorption peaks, one for the strongly

chemisorbed ammonia in the range of 775-925 K (curve a in Figure 4.10) and another at 473 K. However, the amount of ammonia desorbed at low temperature was more than 1.8 times than that at higher temperature. Interestingly, TS-1 showed only one peak in the low temperature region at 373-473 K (curve c in Figure 4.10).

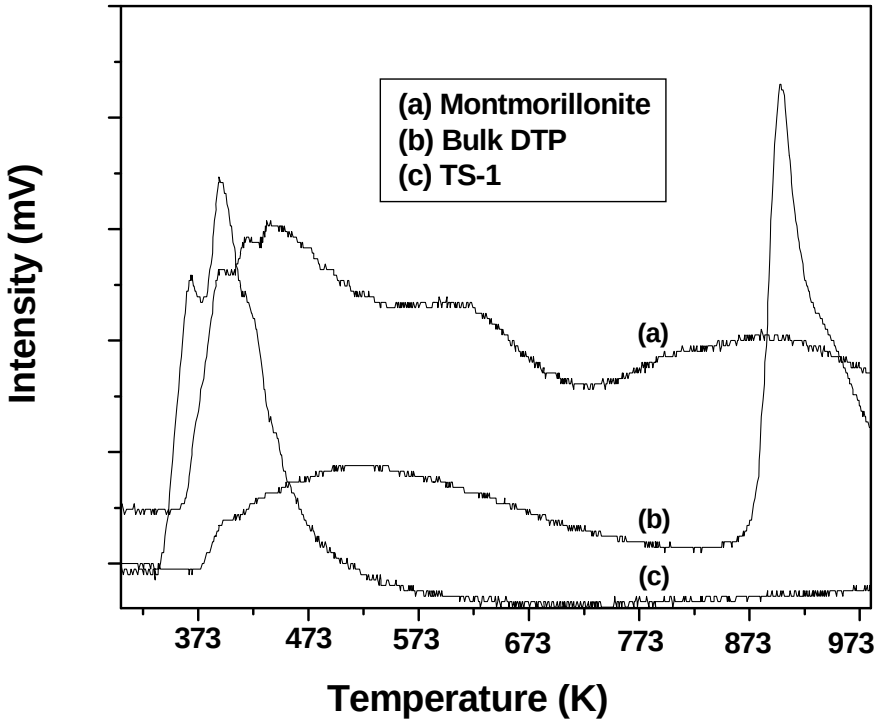

Figure 4.10. Ammonia TPD profiles for montmorillonite clay, DTP and TS-1

4.3.2.2. Catalyst activity measurement

4.3.2.2.1. Catalyst screening

Comparison of activities of montmorillonite clay with those of TS-1 and DTP for hydroxyalkylation of *p*-cresol are presented in Figure 4.11. Performances of various catalysts were evaluated in terms of (%) conversion of *p*-cresol and (%) product selectivity which are defined by Eqs. (4.3) and (4.4) respectively.

$$(\%)\,Conversion = \frac{Initial\ conc.\ of\ p\text{-}cresol - Final\ conc.\ of\ p\text{-}cresol}{Initial\ conc.\ of\ p\text{-}cresol}\ \text{X}\ 100 \qquad (4.3)$$

$$(\%)\ Selectivity = \frac{moles\ of\ a\ product\ formed}{\Sigma\ moles\ of\ all\ the\ products\ formed}\ X\ 100 \qquad (4.4)$$

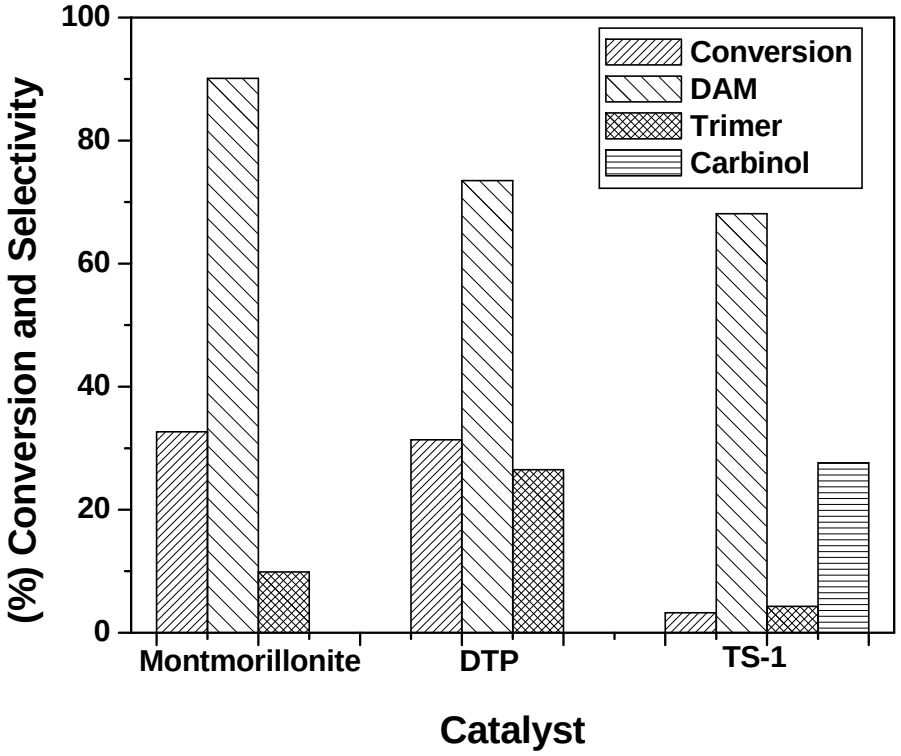

Figure 4.11. Catalyst screening for hydroxyalkylation of *p*-cresol

Reaction conditions: *p*-cresol, 9.26 mmol; catalyst concentration, 0.042 g/cm^3; temperature, 353 K; mole ratio of *p*-cresol to formaldehyde, 5; time, 2 h; solvent, toluene.

Among the three catalysts with different acidity and strength, montmorillonite clay showed highest activity (32% conversion of *p*-cresol with 91% selectivity to DAM) while TS-1 showed the lowest activity (< 4% conversion of *p*-cresol) in spite of it's highest surface area (410 m^2/g). The lowest activity (< 4% conversion of *p*-cresol) of TS-1 could be attributed to its lowest acidity (2.9 μmolS^{-1} NH_3) as well as the presence of only Lewis acidic sites in the low temperature region at 373-473 K [22, 23]. Although, DTP showed

p-cresol conversion similar to montmorillonite, lower selectivity (73%) to DAM was obtained due the predominant formation of a trimer (27%). Montmorillonite showed catalyst activity (*p*-cresol conversion) similar to that of DTP, although the total acidity of later was 4 times higher than that of former, indicating that beyond a certain value, total acidity does not affect the activity of the catalyst. However, selectivity to the desired DAM was maximum (> 90%) in case of montmorillonite which could be due to the presence of acidic sites in the low and high temperature region in an appropriate proportion. DTP showed highest acid strength having 65% acid sites present in a high temperature region (925 K) which results into formation of a trimer hence lowering the DAM selectivity to 73%. In case of TS-1, only low temperature acid sites were present which resulted in lowest selectivity to DAM because of predominant formation of carbinol. This clearly indicates that along with total acidity, the nature of acid sites as well as the acid strength is crucial in determining the activity and selectivity performance for hydroxylation of *p*-cresol. Since, montmorillonite clay was found to be the best catalyst because of its mixed acidic sites [24] for hydroxyalkylation of *p*-cresol, further study on the effect of reaction parameters on activity and selectivity was carried out using the same clay catalyst.

4.3.2.2.2. Effect of mole ratio

Mole ratio of *p*-cresol to formaldehyde plays a significant role in hydroxyalkylation of *p*-cresol (Figure 4.12). For a mole ratio < 2, *p*-cresol conversion was almost negligible while, highest conversion of *p*-cresol achieved was 53% as the mole ratio of *p*-cresol to formaldehyde increased from 2 to 3. However at this mole ratio, selectivity to DAM obtained was 77% while the other product formed was a trimer. The conversion of *p*-cresol decreased from 53 to 32% and selectivity to DAM increased from 77 to 90% when the mole ratio of *p*-cresol to formaldehyde increased from 3 to 5. This decrease in conversion of *p*-cresol was obvious, since *p*-cresol was used in excess as compared to formaldehyde and the reaction was almost ceased when all formaldehyde was consumed in hydroxyalkylation reaction, thus preventing further *p*-cresol conversion. The lower concentration of formaldehyde also retards the further reaction of a DAM with *p*-cresol;

hence selectivity to DAM is maximum for higher molar ratio of *p*-cresol to formaldehyde. Similar results were obtained for the hydroxyalkylation of phenol with acetone for the bisphenol A synthesis [25].

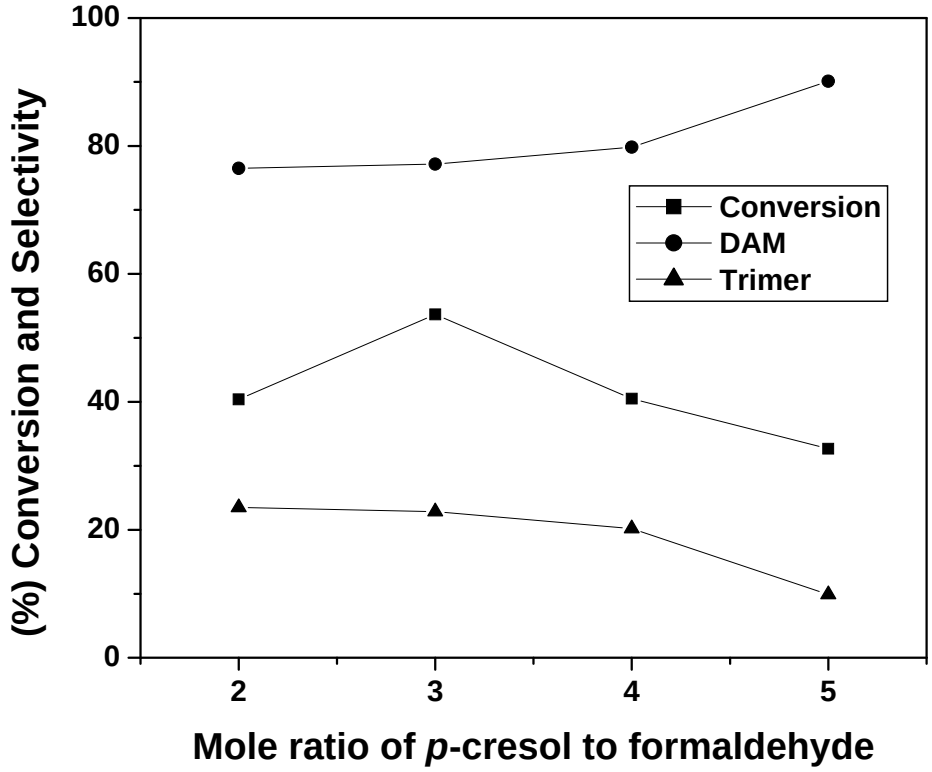

Figure 4.12. Effect of mole ratio of *p*-cresol to formaldehyde on conversion and selectivity

Reaction conditions: *p*-cresol, 9.26 mmol; catalyst concentration, 0.042 g/cm^3; temperature, 353 K; time, 2 h; solvent, toluene.

4.3.2.2.3. Effect of reaction time

Since the hydroxyalkylation reaction involves first the formation of an intermediate carbinol, then DAM and its further reaction with initial substrate to give undesired trimer and oligomers, it was important to study the effect of reaction time on conversion and

selectivity pattern and results are presented in Figure 4.13. *p*-Cresol conversion increased from 12 to 53% while, the selectivity to DAM decreased from 90 to 77% and that of trimer increased from 10 to 23% with increase in reaction time from 0.5 to 2 h. This decrease in selectivity to DAM was mainly because of the reaction of initially formed DAM with formaldehyde followed by, with *p*-cresol.

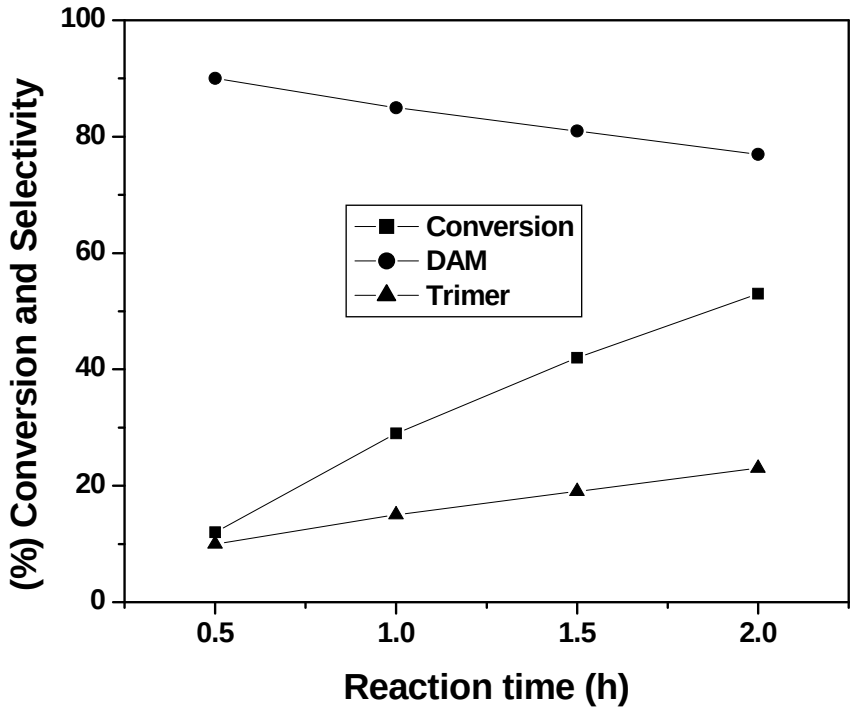

Figure 4.13. Time vs. conversion and selectivity plot

Reaction conditions: *p*-cresol, 9.26 mmol; catalyst concentration, 0.042 g/cm^3; temperature, 353 K; mole ratio of *p*-cresol to formaldehyde, 3; time, 2 h; solvent, toluene.

4.3.2.2.4. Effect of temperature

The effect of temperature on both conversion of *p*-cresol and selectivity to DAM was studied in a temperature range 313-373 K (Figure 4.14). The conversion of *p*-cresol was < 5% at 313 and 333 K which increased to 53% with increase in temperature up to 353 K and remained almost constant up to 373 K. The selectivity to DAM also increased from

53 to 77% with increasing temperature from 333 to 353 K, then remained constant up to 373 K. There was considerable amount of carbinol (2-(hydroxymethyl)-4-methyl phenol) (36%) formed at 333 K, which was then converted into DAM when temperature was raised to 353 K resulting in enhanced selectivity to DAM.

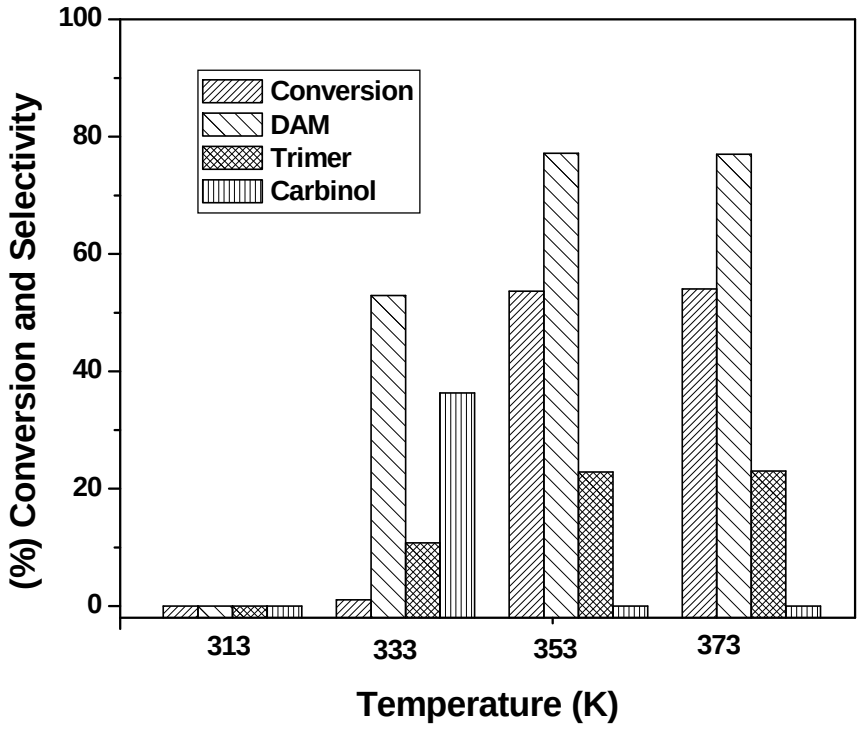

Figure 4.14. Effect of temperature on conversion and selectivity
Reaction conditions: *p*-cresol, 9.26 mmol; catalyst concentration, 0.042 g/cm^3; mole ratio of *p*-cresol to formaldehyde, 3; time, 2 h; solvent, toluene.

4.3.2.2.5. Effect of catalyst concentration

The effect of catalyst concentration on the conversion of *p*-cresol and product distribution was studied in the range of 0.014-0.042 g/cm^3 at 353 K and at the mole ratio of *p*-cresol to formaldehyde as 3. The conversion of *p*-cresol increased from 25 to 53% with increasing catalyst concentration from 0.014 to 0.042 g/cm^3 (Figure 4.15).

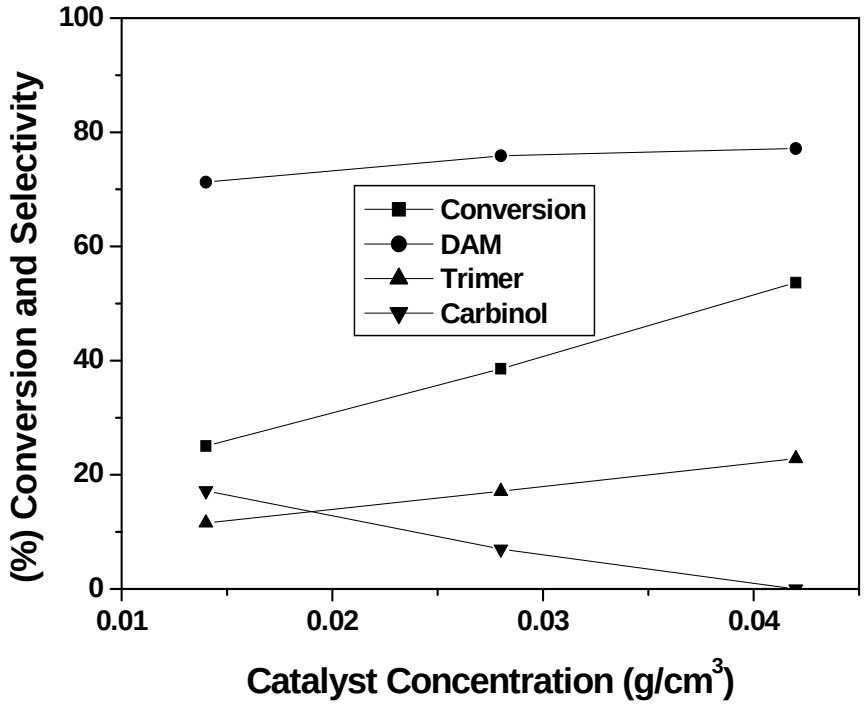

Figure 4.15. Effect of catalyst concentration on conversion and selectivity
Reaction conditions: *p*-cresol, 9.26 mmol; temperature, 353 K; mole ratio of *p*-cresol to formaldehyde, 3; time, 2 h; solvent, toluene.

The maximum conversion (53%) was observed with catalyst concentration of 0.042 g/cm^3. At the lowest catalyst concentration of 0.014 g/cm^3, selectivity to DAM achieved was 71% which marginally increased to 77%, when the catalyst concentration was increased to 0.042 g/cm^3. The selectivity to the trimer [2, 2'-(2-hydroxy-5-methyl-1, 3-phenylene)bis(methylene)bis(4-methylphenol)] increased from 12 to 23% with increasing catalyst concentration from 0.014 to 0.042 g/cm^3. The predominant formation of carbinol (2-(hydroxymethyl)-4-methyl phenol) (17%) was observed at lower catalyst concentration (0.014 g/cm^3) which then decreased steeply due to its further reaction with *p*-cresol to form DAM, with increase in catalyst loading up to 0.042 g/cm^3.

4.3.2.2.6. Effect of solvents

Figure 4.16 shows the role of solvents having different polarity viz decane, toluene and isopropyl alcohol. The *p*-cresol conversion was < 5% for highly polar solvent such as isopropyl alcohol. This could be explained based on the competition between isopropyl alcohol and formaldehyde for active Brønsted acid sites of montmorillonite. Since nucleophilicity of the oxygen atom of isopropyl alcohol is higher than that of formaldehyde, causing better protonation of isopropyl alcohol than formaldehyde resulted in lower conversion of *p*-cresol. With less polar solvents like n-decane and toluene, the conversion of *p*-cresol was much higher than that for polar solvent. Toluene showed the highest conversion of *p*-cresol (53%) and selectivity (77%) to DAM.

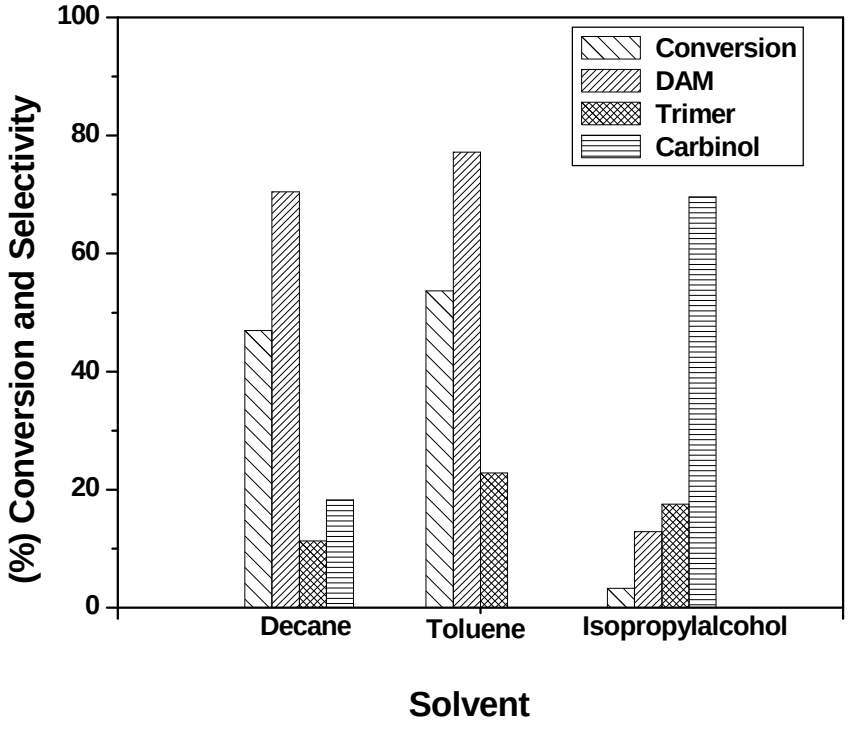

Figure 4.16. Role of solvent in hydroxyalkylation of *p*-cresol

Reaction conditions: *p*-cresol, 9.26 mmol; catalyst concentration, 0.042 g/cm^3; temperature, 353 K; mole ratio of *p* -cresol to formaldehyde, 3; time, 2 h.

4.3.2.2.7. Catalyst recycle

Catalyst recycle experiments were carried out at 353 K using *p*-cresol/ formaldehyde mole ratio 3 for 2 h with catalyst concentration (montmorillonite) 0.042 g/cm^3, as follows. After the first hydroxyalkylation run the used catalyst was filtered and washed with methanol followed by several times with deionized water. Then the catalyst was dried in an oven at 393 K for 8 h and reused for the subsequent run. The procedure was followed for two subsequent hydroxyalkylation experiments. The catalyst was found to retain its activity even after the second recycle without affecting the conversion of *p*-cresol (53%) (Figure 4.17). The selectivity of DAM (77%) was also almost the same for three experiments.

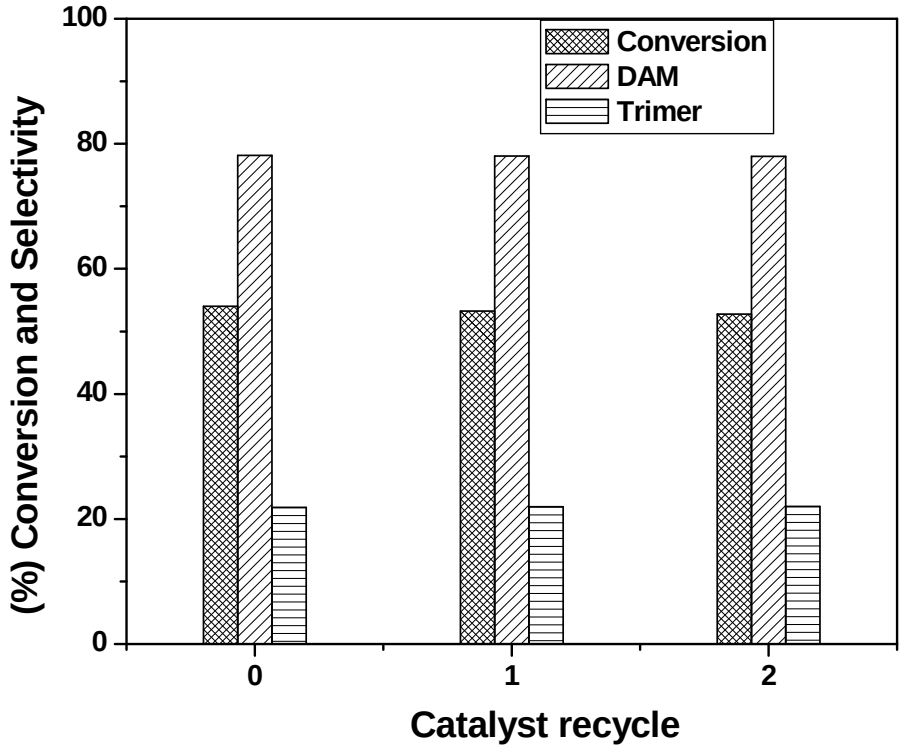

Figure 4.17. Catalyst recycle

Reaction conditions: *p*-cresol, 9.26 mmol; catalyst concn, 0.042 g/cm^3; temperature, 353 K; mole ratio of *p*-cresol to formaldehyde, 3; time, 2 h; solvent, toluene.

4.3.3. Continuous hydroxyalkylation of *p*-cresol to gives DAM over montmorillonite KSF/O

Montmorillonite clays due to their inherent acidity are widely used for the hydroxyalkylation reaction. However, an undesired trimer and higher homologues are predominantly formed in a batch reactor if acidity and strength of montmorillonite clays are very high e.g. montmorillonite KSF/O having high acidity (total acid sites concentration as 15.5 $\mu molS^{-1}NH_3$) and strength (75% acid sites in a high temperature region, 675 K) showed lower DAM selectivity (76%) due to substantial formation of trimer (24%) in a batch reactor. The selectivity to DAM can be enhanced and the catalyst can be effectively used by shifting the hydroxyalkylation process from batch to continuous mode of operation. In the present work, several montmorillonite clays with varying values of surface areas and acidity were evaluated for a continuous hydroxyalkylation of *p*-cresol to DAM.

4.3.3.1. Catalyst characterization

Table 4.5 presents BET surface area and NH_3-TPD results of various montmorillonite samples. The surface areas of various catalysts were in the following order: Montmorillonite K30 > Montmorillonite (Al-Pillared clay) > Montmorillonite K10 > Montmorillonite KP-10 > Montmorillonite KSF/O.

Table 4.5. Textural properties of the montmorillonite K-catalysts

Catalysts	BET (m^2/g)	NH_3 adsorbed ($\mu mol\ S^{-1}$)	TPD of NH_3 (%) distribution of acidic sites	
			LT-Peak (425 K)	HT-Peak (675 K)
Montmorillonite K30	327	4.4	38	62
Montmorillonite(Al-Pillared clay)	251	5.0	25	75
Montmorillonite K10	230	8.1	52	48
Montmorillonite KP10	149	12.2	39	61
Montmorillonite KSF/O	128	15.5	25	75

NH_3-TPD profiles of various montmorillonite clays are shown in Figure 4.18 and the values of ammonia adsorbed are presented in Table 4.5. Among various types of montmorillonite clay materials, montmorillonite KSF/O showed the highest concentration of acid sites (15.5 μmol S^{-1} NH_3) having two desorption peaks in the low (425 K) and high (675 K) temperature region having percentage distribution of 25 and 75% respectively. Similar to the montmorillonite KSF/O, other montmorillonite catalysts also showed two desorption peaks in the low and high temperature regions having acid sites concentration ranging from 4.4 to 12.2 μmol S^{-1} NH_3 (Table 4.5 and Figure 4.18).

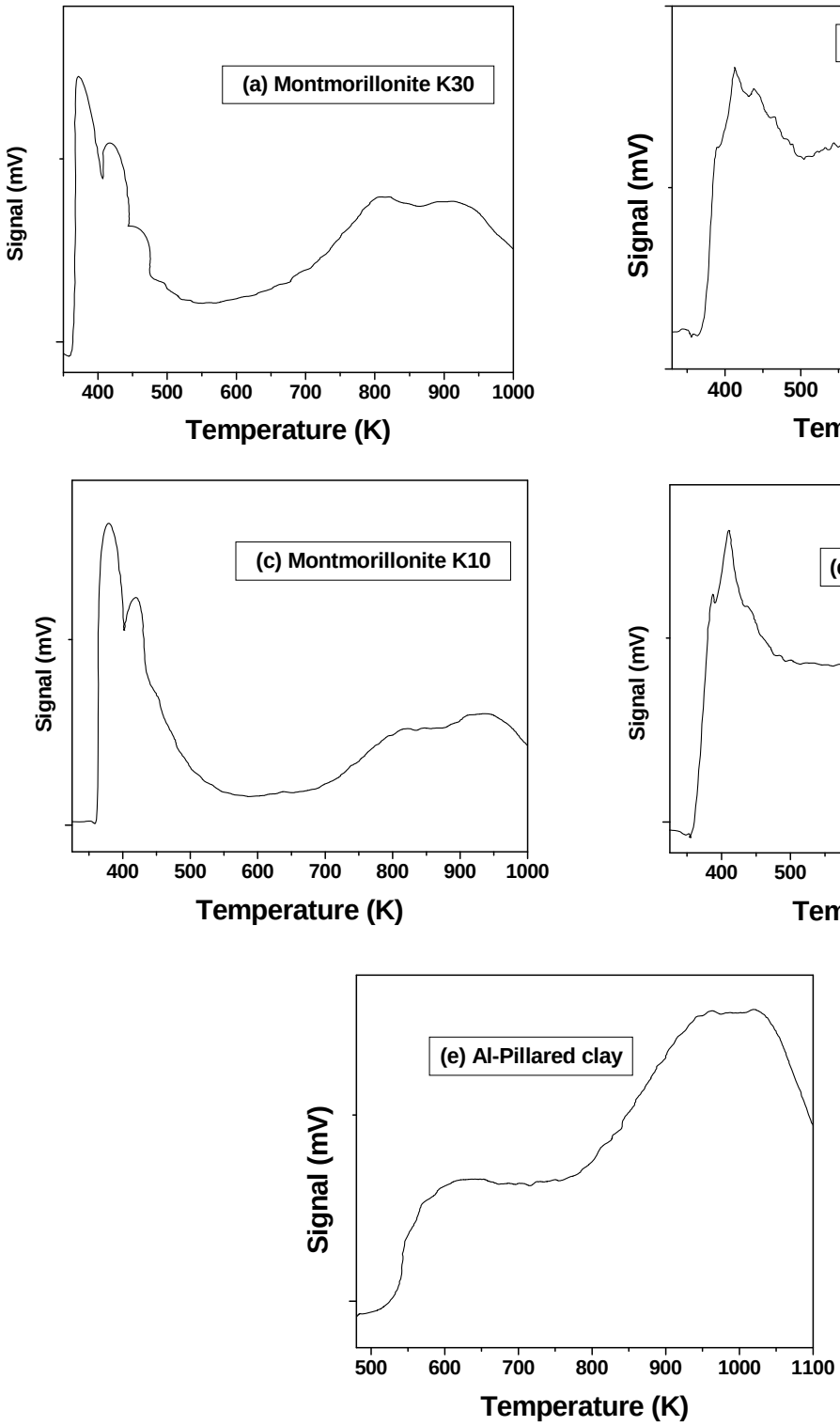

Figure 4.18. Ammonia TPD profiles for various montmorillonite clay catalysts

4.3.3.2. Catalyst activity testing

4.3.3.2.1. Catalyst screening

Montmorillonite KSF/O having strong Brønsted acidity and strength shows low DAM selectivity (75%) due to formation of a trimer as discussed in previous section 4.3.1.2.2 which increases continuously with time in a batch reactor. If time or other parameters like temperature is lowered in order to achieve high DAM selectivity, very low *p*-cresol conversion or DAM yield was observed. These problems associated with batch reactor could be overcome by shifting hydroxyalkylation process from batch to continuous (fixed bed) reactor. The catalyst activity results of montmorillonite KSF/O in a batch and fixed bed reactor are presented in Table 4.6. Montmorillonite KSF/O showed a higher catalyst activity (26% conversion of *p*-cresol with 92% selectivity to DAM) in a continuous fixed bed reactor as compared to batch reactor (< 4% conversion of *p*-cresol) under similar reaction conditions. The higher activity of montmorillonite KSF/O in a continuous fixed bed reactor as compared to a batch reactor could be due to more exposure of reactants to the active acidic sites present on the catalyst surface and less poisoning of active sites by the polar water molecules present in a formalin solution as well as formed during the progress of the reaction as discussed latter in section 4.3.3.2.2.

Table 4.6. Catalyst activity of montmorillonite KSF/O for hydroxyalkylation of *p*-cresol in a batch and fixed bed reactor

Sr. No.	Reactor	Conversion (%)	Selectivity (%)	
			DAM	Trimer
1	Continuous	26	92	8
2	Batch	3.8	88	12

Reaction conditions: *p*-cresol, 42.6 mmol; formaldehyde, 8.52 mmol; mole ratio of *p*-cresol to formaldehyde, 5; catalyst concentration, 0.038 g/cm^3; temperature, 343 K; flow rate, 3 mL/h; solvent, toluene (12 cm^3).

Since montmorillonite KSF/O showed higher catalyst activity in a continuous fixed bed reactor, the activities of other solid catalysts for the hydroxyalkylation of *p*-cresol were also compared with montmorillonite KSF/O in a continuous fixed bed reactor and the results obtained are presented in Figure 4.19. Performances of various catalysts were evaluated in terms of (%) conversion of *p*-cresol and (%) product selectivity which are defined by Eqs. (4.3) and (4.4) respectively discussed in previous section (4.3.2.2.1).

Among the various catalysts screened, montmorillonite KSF/O showed the highest DAM selectivity (92%) with 26% conversion of *p*-cresol, while other montmorillonite K-catalysts (Al-pillared clay and montmorillonite K10) showed low conversion of *p*-cresol, ranging from 2 to 17% with 82-90% DAM selectivity. The highest activity with montmorillonite KSF/O could be attributed to the presence of highest acidity (15.5 μmol S^{-1} NH_3) as well as appropriate combination of acid sites both in low and high temperature regions as compared to the other K-catalysts e. g. montmorillonite K10. Interestingly, montmorillonite K30 showed the same *p*-cresol conversion and DAM selectivity to that of montmorillonite KSF/O in spite of its lower acidity (4.4 μmol S^{-1} NH_3) of former. This indicates that, along with total concentration of acid sites, the nature of acid sites of the catalyst also plays a significant role in the continuous hydroxyalkylation of *p*-cresol. Both montmorillonite KSF/O and montmorillonite K30 showed almost two-fold higher concentration of acid sites in the high temperature region than low temperature region, which is mainly responsible for their high catalyst activity in the continuous hydroxyalkylation process (Table 4.5 and Figures 4.18 a,b). In contrast to montmorillonite KSF/O, montmorillonite K10 showed low acidity (8.1 μmol S^{-1} NH_3) and slightly higher concentrations of acid sites in the low temperature region as compared to those in the high temperature region (Figure 4.18c) resulting in the lower catalyst activity (17% conversion of *p*-cresol) in the continuous hydroxyalkylation process as compared to montmorillonite KSF/O.

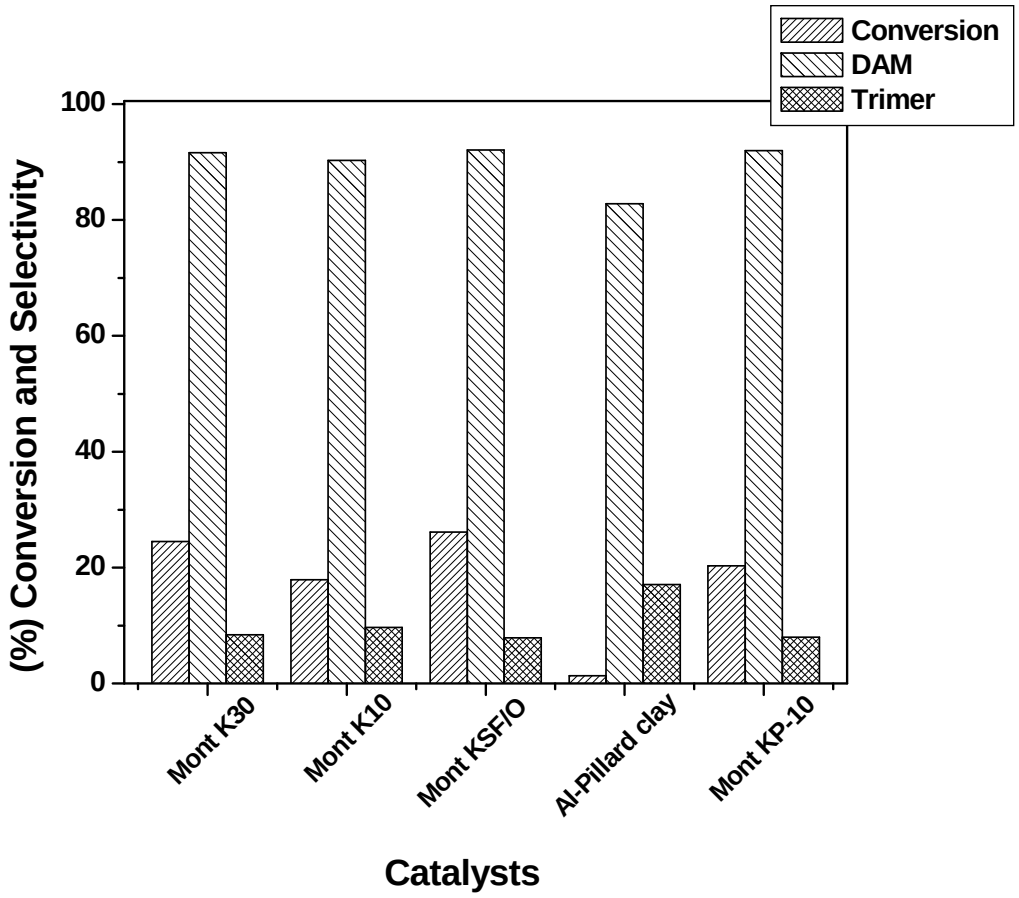

Figure 4.19. Catalyst screening for the continuous hydroxyalkylation of *p*-cresol Reaction conditions: *p*-cresol, 42.6 mmol; formaldehyde, 8.52 mmol; mole ratio of *p*-cresol to formaldehyde, 5; catalyst concentration, 0.038 g/cm^3; temperature, 343 K; flow rate, 3 mL/h; solvent, toluene (12 cm^3).

It was observed from the catalytic activity and NH_3-TPD results that along with total acidity, an appropriate combination of both weak and strong acidic sites were highly desirable for the selective hydroxyalkylation of *p*-cresol to DAM. Interestingly, montmorillonite (Al-pillared clay) showed very low catalyst activity (< 3% conversion of *p*-cresol) in spite of its high concentration of acid sites (5 μmol S^{-1} NH_3). This may be because of the hydrophilic nature of the catalyst due to presence of Al in an excess amount compared to other K-catalysts. The polar molecule like water strongly

coordinated to the Al (Lewis acid sites) as compared to formaldehyde, resulting in the low (< 3%) conversion of *p*-cresol. The amount of water adsorbed is proportional to Al content [26, 27].

4.3.3.2.2. Effect of mole ratio of p-cresol to formaldehyde

The effect of mole ratio of *p*-cresol to formaldehyde on the conversion of *p*-cresol and DAM selectivity was studied by keeping the *p*-cresol concentration fixed and by varying the amount of formaldehyde. Mole ratio of *p*-cresol to formaldehyde plays a significant role in the hydroxyalkylation of *p*-cresol; the results obtained in a fixed bed reactor are presented in Figure 4.20. The conversion of *p*-cresol decreased from 41 to 26% and DAM selectivity increased from 79 to 92% as mole ratio of *p*-cresol to formaldehyde increased from 1 to 5. The decrease in *p*-cresol conversion with an increase in mole ratio was obvious, since formaldehyde was used as a limiting reactant and the reaction almost ceased when all formaldehyde was consumed in the hydroxyalkylation of *p*-cresol. The decrease in DAM selectivity with decreasing mole ratio from 5 to 1 was mainly because of the formation of a trimer by the reaction of initially formed DAM with an excess of formaldehyde.

Interestingly, a very low conversion (< 4%) was observed in a batch reactor as compared to a fixed bed reactor under the same reaction conditions. In the case of a fixed bed reactor, *p*-cresol and formaldehyde get more exposure to the catalyst surface and active acidic sites while passing over the catalyst bed, while in case of a batch reactor, most of the reactants are present in the bulk liquid phase, and thus get less exposure to the catalyst surface and active acidic sites of the catalyst, resulting in low conversion of *p*-cresol.

Secondly, the amount of water molecules (present in formalin solution as well as formed during the reaction) exposed to active acidic sites of the catalyst during the residence time (20 min) was much lower (1.53 mmol) in a continuous operation than in batch operation (17.5 mmol; residence time, 20 min), thereby minimizing the poisoning of active sites of the catalyst which generally decrease the conversion of *p*-cresol to DAM [8].

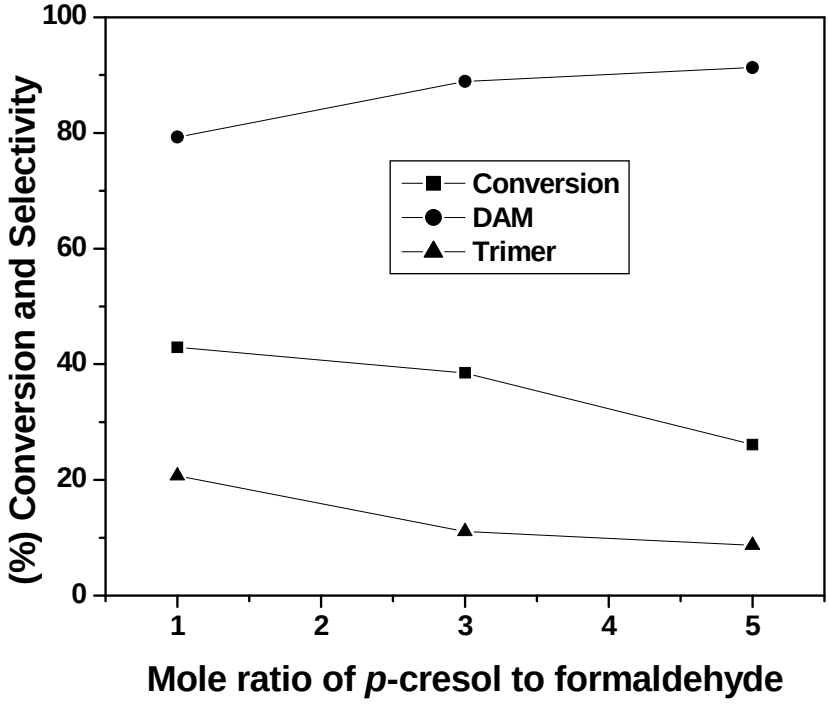

Figure 4.20. Effect of mole ratio of *p*-cresol to formaldehyde

Reaction conditions: *p*-cresol, 42.6 mmol; catalyst concentration, 0.038 g/cm^3; temperature, 343 K; catalyst, mont KSF/O; flow rate, 3 mL/h; solvent, toluene (12 cm^3).

4.3.3.2.3. Effect of temperature

The effect of temperature on *p*-cresol conversion and DAM selectivity was studied in the temperature range of 313 to 343 K at 5 mole ratio of *p*-cresol to formaldehyde and the results are presented in Figure 4.21. The conversion of *p*-cresol increased from 10 to 26% and DAM selectivity increased from 80 to 92% with an increase in temperature from 313 to 343 K. The low selectivity (80%) to DAM at 313 K was mainly due to the formation of an intermediate carbinol (2- (hydroxymethyl)-4-methyl phenol) (18%), which reacts further with another molecule of *p*-cresol at higher temperature (343 K) to give DAM. Very low conversion of *p*-cresol (<3%) was observed in a batch reactor as compared to that in a fixed bed reactor in the temperature range of 313 to 343 K at 5 mole ratio of *p*-cresol to formaldehyde.

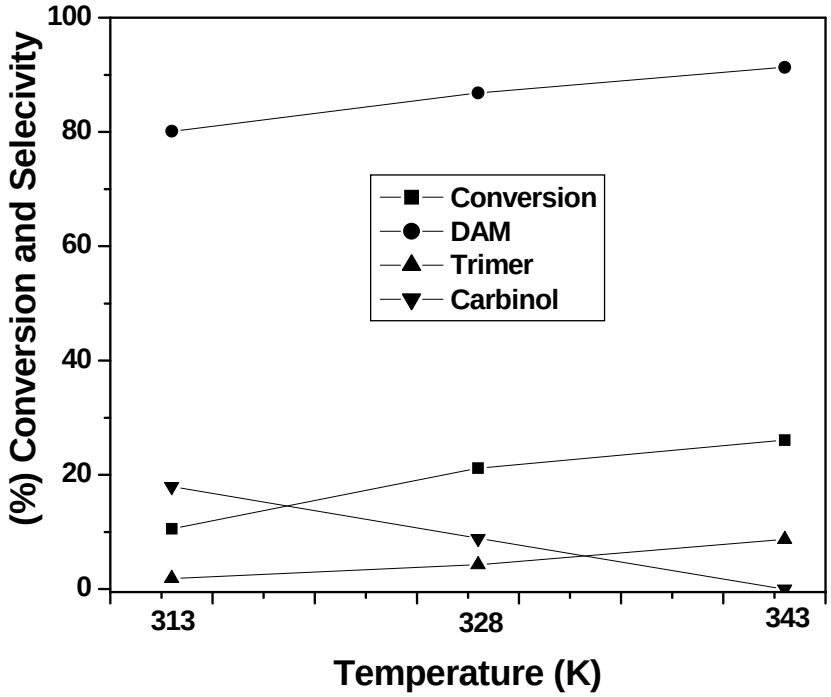

Figure 4.21. Effect of temperature on conversion and selectivity

Reaction conditions: *p*-cresol, 42.6 mmol; formaldehyde, 8.52 mmol; mole ratio of *p*-cresol to formaldehyde, 5; catalyst concentration, 0.038 g/cm^3; catalyst, mont KSF/O; flow rate, 3 mL/h; solvent, toluene (12 cm^3).

4.3.3.2.4. Effect of catalyst concentration

The effect of catalyst concentration on the conversion of *p*-cresol and product distribution was also studied in the range of 0.007 to 0.038 g/cm^3 at 343 K and at a mole ratio of *p*-cresol to formaldehyde = 5 and the results obtained in a fixed bed reactor are presented in Figure 4.22. The *p*-cresol conversion increased from 3 to 26% with increasing the catalyst concentration from 0.007 to 0.038 g/cm^3. The increase in *p*-cresol conversion was mainly because of an increase in active acidic sites with increasing the catalyst concentration. The linear dependence of the conversion of *p*-cresol on the catalyst loading indicates the absence of any mass transfer resistances. Interestingly, the selectivity to DAM decreased marginally from 95 to 92% with increasing the catalyst

concentration from 0.007 to 0.038 g/cm^3. The slight decrease in DAM selectivity from 95 to 92% was due to the formation of a trimer [2, 2′-(2-hydroxy-5-methyl-1, 3- phenylene) bis (methylene) bis (4-methylphenol)] from DAM due to increasing active acidic sites with an increase in the catalyst concentration.

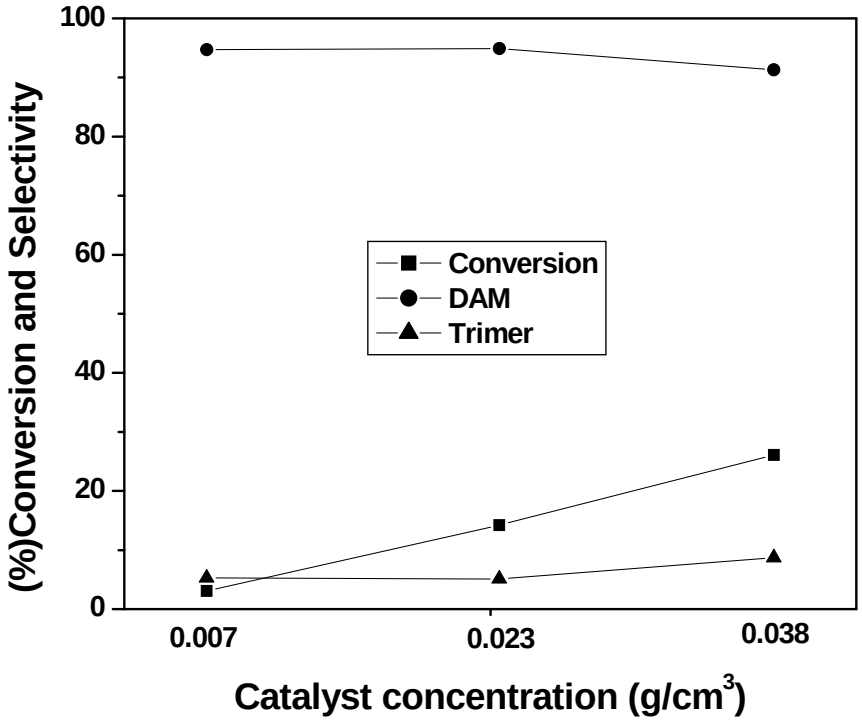

Figure 4.22. Effect of catalyst concentration on conversion and selectivity

Reaction conditions: *p*-cresol, 42.6 mmol; formaldehyde, 8.52 mmol; mole ratio of *p*-cresol to formaldehyde, 5; temperature, 343 K; catalyst, mont KSF/O; flow rate, 3 mL/h; solvent, toluene (12 cm^3).

4.3.3.2.5. Effect of flow rate

The effect of flow rate on the continuous hydroxyalkylation of *p*-cresol was studied in the range of 1 to 6 mL/h and the results are presented in Figure 4.23.

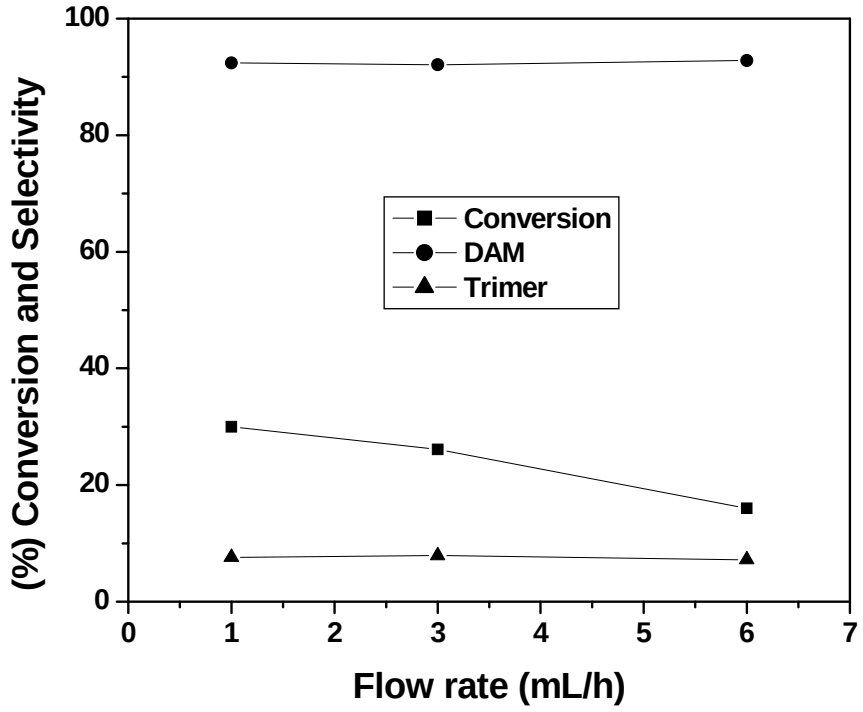

Figure 4.23. Effect of flow rate on conversion and selectivity

Reaction conditions: *p*-cresol, 42.6 mmol; formaldehyde, 8.52 mmol; mole ratio of *p*-cresol to formaldehyde, 5; catalyst concentration, 0.038 g/cm^3; temperature, 343 K; catalyst, mont KSF/O; solvent, toluene (12 cm^3).

The conversion of *p*-cresol decreased from 30 to 16% with increasing the flow rate from 1 to 6 mL/h. The selectivity to DAM (92%) and trimer (8%) remained almost constant over an entire flow rate range (1 to 6 mL/h). The increasing conversion of *p*-cresol with decreasing flow rate was mainly due to the increase in residence time of reactants on the catalyst bed, which increased the interaction between reactants and the active acidic sites of the catalyst.

From the process point of view, the flow rate of 3 mL/h was found to be optimum, since it showed higher conversion of *p*-cresol (26%) with 92% DAM selectivity within a short reaction time (20 min).

4.4. CONCLUSIONS

- The catalytic performance of 20% DTP/BNT prepared by wet impregnation method and commercial montmorillonite was evaluated for the hydroxyalkylation of *p*-cresol to gives DAM.
- DTP impregnated bentonite catalyst (20% DTP/BNT) gave 95% product yield with 94% selectivity to DAM at 353 K and for *p*-cresol to formaldehyde mole ratio of 5. Ammonia-TPD results showed that an increase in total concentration of acid sites from 4.9 of parent BNT to 11.6 $\mu molS^{-1}$ NH_3 of 20% DTP/BNT due to a strong interaction of protons of bulk DTP with surface hydroxyl groups of BNT as evidenced by ^{31}P-CP MASNMR studies, was responsible for its high activity and selectivity.
- Among the three catalysts e.g. montmorillonite, DTP and TS-1 having different acid strengths, montmorillonite showed highest activity (32% conversion with > 90% selectivity to DAM) for hydroxyalkylation of *p*-cresol. Predominant formation of trimer was formed with DTP, while TS-1 showed very low catalyst activity (< 4% conversion of *p*-cresol) with substantial formation of carbinol (16%). Ammonia TPD studies of various catalysts showed that an appropriate combination of both strong and weak acid sites of montmorillonite was mainly responsible for its highest catalyst activity for selective hydroxyalkylation of *p*-cresol to DAM.
- Among various montmorillonite K catalysts screened for the continuous hydroxyalkylation of *p*-cresol to DAM in a fixed bed reactor, montmorillonite KSF/O showed excellent performance (26% conversion of *p*-cresol with > 90% selectivity to DAM). Appropriate combinations of both weak and strong acid sites are highly desirable for the selective hydroxyalkylation of *p*-cresol to DAM. The conversion of *p*-cresol decreased from 41 to 26%, while the DAM selectivity increased from 79 to 92%, with increasing the mole ratio of *p*-cresol to formaldehyde from 1 to 5. The conversion of *p*-cresol increased from 10 to 26% and DAM selectivity increased from 80 to 92% with increasing the temperature from 313 to 343 K. *p*-cresol conversion increased from 3 to 26% and DAM

selectivity decreased marginally from 95 to 92% with increasing the catalyst concentration from 0.007 to 0.038 g/cm^3. The increase in *p*-cresol conversion was mainly because of an increase in active acidic sites with increasing the catalyst concentration. The linear dependence of the conversion of *p*-cresol on the catalyst loading indicates the absence of any mass transfer resistances. The conversion of *p*-cresol decreased from 30 to 16% with increasing the flow rate from 1 to 6 mL. The selectivity to DAM (92%) and trimer (8%) remained almost constant over the entire flow rate range (1 to 6 mL/h). Very low conversion of *p*-cresol (< 4%) was observed in the batch reactor as compared to fixed bed reactor under the same reaction conditions.

4.5. REFERENCES

1. M. Delhorme, C. Labbez, C. Caillet, F. Thomas, *Langmuir*, 26 (2010) 9240.
2. A. Vaccari, *Catal. Today*, 41 (1998) 53.
3. C. Ravindra Reddy, G. Nagendrappa, B. S. Jai Prakash, *Catal. Commun*. 8 (2007) 241.
4. B. Singh, J. Patial, P. Sharma, S. G. Agarwal, G. N. Qazi, S. Maity, *J. Mol. Catal. A: Chem.* 266 (2007) 215.
5. K. Shimizu, T. Higuchi, E. Takasugi, T. Hatamachi, T. Kodama, A. Satsuma, *J. Mol. Catal. A: Chem.* 284 (2008) 89.
6. M. Huglin, G. Knight, W. Wright, *Makromol. Chem.* 152 (1972) 67.
7. A. C. Garade, V. S. Kshirsagar, A. Jha, C. V. Rode, *Catal. Commun.* 11 (2010) 942.
8. A. C. Garade, V. R. Mate, C. V. Rode, *Appl. Clay Sci.* 43 (2009) 113.
9. A. C. Garade, A. M. Hengne, T. N. Deshpande, S. V. Shaligram, M. Shirai, C. V. Rode, *J. Chem. Eng. Jpn.* 42 (2009) 782.
10. Y. Kamiya, Y. Ooka, C. Obara, R. Ohnishi, T. Fujita, Y. Kurata, K. Tsuji, T. Nakajyo, T. Okuhara, *J. Mol. Catal. A: Chem.* 262 (2007) 77.
11. J. A. Dais, J. P. Osegovic, R. S. Drago, *J. Catal.* 183 (1999) 83.
12. H. Su, S. Zeng, H. Dong, Y. Du, Y. Zhang, R. Hu, *Appl. Clay Sci.* 46 (2009) 325.
13. W. Kuang, A. Rives, M. Fournier, R. Hubaut, *Appl. Catal. A: Gen.* 250 (2003) 221.
14. M. H. Bhure, I. Kumar, A. D. Natu, R. C. Chikate, C. V. Rode, *Catal. Commun*. 9 (2008)1863.
15. A. M. Camiloti, S. L. Jahn, N. D. Velasco, L. F. Moura, D. Cardoso, *Appl. Catal. A: Gen*. 182 (1999) 107.
16. S. Udayakumar, S. Ajaikumar, A. Pandurangan, *Appl. Catal. A: Gen.* 302 (2006) 86.
17. S. Uchida, K. Inumaru, M. Misono, *J. Phys. Chem. B* 104 (2000) 8108.
18. P. Madhusudhan Rao, A. Wolfson, S. Kababya, S. Vega, M.V. Landau, *J. Catal.* 232 (2005) 210.

19. V. M. Mastikhin, S. M. Kulikov, A. V. Nosov, I. V. Kozhevnikov, I. L. Mudrakovsky, M. N.Timofeeva, *J. Mol. Catal. A: Chem.* 60 (1990) 65.
20. I. V. Kozhevnikov, K. R. Kloetstra, A. Sinnema, H. W. Zandbergen, H. V. Bekkum, *J. Mol. Catal. A: Chem.* 114 (1996) 287.
21. Z. Hou, T. Okuhara, *J. Mol. Catal. A: Chem.* 206 (2003) 121.
22. M. C. Capel-Sanchez, J. M. Campos-Martin, J. L. G.Fierro, *Appl. Catal. A: Gen.* 246 (2003) 69.
23. R. Mariscal, M. Lopez-Granados, J. L. G. Fierro, J. L. Sotelo, C. Martos, R. Van Grieken, *Langmuir*, 16 (2000) 9460.
24. S. Stackhouse, P. V. Coveney, E. Sandre, *J. Am. Chem. Soc.* 123 (2001) 11764.
25. K. Nowinska, W. Kaleta, *Appl. Catal. A: Gen.* 203 (2000) 91.
26. M. Bolognini, F. Cavani, L. Pozzo, L. Maselli, F. Zaccarelli, B. Bonelli, M. Armandi, E. Garrone, *Appl. Catal. A: Gen.* 272 (2004) 115.
27. D. H. Olson, W. O. Haag, R. M. Lago, *J. Catal.* 61 (1980) 390.

Chapter V

Hydroxyalkylation of guaiacol followed by oxidation of hydroxyalkylated intermediate to give *p*-vanillin

5.1. INTRODUCTION

Vanillin is a high value product (in the range of $ 12-15 per kg) widely used as a flavouring agent for food and confectionary [1, 2]. Due to its growing demand worldwide and limited availability from natural resources, about 80% need is fulfilled by the synthetic vanillin [3]. It is conventionally prepared by the hydroxyalkylation of guaiacol with formaldehyde or glyoxylic acid in presence of strong mineral acids like hydrochloric acid, or quarternary ammonium salts followed by oxidation of side chains of phenol derivatives (intermediate hydroxyalkylated product) using strong oxidants like $K_2Cr_2O_7$ and $KMnO_4$ [4, 5]. Another alternative route for synthesis of vanillin was proposed by Reimer which involves the reaction of guaiacol with chloroform in presence of strong alkali, KOH [6]. However, both these conventional processes based on the stoichiometric use of reagents have major drawbacks like difficulties in separation and recovery of the pure product from the reaction medium, handling of corrosive reagents, and formation of huge quantities of inorganic wastes. In order to overcome these drawbacks, several attempts have been made by researchers using solid acid catalysts [7]. The first one was reported by Rhodia for the production of vanillin (chapter 1, Scheme 1.2) [1]. Among various solid acid catalysts, mainly zeolites were used for the hydroxyalkylation of guaiacol to vanillyl alcohol (VAlc) [8, 9]. Other solid catalysts like heteropoly acids possess strong acidity having potential applications in various organic transformations [10, 11]. Nevertheless, commercial applications of heteropoly acids are rather restricted due to their very low surface area and high solubility in polar solvents [12]. Several reports are available in literature on impregnation of dodecatungstophosphoric acid (DTP) on fumed silica (SiO_2) [13, 14]. Among various applications of these catalysts, selective hydroxyalkylation is a more challenging reaction due to predominant formation of dihydroxydiarylmethane as a by-product [9] and deactivation of the catalyst due to deposition of bulky and higher molecular weight condensation products on the catalyst surface [15]. Hydroxyalkylation of guaiacol is such a reaction in which achieving the highest selectivity to the intermediate VAlc is of great importance for which the guaiacol hydroxyalkylation is carried out at a very high mole ratio (1:15 to 1:20) of guaiacol to formaldehyde [8, 9]. The various products

obtained by the hydroxyalkylation of guaiacol with formaldehyde [9] are presented in Scheme 5.1.

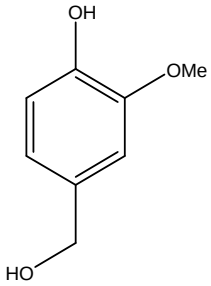

p-Vanillyl alcohol

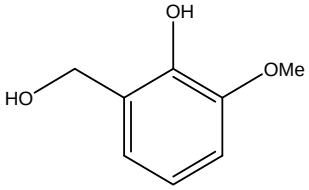

o-Vanillyl alcohol

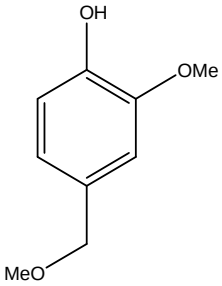

2-methoxy-4-(methoxymethyl)phenol

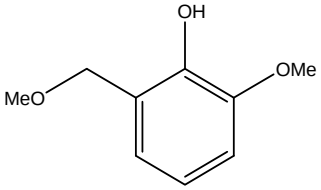

2-methoxy-6-(methoxymethyl)phenol

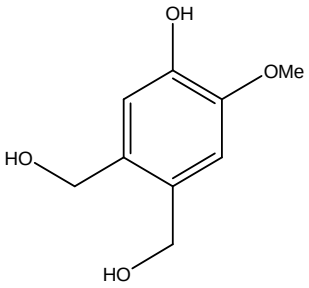

4,5-bis(hydroxymethyl)-2-methoxyphenol

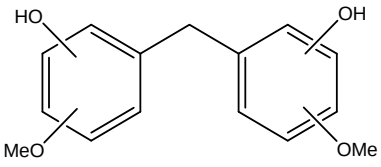

Dihydroxy diarylmethane

Scheme 5.1. Various products obtained by hydroxyalkylation of guaiacol with formaldehyde [9]

Oxidation of side chains of phenol derivatives (*p*-VAlc) which is a second step in the synthesis of *p*-vanillin, are generally carried out using homogeneous cobalt catalysts which pose similar problems associated with conventional oxidants like (i) difficulties in separation from the reaction medium (ii) reusability and (iii) fast deactivation due to the formation of μ-oxo dimer (Co-O-Co) [16, 17]. Hence, it is of great practical importance to design and develop active, selective and reusable catalysts having higher activity and selectivity for the hydroxyalkylation of guaiacol and side chain oxidation of phenol derivatives.

In the present study, the hydroxyalkylation of guaiacol to VAlc using highly dispersed 10% DTP on SiO_2 (Scheme 5.1) at a very low (1:3) guaiacol to formaldehyde mole ratio and oxidation of side chain of phenol derivatives i.e. *p*-vanillyl alcohol (*p*-VAlc) using Co-saponite catalysts were reported (Scheme 5.2).

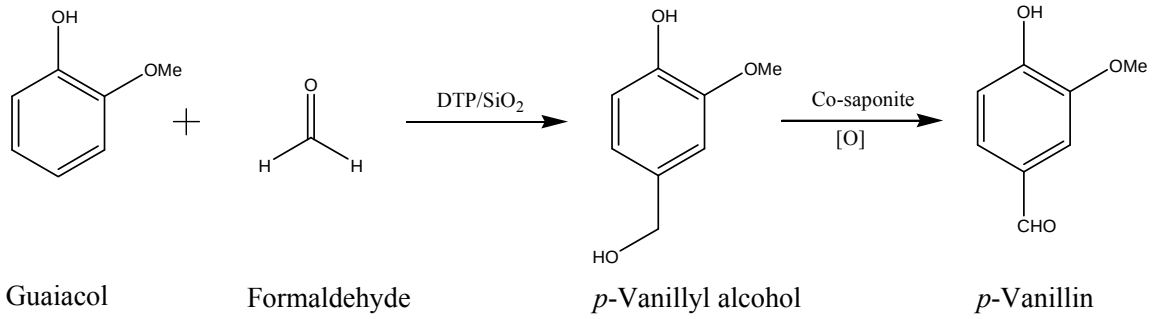

Scheme 5.2. Hydroxyalkylation of guaiacol followed by oxidation of *p*-vanillyl alcohol

After carefully tuning the acidity by appropriate DTP loading, selectivity to VAlc as high as 46% could be achieved in the hydroxyalkylation of guaiacol. Catalyst activity comparison of SiO_2, bulk DTP, amberlyst-15 and montmorillonite K-10 with DTP on SiO_2 was also studied for the hydroxyalkylation of guaiacol. These catalysts were characterized by BET surface area measurement, NH_3-TPD and by XRD. Effect of various reaction parameters like mole ratio of guaiacol to formaldehyde, reaction

temperature, catalyst concentration and reaction time on guaiacol conversion and on product selectivity were also studied for the hydroxyalkylation of guaiacol.

Among various catalysts screened for liquid phase oxidation of *p*-VAlc to *p*-vanillin, 13% Co-saponite showed the highest (99%) selectivity to *p*-vanillin. The catalysts were characterized by various techniques like X-ray powder diffraction (XRD), H_2-temperature programmed reduction (H_2-TPR), N_2-adsorption, Raman, FT-IR, and by thermogravimetry (TGA-DTA). The reusability of the catalyst (13% Co-saponite) was also evaluated by the catalyst recycle experiment.

5.2. EXPERIMENTAL

DTP impregnated on SiO_2 and Co-saponite catalysts having different Co loading were prepared by wet impregnation method and *in situ* precipitation method respectively and detailed experimental procedure of their preparation has been described in chapter 2 (section 2.2.1 and 2.2.2). The catalysts were characterized by various techniques and a detailed characterization procedure is described in section 2.3. The activity of prepared catalysts was evaluated for the hydroxyalkylation of guaiacol and oxidation of *p*-VAlc and its experimental procedure is described in sections 2.4.3 and 2.4.4 respectively.

5.3. RESULTS AND DISCUSSION

5.3.1. Hydroxyalkylation of guaiacol to vanillyl alcohol over DTP impregnated on SiO_2

Hydroxyalkylation of guaiacol with formaldehyde was carried out over the same catalyst (DTP/SiO_2) used for hydroxyalkylation of phenol to give bisphenol F. In order to achieve high VAlc selectivity, reaction was carried out at formaldehyde to guaiacol mole ratio of 3 which is much higher than that used for synthesis of bisphenol F (mole ratio of formaldehyde to phenol, 1:5 = 0.2) and without using any solvent such as toluene.

5.3.1.1. Catalyst characterization

10% DTP/SiO_2 catalyst and other DTP impregnated on SiO_2 catalysts were characterized by various techniques like XRD, NH_3-TPD and BET surface area measurements and results obtained are discussed in chapter 3 (section 3.3.1.1).

5.3.1.2. Catalyst activity measurement

5.3.1.2.1. Catalyst screening

The activity results of various solid acid catalysts for the hydroxyalkylation of guaiacol are presented in Figure 5.1.

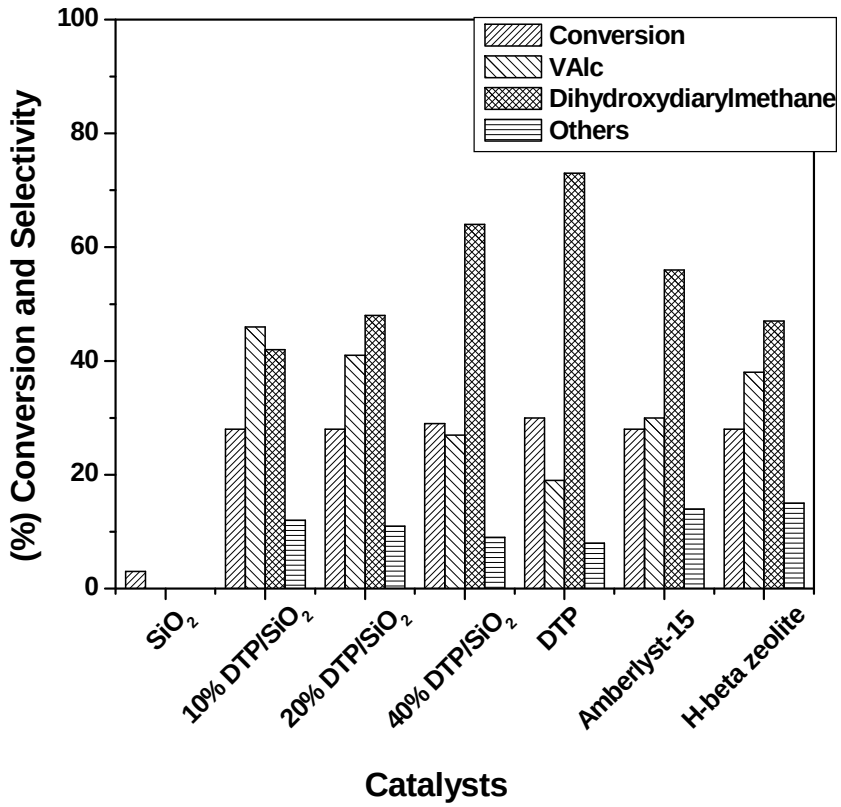

Figure 5.1. Catalyst screening for hydroxyalkylation of guaiacol

Reaction conditions: guaiacol, 8 mmol; formaldehyde, 24 mmol; mole ratio of guaiacol to formaldehyde, 1:3; catalyst concentration, 0.11 g/cm^3; temperature, 353 K; reaction volume, 3 cm^3.

The effect of total acidity and acid strength of various solid acid catalysts on the product selectivity was studied at a fixed guaiacol conversion of 28%. Performances of various catalysts were evaluated in terms of % conversion of guaiacol and % product selectivity, which have been already defined in chapter 4 by eqs. (4.3) and (4.4) respectively.

As can be seen from Figure 5.1, 10% DTP/SiO_2 showed the maximum (46%) selectivity to VAlc (after 30 min) while bulk DTP having the specific BET surface area of 8 m^2/g showed the lowest (19%) selectivity to VAlc at 28% conversion of guaiacol. The selectivity to VAlc decreased from 46 to 27% as DTP loading increased from 10 to 40%. As compared to DTP/SiO_2 catalysts with various DTP loadings, parent SiO_2 showed a very low catalyst activity (< 3% conversion of guaiacol) even after longer reaction time of 2 h in spite of its highest specific surface area of 256 m^2/g (chapter 3, Table 3.1). This indicated that the nature and concentration of acidic sites played a dominant role in the hydroxyalkylation of guaiacol to VAlc. The lowest catalyst activity of SiO_2 could be due to its low acidity (1.1 $\mu molS^{-1}$ NH_3). Interestingly, 10% DTP/SiO_2 showed the highest catalyst activity (46% selectivity to VAlc with 28% conversion of guaiacol) as compared to the parent SiO_2. Higher catalyst activity of 10% DTP/SiO_2 as compared to SiO_2 was due to its increase in concentration of acidic sites (2.1 $\mu molS^{-1}$) in a low temperature region (373-473 K) [chapter 3, Table 3.1 and Figure 3.2b] and stabilization of intermediate carbocation by heteropolyanion of DTP [18]. The product selectivities were found to be dependent mainly on the distribution of weak and strong acid sites. With the stronger acidic catalysts like 20 and 40% DTP/SiO_2, VAlc selectivity decreased from 46% to 41 and 27% respectively, as compared to 10% DTP/SiO_2. The lower VAlc selectivity with these stronger acidic catalysts was mainly due to the presence of acidic sites in high temperature region which facilitate the formation of dihydroxydiarylmethane (Scheme 5.1). As compared to DTP /SiO_2 catalysts, bulk DTP showed very low (19%) VAlc selectivity due to its highest acidity (163.8 $\mu molS^{-1}$ NH_3) and also due its partial solubility in the reaction medium, thus acting as a homogeneous catalyst [19, 20]. The highest acidity (163.8 $\mu molS^{-1}$ NH_3) of DTP and the presence of acidic sites in a high temperature region (high acid strength) facilitate the formation of dihydroxydiarylmethane from initially formed VAlc resulting in to a low selectivity to

VAlc [21]. Other solid acid catalysts such as H-β-zeolite (Si/Al = 12.5) and amberlyst-15 showed lower VAlc selectivity (35 and 30% respectively) than that exhibited by 10% DTP/SiO_2 catalyst. The lower VAlc selectivity with H-β-zeolite catalyst could be again attributed to its high acidity (4.3 $\mu molS^{-1}$ NH_3) and the presence of acidic sites (37%) in a high temperature region. In the case of amberlyst-15 (resin) catalyst, the total acidity reported was 4.7 mmol/g (88 $\mu molS^{-1}$) [22, 23] however, the distribution of its weak and strong acid sites could not be measured by NH_3-TPD due to its instability at temperature > 373 K. The lower VAlc selectivity with amberlyst-15 catalyst was assigned to its higher acidity. In spite of the higher concentration of acidic sites (8 $\mu molS^{-1}$ NH_3), montmorillonite K10 showed a very low (6%) conversion of guaiacol after 30 min which slightly increased to 9% as the reaction time increased from 30 to 120 min. However, selectivity to VAlc decreased from 65 to 49% as reaction time increased from 30 to 120 min. The lower guaiacol conversion with montmorillonite K10 could be explained based on the hydrophilicity of montmorillonite K10 and the competition between polar water molecules and formaldehyde for active acid sites of montmorillonite K10. Since nucleophilicity of the oxygen atom of water molecules is more than that of formaldehyde, the former is strongly co-ordinated with active acid sites of catalyst than the later, hence inhibiting the reaction between formaldehyde and guaiacol that resulted in the lower conversion of guaiacol [24]. The observed activity and selectivity pattern and NH_3-TPD characterization of various catalysts studied in this work strongly indicate that acidic sites of the catalyst present in a low temperature region was highly desirable for the selective hydroxyalkylation of guaiacol to VAlc. Since 10% DTP/SiO_2 showed the highest selectivity (46%) to VAlc, further study on the hydroxyalkylation of guaiacol was carried out using 10% DTP/SiO_2 catalyst.

5.3.1.2.2. Effect of reaction time

The effect of reaction time on the guaiacol conversion and product selectivity was also studied for guaiacol to formaldehyde mole ratio of 1:3 at 353 K. It was found that the guaiacol conversion increased from 0 to 44% with increase in reaction time from 0 to 45 minutes (Figure 5.2). The selectivity to VAlc decreased from 53 to 26% when reaction

time increased from 15 to 45 minutes. This decrease in VAlc selectivity was mainly because of reaction of initially formed VAlc with guaiacol to give dihydroxydiarylmethane and its higher homologues. A high catalyst activity (28% conversion of guaiacol) with 46% VAlc selectivity was obtained after 30 minutes.

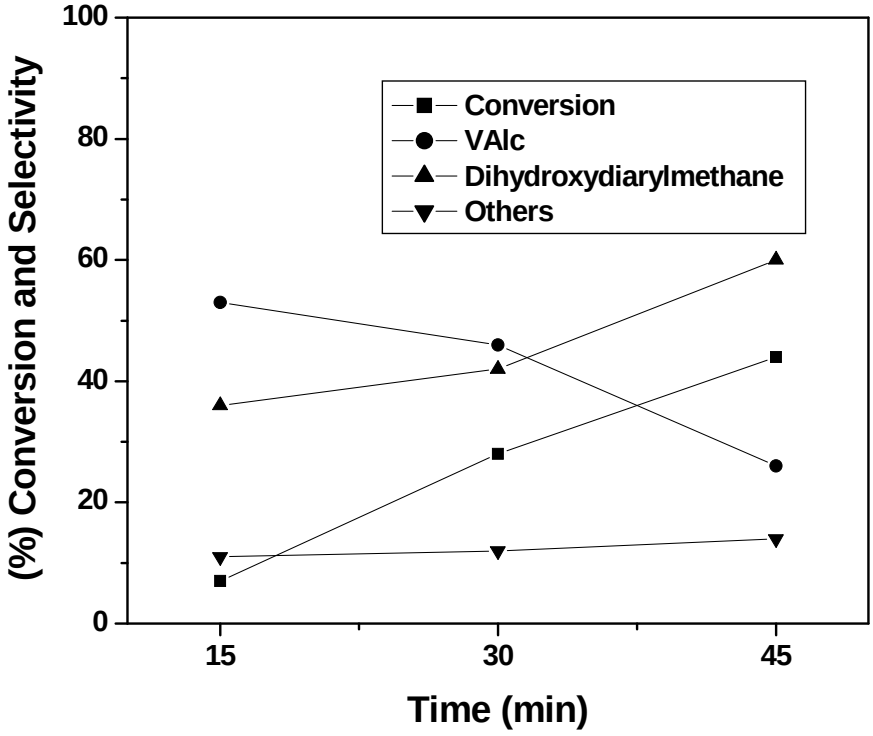

Figure 5.2. Effect of reaction time on conversion of guaiacol and product selectivity Reaction conditions: guaiacol, 8 mmol; formaldehyde, 24 mmol; mole ratio of guaiacol to formaldehyde, 1:3; catalyst concentration, 0.11 g/cm^3; temperature, 353 K; time, 45 min; catalyst, 10% DTP/SiO_2; reaction volume, 3 cm^3.

5.3.1.2.3. Effect of mole ratio of guaiacol to formaldehyde

Effect of mole ratio of guaiacol to formaldehyde on the conversion of guaiacol and product selectivity was studied in the range of 1:1 to 1:5 for 10% DTP/SiO_2 catalyst by

varying the concentration of formaldehyde at a constant guaiacol concentration and the results are presented in Figure 5.3.

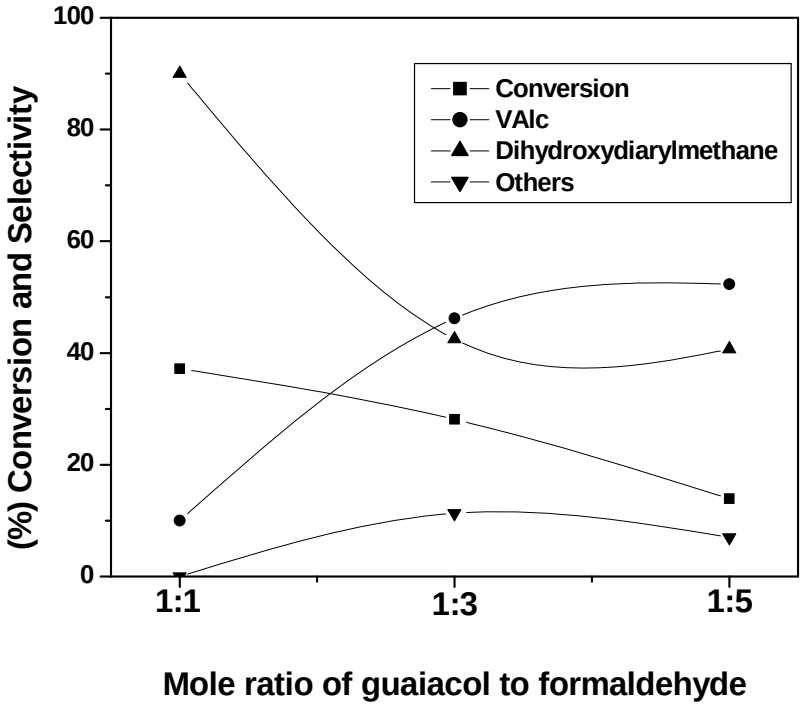

Figure 5.3. Effect of guaiacol to formaldehyde mole ratio
Reaction conditions: guaiacol, 8 mmol; catalyst concentration, 0.11 g/cm^3; temperature, 353 K; time, 30 min; catalyst, 10% DTP/SiO_2; reaction volume, 3 cm^3.

The conversion of guaiacol decreased from 37 to 13% as the mole ratio of guaiacol to formaldehyde increased from 1:1 to 1:5. The selectivity to VAlc increased from 10 to 52% and that of dihydroxydiarylmethane decreased from 90 to 40% with an increase in mole ratio of guaiacol to formaldehyde from 1:1 to 1:5. The other products formed were mainly ether of VAlc e.g. 2-methoxy-4-(methoxymethyl) phenol and 2-methoxy-6-(methoxymethyl) phenol as shown in Scheme 5.1. The lower guaiacol conversion (13%) was mainly because of the blockage of active sites of the catalyst by more polar water molecules present in excess amount for a mole ratio of 1:5 as compared to 1:1 and 1:3

mole ratios. The formation of VAlc (46 and 52%) at mole ratio 1:3 and 1:5 respectively was due to the availability of formaldehyde in excessive amount which minimizes the formation of dihydroxydiarylmethane. Mole ratio of 1:3 shows the best compromise between high catalyst activity (28% conversion of guaiacol) and selectivity to VAlc (46%).

It is interesting to note that the highest selectivity to VAlc (60-70%) has been reported in the literature for a very high mole ratio (1:15 to 1:20) of guaiacol to formaldehyde [7-9]. Among the two isomers of VAlc, *p*-VAlc and *o*-VAlc formed were 67 and 33% respectively at 353 K and at 1:3 mole ratio.

5.3.1.2.4. Effect of catalyst concentration

Effect of catalyst concentration in the range of 0.04 to 0.18 g/cm^3 on guaiacol conversion and product selectivity was also studied and the results are presented in Figure 5.4. The guaiacol conversion increased from 3 to 51% with increase in catalyst concentration from 0.04 to 0.18 g/cm^3. This is obvious since with increase in catalyst concentration; the acidic sites also increased which facilitate the conversion of guaiacol to products. However, the selectivity to VAlc decreased significantly from 46 to 28% and that of dihydroxydiarylmethane increased from 42 to 53% as the catalyst concentration increased from 0.11 to 0.18 g/cm^3. The decrease in VAlc selectivity was due to its further conversion to dihydroxydiarylmethane because of increase in acidic sites at higher catalyst concentration. The selectivity to other products also increased from 12 to 19% with increase in catalyst concentration from 0.04 to 0.18 g/cm^3.

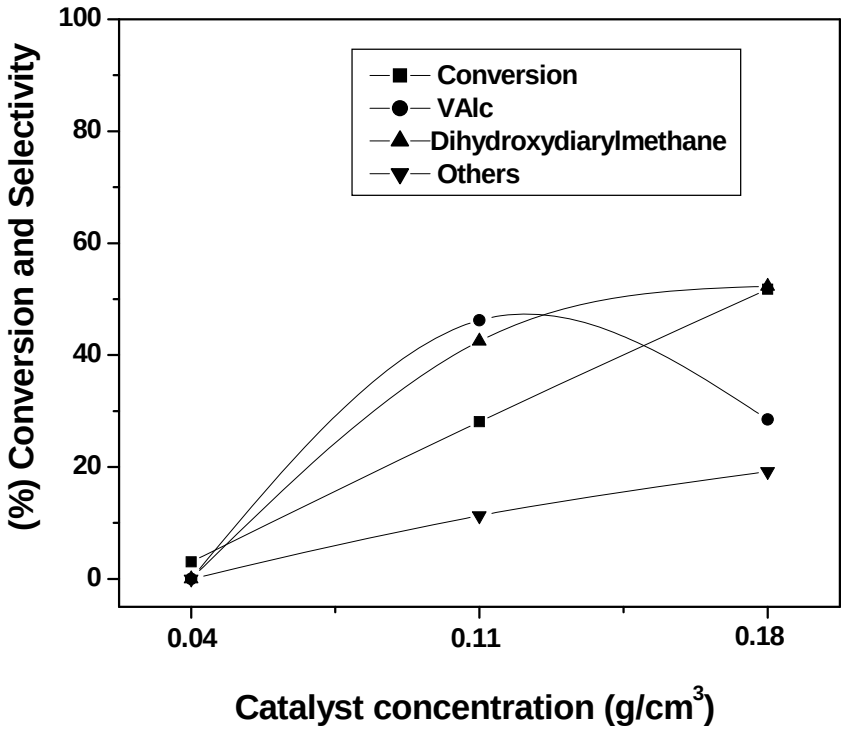

Figure 5.4. Effect of catalyst concentration

Reaction conditions: guaiacol, 8 mmol; formaldehyde, 24 mmol; mole ratio of guaiacol to formaldehyde, 1:3; temperature, 353 K; time, 30min; catalyst, 10% DTP/SiO_2; reaction volume, 3 cm^3.

5.3.1.2.5. Effect of temperature

Figure 5.5 presents the effect of the temperature on guaiacol conversion and product selectivity. This study was performed in the temperature range of 313 to 353 K at 1:3 mole ratio of guaiacol to formaldehyde for 30 min. It was observed that the conversion of guaiacol increased from 2 to 28% with increase in the temperature from 313 to 353 K. However, the VAlc selectivity decreased marginally with increase in the temperature from 323 to 353 K. No appreciable formation of VAlc and dihydroxydiarylmethane was observed at 313 K; but the selectivity to VAlc decreased from 59 to 46% and that of

dihydroxydiarylmethane increased from 34 to 42% with increase in the temperature from 333 to 353 K. The high temperature favored the formation of dihydroxydiarylmethane by the reaction of initially formed VAlc with guaiacol, resulting into decrease in the VAlc selectivity. The best catalytic performance (28% conversion of guaiacol and 46% selectivity to VAlc) was observed at 353 K.

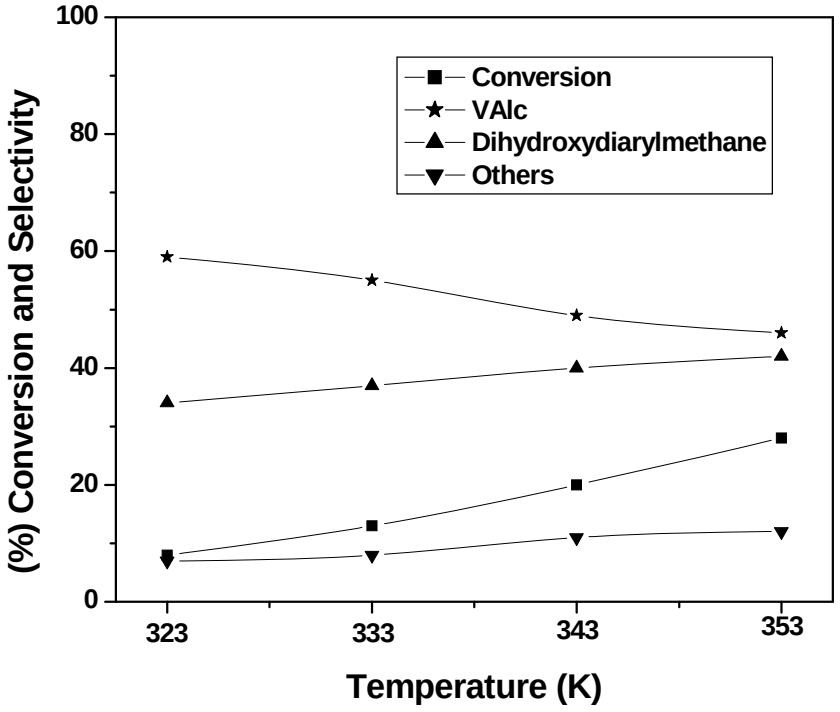

Figure 5.5. Effect of temperature

Reaction conditions: guaiacol, 8 mmol; formaldehyde, 24 mmol; mole ratio of guaiacol to formaldehyde, 1:3; catalyst concentration, 0.11 g/cm^3; temperature, 313-353 K; time, 30 min; catalyst, 10% DTP/SiO_2; reaction volume, 3 cm^3.

5.3.1.2.6. Catalyst recycle

Catalyst recycle experiments were carried out using 20% DTP/Mont K10 catalyst according to the procedure discussed in section 3.3.1.2.6 and results are shown in Figure 5.6. The catalyst was found to retain its activity even after the second recycle. The

conversion of guaiacol slightly decreased from 28 to 26% after the second recycle which could be because of handling losses of the catalyst. The selectivity to VAlc remained almost constant (46%) for all the recycle experiments.

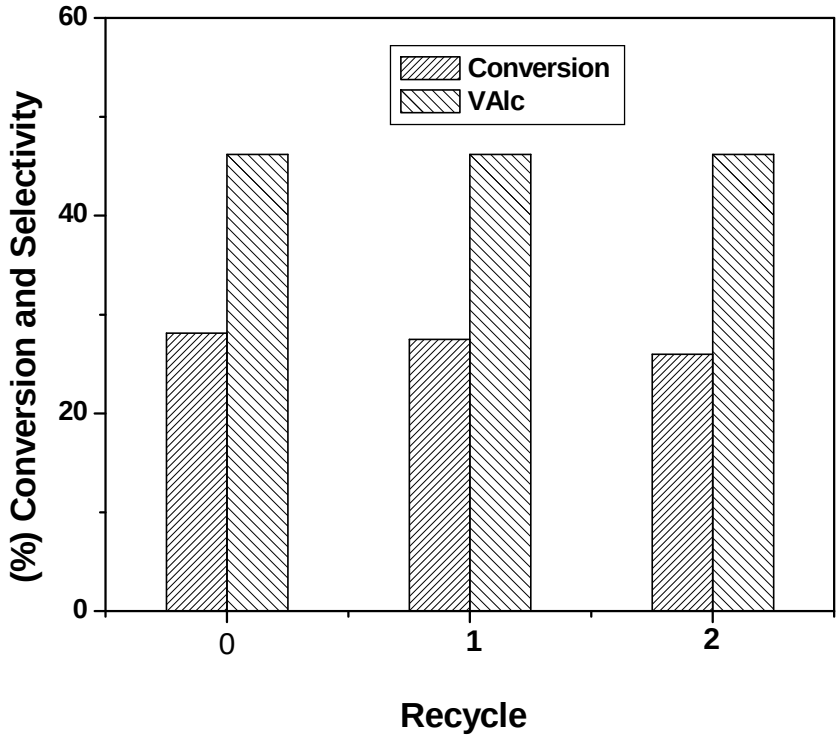

Figure 5.6. Catalyst recycle

Reaction conditions: guaiacol, 8 mmol; formaldehyde, 24 mmol; mole ratio of guaiacol to formaldehyde, 1:3; catalyst concentration, 0.11 g/cm^3; temperature, 353 K; time, 30 min; catalyst, 10% DTP/SiO_2; reaction volume, 3 cm^3.

5.3.2. Oxidation of *p*-vanillyl alcohol to *p*-vanillin

Co-saponite catalysts with varying Co loadings (5-30%) were prepared by *in situ*-precipitation method [25, 26] and their performance was evaluated for liquid phase oxidation of *p*-VAlc to give *p*-vanillin [27]. The objective of this work was to achieve maximum selectivity to *p*-vanillin by tuning the porosity and distribution ratios of Co_3O_4/CoO phases of Co-saponite by varying Co loading in saponite clay. The catalyst characterization and activity results are discussed in the following sections.

5.3.2.1. Catalyst characterization

5.3.2.1.1. X-ray diffraction

XRD patterns of Co-saponite samples with various Co loadings ranging from 5-30% are presented in Figure 5.7.

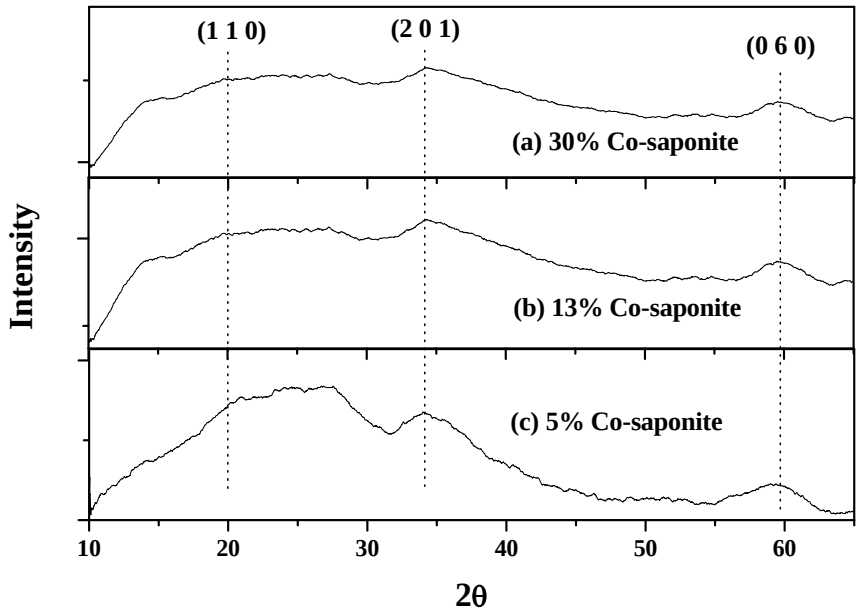

Figure 5.7. XRD patterns of (a) 5% (b) 13% and (c) 30% Co-saponite

A broad (060) reflection at 60° for all the samples indicates the formation of trioctahedral clay structure [28, 29]. Other two broad peaks at 19.5° and 34° were attributed to (110) and (201) reflections. This broadening of peaks could be due to a loss of periodicity in c-direction [30] as a result of incorporation of cobalt in the clay framework. In spite of their amorphous nature, all the Co-saponite samples exhibited the higher activity for selective oxidation of *p*-VAlc to *p*-vanillin.

5.3.2.1.2. H_2-temperature programmed reduction (H_2-TPR)

The H_2-TPR peak at 473-483 K (Figure 5.8) for all the Co-saponite samples with Co loadings ranging from 5 to 30%, could be attributed to the reduction of trivalent cobalt oxide (Co_3O_4) to divalent cobalt oxide (CoO) [31, 32].

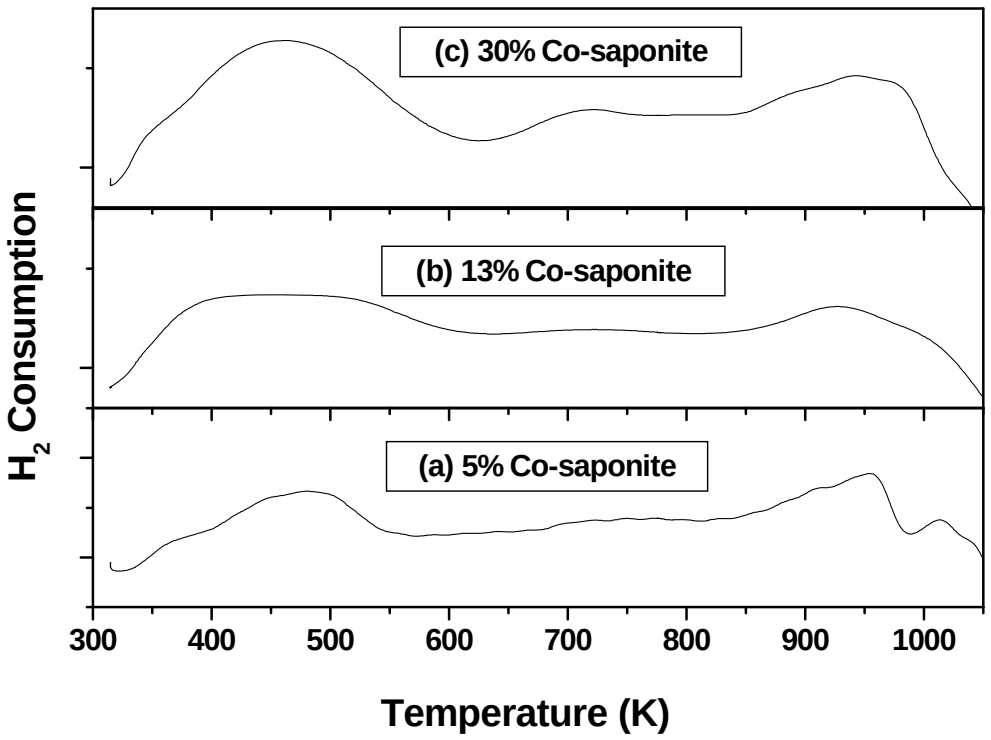

Figure 5.8. H_2-TPR spectra of (a) 5% (b) 13% and (c) 30% Co-saponite samples

Another broad peak at 825-975 K in all the Co-saponite samples was attributed to the reduction of divalent cobalt oxide (CoO) to metallic cobalt (Co^o) [33, 34]. The appearance of an additional peak at 1015 K only in the 5% Co-saponite sample was attributed to the interaction of the support with cobalt could be due to the low Co loading [35].

5.3.2.1.3. N_2-adsorption

Type I isotherm according to IUPAC classification was identified from the nitrogen adsorption-desorption isotherms for the Co-saponite samples with different Co loadings (Figure 5.9). The adsorption occurred at low pressure without any steps and the uptake of gas is governed by the accessible micropore volume rather than by the internal surface area [36]. A sharp inflection step at a relative pressure range > 0.9 was due to the capillary condensation.

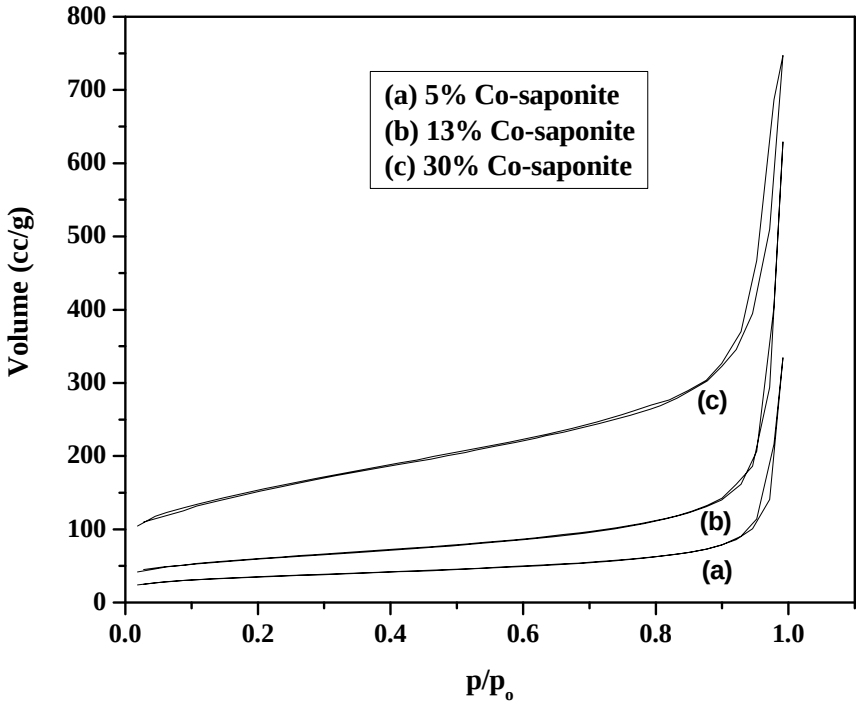

Figure 5.9. Nitrogen adsorption-desorption isotherms of Co-saponite samples

The pore diameter of 5% Co-saponite increased from 1.29 to 1.87 nm when Co loading was increased to 13% (Figure 5.10), which is a characteristic of microporous materials [37].

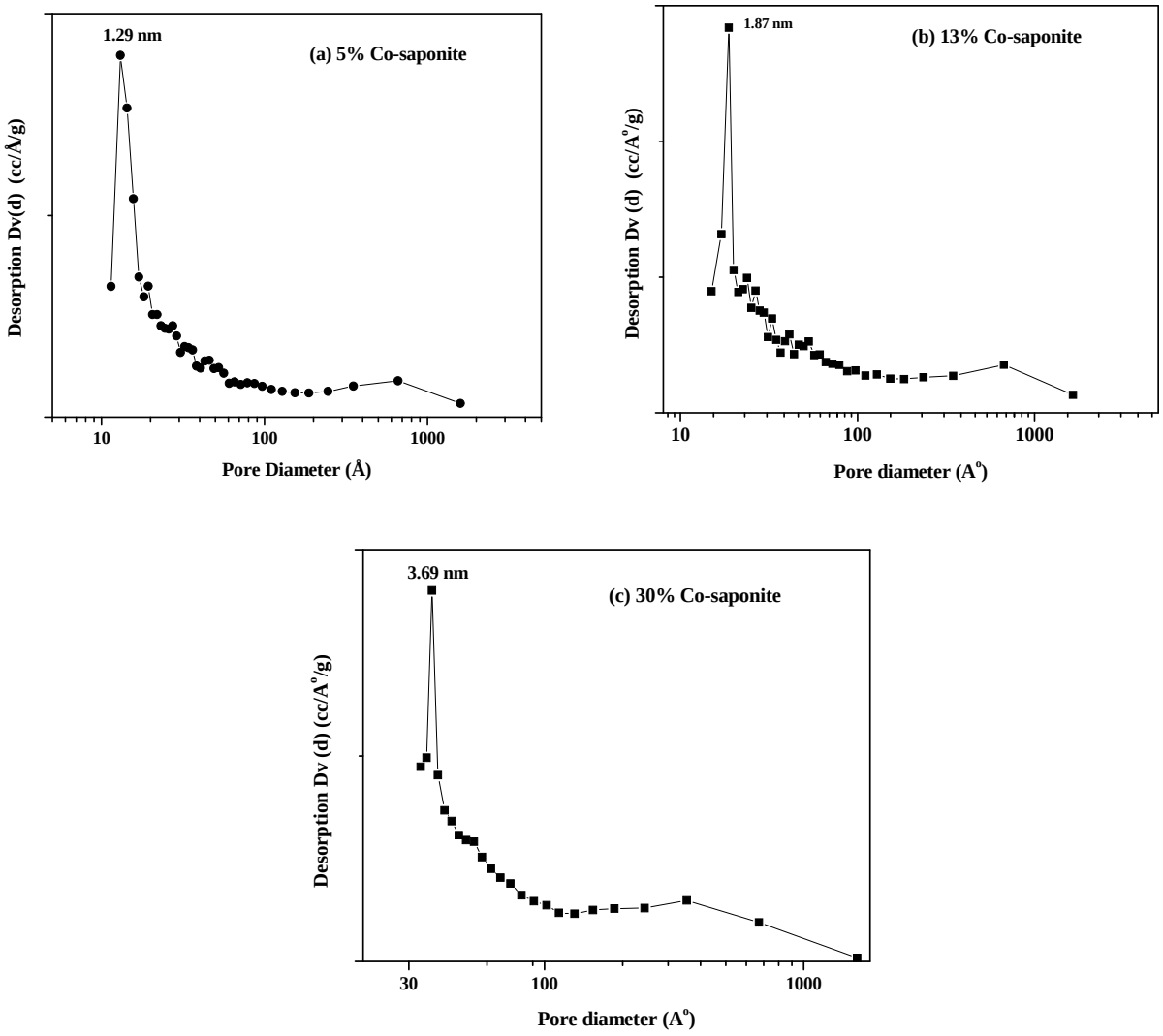

Figure 5.10. Pore size distribution curves for samples (a) 5% (b) 13% and (c) 30% Co-saponite samples

Interestingly, porosity of saponite clay was tuned from *micro*- to *meso*, with increase in Co loading from 13 to 30%. The pore diameter of Co-saponite clay increased almost 2-fold from 1.87 to 3.69 nm with increase in Co loading from 13 to 30%. This tuning of porosity of Co-saponite clay with increase in Co loading could be due to the incorporation of cobalt inside the clay framework and thereby enlarges its pore size and diameter [38]. Such type of observation was also reported in case of V-MCM-41 sample [39].

5.3.2.1.4. Raman analysis

Raman peaks at 200, 450 and 710 cm^{-1} of 5, 13 and 30% Co-saponite samples in Figure 5.11 are characteristic of tri-octahedral saponite clay [40].

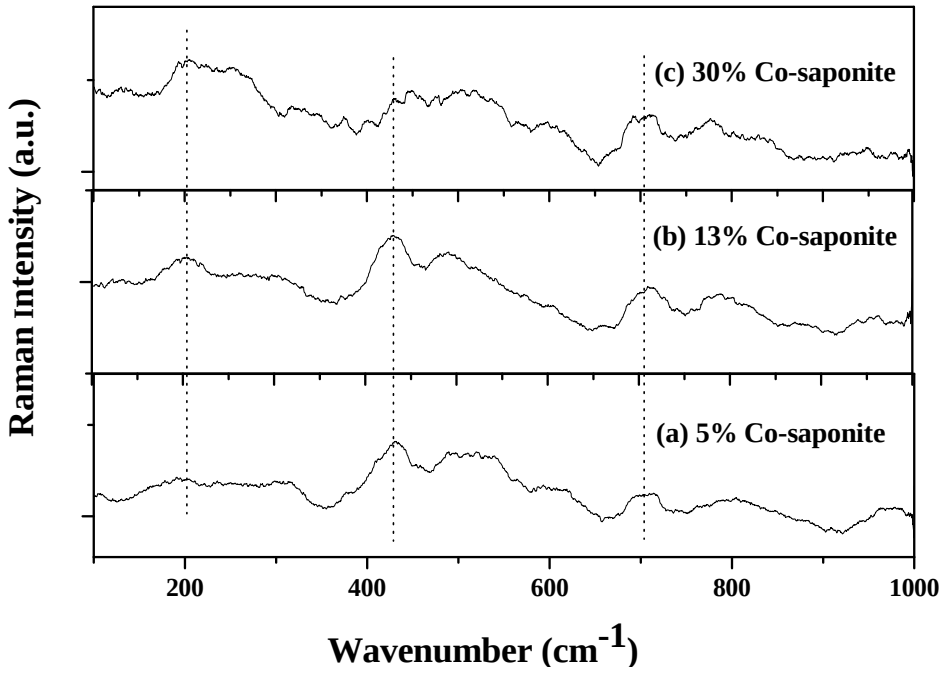

Figure 5.11. Raman spectra of (a) 5% (b) 13% and (c) 30% Co-saponite samples

However the intensity of Raman peaks of Co-saponite samples is low. The intensity or sharpness of Raman peaks generally depends upon the synthesis temperature of saponite samples [41]. The occurrence of peaks with low intensity could be due to the lower synthesis temperature (363 K) used for the preparation of Co-saponite catalysts.

5.3.2.1.5. FT-IR analysis

In FT-IR spectra of Co-saponite samples (Figure 5.12), the broad band at 3000-3500 cm^{-1} along with the band at 1640 cm^{-1} was assigned to stretching and bending vibrations respectively, of surface hydroxyl groups and water molecules bound to Lewis as well as Brønsted acid sites [28, 42]. The presence of bands at 457, 790 and 1017-1090 cm^{-1} in all the Co-saponite samples were due to the amorphous SiO_2 and Si-O stretching, respectively [43]. Another additional weak band at 667 cm^{-1} in 30% Co-saponite sample was assigned to a_1^2 stretching mode of SiO_2 [41].

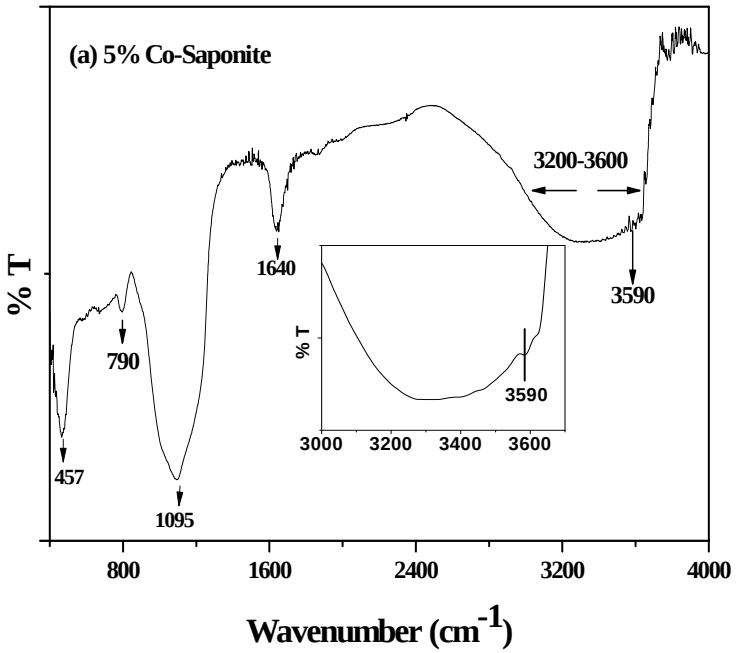

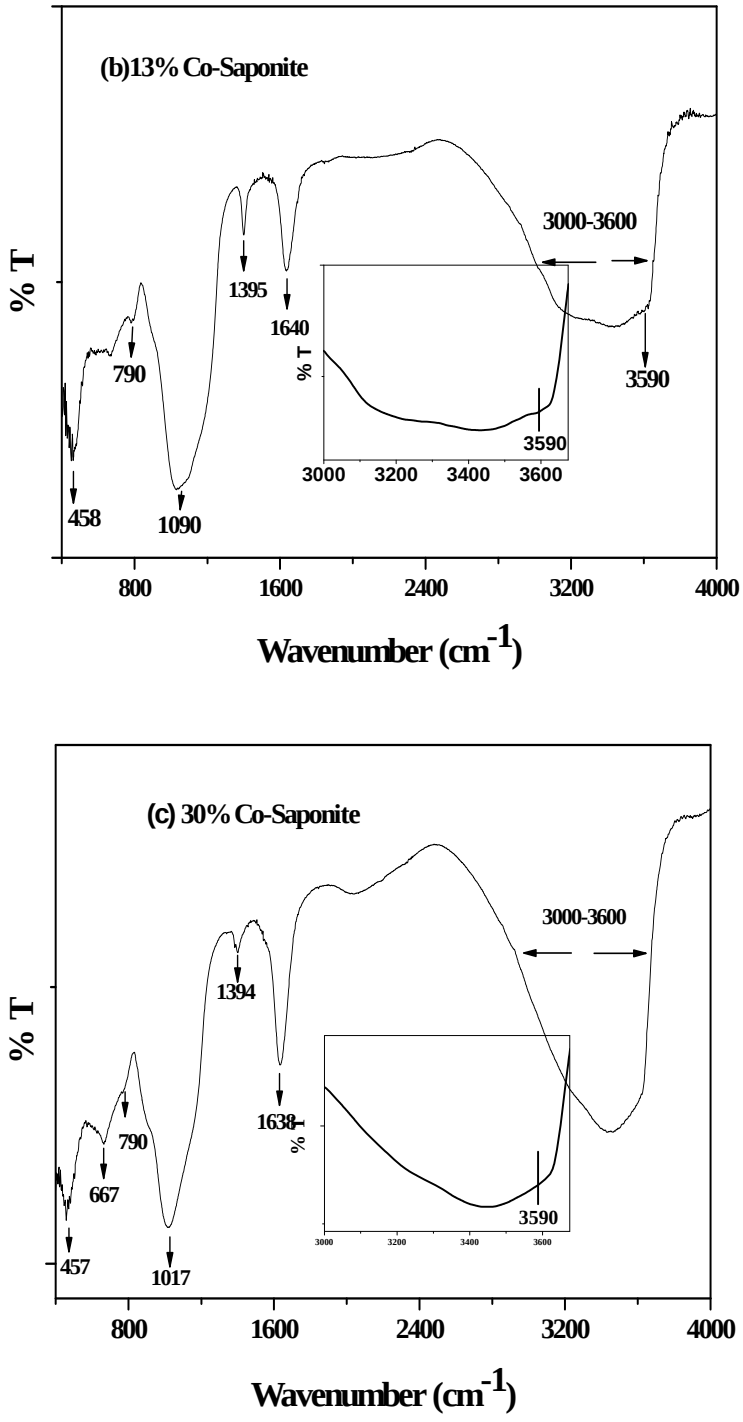

Figure 5.12. FT-IR spectra of (a) 5% (b) 13% and (c) 30% Co-saponite samples

An additional shoulder band at 3590 cm^{-1} along with a broad band at 3000-3500 cm^{-1} for 5% Co-saponite (inset Figure 5.12 a,b,c) disappeared completely with increase in Co loading from 5 to 30%. The presence of a band at 3590 cm^{-1} was assigned to the stretching mode of surface Si-O (H)-Al groups formed by isomorphous substitution of Si (IV) by Al (III) in tetrahedral sheet of saponite clay [44, 45]. A sharp band at 1395 cm^{-1} for both 13 and 30% Co-saponite samples could be probably due to the octahedral substitution of Al^{3+} by Co^{2+} similar to that in case of Ni-saponite sample [28] .

5.3.2.1.6. TGA-DTA analysis

In TGA analysis of 5% Co-saponite, weight loss of 12% occurred at < 473 K while that of 4% occurred in a range of 473-1073 K, respectively (Figure 5.13a).

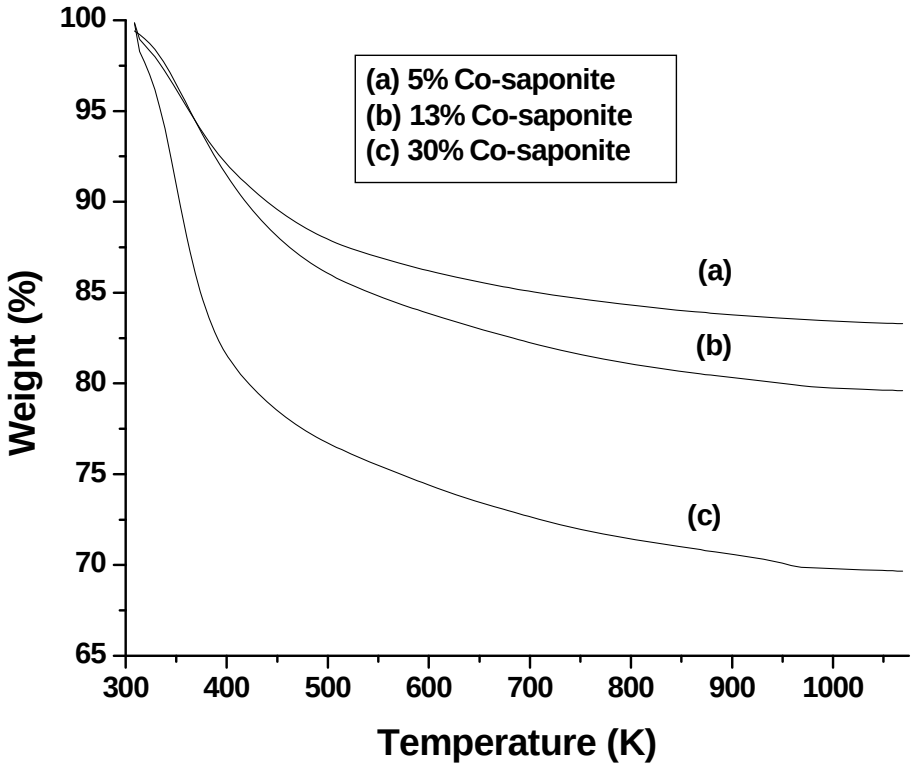

Figure 5.13. TGA curves of (a) 5% (b) 13% and (c) 30% Co-saponite samples

The endothermic peak near 373 K in DTA of the same sample (Figure 5.14a) indicates the release of water molecules absorbed as well as co-coordinated to the interlayer cations. A weight loss of 13% occurred at < 473 K while 7% weight loss occurred in a range of 473-1073 K respectively (Figure 5.13b). An endothermic peak at 373 K in DTA curve of 13% Co-saponite (Figure 5.14b) occurred due to the release of adsorbed water molecules while another weak exothermic peak at 1013 K was due to dehydroxylation of the sample [46]. The weight losses of 23 and 7% for 30% Co-saponite sample were in a temperature range of < 473 K and 473-1073 K respectively (Figure 5.13c). In DTA analysis of 30% Co-saponite (Figure 5.14c), the sharpening of an exothermic peak and its shifting toward lower temperature from 1013 to 963-973 K indicates the strong interaction of –OH with cobalt which facilitates the dehydroxylation of –OH groups due to enhancement in acidity with increase in Co loading from 13 to 30% [47-49].

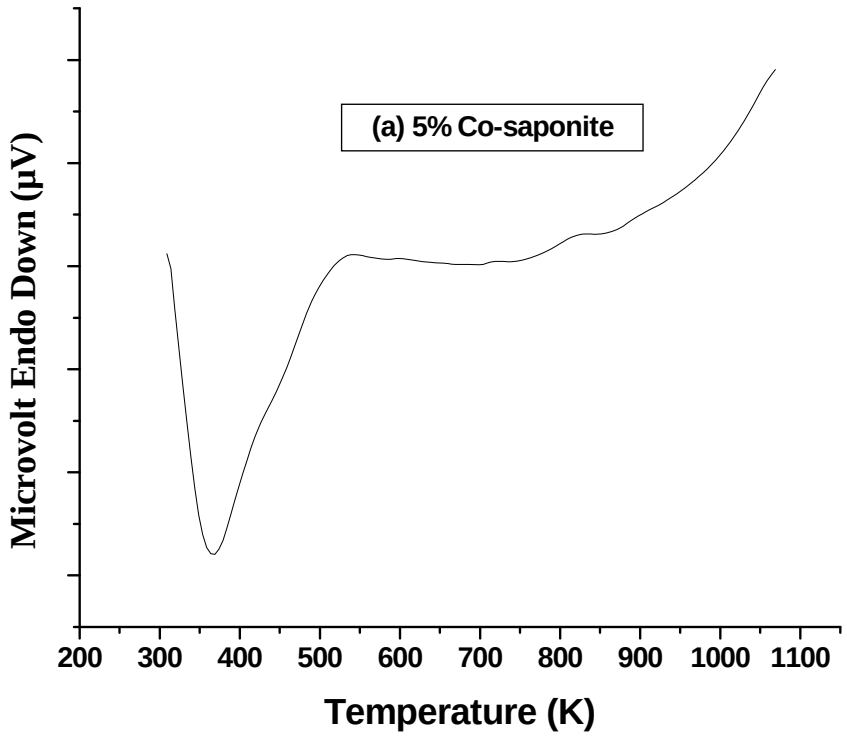

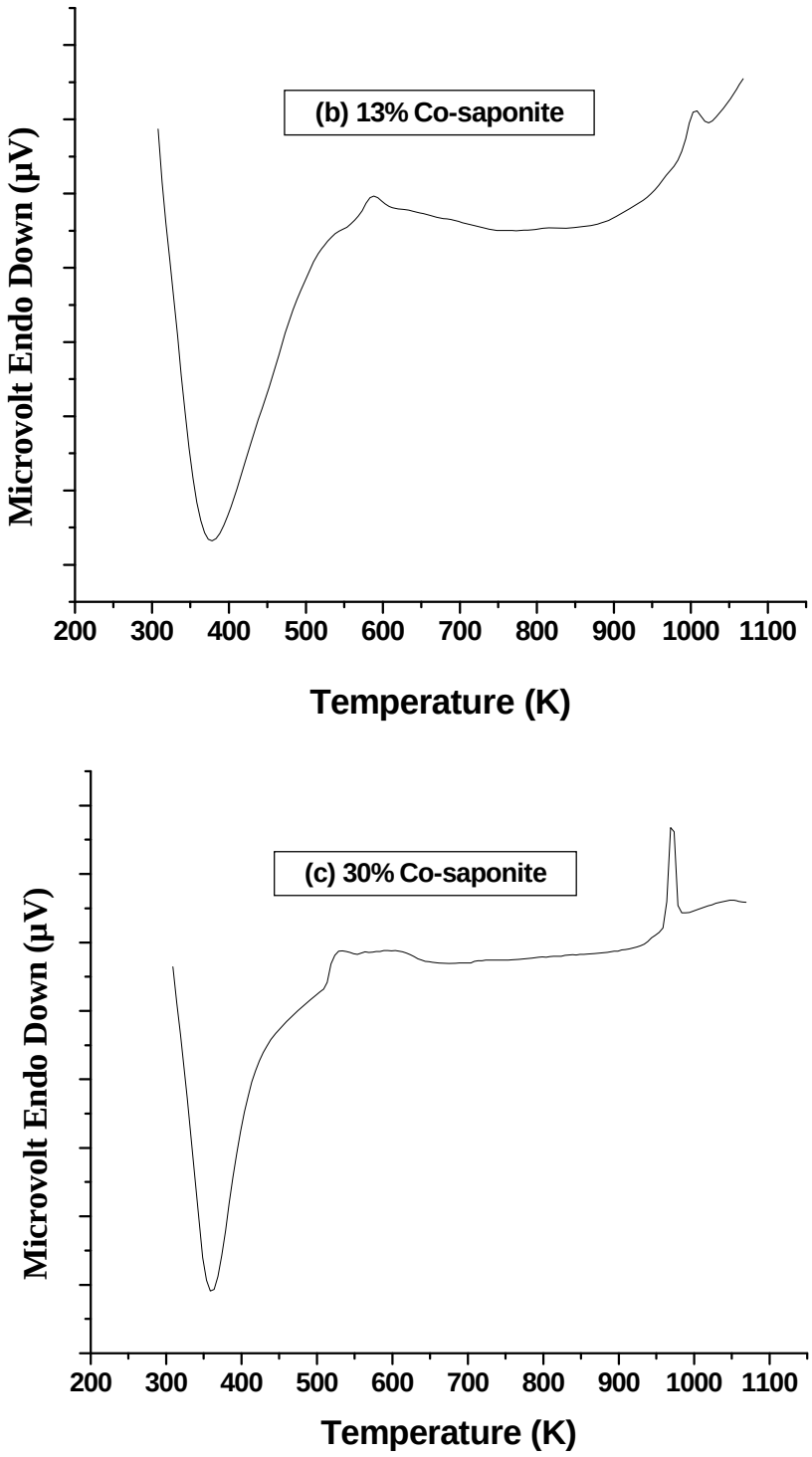

Figure 5.14. DTA curves of (a) 5% (b) 13% and (c) 30% Co-saponite samples

5.3.2.2. Catalyst activity measurement

5.3.2.2.1. Catalyst screening

Among the various catalysts (Co loadings ranging from 5-30%) screened, 13% Co-saponite gave the highest *p*-VAlc conversion of 55% with 99% selectivity to *p*-vanillin (Figure 5.15). The distribution ratios of Co_3O_4/CoO phases as estimated from TPR studies (Figure 5.8) were: 0.84, 1.67 and 1.7 for 5, 13 and 30% Co loadings respectively. Thus, the highest activity with 13% Co-saponite catalyst as compared to that of 5% Co-saponite was due to the increase in distribution ratio of Co_3O_4/CoO phase (increase in number of active sites) with increase in Co loading from 5 to 13%. Interestingly, the selectivity to alkylated product steeply decreased from 6 to 1% as Co loading increased from 5 to 13%. It is well known that Co_3O_4 having +2 and +3 oxidation states forms a dynamic equilibrium with oxygen under reaction conditions which is highly desirable for oxidation reactions [50, 51]. The oxidation proceeds through the activation of the C-H bond and dissociation of the C-H bond to give *p*-vanillin as presented in Scheme 5.3 (Ph- represents aromatic ring containing –OH and –OMe groups).

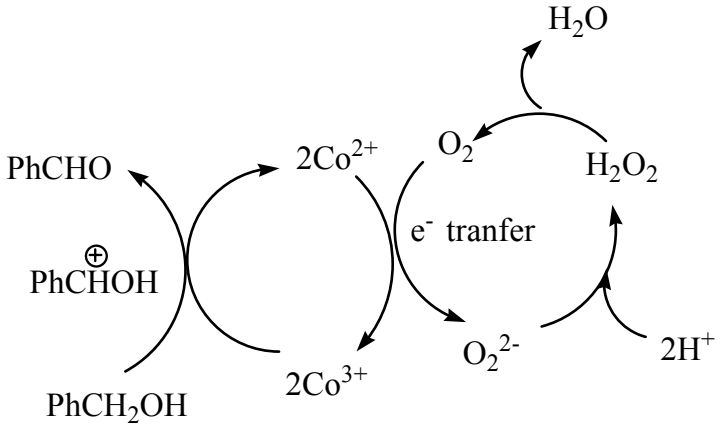

Scheme 5.3. Oxidation reaction pathway for the formation of *p*-vanillin

Beyond 13% Co-loading, the conversion of *p*-VAlc marginally increased from 55 to 58%, which is in accordance with a marginal increase in Co_3O_4/CoO ratio (from 1.67 to 1.7). However, selectivity to *p*-vanillin decreased substantially from 99 to 92% due to the formation of *p*-vanillic acid by further oxidation of *p*-vanillin. Since formation of *p*-

vanillic acid involves re-adsorption of *p*-vanillin (product) on the catalyst surface, followed by its interaction with active sites and molecular oxygen, increase in pore size as well as Co loading facilitates a diffusion of *p*-vanillin through the pores and enhances its interaction with active catalytic sites and thereby causes its further oxidation into *p*-vanillic acid. No alkylated product was observed with 30% Co-saponite catalyst. It was concluded from the catalyst activity and characterization results that the distribution ratio of Co_3O_4/CoO phase in saponite clay as well as pore size with appropriate magnitude is necessary for achieving highest activity and selectivity to *p*-vanillin.

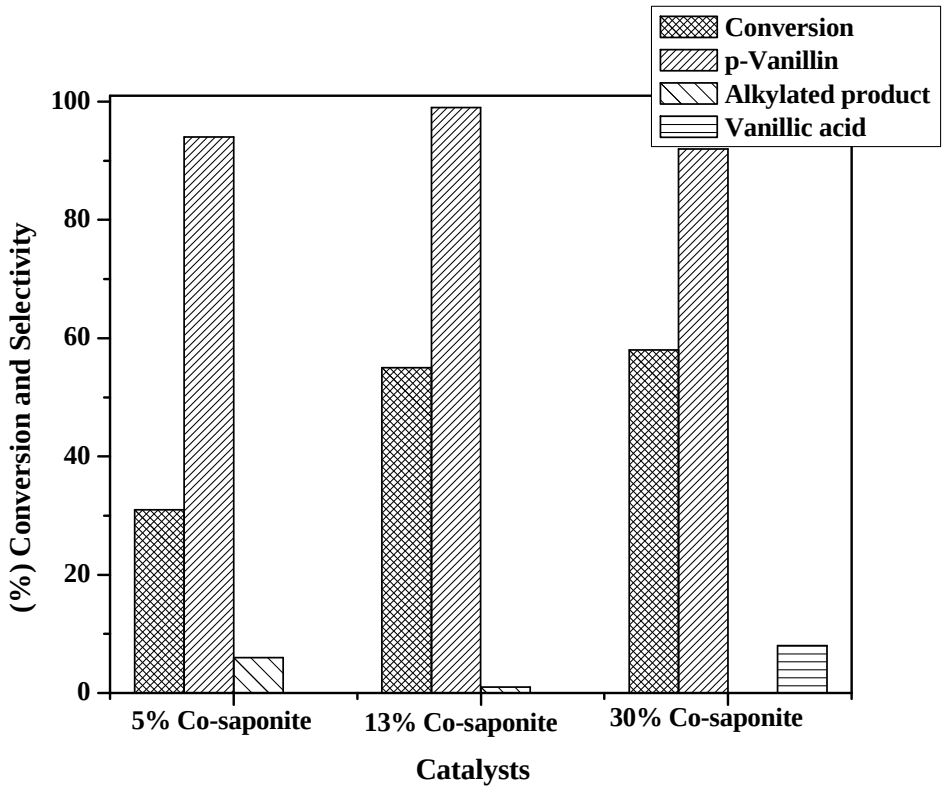

Figure 5.15. Effect of Co loading on conversion and selectivity patterns
Reaction conditions: *p*-vanillyl alcohol, 6.5 mmol; NaOH, 26 mmol, iso-propanol, 50 mL; catalyst, 10 mol% of Co w.r.t. *p*-vanillyl alcohol; temperature, 338 K; air flow rate, 60 mL/min; reaction time, 3 h.

The activity of prepared 13% Co-saponite catalyst (BET surface area of 405 m^2/g) was also compared with a commercial Co_3O_4 catalyst (BET surface area of 14 m^2/g) (Figure 5.16). Under similar cobalt loading (0.065 mmol of Co) and reaction conditions, the higher activity of 13% Co-saponite (55% conversion of *p*-VA with 99% selectivity to *p*-vanillin) than that of the commercial Co_3O_4 (44% conversion of *p*-VA) with 98% selectivity to *p*-vanillin could be attributed to the higher porosity (1.87 nm) and BET surface area (405 m^2/g) of the former sample as compared to that of commercial Co_3O_4.

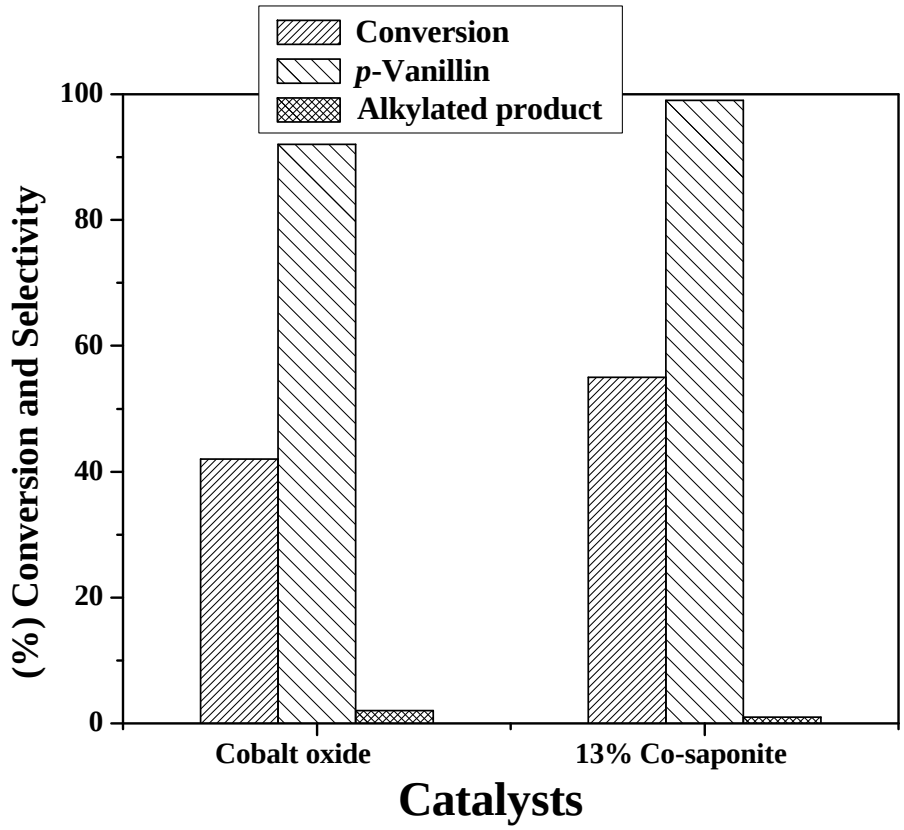

Figure 5.16. Catalytic performance of (a) 13% Co-saponite and (b) cobalt oxide for oxidation of *p*-vanillyl alcohol

Reaction conditions: *p*-vanillyl alcohol, 6.5 mmol; NaOH, 26 mmol, iso-propanol, 50 mL; catalyst, 10 mol% of Co w.r.t. *p*-vanillyl alcohol (0.065 mmol of Co); temperature, 338 K; air flow rate, 60 mL/min; reaction time, 3 h.

5.3.2.2.2. Effect of reaction time

Since 13% Co-saponite shows the best performance for oxidation of *p*-VAlc, the effect of reaction time on the *p*-VAlc conversion and *p*-vanillin selectivity was also studied for this catalyst (Figure 5.17). *p*-VAlc conversion increased from 24 to 55% while selectivity to *p*-vanillin remained almost constant (~ 99%) with increase in reaction time from 1 to 3 h. Thereafter, the conversion of *p*-VAlc marginally increased from 55 to 59% and *p*-vanillin selectivity decreased from 99 to 94% due to the formation of base catalyzed alkylated products with increase in reaction time from 3 to 5 h.

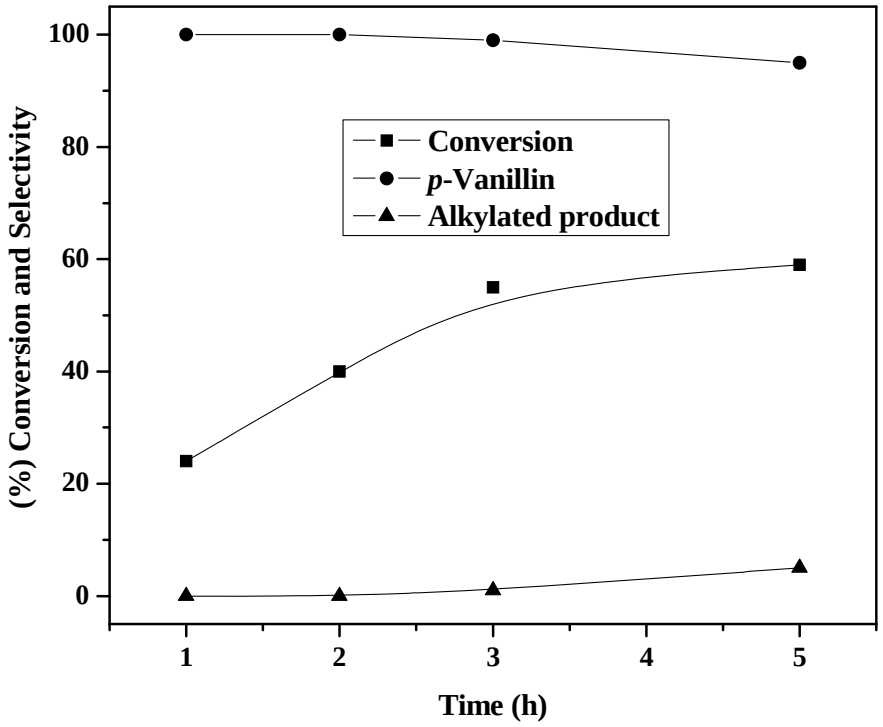

Figure 5.17. Effect of reaction time on the conversion of *p*-vanillyl alcohol and product selectivity

Reaction conditions: *p*-vanillyl alcohol, 6.5 mmol; NaOH, 26 mmol, iso-propnol, 50 mL; catalyst (13% Co-saponite), 10 mol% of Co w.r.t. *p*-vanillyl alcohol; temperature, 338 K; air flow rate, 60 mL/min; reaction time, 3 h.

5.3.2.2.3. Catalyst recycle

Catalyst recycle experiments were carried out as follows. After the first oxidation run, the used catalyst was filtered and washed several times with iso-propanol. Then the catalyst was dried at 383 K for 2 h and reused for the subsequent runs. The same procedure was followed for two subsequent oxidation experiments. The catalyst retained its activity even after the 2nd recycle experiment (Figure 5.18). The conversion of *p*-VAlc marginally decreased from 55 to 50% after 2nd recycle experiment that could be due to the handling losses of the catalyst. The selectivity to *p*-vanillin (99%) also remained constant for all the recycle experiments.

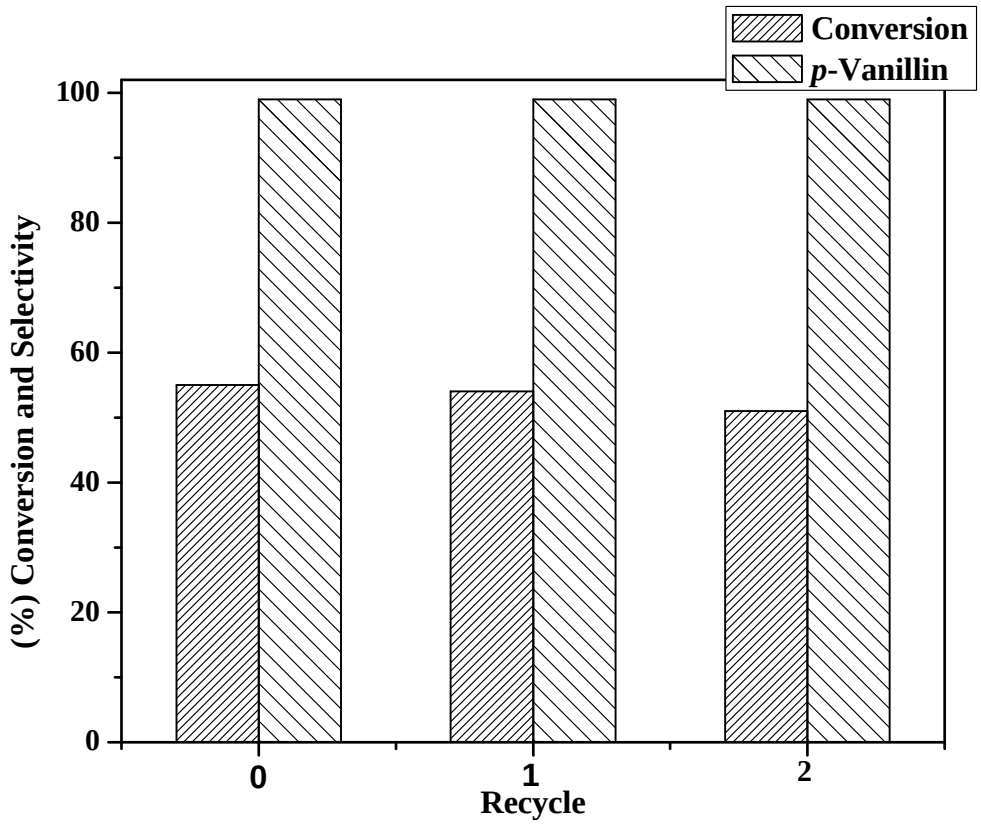

Figure 5.18. Catalyst recycle

Reaction conditions: *p*-vanillyl alcohol, 6.5 mmol; NaOH, 26 mmol, iso-propanol, 50 mL; catalyst(13% Co-saponite), 10 mol% of Co w.r.t. *p*-vanillyl alcohol; temperature, 338 K; air flow rate, 60 mL/min; reaction time, 3 h.

The stability of Co-saponite catalyst under the reaction conditions was confirmed by conducting a leaching test. For this purpose, the oxidation experiment was interrupted after 1 h at a partial conversion of 24% and the catalyst was removed by filtration and the reaction was further continued up to 3 h without the catalyst. The conversion of *p*-VAlc remained constant at 24% after continuing the reaction without the catalyst indicating that no leaching of Co metal was observed .

5.4. CONCLUSIONS

- Several types of solid acid catalysts were prepared and screened for the hydroxyalkylation of guaiacol among which 10% DTP/SiO_2 was found to be an effective catalyst giving the highest selectivity (46%) to VAlc. 20 and 40% DTP/SiO_2 catalysts with higher acidity showed lower selectivity to VAlc (41 and 27% respectively). Predominant formation of dihydroxydiarylmethane (73%) was observed with bulk DTP due to its highest acidity (163.8 $\mu molS^{-1}$ NH_3) and high acid strength. H-β-zeolite and amberlyst-15 showed very low VAlc selectivity (35 and 30% respectively) as compared to 10% DTP/SiO_2, due to their stronger acidity. The highest selectivity of 46% to VAlc with 10% DTP/SiO_2 catalyst could be due to acidic sites concentration in a low temperature region as evidenced by NH_3-TPD studies and the stabilization of intermediate carbocation by heteropoly anions of DTP. The conversion of guaiacol decreased from 37 to 14% and the selectivity to VAlc increased from 10 to 52% as the mole ratio of guaiacol to formaldehyde increased from 1:1 to 1:5. The conversion of guaiacol was found to increase with increase in the temperature and catalyst concentration.

- Co-saponite samples having various Co loadings (5-30%) were prepared by *in situ*-precipitation method. The formation of trioctahedral saponite clay was confirmed by XRD, Raman and FT-IR analysis. Effect of Co loading on the change in porosity of saponite clays was also studied systematically. The porosity of the clay samples altered from *micro*- to *meso* with increase in Co loadings from 13 to 30%. Among various Co-saponite samples prepared, 13% Co-saponite

showed an excellent performance (99% selectivity to *p*-vanillin with 55% conversion of *p*-VAlc) for the liquid phase air oxidation of *p*-VAlc to *p*-vanillin. Co-saponite catalyst having higher Co loading (30%) showed lower selectivity (92%) to *p*-vanillin due to the formation of *p*-vanillic acid as a byproduct. The distribution ratios of Co_3O_4/CoO phases increased from 0.84 to 1.67 with increase in Co loading from 5 to 13%, leading to its highest activity and selectivity.

5.5. REFERENCES

1. R. A. Sheldon, H. van Bekkum (Eds.), *Fine Chemicals through Heterogeneous Catalysis*, Wiley/VCH, New York/Weinheim, 2001.
2. P. Metivier, in: R. A. Sheldon, H. van Bekkum (Eds.), *Fine Chemicals through Heterogeneous Catalysis*, Wiley/VCH, New York/Weinheim, 2001, p.173.
3. M. B. Hocking, *J. Chem. Edu*. 74 (1997) 1055.
4. W. C. Muench, T. S. Hormel, P. M. Kirchhoff, L. A. Robbins, *US Pat. 4205188* (1980).
5. H. Iwane, T. Sugawara, N. Suzuki, K. Kaneko, *US Pat. 5220079* (1993).
6. K. Reimer, *Berichte der deutschen chemischen Gesellschaft* 9 (1876) 423.
7. C. Moreau, S. Razigade-Trousselier, A. Finiels, F. Fajula, L. Gilbert, *US Pat. 5811587* (1998).
8. M. Bolognini, F. Cavani, L. Dal Pozzo, L. Maselli, F. Zaccarelli, B. Bonelli, M. Armandi, E. Garrone, *Appl. Catal. A: Gen*. 272 (2004) 115.
9. F. Cavani, M. Corrado, R. Mezzogori, *J. Mol. Catal. A : Chem.* 182-183 (2002) 447.
10. M. H. Bhure, I. Kumar, A. D. Natu, R. C. Chikate, C. V. Rode, *Catal. Commun*. 9 (2008) 1863.
11. S. Udayakumar, S. Ajaikumar, A. Pandurangan, *Appl. Catal. A: Gen*. 302 (2006) 86.
12. T. Okuhara, *Chem. Rev*. 102 (2002) 3641.
13. F. Marme, G. Coudurier, J. C. Vedrine, *Micropor. Mesopor. Mater.* 22 (1998) 151.
14. A. Tarlani, M. Abedini, A. Nemati, M. Khabaz, M. M. Amini, *J. Colloid Interface Sci*., 303 (2006) 32.
15. M. Alvaro, H. Garcia, A. Sanjuan, M. Espla, *Appl. Catal. A: Gen*. 175 (1998) 105.
16. R. A. Sheldon, N. de Heiji, in: W. Ando, Y. Morooka (Eds.) *The role of Oxygen in Chemistry and Biochemistry*, Elsevier, Amsterdam, 1988, p. 243.
17. M. P. J. Peetrs, M. Busio, P. Leijten, *Appl. Catal. A: Gen.* 118 (1994) 51.

18. Z. Hou, T. Okuhara, *J. Mol. Catal. A : Chem.* 206 (2003) 121.
19. K. Nowinska, W. Kaleta, *Appl. Catal. A: Gen.* 203 (2000) 91.
20. L. C. Passoni, F. J. Luna, M. Wallau, R. Buffon, U. Schuchardt, *J. Mol. Catal. A: Chem.* 134 (1998) 229.
21. A. C. Garade, V. S. Kshirsagar, C. V. Rode, *Appl. Catal. A: Gen.* 354 (2009) 176.
22. T. A. Peters, N. E. Benes, A. Holmen, J. T. F. Keurentjes, *Appl. Catal. A: Gen*. 297 (2006) 182.
23. K. Klepacova, D. Mravec, A. Kaszonyi, M. Bajus, *Appl. Catal. A: Gen*. 328 (2007) 1.
24. A. C. Garade, V. R. Mate, C. V. Rode, *Appl. Clay Sci*. 43 (2009) 113.
25. V. S. Kshirsagar, A. C. Garade, K. R. Patil, M. Shirai, C. V. Rode, *Top. Catal*. 52 (2009) 784.
26. V. S. Kshirsagar, A. C. Garade, K. R. Patil, R. K. Jha, C. V. Rode, *Ind. Eng. Chem. Res*. 48 (2009) 9423.
27. A. C. Garade, N. S. Biradar, S. M. Joshi, V. S. Kshirsagar, R. K. Jha, C. V. Rode, *Appl. Clay Sci*. (2010) doi: 10.1016/j.clay.2010.10.026.
28. C. Bisio, G. Gatti, E. Boccaleri, L. Marchese, G. B. Superti, H. O. Pastore, M. Thommes, *Micropor. Mesopor. Mater*. 107 (2008) 90.
29. R. Prihod'ko, E. J. M. Hensen, M. Sychev, I. Stolyarova, T. E. Shubina, I. Astrelin, R. A. Santen, *Micropor. Mesopor. Mater*. 69 (2004) 49.
30. O. Prieto, M. A. Vicente, M. A. Banares-Munoz, *J. Porous Mater*. 6 (1999) 335.
31. M. Voß, D. Borgmann, G. Wedler, *J. Catal*. 212 (2002) 10.
32. M. M. Hossain, *Chem. Eng. J.* 123 (2006) 15.
33. F. B. Noronha, A. Frydman, D. A. G. Aranda, C. Perez, R. R. Soares, B. Morawek, D. Castner, C. T. Campbell, R. Frety, M. Schmal, *Catal. Today* 28 (2006)147.
34. R. Lago, G. Bini, M. A. Pena, J. L. Fierro, *J. Catal*.167 (1997)198.
35. M. M. Hossain, M. A. Al-Saleh, M. Shalabi, T. Kimura, T. Inui, *Appl. Catal. A: Gen.* 278 (2004) 65.

36. K. S. W. Sing, D. H. Everett, R. A. W. Haul, L. Moscou, R. A. Pioretti, J. Rouquerol, T. Siemieniewska, *Pure Appl. Chem*. 57 (1985) 603.
37. T. J. Barton, L. M. Bull, W. G. Klemperer, D. A. Loy, B. McEnaney, M. Misono, P. A. Monson, G. Pez, G. W. Scherer, J. C.Vartuli, O. M.Yaghi, *Chem.Mater*.11 (1999) 2633.
38. S. S. Bhoware, S. Shylesh, K. R. Kamble, A. P. Singh, *J. Mol. Catal. A: Chem*. 255 (2006) 123.
39. S. Shylesh, A. P. Singh, *J. Catal*. 228 (2004) 333.
40. R. L. Frost, L. Rintoul, *Appl. Clay Sci*. 11 (1996) 171.
41. J. T. Kloprogge, R. L. Frost, *Vib. Spectrosc*. 23 (2000) 119.
42. L. Marchese, J. Chen, P. A. Wright, J. M. Thomas, *J. Phys. Chem*. 97 (1993) 8109.
43. Z. Shan, P. Waller, W. Zhou, J. C. Jansen, P. Yeh, G. Tartaglione, L. Marchese, T. Maschmeyer, *Chem. Eur. J.* 10 (2004) 4970.
44. A. Janin, M. Maache, J. C. Lavalley, J. F. Joly, F. Raatz, N. Szydlowski, *Zeolites* 11 (1991) 391.
45. J. Weitkamp, *Solid State Ionics* 131 (2000)175.
46. M. A. Vicente, M. A. Bañares-Muñoz, L. M. Gandia, A. Gilb, *Appl. Catal. A: Gen.* 217 (2001)191.
47. S. Yariv, L. Heller-Kallai, *Clays Clay Miner*. 21 (1973) 199.
48. V. Balek, Z. Malek, S. Yariv, G. J. Matuschek, *Therm. Anal. Cal.* 56 (1999) 67.
49. E. Eren, B. Afsin, *J. Hazardous Mater*. 151 (2008) 682.
50. A. Bielanski, J. Haber, *Cat. Rev. Sci. Eng*. 19 (1979)1.
51. V. S. Kshirsagar, S. Vijayanand, H. S. Potdar, P. A. Joy, K. R. Patil, C. V. Rode, *Chem. Lett*. 37 (2008) 310.

Chapter VI

Oxidation of *p*-hydroxybenzyl alcohol to *p*-hydroxybenzaldehyde

6.1. INTRODUCTION

Oxidation of *p*-hydroxybenzyl alcohol (PHBAlc) is an industrially important reaction whose end products e.g. *p*-hydroxybenzaldehyde (PHB) and *p*-hydroxybenzoic acid (PHBA) are widely used as building blocks for fine chemicals [1, 2]. PHB and PHBA are mainly used in the synthesis of various agrochemicals, flavoring and fragrance agents, petroleum products and in electroplating. Generally, cobalt based catalysts both in homogeneous and heterogeneous forms have been reported in the literature for the synthesis of PHB and PHBA by oxidation of phenol derivatives [3-5]. The first process reported by Nishizawa et al. for the side chain oxidation of phenol derivatives used homogeneous cobalt catalyst [6] which was then followed by several other researchers [7-9]. In case of soluble cobalt catalysts, formation of inactive, OH-bridged Co complexes under aqueous basic conditions causes catalyst deactivation while in non-aqueous solvents such as methanol; the predominant formation of the corresponding ether was observed [10]. Homogeneous catalyst system also suffers from a major drawback of the catalyst recovery and its reuse affecting the overall economics of the process. In case of heterogeneous cobalt-aluminophosphate (Co-APO) type catalysts, oxidation of the substrate was found to take place mainly due to the dissolved cobalt species that leach out from the support during the reaction [11]. Other heterogeneous catalysts containing cobalt alone or together with copper or manganese supported on molecular sieves, carbon or resins were also reported for such oxidations [12, 13]. Novel heterogeneous nano structured catalyst systems based on cobalt also have been reported recently [14]. Thus, environmentally benign and relatively cheaper catalyst system than cobalt and working at atmospheric pressure for the air oxidation of hydroxybenzyl alcohols is highly desirable [15, 16]. In this context, γ-Fe_2O_3 is a versatile iron oxide well known for its application as a catalyst in several reactions [17, 18]. Since, iron also has an ability to form a redox couple (Fe^{+2}/Fe^{+3}) similar to cobalt, it can be explored as an economically viable oxidation catalyst. However bulk Fe_2O_3 has very low surface area (9 m^2/g), hence developing Fe_2O_3 with larger surface area would be highly desirable for its application as a catalyst. Another advantage of iron oxide catalyst is its easy separation from reaction medium by applying an external magnetic field. In the present work, the synthesis of

highly pure single phase γ-Fe_2O_3 (rod and spherical shaped) catalysts for the liquid phase air oxidation of PHBAlc is reported (Scheme 6.1).

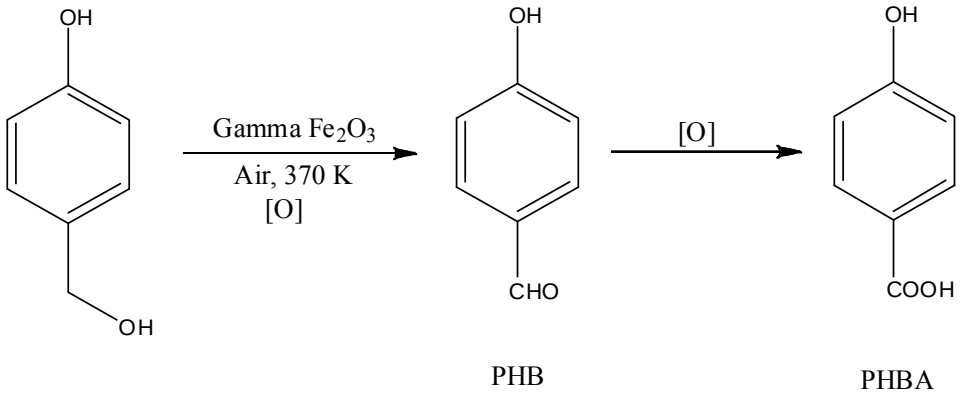

Scheme 6.1. Oxidation of *p*-hydroxybenzyl alcohol

γ-Fe_2O_3 (maghemite) catalysts were synthesized at two different temperatures i.e. 278 (low tempaerture, LT) and 368 K (high temperature, HT) by co-precipitation method. The prepared catalysts were characterized by different techniques such as XRD, XPS, Mössbauer spectroscopy, SEM, FT-IR, and by BET surface area measurement. The major reflection in the X-ray diffractogram was observed to be of the γ-Fe_2O_3 phase which was further supported by the Mössbauer analysis. The characterization by XPS confirmed the presence of Fe^{3+} species that are responsible for initiation of the oxidation of PHBAlc. Both the catalysts were found to be highly active and selective for liquid phase air oxidation of PHBAlc under ambient pressure conditions. The reusability of the catalysts was evaluated by the catalyst recycle experiments.

6.2. EXPERMENTAL

Single phase γ-Fe_2O_3 catalysts with different morphologies as a function of synthesis temperature, were prepared by co-precipitation method and detailed experimental procedure of their preparation has been described in section 2.2.3. The catalysts were characterized by various techniques and the detailed experimental procedure of catalyst characterization is described in section 2.3. The activity of prepared catalysts was

evaluated for the oxidation of PHBAlc to give PHB and PHBA. The experimental procedure for oxidation of PHBAlc is described in section 2.4.4.

6.3. RESULTS AND DISCUSSION

γ-Fe_2O_3 catalysts prepared by co-precipitation method were characterized by different techniques and their activity was evaluated for liquid phase oxidation of PHBAlc. The catalyst characterization and activity results are discussed in the following sections.

6.3.1. Catalyst characterization

6.3.1.1. X-ray diffraction

Iron oxide synthesis is often known to yield mixed phases however, in the present work a single phase γ-Fe_2O_3 material was successfully prepared [19, 20]. The X-ray diffractograms of the two samples synthesized at 278 (LT) and 368 K (HT) respectively are presented in Figure 6.1.

In each case, the major reflections at 2θ of 30.3^o (220), 35.8^o (311), 44.5^o (400) and 63^o (440) correspond to the characteristic γ-Fe_2O_3 (maghemite) together with others observed at 54.5^o (422) and 58.3^o (511) [21]. A small peak at 2θ of 21.2^o (111) implies that the product belongs to the spinel family bearing a cubic structure with an unit cell dimension of 8.35 Å with the space group of *Fd*3*m*. The cubic structure was derived from oxygen anions having arrays parallel to the (111) plane. Absence of any other peaks indicates the formation of pure maghemite phase of iron oxide. The drift in the diffractogram at low 2θ values in case of LT sample can be attributed to the difference in the morphology of crystallites [22].

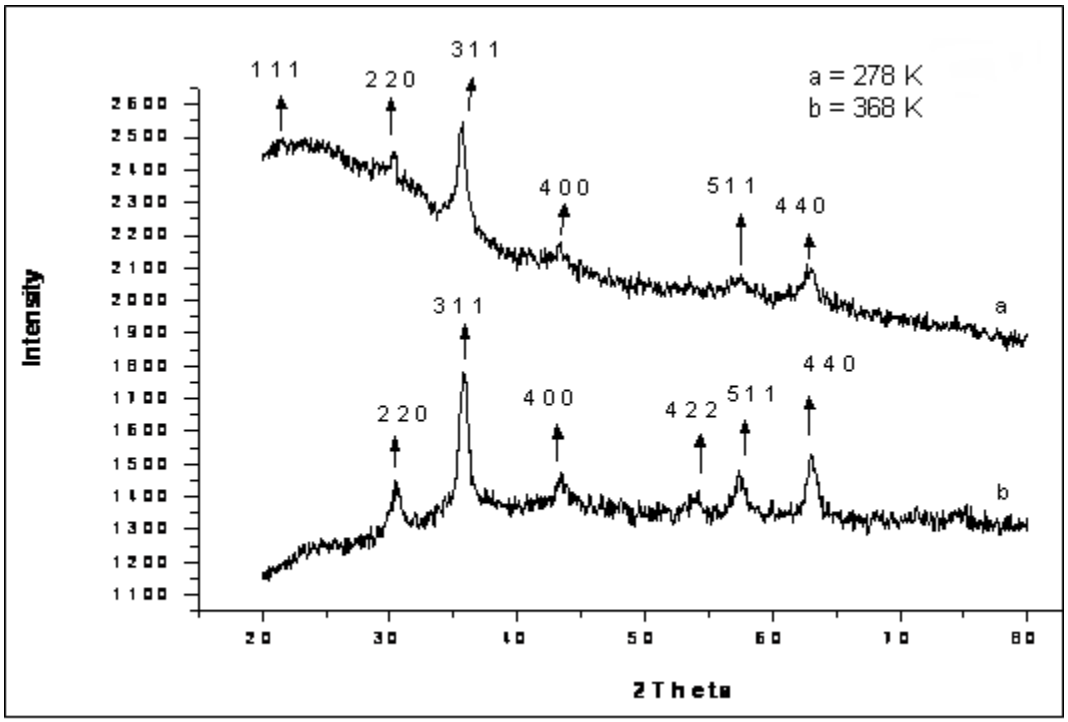

Figure 6.1. X-ray diffraction of γ - Fe_2O_3 particles synthesized at two different temperatures i.e. 278 K and 368 K

6.3.1.2. X-ray photoelectron spectroscopy

Since, both γ-Fe_2O_3 (cubic maghemite) and Fe_3O_4 (magnetite) possess the inverse spinel structure, XPS was also used to confirm the formation of pure γ-Fe_2O_3 along with XRD. Both the samples showed characteristic doublet of Fe $2p_{3/2}$ and $2p_{1/2}$ as photoelectron peaks (Figures 6.2a and 6.2b) at 710.6 and 724.12 eV respectively, which matched with those of γ-Fe_2O_3 reported in the literature [23, 24]. No signals corresponding to any other forms of iron were observed in XPS. O1s XPS of sample showed a single peak at 529.9 eV (Figures 6.2b and 6.2d) corresponding to oxide oxygen (O^{2-}) [25].

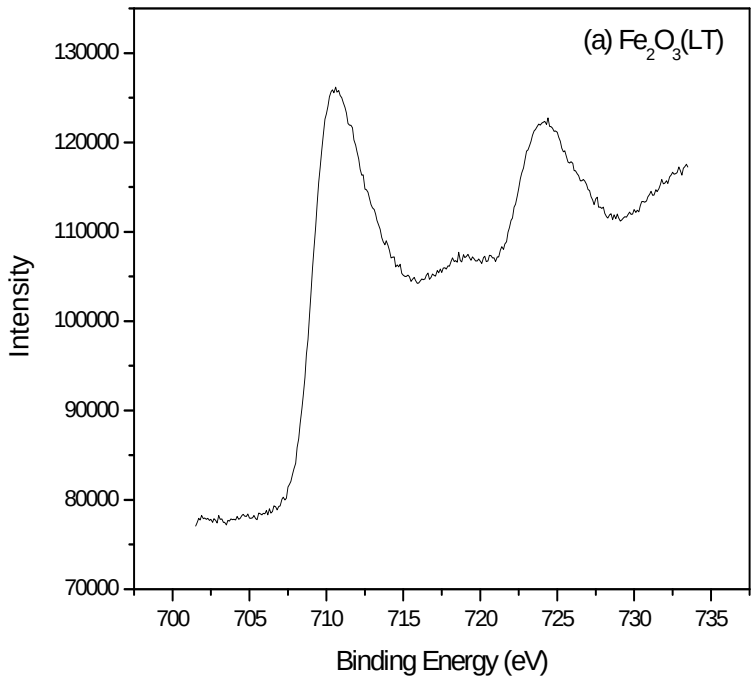
(a) Fe_2O_3(LT)
Intensity
130000
120000
110000
100000
90000
80000
70000
700
705
710
715
720
725
730
735
Binding Energy (eV)

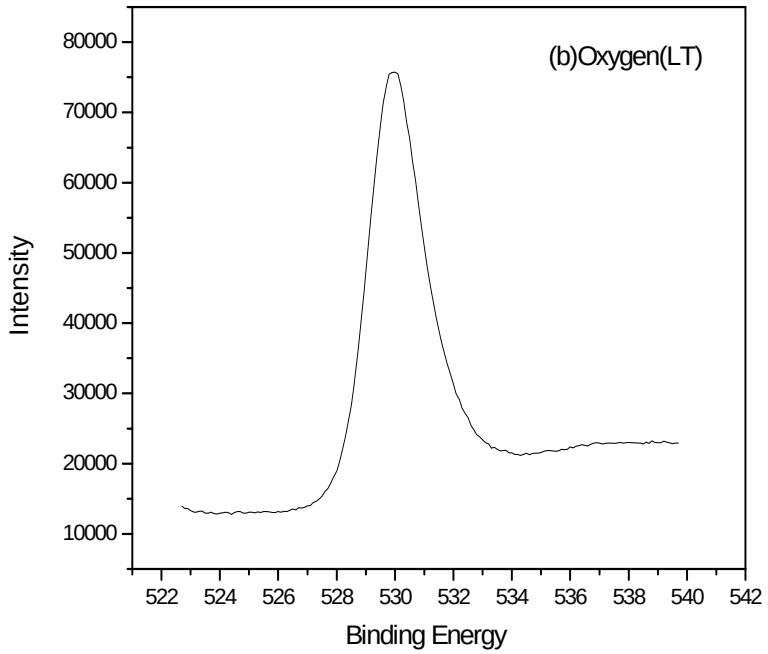
(b)Oxygen(LT)
Intensity
80000
70000
60000
50000
40000
30000
20000
10000
522
524
526
528
530
532
534
536
538
540
542
Binding Energy

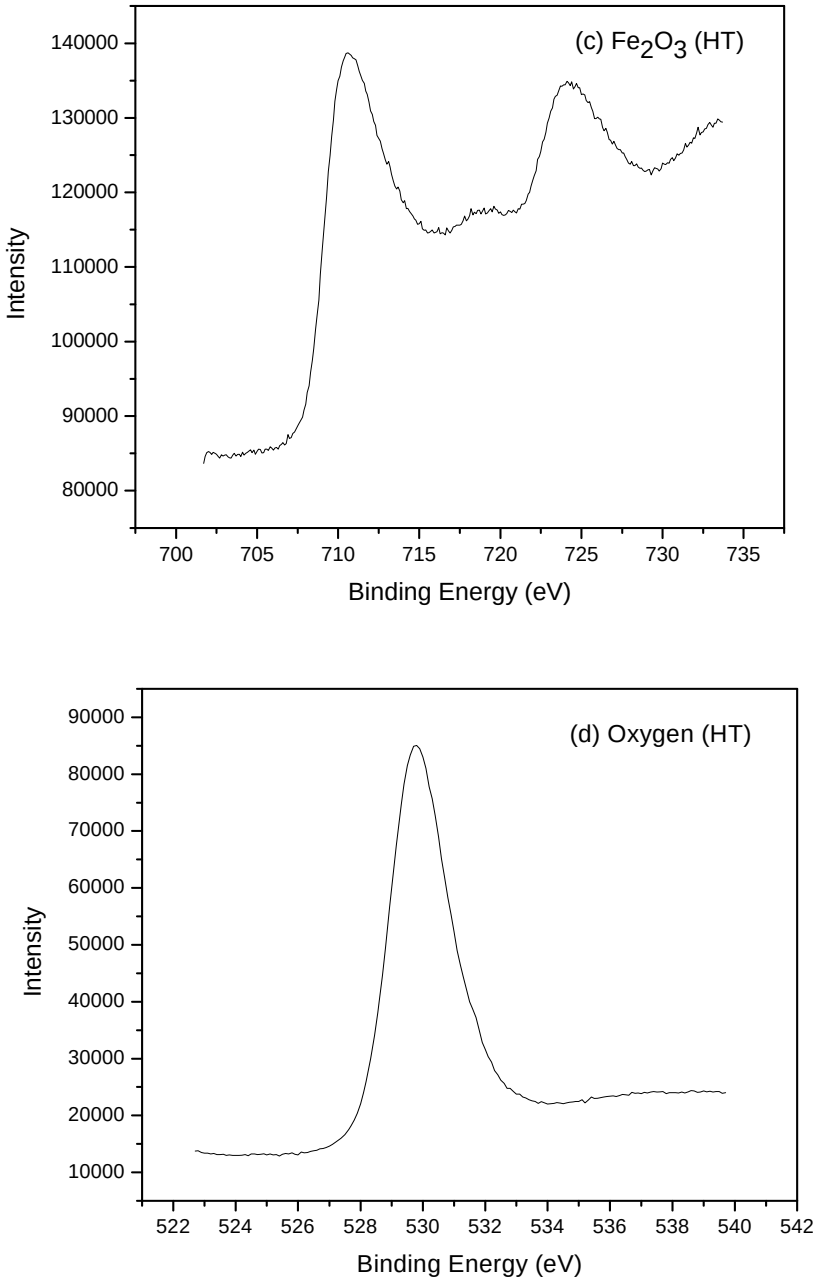

Figure 6.2. XPS spectra of Fe $2p_{3/2}$ and $2p_{1/2}$ in γ-Fe_2O_3 prepared at (a) 278 K (LT) and (c) 368 K (HT)

XPS spectra of O 1s in γ-Fe_2O_3 prepared at (b) 278 K (LT) and (d) 368 K (HT)

6.3.1.3. Mössbauer analysis

In order to gain insight into the structural and magnetic properties of the iron phases, a Mössbauer study has been performed on both LT and HT samples synthesized at 278 and 368 K respectively and these spectra are shown in Figures 6.3 (a) and (b). Asymmetrical and broad lines could be fitted by means of a discrete distribution of hyperfine field. Isomer shift (IS) values obtained from the Mössbauer spectrum for each sample (LT and HT) were identical, i.e. IS = 0.33 mm/s, while the average B values were 40 and 39 T respectively. The hyperfine parameters were not characteristic of bulk-like magnetite (x = 0) or maghemite (x = 1/3) but typical of small sized magnetite and maghemite. Usually, iron compounds with $3d^5$ configuration are found to exhibit IS values between 0.2 – 0.4 mm/s which represents the presence of Fe^{3+} ions on both tetrahedral and octahedral sites [26]. On the contrary, the values for Fe^{2+} ions are comparatively higher and electron transfer process between Fe^{2+} and Fe^{3+} ions in the octahedral site yields intermediate value (0.6 – 0.8 mm/s) [26]. Nevertheless for small size particles with broad spectra, it is not always possible to identify the valence state from IS value. The asymmetry of the spectrum is a qualitative benchmark, with a broader and less intense line 1 than line 6 for magnetite and opposite spectrum asymmetry typical for pure maghemite. Therefore, in the present case the product obtained was pure γ-Fe_2O_3. These results are further confirmed from the Mössbauer analysis of both the samples at lower temperature (30 K Figure 6.3 b). The spectra, with sharp peaks, were composed of two main magnetic components with the following isomeric shift and hyperfine field values: IS = 0.46 mm/s, 0.42 mm/s and B = 52.4, 50.5 T respectively for LT sample, and IS = 0.47 mm/s, 0.43 mm/s and B = 52.0, 49.6 T respectively for HT sample. These hyperfine parameters were found to be very close to that of octahedral and tetrahedral Fe^{3+} in γ–Fe_2O_3 phase.

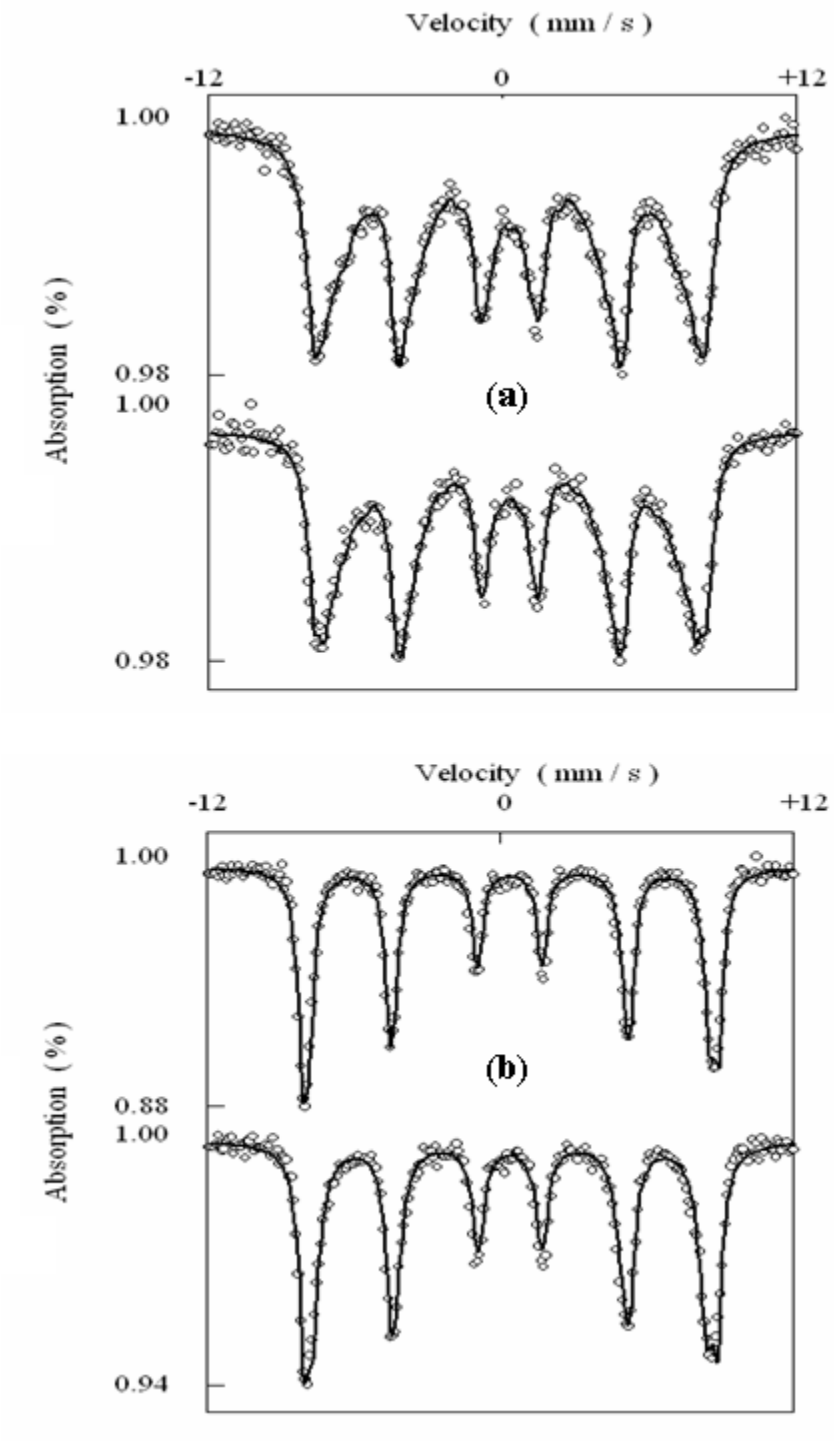

Figure 6.3. Mössbauer spectra of LT and HT-γ-Fe_2O_3 recorded at (a) 300 K and (b) at 30 K

6.3.1.4. SEM analysis

The SEM images of LT and HT samples of Fe_2O_3 clearly reveal two different types of morphologies as shown in Figure 6.4.

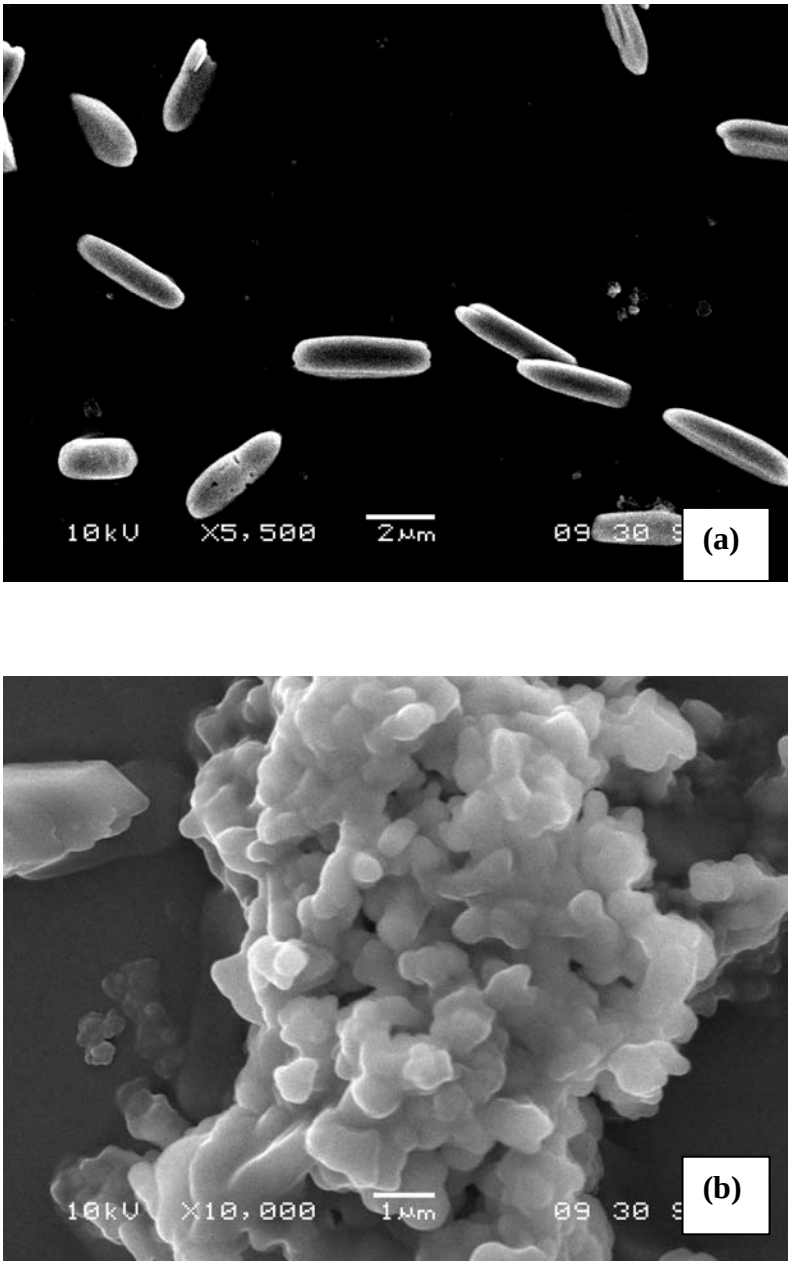

Figure 6.4. SEM (a) γ-Fe_2O_3 particles at 278 K after 3 h (b) γ-Fe_2O_3 particles at 368 K after 3 h

LT sample showed a rod shaped morphology (Figure 6.4 a) with almost homogenous distribution of particle size (diameter with 400 – 500 nm and length up to 2.8 μm) while the particles of HT sample were spherical in shape (Figure 6.4 b). Close observation of a single rod reveals that the surface is rough which could be highly desirable for a catalytic reaction.

6.3.1.5. FT-IR analysis

The FT-IR spectra of γ-Fe_2O_3 catalysts prepared at different temperatures are shown in Figure 6.5.

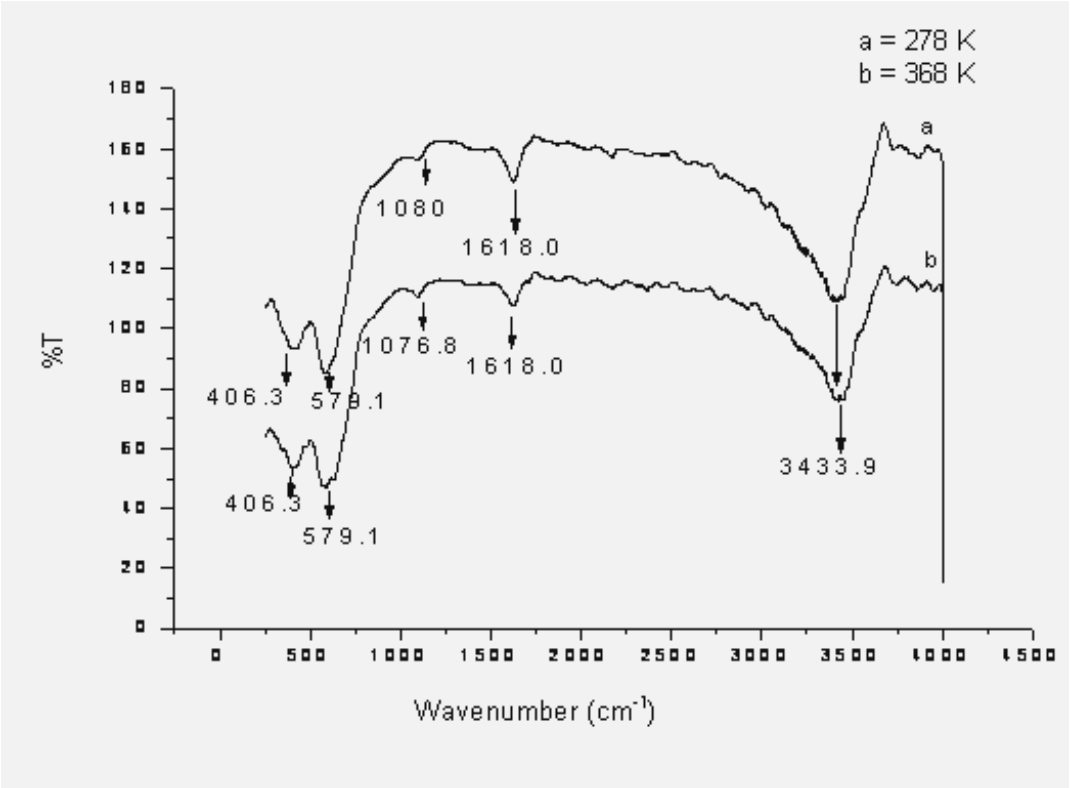

Figure 6.5. FT-IR spectra of (a) γ-Fe_2O_3 particles at 278 K (b) γ-Fe_2O_3 particles at 368 K after 3 h

Both LT and HT samples showed the peaks in the regions between 300 – 700 cm^{-1} corresponding to γ-Fe_2O_3 spinel phase [27, 28]. The peaks at 1080, 1076.8 cm^{-1} can be attributed to the presence of some overtones. The maghemite structure consists of FeO_6 octrahedra and FeO_4 tetrahedra. The cations (Fe^{3+}) are located at the tetrahedral sites along with certain vacancies. These vacancies are filled up with oxygen anions which compensate for the increased positive charge. The IR analysis enabled in locating the metal-oxygen bonds.

.

6.3.1.6. BET surface area measurement

Significant difference was observed between BET surface area of LT and HT γ-Fe_2O_3 as compared to the bulk γ-Fe_2O_3. Both LT and HT γ-Fe_2O_3 showed high surface area (109 and 97 m^2/g respectively) as compared to bulk Fe_2O_3 which showed a very low surface area (9 m^2/g).

6.3.2. Catalyst activity testing

6.3.2.1. Catalyst screening

The activity of the prepared γ-Fe_2O_3 catalysts were evaluated for liquid phase oxidation of PHBAlc and the results obtained are presented in Table 6.1. Both LT and HT samples of γ-Fe_2O_3 showed higher activities (42-44% conversion of PHBAlc with 82-89% selectivity to oxidation product) than that shown by the bulk Fe_2O_3 (26% conversion of PHBAlc with 22% selectivity to oxidation product). This can be attributed to the particle size of 400-500 nm having very high surface area (109 and 97 m^2/g) of LT and HT catalysts respectively as compared to the very low surface area of bulk Fe_2O_3 (9 m^2/g). Table 6.1 also presents the influence of reaction time on conversion and selectivity pattern for the oxidation of PHBAlc. With increase in reaction time from 8 to 24 h, conversion of PHBAlc increased from 44 to 84% and 42 to 80% while selectivity to oxidation products (PHB and PHBA) increased from 89 to 94% and 82 to 90% for γ-Fe_2O_3 (LT) and γ-Fe_2O_3 (HT) catalysts respectively. The selectivity to other products mainly alkylated product (4, 4'-dimethylene diphenol) decreased from the range of 11-19% to 6-10% with increase in reaction time from 8 to 24 h.

Table 6.1. Effect of reaction time on conversion and selectivity pattern.[a]

Entry	Reaction time (h)	Catalyst	Conversion (%)	Selectivity (%)		
				PHB	PHBA	Other
1	8	γ-Fe_2O_3 (LT)	44	68	21	11
		γ-Fe_2O_3 (HT)	42	63	19	18
		Bulk γ-Fe_2O_3	26	22	-	78
2	24	γ-Fe_2O_3 (LT)	84	56	38	6
		γ-Fe_2O_3 (HT)	80	53	37	10

[a] Reaction conditions: *p*-hydroxybenzyl alcohol, 8 mmol; NaOH, 32 mmol; mole ratio (*p*-hydroxybenzyl alcohol to NaOH), 1: 4; temperature, 370 K; air flow rate, 40 mL/min; catalyst concentration, 0.4 g; solvent, water; total reaction volume, 50 cm^3.

6.3.2.2. Effect of catalyst concentration

Figure 6.6 shows the effect of catalyst concentration on the activity and selectivity pattern. It was observed that two fold increase in catalyst concentration of γ-Fe_2O_3 (LT) and γ-Fe_2O_3 (HT) resulted in enhancing the conversion of PHBAlc from 34 to 44% and 30 to 42% respectively. Interestingly, selectivity to oxidation products also increased from 37 to 89% and 33 to 82% with increase in catalyst concentration for γ-Fe_2O_3 (LT)

and γ-Fe_2O_3 (HT) catalysts respectively. The two-fold increase in activity was mainly due to the increase in active sites with increase in catalyst concentration.

Although, about 20% conversion was observed for a blank run (without catalyst), but only a base (NaOH) catalyzed coupling products (4, 4'-dimethylene diphenol and tarry product) were formed without formation of any oxidation products. Under oxidation conditions, spinel type Fe_2O_3 has an ability to form a redox couple, Fe^{+2} / Fe^{+3} responsible for a dynamic equilibrium with the lattice oxygen. Activation followed by dissociation of a C-H bond of PHBAlc gives PHB. γ-Fe_2O_3 showed three fold higher catalyst activity due to higher aspect ratio as compared to the bulk Fe_2O_3. Such type of catalytic activity has been reported for Co_3O_4 for the liquid phase oxidation reactions of phenol derivatives [12, 14].

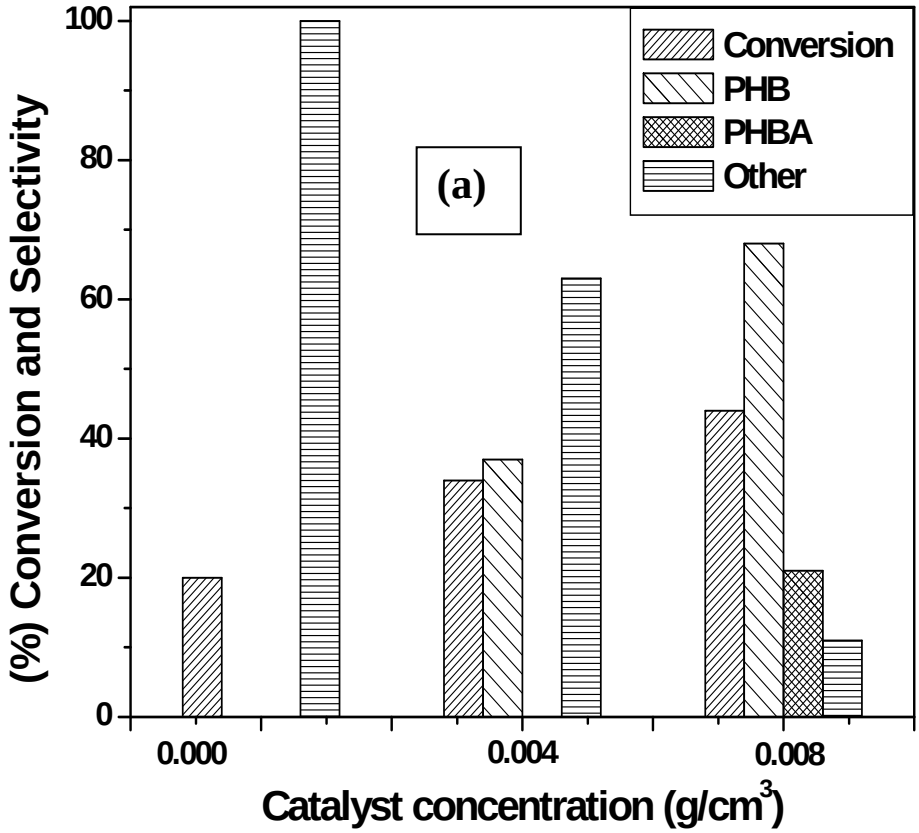

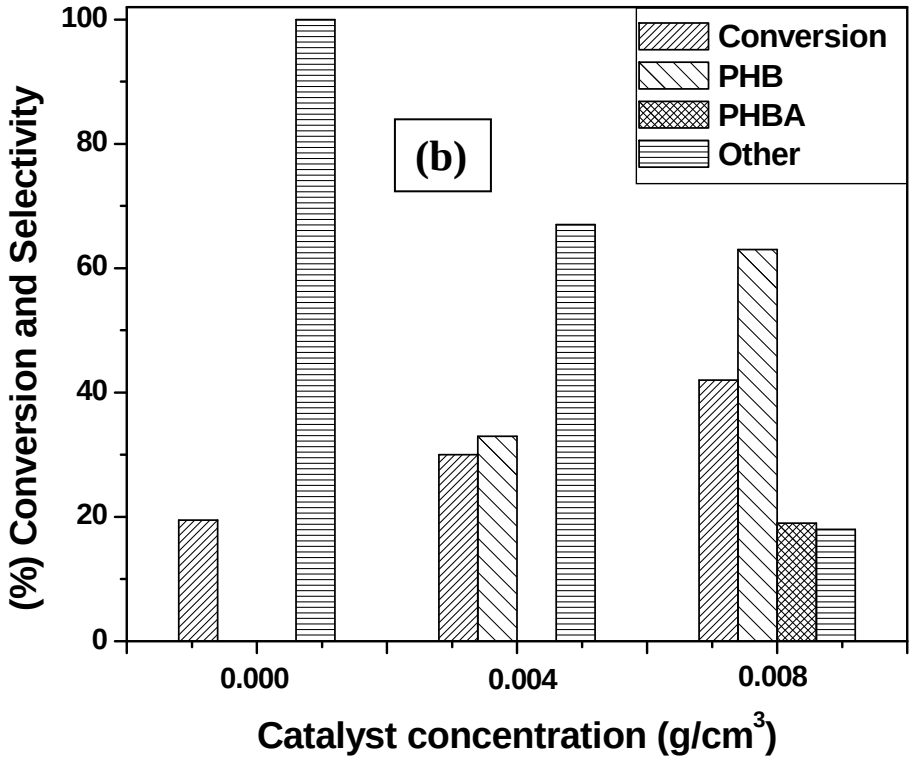

Figure 6.6. Effect of catalyst concentration for (a) γ-Fe_2O_3, low temperature (LT) and (b) γ-Fe_2O_3, high temperature (HT) samples on oxidation of *p*- hydroxybenzyl alcohol

Reaction conditions: *p*-hydroxybenzyl alcohol, 8 mmol; NaOH, 32 mmol; mole ratio (*p*-hydroxybenzyl alcohol to NaOH), 1: 4; temperature, 370 K; air flow rate, 40 ml/min; reaction time, 8 h; solvent, water; total reaction volume, 50 cm^3.

6.3.2.3. Catalyst recycle

In order to establish the reusability of the catalysts for oxidation of PHBAlc, after the first oxidation experiment, the catalyst (γ-Fe_2O_3-LT) was separated from reaction medium using strong bar magnet and washed with water followed by methanol for several times, dried it at room temperature and then in an oven at 383 K for 2 h and reused it for

subsequent runs. This procedure was followed for three subsequent oxidation experiments and the results obtained are shown in Figure 6.7.

The catalyst was found to retain its activity even after the third recycle. The PHBAlc conversion slightly decreased from 84 to 80% after the third recycle; this could be because of handling losses of the catalyst. The selectivity to oxidation products remained almost constant (94%) for all the recycle experiments.

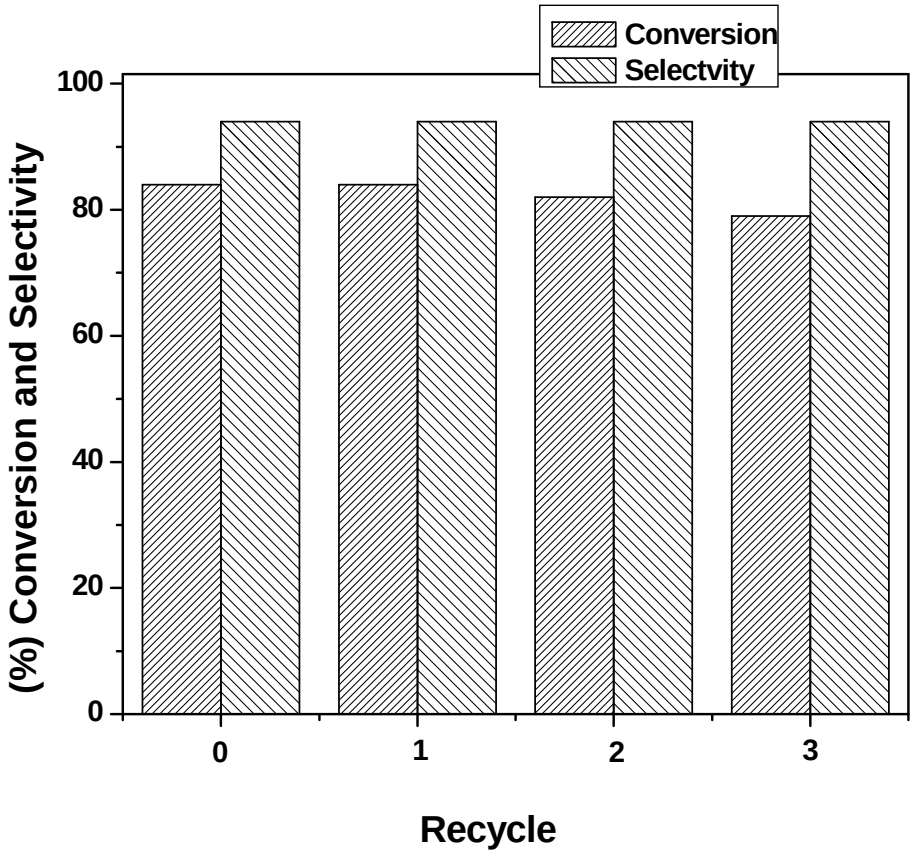

Figure 6.7. Catalyst recycle

Reaction conditions: *p*-hydroxybenzyl alcohol, 8 mmol; NaOH, 32 mmol; mole ratio (*p*-hydroxybenzyl alcohol to NaOH), 1: 4; temperature, 370 K; air flow rate, 40 mL/min; catalyst concentration, 0.008 g/cm^3; reaction time, 24 h; solvent, water; total reaction volume, 50 cm^3; catalyst, γ-Fe_2O_3 (LT).

6.3.3. Plausible mechanistic pathway

A plausible mechanistic pathway for the oxidation of PHBAlc catalyzed by γ-Fe_2O_3 is presented in Scheme 6.2. Under basic conditions, PHBAlc is converted into corresponding aninon (I). In the first oxidation step, anion of PHBAlc (I) is oxidized to give radical (II), during this process, Fe (III) is reduced to Fe (II) by abstracting an electron from (I) [29]. Fe (II) in turn, donates an unpaired electron to paramagnetic ($^3O_2$) oxygen molecule to form a superoxo species (III) as shown below in Figure 6.8.

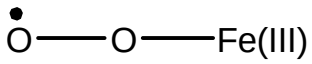

Figure 6.8. Formation of superoxo species in oxidation of *p*-hydroxybenzyl alcohol

The formation of such superoxo species is reported under mild temperature conditions in a polar solvent [30]. Superoxo species (III) is then converted into hydroperoxo species (IV) in presence of water. The radical (II) combines with hydroperoxo species (IV) and to form an iron-substrate intermediate (V) with elimination of H_2O_2. This is analogous to hydridometal mechanistic pathway [31]. Iron substrate intermediate (V) is then converted into anion of PHB (VI) and Fe (II) with the rupture of Fe-O bond. Fe (II) is again reoxidized to give back Fe (III) and the catalytic cycle is continued.

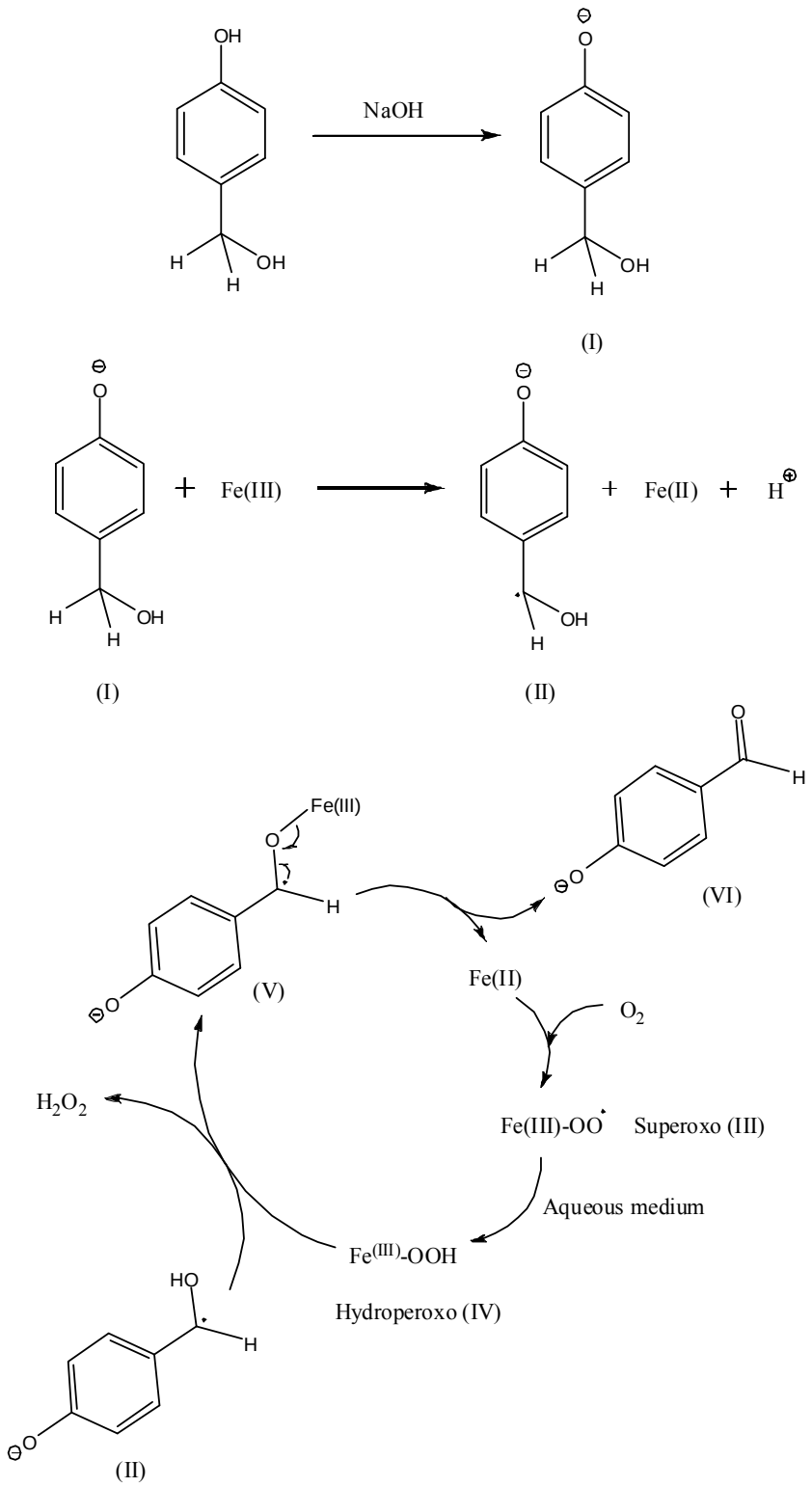

Scheme 6.2. Plausible mechanistic pathway for oxidation of *p*-hydroxybenzyl alcohol

6.4. CONCLUSIONS

- Highly pure single phase γ-Fe_2O_3 samples were prepared by a simple protocol involving precipitation at low temperature using NH_4OH.
- XRD pattern showed major reflections at 2θ of 30.3^o (220), 35.8^o (311), 44.5^o (400) and 63^o (440) characteristic of γ-Fe_2O_3 (maghemite). The characteristic doublet of Fe 2p3/2 and 2p1/2 were observed as photoelectron peaks at 710.6 and 724.12 eV respectively which confirmed Fe_2O_3 species. The hyperfine parameters observed in Mössbauer analysis also confirmed the formation of γ-Fe_2O_3 phase.
- Two different morphologies due to precipitation carried out at two different temperatures (278 and 368 K) were observed in SEM analysis.
- Both LT and HT samples of γ-Fe_2O_3 particles showed about three times higher activities than that shown by the bulk Fe_2O_3 for the air oxidation of PHBAlc under mild conditions.

6.5. REFERENCES

1. S. Mitchell, *Kirk-Othmer Encyclopedia of Chemical Technology*, (4th Eds.), Willy-Interscience: New York, 1998, p.1030.
2. S. Torii, H. Tanaka, T. Siroi, M. Akada, *J. Org. Chem.* 44 (1979) 3305.
3. C. V. Rode, M. V. Sonar, J. M. Nadgeri, R. V. Choudary, *Org. Proc. Res. Dev.* 8 (2004) 873.
4. C. V. Rode, V. S. Kshirsagar, J. M. Nadgeri, K. R. Patil, *Ind. Eng. Chem. Res.* 46 (2007) 8413.
5. V. S. Kshirsagar, S. Vijayanand, H. S. Potdar, P. A. Joy, K. R. Patil, C. V. Rode, *Chem. Lett*. 37 (2008) 310.
6. K. Nishizawa, K. Hamada, T. Aratani, *Eur. Pat.* 0012939 (1979).
7. E. Marko, L. Treindl, *React. Kinet. Catal. Lett.* 46 (1992) 345.
8. P. Li, H. Alper, *J. Mol. Catal. A: Chem.* 72 (1992) 143.
9. P. Campo, P. Cocolios, P. Dognin, H. Ledon, *Eur. Pat*. 0323290 (1987).
10. R. A. Sheldon, N. de Heiji, in: W. Ando, Y. Morooka (Eds.) *The role of Oxygen in Chemistry and Biochemistry*, Elsevier, Amsterdam, 1988, p. 243.
11. M. P. J. Peetrs, M. Busio, P. Leijten, *Appl. Catal. A: Gen.* 118 (1994) 51.
12. F. Wang, G. Yang, W. Zhang, W. Wu, J. Xu, *Chem. Commun.* 5 (2003) 1172.
13. L. Yumin, L. Shetain, Y. Xingkai, W. Yue, *Appl. Catal. A: Gen.* 169 (1998) 127.
14. V. S. Kshirsagar, S. Vijayanand, H. S. Potdar, P. A. Joy, K. R. Patil, C. V. Rode, *Chem. Lett.* 37 (2008) 310.
15. M. D. Tzirakis, I. N. Lykakis, G. D. Panagiotou, K. Bourikas, A. Lycourghiotis, M. Orfanopoulos, *J. Catal.* 252 (2007) 178.
16. F. Shi, M. K. Tse, M. M. Pohl, J. Radnik, A. Brückner, S. Zhang, M. Beller, *J. Mol. Catal. A: Chem.* 292 (2008) 28.
17. E. Rombia, I. Ferino, R. Monaci, C. Picciau, V. Solinas, R. Buzzoni, *Appl. Catal. A: Gen*. 73 (2004) 266.
18. J. D. Desai, H. M. Pathan, S. Min, K. Jung, O. Joo, *Appl. Surf. Sci.* 252 (2006) 2251.
19. M. I. Shukoor, F. Natalio, M. N. Tahir, V. Ksenofontov, H. A. Therese, P. Theato, H. C. Schroder, W. E. G. Muller, W. Tremel, *Chem Commun*. (2007) 4677.

20. L. Duraes, B. F. O. Costa, J. Vasques, J. Campos, A. Portugal, *Mater. Lett.* 59 (2005) 859.
21. V. Sreeja, P. A. Joy, *Mater. Res. Bull.* 42 (2007) 1570.
22. D. S. Xue, L. Y. Zhang, F. S. Li, *Hyperfine Interact.* 41 (2004) 156.
23. T. Fujii, F. M. F. de Groot, G. A. Sawatzky, F. C. Voogt, T. Hibma, K. Okada, *Phys. Rev. B* 59 (1999) 3195.
24. X. M. Liu, S. Y. Fu, H. M. Xiao, *J. Solid State Chem.* 179 (2006) 1554.
25. M. Mullet, Y. Guillemin, C. Ruby, *J. Solid State Chem.* 181 (2008) 81.
26. G. Connell, J. A. Dumesic, *J. Catal*. 101 (1986) 103.
27. A. Lagashetty, V. Havanour, S. Basavaraja, S. D. Balaji, A. Venkataraman, *Sci. Technol. Adv. Mater.* 8 (2007) 484.
28. B. Gillot, *Vib. Spectrosc.* 6 (1994) 127.
29. F. R. Keene, *Coord. Chem. Rev*. 187 (1999) 121.
30. E. Niederhoff, J. Timmon, A. E. Martell, *Chem. Rev.* 84 (1984) 137.
31. R. A. Sheldon, I. W. C. E. Arends, A. Dijksman, *Catal. Today* 57 (2000) 157.

Chapter VII

Summary and conclusions

7. SUMMARY AND CONCLUSIONS

In this thesis, the work on development of various solid acid catalysts involving dodecatungstophosphoric acid (DTP) dispersed on silica and clay materials and Co, Fe based oxidation catalysts is presented. The prepared as well as commercial catalysts were thoroughly characterized by various physico-chemical methods mainly to evaluate their surface acidity, phase identification, morphologies and oxidation states. The solid acid catalysts were highly selective in hydroxyalkylation of phenol and *p*-cresol to give the corresponding dihydroxydiarylmethane derivatives while, Co-saponite gave > 99% selectivity to vanillin in the liquid phase oxidation of *p*-vanillyl alcohol. The observed activity results of the hydroxyalkylation and oxidation reactions were co-related with catalyst characterization data. The summary and main conclusions of this work are given below.

1) Among the various DTP/SiO_2 catalysts having DTP loadings ranging from 0 to 40%, 20% DTP/SiO_2 gave the highest selectivity of 90% to bisphenol F in hydroxyalkylation of phenol. The optimum performance (product yield, 34%) with the highest selectivity of 90% to bisphenol F could be due to interaction of DTP with SiO_2 giving moderate acidity with an appropriate combination of both strong and weak acid sites, as evidenced by NH_3-TPD studies. The interaction between DTP and SiO_2 support was also confirmed by ^{31}P CPMAS NMR which showed a slightly broader peak at -15.49 ppm in 20% DTP/SiO_2 sample as compared to bulk DTP. Formation of a carbinol intermediate was observed for 10% DTP/SiO_2 catalyst, while a byproduct (trimer) formation was found to be substantial for bulk DTP, 40% DTP/SiO_2 and montmorillonite KSF/O catalysts due to their higher acidity.

In case of various DTP impregnated Mont K10 catalysts screened, 20% DTP/Mont K10 showed the highest activity (90% selectivity to bisphenol F with 28% conversion of phenol) for the hydroxyalkylation of phenol to give bisphenol F. The acidity and strength of montmorillonite K10 was significantly altered after impregnation with DTP as evidenced by NH_3-TPD and pyridine IR results. The ratio of Brønsted to Lewis acid sites (B/L) increased from 0.47 to 1.45 with increase in DTP loading from 0 to 60%. This

variation in acid sites led to marked differences in their catalyst activity for the hydroxyalkylation of phenol to bisphenol F.

2) 20% DTP/BNT gave 95% product yield with 94% selectivity to DAM at 353 K, for the hydroxyalkylation of *p*-cresol with formaldehyde. Ammonia-TPD results showed that an increase in total concentration of acid sites from 4.9 of parent BNT to 11.6 $\mu molS^{-1}$ NH_3 of 20% DTP/BNT was due to a strong interaction of protons of bulk DTP with surface hydroxyl groups of BNT, as evidenced by ^{31}P-CP MASNMR studies also. The catalyst retained its activity even after 3rd recycle experiment.

Continuous hydroxyalkylation of *p*-cresol to DAM in a fixed bed reactor was studied using montmorillonite KSF/O catalyst. The effect of various reaction parameters like mole ratio of *p*-cresol to formaldehyde, temperature, catalyst concentration and flow rate on conversion and selectivity was also studied for the continuous hydroxyalkylation operation. Very low conversion of *p*-cresol (< 4%) was observed in the batch reactor as compared to the fixed bed reactor under the same reaction conditions.

3) For the hydroxyalkylation of guaiacol to vanillyl alcohol (VAlc), 10% DTP/SiO_2 was found to be an effective catalyst giving the highest selectivity (46%) to (VAlc). 20 and 40% DTP/SiO_2 catalysts with higher acidity and strength showed lower selectivity to VAlc, due to the predominant formation of dihydroxydiarylmethane. H-β-zeolite and amberlyst-15 showed very low VAlc selectivity (35 and 30% respectively) as compared to 10% DTP/SiO_2 due to their stronger acidity. The highest selectivity of 46% to VAlc with 10% DTP/SiO_2 catalyst could be due to acidic sites concentration in a low temperature region as evidenced by NH_3-TPD studies and the stabilization of intermediate carbocation by heteropoly anions of DTP.

4) For liquid phase oxidation of *p*-vanilyl alcohol formed in the first step of the hydroxyalkylation of guaiacol, Co-saponite catalysts with various Co loadings ranging from 5 to 30% were prepared by *in situ*-precipitation method. The porosity of the clay samples altered from *micro*- to *meso* with increase in Co loading from 13 to 30%. Among

various Co-saponite samples prepared, 13% Co-saponite showed an excellent performance (99% selectivity to *p*-vanillin with 55% conversion of *p*-VAlc) for the liquid phase air oxidation of *p*-VAlc to *p*-vanillin. Co-saponite catalyst having higher Co loading (30%) showed lower selectivity (92%) to *p*-vanillin due to the formation of *p*-vanillic acid as a byproduct. The distribution ratios of Co_3O_4/CoO phases increased from 0.84 to 1.67 with increase in Co loading from 5 to 13%, leading to its highest activity and selectivity.

5) Highly pure single phase γ-Fe_2O_3 samples were prepared by precipitation method at low and high temperatures conditions. XRD pattern showed major reflections at 2θ of 30.3^o (220), 35.8^o (311), 44.5^o (400) and 63^o (440) characteristic of γ-Fe_2O_3 (maghemite) phase. The characteristic doublet of Fe 2p3/2 and 2p1/2 were observed as photoelectron peaks at 710.6 and 724.12 eV respectively which confirmed Fe_2O_3 species. The hyperfine parameters observed in Mössbauer analysis also confirmed the formation of γ-Fe_2O_3 phase. Two different morphologies due to precipitation carried out at two different temperatures (278 and 368 K) were observed in SEM analysis. Both low temperature (LT) and high temperature (HT) samples of γ -Fe_2O_3 particles showed about three times higher activities than that shown by the bulk Fe_2O_3 for the air oxidation of PHBAlc under mild conditions.

List of publications

Research paper published in peer reviewed journals

1. **A. C. Garade**, V. S. Kshirsagar, C. V. Rode, "Selective hydroxyalkylation of phenol to bisphenol F over dodecatungstophosphoric acid (DTP) impregnated on fumed silica." *Appl. Catal A: Gen. 354 (2009) 176.*

2. **A. C. Garade**, V. R. Mate, C. V. Rode, "Montmorillonite for selective hydroxyalkylation of *p*-cresol." *Appl. Clay Sci. 43 (2009) 112.*

3. C. V. Rode, **A. C. Garade**, R. C. Chikate, "Solid acid catalysts: Modification of acid sites and its effect on activity, selectivity tuning in various reactions" *Catal. Surv. Asia 13 (2009)205.*

4. **A. C. Garade**, M. Bharadwaj, S. V. Bhagwat, A. A. Athawale, C. V. Rode, "An efficient γ-Fe_2O_3 catalyst for liquid phase air oxidation of *p*-hydroxybenzyl alcohol under mild conditions." *Catal. Commun. 10 (2009) 485.*

5. V. S. Kshirsagar, **A. C. Garade**, K. R. Patil, M. Shirai, C. V. Rode, "Liquid phase oxidation of *p*-cresol over cobalt saponite." *Top. Catal. 52 (2009) 784.*

6. **A. C. Garade**, V. S. Kshirsagar, R. B. Mane, A. A. Ghalwadkar, C. V. Rode, "Acidity tuning of montmorillonite K10 by impregnation of dodecatungstophosphoric acid and its effect on hydroxyalkylation of phenol." *Appl. Clay Sci. 48 (2010) 164.*

7. **A. C. Garade**, A. M. Hengne, T. N. Deshpande, S. V.Shaligram, M. Shirai, C. V. Rode, "Continuous hydroxyalkylation of *p*-cresol to 2, 2′-methylenebis(4-methylphenol) in a fixed bed reactor." *J. Chem. Eng. Jpn. 42 (2009) 782.*

8. **A. C. Garade**, P. S. Niphadkar, P. N. Joshi, C. V. Rode, "Hydroxyalkylation of *p*-cresol to 2, 2'-methylenebis(4-methyl)phenol using Sn-MCM-41 catalyst." *Chem. Lett. 39 (2010)126.*

9. **A. C. Garade**, V. S. Kshirsagar, C. V. Rode, "Structure-Activity studies of dodecatungstophosphoric acid impregnated bentonite clay catalyst in hydroxyalkylation of *p*-cresol." *Catal. Commun. 11 (2010) 942.*

10. V. S. Kshirsagar, **A. C. Garade**, K. R. Patil, R. K. Jha, C. V. Rode, "Heterogeneous cobalt-saponite catalyst for liquid phase air oxidation of *p*-cresol." *Ind. Eng. Chem. Res. 48 (2009) 9423.*

11. V. S. Kshirsagar, **A. C. Garade**, K. R. Patil, A. Yamaguchi, M. Shirai, C. V. Rode, "Characterization of clay intercalated cobalt salen catalysts for the oxidation of *p*-cresol." *Appl. Catal. A: Gen. 370 (2009) 16.*

12. J. M. Nadgeri, **A. C. Garade**, R. A. Tambe, S. P. Gokhale, C. V. Rode, "Pd-Functionalized carbon nanotubes for selective hydrogenation of 2-butyne-1, 4 diol." *Adv. Sci. Lett. 3 (2010) 1.*

13. P. S. Niphadkar, **A. C. Garade**, R. K. Jha, C. V. Rode, P. N. Joshi, "Micro-/meso-porous stannosilicate composites (Sn-MFI/MCM-41) via two step crystallization process: process parameter-phase relationship." *Microporous Mesoporous Mater. 136 (2010) 115.*

14. **A. C. Garade**, N. S. Biradar, S. M. Joshi, V. S. Kshirsagar, R. K. Jha, C. V. Rode, "Liquid phase oxidation of *p*-vanillyl alcohol over synthetic Co-saponite catalyst." *Appl. Clay Sci.* (2010) doi: 10.1016/j.clay.2010.10.026.

Posters/Oral presentation for national/international symposium

1. **A. C. Garade**, C. V. Rode, "Selective hydroxyalkylation of *p*-cresol to dihydroxydiarylmethane using montmorillonite clay."
   Poster presented in ***National Workshop on Catalysis-Futuristic Materials as Catalysts and Adsorbents (CATWORKSHOP 2008)***, organized by *Catalysis Society of India*, Bhubaneswar, Orissa (India) during 18-20 February 2008.

2. C. V. Rode, **A. C. Garade**, M. Shirai, "Continuous hydroxyalkylation of *p*-cresol to 2, 2'-methylenebis (4-methylphenol) in a fixed bed reactor."
   Oral presented in ***International Workshop on Process Intensification (IWPI 2008)***, organized by *The Society of Chemical Engineers, Japan*, Tokyo (Japan) during 15-18 October 2008.

3. **A. C. Garade**, A. M. Hengne, A. A. Ghalwadkar, C. V. Rode, "Comparison of batch and continuous processes for hydroxyalkylation of *p*-cresol to 2, 2-methylenebis (4-methylphenol)."
   Oral presented in ***61 st Annual Session of Indian Institute of Chemical Engineers (CHEMCON 2008) on Green Technology and Sustainable Development*** , organized by Indian Institute of Chemical Engineers- Chandigarh Regional Centre, Chandigarh (India) during 27-30 December 2008.

4. **A. C. Garade**, S. T. Jadkar, C. V. Rode, "Selective hydroxyalkylation of phenol using dodecatungstophosphoric acid impregnated on montmorillonite K10 catalyst."
   Poster presented in ***19th National Symposium on Catalysis (CATSYMP-19) on Catalysis for Sustainable Energy and Chemicals*** organized by *Catalysis Society of India*, Pune (India) during 18-21 January 2009.

5. **A. C. Garade**, V. S. Kshirsagar, C. V. Rode, "Selective hydroxyalkylation of phenol to bisphenol F over solid acid catalysts."

Poster presented in ***Science Day*** organized by *National Chemical Laboratory,* Pune (India) in February 2009.

6. **A. C. Garade**, R. P. Patil, C. V. Rode, "Hydroxyalkylation of phenol to bisphenol F in a batch reactor: catalytic activity and kinetic studies."
   Poster presented in ***NCL Diamond Jubilee Symposium*** (***ACEPT-2009) on Advances in Chemical Engineering & Process Technology*** organized by *National Chemical Laboratory*, Pune (India) during 4-6 June 2009.

7. **A. C. Garade**, A. Jha, C. V. Rode, "Comparison of batch and continuous processes for hydroxyalkylation of *p*-cresol to 2, 2-methylenebis (4-methylphenol)."
   Poster presented in ***NCL Diamond Jubilee Symposium*** (***ACEPT-2009) on Advances in Chemical Engineering & Process Technology*** organized by *National Chemical Laboratory*, Pune (India) during 4-6 June 2009.

8. **A. C. Garade**, A. Jha, C.V.Rode, "Acidity tuning of fumed silica for the hydroxyalkylation of phenol to bisphenol F."
   Poster presentated in ***International Workshop on Nanotechnology and Advanced Functional Materials (NTAFM-09)*** organized by *Material Research Society of India* (Pune Chapter), *National Chemical Laboratory* and *Indian Institute of ScienceEducation and Research*, Pune (India) during 9-11 July 2009.